The Role of IKKε in the Initiation and Progression of Breast Cancer Bone Metastasis

A thesis submitted in fulfilment of the requirements

for the degree of Doctor of Philosophy

by

Ryan T. Bishop

June 2018

Department of Oncology and Human Metabolism

Faculty of Medicine, Dentistry and Health

The University of Sheffield

To my family

Contents

List of Abbreviations

Akt	Protein Kinase B
ALP	Alkaline Phosphatase
ALZ	Alizarin Red
AMX	Amlexanox
BAFF	B-cell activating factor
BCa	Breast cancer
BCA	Bicinchoninic acid
Bcl-2	B-cell lymphoma-2
BDNF	Brain-derived neurotrophic factor
BMP	Bone morphogenetic protein
BSA	Bovine Serum Albumin
CD	Cluster of differentiation
c-Fms	Receptor of M-CSF
cIAP	Cellular Inhibitor of Apoptosis Protein
CRISPR	Clustered Regularly Interspaced Short Palindromic Repeats
COX2	Cyclooxygenase-2
CCL	Chemokine ligand
CNA	Copy number alteration
CNV	Copy number variation
CTC	Circulating tumour cell
CXCL	chemokine (C-X-C motif) ligand

CYLD	Cylindromatosis protein
DAMP	Damage associated molecular pattern
DKK-1	Dickkopf-1
DMSO	Dimethyl sulphoxide
DNA	Deoxyribose nucleic acid
DoC	Docetaxel
DTC	Disseminated Tumour cell
ECM	Extracellular matrix
EDTA	Ethylenediaminetetraacetic acid
EGF	Epidermal growth factor
EGFR	EGF receptor
EMT	Epithelial to Mesenchymal Transition
EMMPRIN	Extracellular matrix metalloproteinase inducer *aka* CD147
ER	Oestrogen receptor
ERK	Extracellular signal–regulated kinases
ET-1	Endothelin-1
FCS	Foetal calf serum
FDA	Food and Drug Administration
FGF	Fibroblast growth factors
FGFR	FGF receptor
FLT3L	FMS-like tyrosine kinase 3 ligand
FOXO3	Forkhead Box O3

G-CSF	Granulocyte-colony stimulating factor
GF	Growth Factor
HER2	Human epidermal growth factor receptor 2
HSC	Haemopoeitic stem cell
ICAM	Intercellular Adhesion Molecule
IFN	Interferon
IGF-1	Insulin growth factor 1
IκBα	Inhibitor of κB alpha
IκBβ	Inhibitor of κB beta
IκBε	Inhibitor of κB epsilon
IκB ζ	Inhibitor of κB zeta
IKK	IκB kinase
IKKα	IκB kinase subunit alpha
IKKβ	IκB kinase subunit beta
IKKε	IκB kinase subunit epsilon (*aka* IKK-i)
IKKγ	IκB kinase subunit gamma
IKK-i	IκB kinase inducible subunit
IL	Interleukin
i.p.	Intraperitoneal
IRF	Interferon regulatory factor
ISGF	IFN-stimulated gene factor
IVIS	*In vivo* imaging system

JAK	Janus Kinase
JNK	c-Jun N-terminal kinases
KDa	Kilodaltons
KD	Knockdown
LB	Luria broth
LOX	Lysyl oxidase
LPS	Lipopolysaccharide
LTβ	Lymphotoxin-Beta
MAPK	Mitogen activated protein kinases
M-CSF	Macrophage colony stimulating factor
MCP-1	Monocyte chemotactic protein-1
MMP	Metalloproteinase
MSC	Mesenchymal stem cells
NAK1	NF-κB-activating kinase *aka* TBK1
NAP	NAK associated protein 1
nCOR	Nuclear co-repressor proteins
NEMO	NFκB essential modulator
NFκB	Nuclear factor kappa B
NIK	NF-κB-inducing kinase
NPI	Nottingham Prognostic Index
NOX	Nicotinamide adenine dinucleotide phosphate (NAPDH) oxidase
OB	Osteoblasts

OC	Osteoclasts
OE	Overexpression
OPG	Osteoprotegerin
OPN	Osteopontin
PAMP	Pathogen associated molecular pathogen
PBS	Phosphate-buffered saline
PDGF	Platelet-derived growth factors
PEI	Polyethylenimine
PI3K	Phosphoinositide 3-kinase
PML	Promyelocytic Leukemia
PQIP	cis-3-[3-(4-methyl-piperazin-l-yl)-cyclobutyl]-1-(2-phenyl-quinolin-7-yl)-imidazo[1,5-a]pyrazin-8-ylamine
PR	Progesterone receptor
PTHrP	Parathyroid hormone-related protein
RANK	Receptor activator of nuclear factor κB
RANKL	Receptor activator of nuclear factor κB ligand
RNA	Ribose nucleic acid
RNAi	RNA interference
Runx2	Runt-related transcription factor
SDF-1α	Stromal cell-derived factor 1 *aka* CXCL12
shRNA	Short hairpin RNA
siRNA	Small interfering RNA
SINTBAD	Similar to NAP1 and TBK-1 adaptor

SIKE	Suppressor of IKKε
SOST	Sclerostin
SUMO	Small Ubiquitin-like Modifier
STAT	Signal transducers and activators of transcription
TANK	TRAF Family Member Associated NFκB Activator
TBK1	TANK-binding kinase 1
TBS	Tris buffered saline solution
TFF3	Trefoil factor 3
TGFβ	Transforming growth factor-β
TLR	Toll-like receptor
TNBC	Triple negative breast cancer
TNFα	Tumour necrosis factor
TNFR	Tumour necrosis factor receptor
TOPORS	Topoisomerase I-binding protein arginine serine-rich protein
TRAF	TNF receptor associated factor
UK	United Kingdom
VEGF	Vascular endothelial growth factor
VCAM-1	Vascular cell adhesion molecule 1
Wnt	Wingless and Int-1

Declaration

I confirm that I shall abide by the University of Sheffield's regulations on plagiarism and that all written work shall be my own and will not have been plagiarised from other paper-based or electronic sources. Where used, material gathered from other sources will be clearly cited in the text.

Acknowledgments

Firstly, I would like to thank Dr Aymen Idris, my primary supervisor for allowing me to be a part of your lab group as both an MSc student and PhD candidate and to pursue multiple research projects in the field of bone and translational oncology. I would like to express my gratitude at the opportunities you have offered to me, allowing me to travel with my research, contributing to papers, books, articles, websites, reviews, grants and even your company. The insight I have gained from these experiences has been invaluable.

I am also very grateful to Breast Cancer Now for their continued support and funding allowing me to do these studies and progress as a young scientist.

I would also like to express my gratitude to my co-supervisor Dr Penny Ottewell, for her in-depth knowledge of breast cancer and bone research, for her collaboration, and support throughout my PhD. Thank you to Diane Lefley for her advice and guidance with µCT, histology and the IVIS system. I would also like to thank Dr. Ning Wang and Richard Allan for their contribution to the *in vivo* experiment of my PhD. I would also like to say a thank you to Dr Neil Chapman for his constant support and advice on research, careers and life in general.

I cannot express my appreciation of Dr Silvia Marino enough, for teaching me all I know, for encouraging me to pursue a career in research, for spurring me on when times were hard, thank you for being a great mentor but most importantly an amazing friend. A special thanks to soon-to-be Drs. Daniëlle de Ridder and Abdullah Al Jeffrey for their constant support and for being the best of friends over the past four years, I could not have done this without you both. I'd also like to say a huge thank you to almost Dr. Gloria Alloca, for being part of my *ohana* both in and out of the lab.

Finally, I will forever be grateful to my family for their love and support not just throughout my PhD but my entire life. Thank you for helping me to get to where I am today.

Accepted Publications

Marino S, **Bishop RT**, Logan JG, Capulli M, Sophocleous A, Mollat P, Mognetti B, Ventura L, Sims AH, Rucci N, Ralston SH and Idris AI**.** Contribution of cancer-specific IKKβ to bone metastasis, skeletal tumour burden and osteolysis **Oncotarget.** 2018; 9:16134-16148

Marino S, **Bishop RT**, Logan JG, Capulli M, Sophocleous A, Mollat P, Mognetti B, Ventura L, Sims A H, Rucci N, Ralston SH and Idris AI**.** Pharmacological inhibition of the skeletal IKKβ reduces breast cancer-induced osteolysis**. Calcified Tissue International.** 2018**.**

Marino S, **Bishop RT**, Logan J**.** G, Sophocleous A, Mollat P**.** and Idris AI**.**, Pharmacological evidence for the bone-autonomous contribution of the NFκB/β-catenin axis to breast cancer related osteolysis**. Cancer Letters.** 2017; 410:180-190

Peramuhendige P, Marino S, **Bishop RT**, de Ridder D, Khooger A, Baldini I, Capulli M, Rucci N and Idris A**.** I**.** TRAF2 in osteotropic breast cancer cells enhances skeletal tumour growth and promotes osteolysis**. Scientific Reports.** 2018; 8(39)

de Ridder D, Marino S, **Bishop RT,** Renema N, Chenu C**.** Heymann D, Idris AI**.** Bidirectional regulation of bone formation by exogenous and osteosarcoma-derived Sema3A. **Scientific Reports.** 2018. 8. 6877.

Manuscripts under review

Bishop RT, Marino S, de Ridder D, Allen RJ, Lefley DV, Wang N, Ottewell PD and Idris AI**.** Contribution of the IKKε/TBK-1 axis to breast cancer metastasis and osteolysis (*Oncogene*)

Manuscripts in preparation

Bishop RT, Marino S, de Ridder D, Carrasco DG, Allen RJ, Wang N**.**, and Idris AI**.** Targeting TRAF6/NFκB reduces breast cancer metastasis, skeletal tumour burden and osteolysis**.**

Conference Papers

Bishop RT, Marino S, de Ridder D, Lefley DV, Ottewell PD and Idris AI**.** Regulation of breast cancer metastasis and osteolysis by IKKε**. Calcified Tissue International** (2017) 100:S1–S174

- Plenary Oral presentation at the European Calcified Tissue Society (ECTS) meeting, Salzburg 2017.

Bishop RT, Marino S, Carrasco G, Allen RJ, Wang N and Idris AI. A small molecule inhibitor of TRAF6 signalling in combination with Docetaxel reduces breast cancer skeletal tumour burden and osteolysis**. Journal of Bone Oncology** (2018 *in press*)

- Poster presentation at the Cancer and Bone Society (CABs) meeting, Oxford, 2018

Book Chapters

Marino S, **Bishop RT**, de Ridder D, Delgado-Calle J, and Reagan MR, 2D and 3D *in vitro* co-culture for cancer and bone cell interaction studies. (Springer Bone Research Protocols. 3rd ed. In press)

Awards

The European Calcified Tissue Society (ECTS) New Investigator Award, Salzburg, Austria (2017)

The Learned Society Travel Award, Sheffield, UK (2017)

The Mellanby Centre Research Day Best Oral Presentation, Sheffield, UK (2016)

List of Tables

List of Figures

Abstract

Breast cancer is the most common cancer in the UK with the second highest cancer mortality rate for women. Primary tumours can be successfully treated locally through surgery and adjuvant chemotherapy or hormone therapy. However, it is the recurrence of, often chemoresistant, metastatic tumours at distant sites in the body that are the leading cause of breast cancer mortality. Breast cancers preferentially metastasise to bone. Once in the skeleton, breast cancer cells produce factors that influence the cells of the bone including osteoclasts and osteoblasts inducing osteolytic lesions. Due to the high mortality rate observed in metastatic breast cancer, there is a real need to identify the molecular mechanisms through which tumour cells escape the primary tumour and to establish novel drug targets for the prevention and treatment of metastatic breast cancer. IκB kinase subunit epsilon (IKKε), a key component of NFκB and IRF signalling, has been shown to act as a breast cancer oncogene However, its role in the development and progression of breast cancer osteolytic metastasis has yet to be elucidated. Here, I have shown breast cancer specific knockdown in triple negative human MDA-MB-231-BT cells reduced skeletal tumour growth and subsequent osteolytic bone damage, similarly the IKKε/TBK-1 inhibitor, Amlexanox reduced tumour growth and osteolysis in the 4T1 mouse model of breast cancer. I have demonstrated through functional and mechanistic studies that IKKε/TBK-1contribute to the ability of osteotropic MDA-MB-231 cells to proliferate, move and enhance osteoclast formation through the activation of the IRF3 and NFκB signalling pathways. Furthermore, combined treatment of Amlexanox and Docetaxel in the neo-adjuvant setting in mice reduced primary breast tumour growth of syngeneic breast cancer cells and inhibited metastasis and prolonged metastasis-free survival. Thus IKKε/TBK-1 inhibition shows great promise for the treatment of primary and skeletal tumour burden in advanced breast cancer

Graphical Abstract

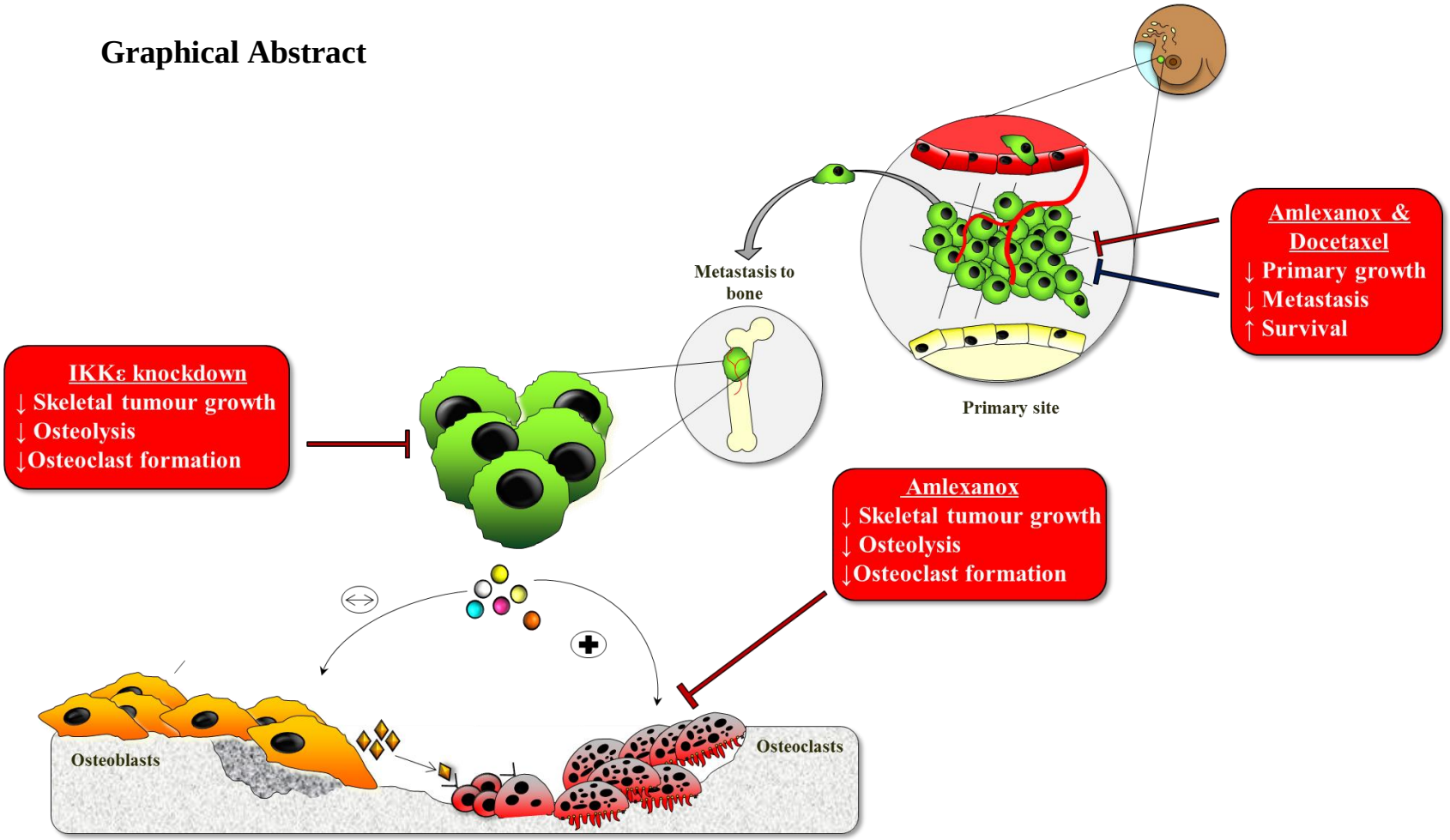

Figure 1. Targeting of IKKε, alone and in combination with conventional chemotherapies, may show promise for all stages of breast cancer.

Therapeutic targeting of IKKε in the bone microenvironment using knockdown or Amlexanox reduces skeletal tumour growth of breast cancer cells, osteolysis and reduces osteoclast formation. Combined administration of Amlexanox and Docetaxel in the neoadjuvant setting reduces primary growth, metastasis and improves survival. Targeting of IKKε, alone and in combination with conventional chemotherapies, may show promise for all stages of breast cancer.

Chapter 1

General Introduction

1 Introduction

1.1 Breast cancer

Breast cancer is the most common cancer in the United Kigdom (UK) (Office for National Statistics, 2014). It is estimated that 1 in 8 women will develop breast cancer throughout their lives. Despite improved methods of early detection and treatment, breast cancer represents the second most common cause of cancer death in women, with 12,000 deaths in the UK associated with the disease in 2010 (Office for National Statistics, 2014).

1.1.1 Breast Cancer Risk Factors

Several studies carried out over the past few decades have identified various risk factors associated with initial breast cancer development, reviewed extensively by (Ciriello et al., 2013, Kerlikowske et al., 2017). These risk factors can be broadly divided into intrinsic and extrinsic factors that influence the disease. Intrinsic factors include sex, age, genetic background and age at onset of menarche and menopause, whereas extrinsic risk factors include high fat diet, high alcohol consumption and intake of exogenous sex hormones. Many of said factors are linked to estrogen exposure, a class of female sex hormones associated with disease initiation and progression. Estrogen binding to its receptor induces cellular proliferation and thus may drive mammary epithelial cells through the cell cycle to continue dividing (Hilakivi-Clarke et al., 2002).

1.1.2 Pathology of Invasive Breast Cancer

Invasive breast cancer is not regarded as a singular disease but in fact a diverse group of lesions with varying molecular characteristics, prognoses and treatment options. Breast cancers are mostly carcinomas, specifically adenocarcinomas arising from the mammary glandular epithelia. Breast carcinomas usually start as

a local hyperplastic disease known as carcinoma *in situ*. Division of breast carcinomas in to histological classifications is based upon both growth and cytological features whereas further subdivisions are assigned by molecular characteristics. Specific classifications have been devised in order to predict progression and response to treatment (Malhotra et al., 2010).

1.1.3 **Histological Grading of Tumours**

Following recognition of a histological type, breast cancers are assigned a histological grade. The Nottingham Prognostic Index (NPI) is the most widespread system in use in the clinic (Rakha et al., 2014). The NPI assigns a value of one to three, to three characteristics of normal breast tissue: tubule formation, nuclear grade and mitotic rate. Breast tissue is arranged as tubular glands, thus tumours with loss of this structure are given higher scores. Nuclear grade considers changes in cell size and uniformity, less uniformity in the cells is related to higher grades. Mitotic rate is defined by the number of mitotic figures in ten high power fields, where mitotic figures are the chromosomes seen as a dark threadlike tangle. More mitotic figures correlate with a higher grade. The overall values are calculated and those with scores of three to five are described as grade 1, scores of six and seven are grade 2 and grade 3 tumours have a score of eight or nine. The grading of tumours is indicative of prognosis, whereby a higher grade has a less favourable outcome.

1.1.4 **Estrogen Receptor, Progesterone Receptor and HER2 Protein Status**

Standard practice in the assessment of breast tumours is the screening of tumours for expression of oestrogen receptor (ER), progesterone receptor (PR) and human epidermal growth factor receptor 2 (HER2). This is due to the development of targeted treatments against these proteins (Allison, 2012). ER and PR are expressed in up to 70% and 65% of all breast carcinomas respectively. Although they are not necessarily strong prognostic markers, tumours that express ER/PR have the best response to hormone therapy such as tamoxifen and aromatase inhibitors. HER2 is an oncogene that codes for a tyrosine kinase receptor, which regulates processes involved in proliferation, survival and invasion of cells. Identification of HER2 overexpression led to the development of HER2-targeted treatment, Herceptin. The combined treatment of Herceptin with standard chemotherapy (doxorubicin) improved survival rates of patients by 8.8% above doxorubicin alone after 10 years (Perez et al., 2011). A third histological type of breast cancer is represented by those lacking the aforementioned receptors known as triple negative breast cancers. As such, these breast cancers lack known druggable targets and such have a poor prognosis (Negi et al., 2016). Moreover, recent evidence indicates that a triple negative breast cancer subtype exists that expresses the androgen receptor and as such has been deemed the luminal androgen receptor (LAR) subtype (Lehmann et al., 2011). Patients with LAR breast cancer exhibit decreased relapse-free survival, however on-going clinical trials suggest that these patients benefit from anti-androgen therapy (Barton et al., 2016). The development of new targeted treatments for triple negative breast cancers is an unmet clinical need.

1.1.5 **Molecular Subtypes of Invasive Breast Cancer**

With the development of gene profiling technologies, six molecular subtypes of invasive breast carcinoma have been identified with varying outlooks, treatments options and overall rate of survival (Perou et al., 2000, Prat and Perou, 2010, Yersal and Barutca, 2014). These classifications were deemed as: luminal-A, luminal-B, HER2 enriched, normal breast-like, basal-like and claudin-low (Table 1). It should be noted that, there is some disagreement over the existence of normal-like breast cancers; some researchers have stated that this classification is actually an artefact due to high contamination of normal tissue in tumour samples (Weigelt et al., 2010). The characterisation of breast carcinomas into molecular subtypes improves the definition of prognostic signatures and tumour specific treatments.

Table 1. Molecular taxonomy of invasive breast cancer and their characteristics (Malhotra et al., 2010)

Subtype	Prevalence	Molecular profile	Prognosis
Luminal-A	~40%	ER^{high}, $HER2^{low}$	Good prognosis.
Luminal-B	~20%	ER^{low}, $HER2^{low}$, high proliferation	Favourable prognosis
HER2 enriched	10-15%	$HER2^{high}$, ER/PR^{-}	Poor prognosis
Normal like	8%	Increased adipose gene signature, ER^{-}, PR^{-}, $HER2^{-}$,	Poor prognosis
Basal-like	15-20%	ER^{-}, PR^{-}, $HER2^{-}$, cytokeratin5/14^{+}, laminin^{+}, $EGFR^{+}$	Poor prognosis
Claudin-Low	12-14%	ER^{-}, Claudins 3/4/7^{low}, vimentin^{+}, E-cadherin^{low}, occludins^{low}, $Zeb1^{+}$	Poor prognosis

1.1.6 **Metastatic Breast Cancer**

The vast majority of deaths from breast cancer are not due to the primary tumour but to the development of metastasis at distal sites in the body. Around 10-15% of breast cancer patients develop metastases within 3 years of initial disease detection (Weigelt et al., 2005). Furthermore, it is not uncommon for patients to develop secondary metastases 10 or more years after initial diagnoses (Weigelt et al., 2005). Breast cancer metastases have been recorded in all organs of the body with secondary tumours developing concomitantly at multiple locations. Breast cancers appear to preferentially metastasise to bone followed by the liver, pleura, lung, adrenal glands and brain (Coleman and Rubens, 1987). Many breast cancer patients will always be at risk of secondary cancers, thus it is necessary to identify targets within the tumour and the new niche that drive metastasis in order to develop new potential therapies.

1.1.7 **The Metastatic Process**

The idea that cancers spread to specific secondary sites has been around since the turn of the 19^{th} century, in which Stephen Paget suggested the 'seed and soil 'hypothesis (Paget, 1989). This hypothesis denotes that in certain cancers, the seeds, are primed to metastasise to particular organs, the soil, due to their 'fertile' conditions that permit them to proliferate.

Progression to metastasis and the subsequent development of secondary tumours can be considered as a stepwise set of events (Nguyen et al., 2009). Genomic instability in cancer cells may lead to the expression of gene sets that ensure metastatic competence of certain cells and progression through the metastatic steps: invasion of local tissues; intravasation and survival in the circulation; extravasation of the circulation followed by organ-specific colonisation (Figure 2).

Metastasis initiating genes are those that facilitate cell motility and extracellular matrix degradation, epithelial-to-mesenchymal transition (EMT – the process by

which cells change from a epithelial-like cell to an invasive mesenchymal-like cell) and evasion of the immune system (Nguyen and Massagué, 2007). For example, in breast carcinoma gain of metadherin and N-cadherin, induce EMT and thus enhances invasion (Li et al., 2011). Metastasis progression genes enable extravasation and aid survival in a new niche. Examples of such in breast cancer include COX2, LOX, MMP1, and epiregulin (Gupta et al., 2007). The third class of metastatic genes has been deemed metastatic virulence genes (Nguyen and Massagué, 2007). These types of genes provide disseminated cancer cells with the ability to colonize specific organs. Additionally recent evidence suggests that tumour derived exosomes, 30-50nm membranous vesicles that contain protein, RNA, DNA and lipids are able to prime the metastatic niche and determine organotropism of cancers. Hoshino and colleagues (2015) demonstrated that exosomes from cancer cells with specific organotropism were specifically taken up by cells in their respective preferential secondary sites. Furthermore, they showed that pretreatment of mice with exosomes could redirect cancer cells to organs that they were unable to previously colonise. In addition, it was established that exosomal expression of integrins facilitated their organotropism, as knockdown of integrin β4 reduced lung metastasis of cancer cells. Exosomes once in the metastatic niche activated the Src-S100 pathway to induce an inflammatory environment and promote metastasis (Hoshino et al., 2015).

Following a period of latency, in which cancer cells survive, often undetected as single cells or micrometastases, in the new niche, the disseminated tumour cells reacquire an aggressive proliferative phenotype and reinitiate growth such that clinically detectable metastases are visible (Nguyen et al., 2009). In addition, it is often the case that metastatic disease is associated with resistance to therapeutics and increased morbidity.

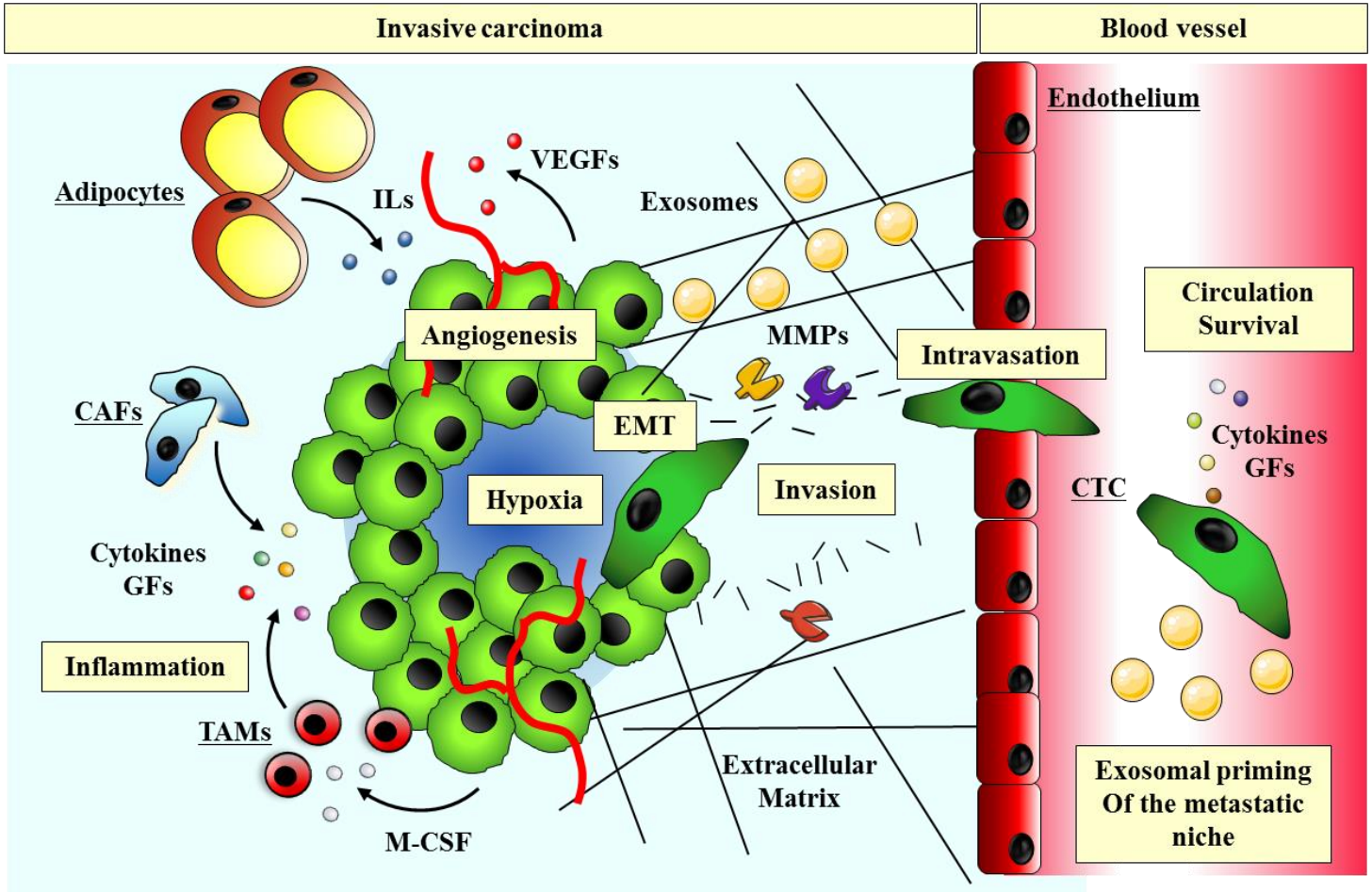

Figure 2. Schematic diagram of tumourigenesis and the metastatic process.

Cancer cells gain a proliferative advantage over healthy cells. Enhanced proliferation leads to growth of primary tumour Hypoxia and inflammation induce cytokine production and angiogenesis. Gain of metastasis initiating genes leads to EMT and increase invasive capacity. Invasion is promoted by cytokines and facilitated by ECM remodelling proteins. Release of exosomes from the primary tumour promote organotropism. Circulating tumour cells (CTCs) survive in the vasculature through expression of metastasis progression gene sets. Upon arrival and arrest in the vasculature of the secondary organ. CTCs may undergo a period of dormancy and upon reactivation and the expression of metastasis virulence genes colonize the secondary organs. See text in section 1.1.7.

1.1.8 **Patterns of breast cancer metastasis**

Breast cancers with particular molecular patterns have characteristic sites to which they metastasise. Characteristics that have been shown to affect the pattern of disseminated disease include hormone receptor status, tumour grade and histological type. A lower histological grade has been associated with the increased frequency of pleural metastatic lesions, whereas a higher grade is associated with a shorter metastasis-free survival and lesions in the lung and liver. In addition, it has been shown that different subgroups of breast cancer have different patterns of spread (Wu et al., 2017)(Figure 3). ER+ disease (Luminal A/B) have the highest skeletal involvement (A – 58.52%, B- 47.28%) and the lowest brain involvement (A - 4.30%; B - 5.89%). HER2-enriched tumours metastasise more frequently to the skeleton and the liver (34.49% and 31.72%) followed by lung and brain (25.48% and 8.31%). Triple negative breast cancers metastasise commonly to bone followed by lung and liver (36.39%, 32.09% and 22.40%). TNBCs also have the highest proportion of breast cancer patients developing brain metastases at 9.12% (Wu et al., 2017).

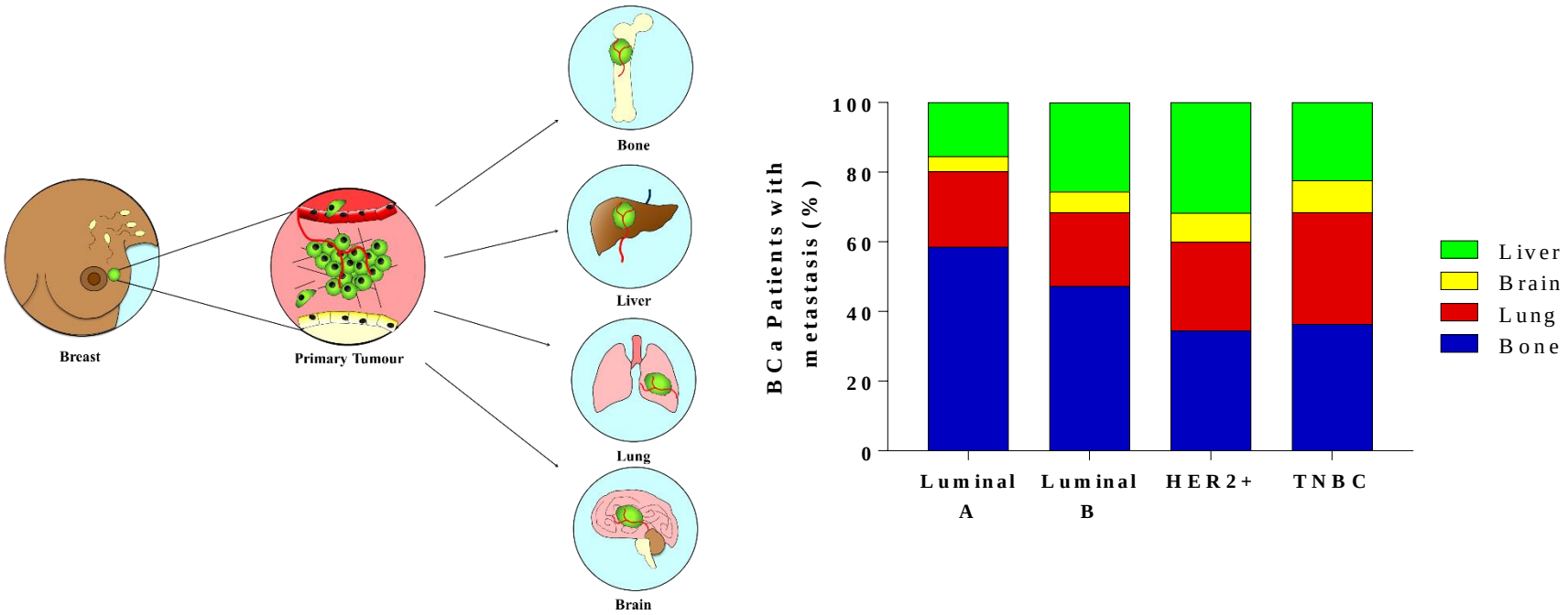

Figure 3. Patterns of breast cancer metastatic dissemination.

Localised primary breast cancer has a favourable prognosis if caught at an early stage. However, breast cancer cells can enter the circulatory or the lymphatic systems and metastasise to the lymph nodes (yellow nodes) Breast cancers also metastasise to distant sites, primarily bone, liver, lung and brain, which, at this stage is incurable. Breast cancers frequently metastasise to the bone. This is more commonly associated with ER+ disease. TNBCs more frequently metastasise to lung followed by bone. Data taken from (Wu et al., 2017).

1.2 Bone

The skeleton has a multitude of functions in vertebrates, which includes: acting as a scaffold for muscles; protection for organs and marrow; storage and release of ions and growth factors from its matrix; and regulation and release of haematopoietic cells. The skeleton is a dynamic organ that is constantly broken down and replaced by the cells of the bone. Many of the cells in the bone are derived from either mesenchymal or haemopoeitic progenitor cells. The mesenchymal progenitors can give rise to osteoblasts, chondrocytes, adipocytes, myocytes and endothelial cells. The osteoclast is formed following the fusion of bone marrow resident macrophages and are derived from myeloid progenitor cells of the haematopoietic lineage (Figure 4).

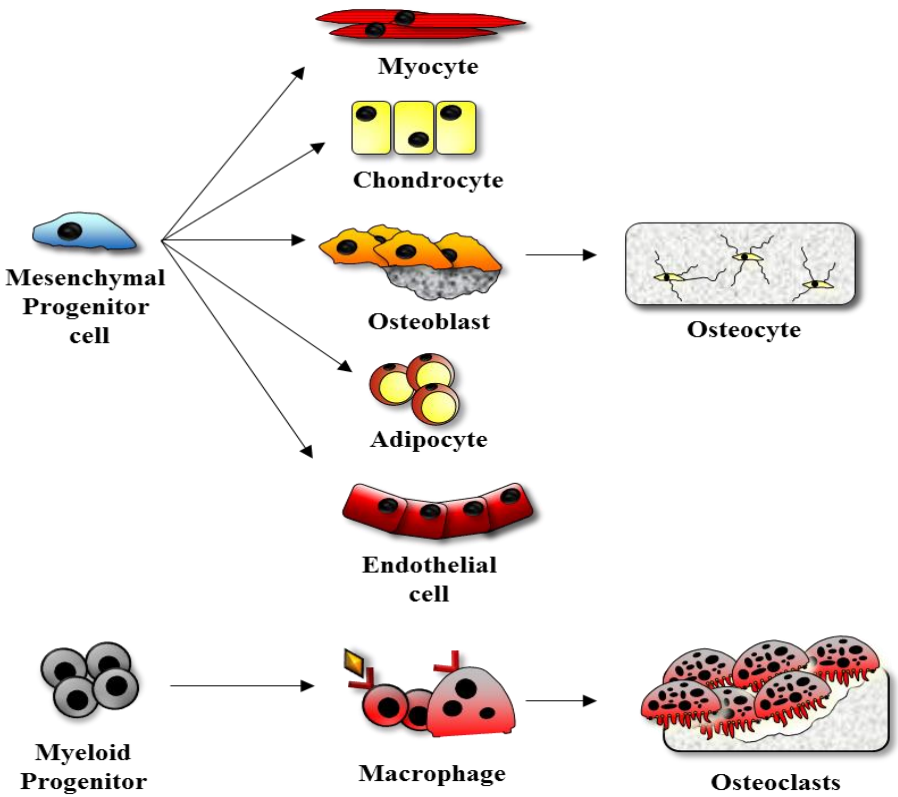

Figure 4. Cells of the bone and their lineage.

Mesenchymal progenitor cells differentiate into various cells including myocytes, chondrocytes, adipocytes, endothelial cells and osteoblasts. Osteoblasts, the bone forming cells, lay down osteoid and then can become embedded in the bone matrix and become osteocytes. Osteoclasts, the cells that remove bone, are formed following the fusion of macrophage precursors of myeloid lineage. See section 1.2 for details.

1.2.1 **Bone remodelling**

Much of the adult skeleton is covered by quiescent bone lining cells. These cells lie over a layer of mineralised and generally quiescent bone. Following micro-damage or mechanical stress, osteoclast precursors and mature osteoclasts travel to the area where resorption is required. This process of bone remodelling serves to remove and replace old or damaged bone in the adult skeleton. Bone resorption phase has a median duration of 30 days whereas bone formation last for up to 3 months (Eriksen, 2010).

This process is initiated by the removal of old/damaged bone by mature resorbing osteoclasts. Mature osteoblasts migrate to these resorption pits and lay down layers of unmineralised bone, known as osteoid, after around seven days this matrix becomes mineralised following the influence of Vitamin D-3 and other factors. A fraction of these osteoblasts become implanted within the osteoid matrix and remain there as osteocytes. Osteocytes have dendritic extensions on their surface, which interconnect through channels within the bone. Through these connections, the osteocytes/osteoblasts sense mechanical strains, which regulates bone remodelling.

1.2.1.1 Bone resorption

The initial phase of the bone remodelling cycle involves a multitude of cells in the bone marrow including osteocytes, osteoblasts and lining cells. (Hadjidakis and Androulakis, 2006). Many researchers have suggested that osteocytes embedded within the mineralised matrix instruct osteoblasts and lining cells to secrete MMPs, collagenases and gelatinases that in turn break down the mineralised layer, thereby facilitating the migration of osteoclasts and their precursors to the remodelling site. (Lerner, 2000; Suda et al., 1997; Manolagas, 2000; Troen, 2003). In addition, osteoclast precursors are drawn to the site of resorption by bone-derived factors such as TGFβ, type-1 collagen and osteocalcin (Suda et al., 1997).

The proliferation of osteoclast precursors and their subsequent fusion into multinucleated active osteoclasts is controlled by the main osteoclastic factors, RANKL and MCSF (Weir et al., 1993; Sarma and Flanagan, 1996; Morohashi et al., 1994 and the decoy RANKL receptor, osteoprotegerin (OPG), produced by osteocyte sand osteoblasts and lining cells (Nakashima et al., 2011 Proff and Romer, 2009; Boyce and Xing, 2008, Hsu et al., 1999).

In response to these factors, osteoclasts utilise proteins of the integrin superfamily, specifically the $\alpha_V\beta_3$ vitronectin receptor to attach to proteins such as vitronection, collagen type I and fibronectin exposed on the mineralised bone surface (Lakkakorpi et al., 1991). Following adhesion to the extracellular matrix of the bone, the osteoclast membrane becomes polarised in order to form specialised organelles known as podosomes. This allows the formation of an actin ring (Lakkakorpi et al., 1991; Hill, 1998).The structure of the actin ring allows for an intimate binding of the active osteoclast to the surface of the bone, surrounding an isolated region of bone called Howship's lacuna or the sealing zone (Roodman, 1996). Inside the sealing zone, the ruffled border of the osteoclast allows for the secretion of protons and chloride ions (Teti et al., 1989; Schaller et al., 2005). This creates a localised low pH environment which aids the demineralisation and degradation of the bone matrix. Hydroxyapatite crystals are then converted in to Ca^{2+}, HPO_4^{2-} and water in the process (Bar-Shavit, 2007). Subsequently, the organic bone matrix is exposed, which is degraded following the release of vesicles containing cathepsin K, active at low pH, which digest collagen type I, thus removing the organic component of bone (Teitelbaum, 2000; Blair et al., 1989;(Garnero et al., 1998). Additionally, MMP9 removes organic bone matrix outside the acidic ruffled border (Everts et al., 1992). Once degraded, the organic and inorganic components of the bone are endocytosed at the ruffled border membrane, transported through the cell in vesicles and then secreted in to the extracellular space (Vaananen and Laitala-Leinonen, 2008). Once the bone resorption process is complete, osteoclasts undergo apoptosis and are subsequently and readily removed by phagocytes. (Hill, 1998).

1.2.1.2 Bone formation

In the latter stage of the bone remodeling cycle, osteoblast precursors are recruited to the site of resorption in which new bone is deposited. The release of chemotactic agents, such as osteocalcin (OCN), TGF-β, IGF-1 and collagen type I are released from the bone matrix during resorption which promotes the migration of pre-osteoblasts to the site of resorption. (Mundy et al., 1982, Lerner, 2006). On arrival at the resorbed site, the osteoblast progenitors proliferate and differentiate in to mature osteoblasts. The maturation process is also mediated by bone-derived factors released during resorption including IGF-1 and 2, FGFs, TGFβ, Bone morphogenic protein 2 (BMP2), and platelet-derived growth factors (PDGFs) (Hill, 1998). Mature osteoblasts produce collagen type I along with OCN, osteopontin (OPN), bone sialoprotein (BSP), osteonectin (OSN) and proteoglycans which collectively form the unmineralised bone matrix known as osteoid (Ducy, 2000; Mackie, 2003; Katagiri and Takahashi, 2002). Alkaline phosphatase (ALP), is also produced and secreted by osteoblasts, which functions to degrade proteins such as pyrophosphate that inhibit mineralisation. In addition to these factors, osteoblasts also release matrix vesicles at sites within the osteoid. Matrix vesicles are membrane bodies which contain proteins, acidic phospholipids, phosphate and calcium that prompt the formation of hydroxyapatite crystals. One such highly phosphorylated protein that regulates the formation of hydroxyapatite is BSP. Expression of BSP is limited to actively mineralising bone and has been shown to nucleate hydroxyapatite crystals at nano-molar concentration under steady-state conditions (Hunter and Goldberg, 1993, Tye et al., 2003). Deposition of hydroxyapatite induces the conversions of osteoid into mineralised matrix, thus ensuring bones rigidity and strength (Katagiri and Takahashi, 2002; Murray J.Favus, 2006).

Currently, the mechanisms by which bone deposition is terminated are not fully understood. Thus far two mechanisms have been hypothesised. One postulated mechanism involves the release of sclerostin (SOST) by osteocytes. SOST is a negative regulator of bone formation. It inhibits osteoblast activity whilst also inducing the transition of osteoblasts in to quiescent lining cells (Sutherland et

al., 2004). A second mechanism may be that bone deposition is terminated following the osteoblasts apoptosis initiated by bone-derived factors. In humans the bone formation phase lasts around three months and ends with up to 65% of osteoblasts undergoing apoptosis (Jilka et al., 1998).

The remaining osteoblasts are either converted in to lining cells that cover the majority of the quiescent bone or they become buried within the new bone matrix and become osteocytes (Murray J.Favus, 2006).

1.2.2 **Metastasis to Bone**

Approximately, 70% of all advanced breast cancer cases develop metastases in one or more bone sites (Manders et al., 2006) . Breast cancer bone metastases are coupled with osteolysis (breakdown of the bone), bone pain, fragility, hypercalcaemia and deformity (Guise, 2000). The osseous microenvironment provides a unique setting in which a plethora of cell types from multiple lineages exist. The bone contains cells of a mesenchymal lineage; chondrocytes, endothelial cells, adipocytes osteoblasts and osteocytes, in addition to cells of the haemopoeitic lineage such as macrophages, osteoclasts, T- and B-cells and also cells of a vascular nature such as pericytes and endosteal cells (Krzeszinski and Wan, 2015). Cancer cells influence cells of the bone in two main ways (Yin et al., 2005). Arrival of cancer cells within the bone leads to the formation of osteolytic lesions following an increase in the formation and activity of osteoclasts, resulting in bone resorption. In normal physiological conditions, there is no net difference in bone formation and bone resorption. However, in osteolytic bone metastases, increased cancer cell induced-osteoclastic bone resorption exceeds inherent bone remodelling by osteoblasts resulting in the loss of mineralised tissue (Krzeszinski and Wan, 2015). Comparatively, cancer cells can also enhance the bone forming abilities of osteoblasts culminating in osteoblastic metastatic lesions. These lesions, although occuring through the enhanced formation of bone and are weak, due to the disorganised bone growth, which leads to fracture development. The

development of osteolytic or osteoblastic metastases is not mutually exclusive and individuals with bone metastases may possess both.

1.2.2.1 Tumour cell dormancy

Dissemination of tumour cells to the bone microenvironment is believed to occur early in the metastatic process (Braun et al., 2000). Disseminated tumour cells (DTCs) compete with haematopoietic stem cells (HSCs) to adhere to the endosteal niche (Shiozawa et al., 2011), the perivascular niche or the HSC niche . DTCs have been shown to remain in the bone marrow for years and even decades (Braun et al., 2000). Evidence suggests DTCs remain in the pre-metastatic niche in a dormant quiescent state resistant to cytotoxic therapies (Shiozawa et al., 2010).

1.2.2.2 Osteolytic Metastases

Tumour cells that have colonised the bone induce the formation of osteolytic lesions through the secretion of factors that act directly on osteoclasts and their precursors or indirectly on osteoblasts to enhance osteoclastogenesis and later activity. These factors include a plethora of cytokines including ILs, TNFα, MCS-F, VEGF, MMPs, IGF-1, TGF-β and parathyroid hormone related protein (PTHrP)(Ibrahim et al., 2010; Rose and Siegel, 2006). A number of these secreted factors induce osteoclast formation directly by stimulating osteoclast precursors and mature resorbing osteoclasts (e.g. TNFα and MCS-F) whilst others act on osteoblasts to enhance the production of RANKL and other osteoclastic cytokines and reduce the production of factors that inhibit osteoclast formation (Thomas et al., 1999; Ohshiba et al., 2003 IL-1, IL-8, IL-11, TNFα and M-CSF all directly promote osteoclast differentiation, function and survival whereas other factors such as IL-1, IL-6 and TGFβ indirectly induce osteoclast formation by stimulating the release of factors such as PTHrP and (PGE) that enhance RANKL production by osteoblasts (Guise, 2002). PTHrP is a highly studied secreted factor and has been demonstrated to induce osteolysis by increasing the production of RANKL by osteoblasts whilst simultaneously reducing the production of OPG (Thomas et al., 1999; Karaplis and Goltzman, 2000).

Arrival of malignant cancer cells, disturbs the normal bone remodelling process and ultimately leads to osteolysis and bone loss. As a consequence of the increased bone resorption stored growth factors such as IGFs, TGF-β and BMPs are freed from the bone matrix into the tumour-bone microenvironment. These factors act on the tumour cells to enhance survival, proliferation and migration (Guise et al., 2006). The high levels of extracellular calcium, coupled with the hospitable acidic local environment stimulate the growth of tumour cells through activation of the MAP kinase pathways (Guise et al., 2006) and augment the cancer cell production and secretion of PTHrP. Additionally, the reduction in trabecular bone enhances tumour burden by providing the tumour cells the space to grow (Guise et al., 2006).

Collectively, the vicious cycle involves the tumour cells entering the bone microenvironment and after a period of dormancy, perturbing the balance of bone remodelling, in favour of destruction of the bone (Figure 5). The enhanced bone resorption releases factors stored within the bone matrix and induces the proliferation of the tumour cells. Ultimately, the growth of the tumour cells leads to more osteoclast formation and destruction of the bone until progressively more and more bone is lost and the tumour burden worsens. The observation that breast carcinomas are highly bone tropic and osteolytic in nature is well documented, thus it is necessary to identify cancer-specific drivers of metastases in order to significantly reduce the development of metastatic disease.

1.2.2.3 Osteoblastic bone metastasis

Osteoblastic lesions are induced by the excessive stimulation of osteoblast activity that culminates in the formation of disorganized and weak new bone (Guise et al., 2006). Many osteoblastic bone metastases have areas of both osteoblastic and osteolytic lesions with recent evidence from the clinic indicating that both processes contribute to the phenotype in the same patient (Mundy, 2002; Keller and Brown, 2004). Osteoblasts produce the main osteoclastic cytokines RANKL and MCSF and a significant increase in the number of mature osteoblasts leads to an increase in osteoclast number with a

resulting increase in bone resorption with bone formation. The development and regulation of bone is modulated by a number of complex endocrine and paracrine factors such as urokinase plasminogen activator (uPA), Wnt signalling factors and endothelin-1 (ET-1). These factors are involved in the regulation of osteoblasts by modulating their proliferation, differentiation and activity. These same factors that regulate normal bone physiology are also involved in the development of osteoblastic lesions (Guise et al., 2006; Mundy, 2002; Logothetis and Lin, 2005). Cancer cells that metastasise to bone produce these factors that directly stimulate the proliferation and enhanced activity of osteoblasts or these cancer cells can indirectly influence bone formation by modifying the bone matrix and microenvironment.

ET-1 and IGF-1 are two heavily studied factors in the process of osteoblastic metastases. Both of which are known to directly stimulate the proliferation and function of osteoblasts. Additionally ET-1 has been shown to reduce osteoblast apoptosis (Van et al., 2007). The exact mechanisms through which ET-1 stimulates bone formation is unknown, however, some studies have shown ET-1 leads to the nuclear translocation of the pro-survival factor NFATc1 (Van Sant et al., 2007). Moreover, ET-1 has previously shown to both reduce osteoclast formation and motility (Alam et al., 1992). BMPs and TGF-β directly stimulate osteoblast activity, whilst uPA activates TGF-β and IGF-1 release from IGF binding proteins ultimately stimulates osteoblasts activity (Guise et al., 2006; Guise, 2002; Papachristou et al., 2012). IGF-1 has been shown to stimulate both the MAPK and PI3K/AKT signalling pathways in osteoblasts and increase the expression of RUNX2, the master regulator of osteoblastogenesis, in osteoblast precursors. Selective inhibition of the IGF-1 receptor with the pharmacological inhibitor, PQIP was shown to reduce RANKL/OPG ratio in IGF-1 stimulated osteoblasts, prevent their ability to induce osteoclast formation and also reduced breast cancer induced osteolysis *in vivo* (Logan et al., 2013). Additionally, tumour derived VEGF has been shown to promote osteoblast activity and osteoblastic lesions (Dai et al., 2004). Furthermore, recent phase III clinical trials indicate that inhibition of VEGFR2 and c-Met with the dual inhibitor cabozantinib modestly improved overall

survival in previously treated metastatic prostate cancer patients (Pond et al., 2018).

Overall, the effect of cancer-induced osteoblast activity results in enhanced bone formation and osteoclastic bone resorption. Tumour and osteoblast released factors such as RANKL enhance osteoclast bone resorption and in turn cytokines and bone-derived factors in the osteolytic lesions enhance tumour growth further enhancing the vicious cycle (Ibrahim et al., 2010) .

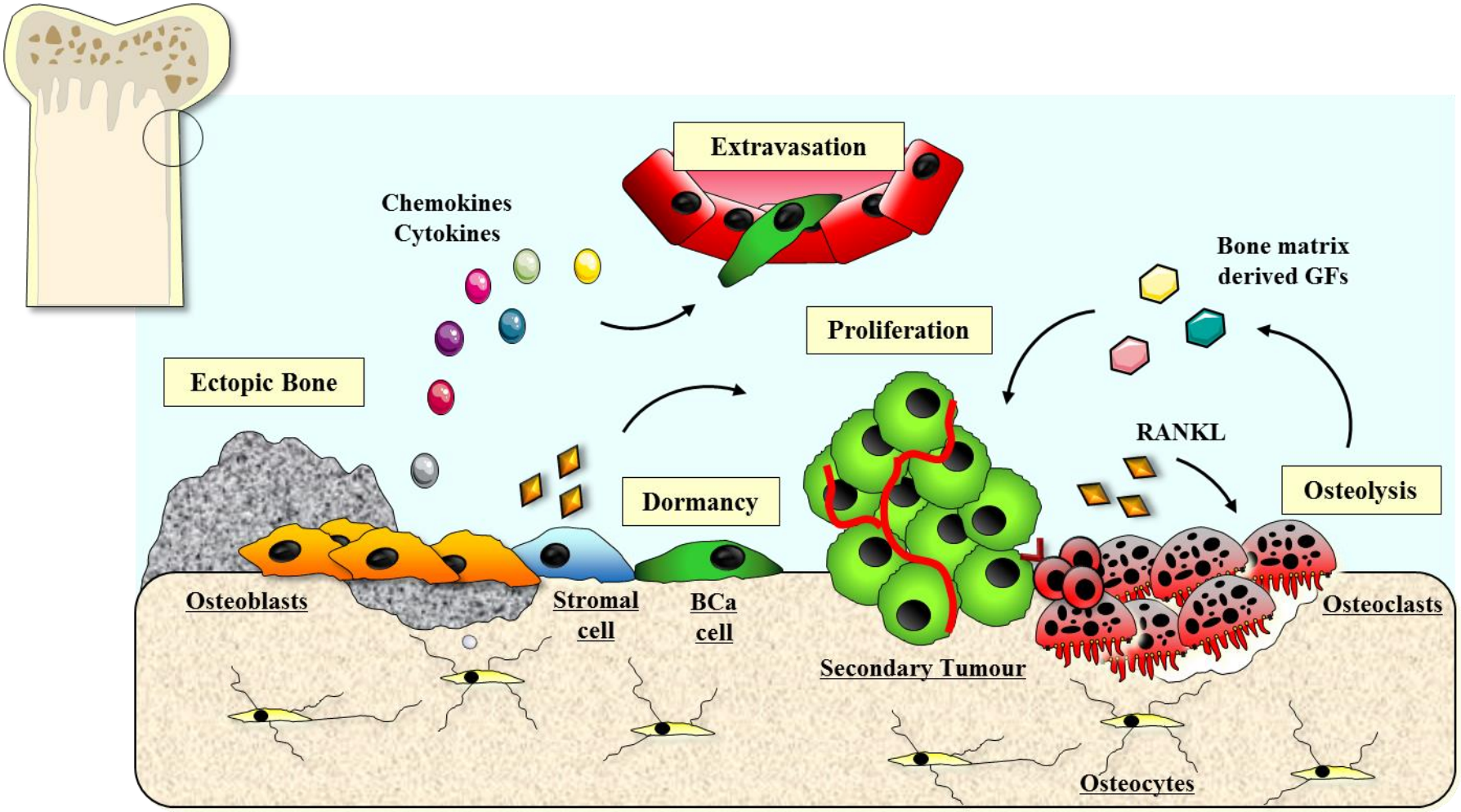

Figure 5. The bone metastatic process.

Diagram of the bone metastatic process and vicious cycle. Colonisation of the bone by disseminated tumour cells follows a period of dormancy. Upon reactivation, tumour cells secrete factors that influence osteoblasts to produce weak ectopic bone and RANKL which stimulates osteoclast formation and osteolysis. Growth factors in the bone lead to tumour cell proliferation. See section 1.2.2 for details.

1.3 IKKε

Inhibitor of nuclear factor kappa-B kinase subunit epsilon, also known as IκB kinase epsilon, IKKε or IKK-inducible (IKK-i), is a protein encoded by the gene *IKBKE*. Through an integrative genomics approach that utilised RNA interference (RNAi) screens, overexpression screens and comparative genomics, *IKBKE* was identified as a breast cancer oncogene (Boehm et al., 2007). It was demonstrated that *IKBKE* is overexpressed and amplified in 16.3% of breast cancer cell lines and in 30% of breast cancer patient samples. In addition, they showed that IKKε-transformed breast epithelial cells into tumour cells and up-regulated NFκB response genes, thus implicating the NFκB pathway in the tumourigenesis and survival of some breast carcinomas.

1.3.1 **The NFκB Pathway**

The NFκB pathway is a key regulator of many vital biological process including innate immunity, inflammation, cell proliferation and survival. These processes have been implicated in cancer development and progression, whether through aberrant cancer-intrinsic NFκB signalling activation or through deregulation of the pathway in cells of the microenvironment leading to inflammation (Hanahan and Weinberg, 2011).

The NFκB family are a group of five transcription factors consisting of RelA(p65), RelB, c-Rel, p52 (p100 precursor) and p50 (p105 precursor) reviewed extensively by (Hayden and Ghosh, 2004). The NFκB transcription factors all contain a shared Rel homology domain (RHD), which enables specific DNA binding and subsequent transcription of target genes.

In the cytosol of unstimulated cells, the NFκB transcription factors remain bound to the inhibitors of κB (IκB) proteins preventing their nuclear translocation. The IκB family consists of seven proteins with different binding affinities for NFκB proteins (Hayden and Ghosh, 2004). The seven family

members include IκBα, IκBβ, IκBε, the REL-precursory p100 and p105 proteins and the atypical IκBζ and Bcl-3. Phosphorylation of the IκB proteins on two conserved serine residues (-32 and -36) by members of the inhibitor of IκB (IKK) family results in their subsequent ubiquitin-directed proteasomal degradation. This is a prerequisite to NFκB activation (Hayden and Ghosh, 2004).

The members of the IKK family are a collection of serine/threonine kinases compromised of IKKα/IKK1, IKKβ/IKK2, IKKε/IKK-i, TANK-binding kinase-1 (TBK-1) and the regulatory IKKγ/NEMO. The distinct ways in which the IKKs are regulated by upstream proteins enable the strict control of the NFκB response by various stimuli.

1.3.2 **Canonical versus Non-Canonical NFκB Activation**

The canonical NFκB pathway involves the assembly of the classical IKK complex consisting of IKKα,β,γ. This complex phosphorylates IκB proteins leading to the release of NFκB proteins, their nuclear translocation and transcription of NFκB-related genes (Figure 6)(Hayden and Ghosh, 2004). The classical pathway is activated by numerous cytokines and through their receptors including the Toll-like receptors (TLRs), interleukin-1 receptor -1 (IL1R1) and the tumour necrosis factor-α receptor (TNFR). When these receptors are stimulated by their respective ligands, a signalling cascade ensues and converges upon the IKK complex through phosphorylation and activation of IKKβ. Adaptor proteins such as the TNFα receptor associated factors (TRAFs) and certain kinases such as TGF-β activated kinase-1 (TAK1) are brought into close proximity upon stimulation by distinct ligands leading to IKKβ phosphorylation. Once activated the IKK complex in turn phosphorylates IκBα at serine-32 and serine-36 leading to its ubiquitination and destruction by the proteasome. This allows liberation of the p65/p50 heterodimers to

translocate to the nucleus where it activates the transcription of various NFκB target genes (Hayden and Ghosh, 2004).

The non-canonical pathways are believed to be IKKγ independent. The best characterised is the activation of IKKα homodimer by a subset of receptors (Figure 6). In an unstimulated cell, NFκB inducing protein (NIK) is subject to constant proteosomal degradation. However, following stimulation, NIK is stabilised allowing it to phosphorylate the IKKα homodimer. In turn the IKKα homodimer phosphorylates p100 such that it is undergoes ubiquitin-mediate proteosomal degradation. The catalytically active p52 protein is free to translocate as a heterodimer with RelB to the nucleus and induce gene transcription (Hayden and Ghosh, 2004).

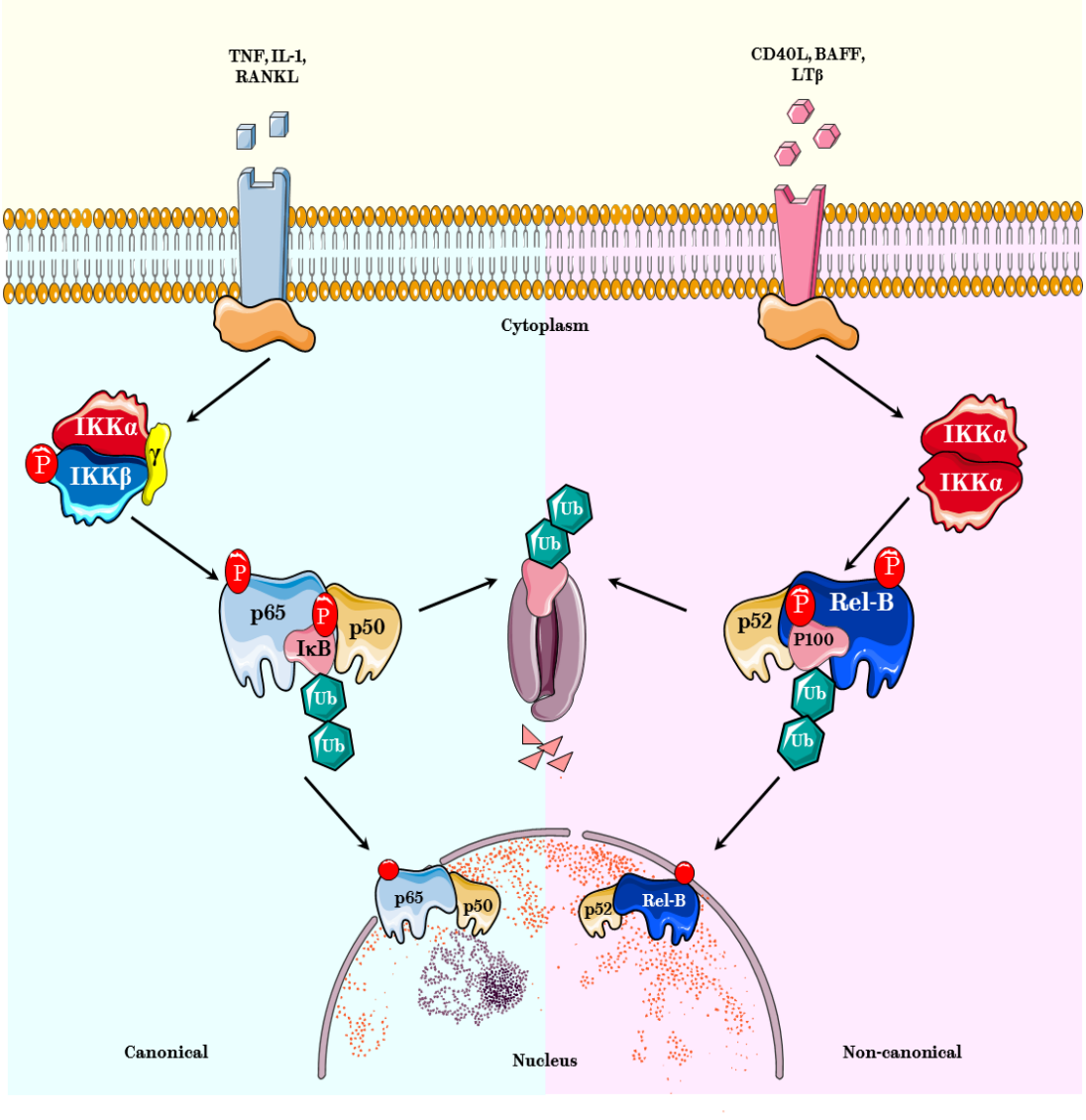

Figure 6. Canonical and non-canonical NFκB activation.

NFκB transcription factors remain catalytically inactive in the cytoplasm bound to IκB proteins. Upon stimulation IκB proteins are phosphorylated by IKK complexes and undergo lysine-48 linked ubiquitin dependent proteosomal degradation allowing NFκB proteins to translocate to the nucleus and induce gene transcription. See text for details.

1.3.3 **The IKK-related Kinases - IKKε and** TBK-1

The discovery of IKKε occurred simultaneously by two separate groups and was named IKKε and IKK-inducible (IKK-i)**.** IKKε was discovered through a database search for proteins similar to IKKα and IKKβ and was shown to activate NFκB upon stimulation of Jurkat T-cells with phorbol esters (Peters et al**.**, 2000)**.** IKK-i was discovered by Shimada and colleagues who showed IKK-i expression was induced following lipopolysaccharide stimulation of murine macrophages and its mRNA could be induced by other proinflammatory signals including TNFα, IL-1, IL-6 and IFNγ (Shimada et al**.**, 1999)**.** TBK-1 was initially identified, through a yeast two-hybrid system, as a protein that binds to TANK (Pomerantz and Baltimore, 1999)**.** IKKε and TBK-1 share 33% and 31% kinase sequence similarity to IKKα and IKKβ, respectively, whereas they share 65% sequence similarity to one another (Clément et al**.**, 2008)**.** In addition, TBK-1 and IKKε both contain multimerisation domains allowing them to from homo-dimers and heterodimers with each other**.** In addition, TBK-1, similarly to IKKα and IKKβ, is a constitutively expressed protein and knockout of TBK-1 in mice leads to embryonic lethality due to liver apoptosis (Bonnard et al**.**, 2000)**.** However, IKKε protein is undetectable in almost all tissues and is only expressed constitutively in certain tissues such as the pancreas, thymus, spleen and also peripheral blood leukocytes (Shimada et al**.**, 1999)**.** Furthermore, IKKε deficient mice are viable, yet are hyper-susceptible to viral infection due to deficient IFN signalling (Hemmi et al., 2004, Tenoever et al., 2007)**.**

1.3.4 **The role of IKKε and TBK-1 in NFκB Signalling**

IKKε and TBK-1 were initially deemed IκB kinases through their ability to phosphorylate IκBα when overexpressed and both proteins were shown to only phosphorylate IκBα on serine 36, which is insufficient to result in IκBα degradation (Peters et al., 2000, Shimada et al., 1999). Comparatively, IKKβ phosphorylates IκBα on both serine-36 and serine-32, which leads to its subsequent degradation. Knockout of IKKε and TBK-1 of mouse embryonic fibroblasts show no inherent deficiency in IκBα degradation and NFκB activation in response to TNF and other inducers. This suggests that IKKε and TBK-1 do not activate NFκB through direct phosphorylation of IκB (Hemmi et al., 2004). Interestingly, IKKε deficient MEFs show abrogation of NFκB specific genes including *MMP2, IL6, MCP1, COX2* and *ICAM-1* suggesting that phosphorylation of p65 by IKKε is necessary for transcription of certain genes (Kravchenko et al., 2003). Studies have revealed that NFκB activation by IKKε is a result of direct phosphorylation of NFκB proteins (p65 and c-Rel). IKKε phosphorylates serine 468 and serine 536 on p65; post-translational modifications necessary for proper transcription of specific NFκB related genes (Buss et al., 2004). These modifications successively facilitate co-translocation of p65 and IKKε to the nucleus and to DNA regions that contain NFκB binding sites. Once at these sites, IKKε phosphorylates c-Jun and initiates the clearance of nuclear receptor co-repressor proteins (nCOR) allowing for transcription of c-Jun specific genes (Huang et al., 2009). It is worth noting that such c-Jun specific genes include matrix remodelling enzymes matrix metalloproteinases (MMP). Furthermore, IKKε-deficient murine fibroblast-like synoviocytes do not up-regulate production of MMP3 and MMP13 in response to classical inflammatory stimuli (Sweeney et al., 2005). IKKε and TBK-1 also phosphorylate c-Rel leading to its nuclear accumulation independently of IκBα serine-32 and serine-36

phosphorylations. However, these phosphorylation events do not suffice in potentiating c-Rel activation and subsequent induction of survival and proliferation gene expression suggesting the necessity of other post-translational modifications (Harris et al., 2006).

1.3.5 **The role of IKKε and TBK-1 in Interferon Regulatory Factor (IRF) Signalling**

The overlapping functions of NFκB proteins and innate immunity is evidenced by the role of the IKK-related proteins in IRF signalling (Figure 7) (Clément et al., 2008). The IRF transcription factors regulate the expression of type-I interferons (IFNs), important pro-inflammatory cytokines involved in the innate immune response against viral infection. IFNα and IFNβ induce growth arrest and programmed cell death in virally infected cells. Both IKKε and TBK-1 phosphorylate IRF-3, -5 and -7 in response to a number of pathogen associated molecular patterns (PAMPs) and damage-associated molecular patterns (DAMPs) including LPS, double stranded RNA (dsRNA) and cytosolic DNA through TLR-dependant pathways. Activation of PAMP and DAMP sensing TLRs by their ligands leads to the recruitment of adaptor proteins such as TNFR-associated factors 2 (TRAF2), -3 and -6 leading to recruitment of scaffold proteins. IKKε and TBK-1 form distinct complexes with TANK, NAK associated protein 1 (NAP-1) and the similar to NAP1 and TBK-1 adaptor (SINTBAD) (Chau et al., 2008). It is believed that these scaffold proteins assemble IKKε and TBK-1 as hetero- and homodimers. Dimers form in response to specific upstream signals (i.e. PAMPs and DAMPs) that in turn phosphorylate IRF3 and IRF7 on specific serine residues to stabilise and activate IRF dimers leading to nuclear translocation and transcription of IRF target genes (Figure 7). Stringent controls are in place to prevent continued IRF signalling and prolonged IFN production (Chau et al., 2008). The deubiquitinating protein, CYLD negatively regulates IRF signalling (and NFκB signalling) by deubiquitinating adaptor proteins and also IKKε and TBK-1 to

diminish their activation. A20 is a ubiquitin ligase that adds K48 linked ubiquitin to various proteins within the NFκB and IRF signalling pathways leading to their proteolytic degradation. Another example is the suppressor of IKKε (SIKE), a protein with high binding affinity for both TBK-1 and IKKε. In unstimulated cells, SIKE is found bound to TBK-1 in the cytoplasm and inhibits its interaction with IRF3 thus diminishing the IRF3 dependant response but not NFκB signalling (Huang et al., 2005).

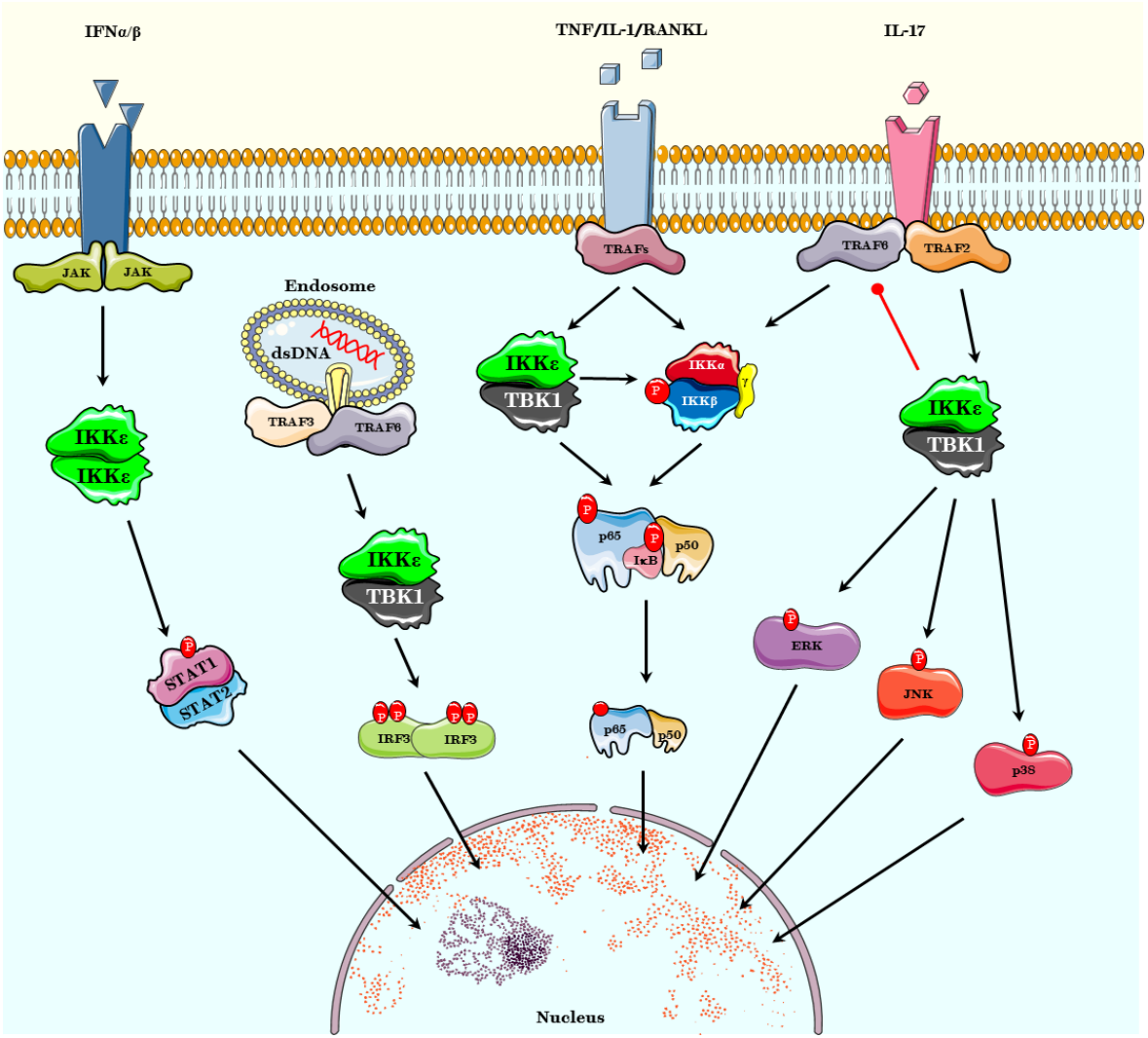

Figure 7. IKKε/TBK-1 ***signalling pathways in innate immunity.***

IKKε and TBK-1 functions as homo- and heterodimers to phosphorylate a number of adaptor proteins (TRAFs), kinases (IKKs) and transcription factors (NFκB, IRFs, STATs, p38, JNK and ERK) to maintain a pro-inflammatory and anti-viral state in response to cytokines, PAMPs and DAMPs, see text in sections 1.3.4 to 1.3.7.

1.3.6 **The role of IKKε and TBK-1 in JAK-STAT signalling**

The signal transducers and activators of transcription (STAT) proteins are important for the induction of genes involved in an anti-viral IFN-induced state. IKKε has recently been shown to phosphorylate STAT1, a protein that forms part of the IFN-stimulated gene factor 3 complex (ISGF3) with STAT2 and IRF-9. Phosphorylation of STAT-1 by IKKε allows it to form a more stable heterodimer with STAT2 and bind to target gene sequences (Figure 7) (Tenoever et al., 2007).

1.3.7 **The role of IKKε and TBK-1 in IL-17 Signalling**

IL-17 is an inflammatory cytokine produced by a subset of T-cells, immune cells and cancer cells including breast cancer which induces the activation of a variety of transcription factors leading to transcription and production of proinflammatory cytokines, MMPs and vascular endothelial growth factor (VEGF) (Welte and Zhang, 2015). Upon IL-17 binding to its receptor, NFκB activator 1 (Act-1) is recruited and forms a complex with TRAF6 leading to NFκB activation via the canonical pathway. At the same time, IKKε and/or TBK-1 are recruited to IL-17R where it phosphorylates Act1 inducing a conformational change (Figure 7). This change decreases its binding affinity to TRAF6 and increases its affinity to a TRAF2/5 complex leading to activation of p38, JNK, and ERK transcription factors and inflammatory chemokine expression (Bulek et al., 2011)

1.4 The role of IKKε in Breast Cancer

The association between IKKε and cancer was first established by Eddy and colleagues who implicated IKKε overexpression in primary human breast cancer samples, breast cancer cell lines as well as mouse tumours of the breast. In addition it was shown that expression of casein kinase 2 (CK2), a member of the Wnt signalling pathway, in numerous cell lines induced expression of IKKε whilst inhibition of CK2 reduced IKKε in mammary carcinoma cell lines (Eddy et al., 2005). Following these observations, Adli and Baldwin reported that IKKε is expressed in several breast and prostate cancer cell lines. Moreover, IKKε was found to be involved in basal and constitutive phosphorylation of p65 at serine 536. This posttranslational modification is necessary for increasing p65 transactivation potential (binding to other transcription factors in the nucleus) and continued activity. Importantly, it was shown that phosphorylation of IKKε was constitutive and independent of cytokines (Adli and Baldwin, 2006)

Compounding on previous work Boehm *et al.* described IKKε as a breast cancer oncogene, a gene whose product drives cellular transformation, through multiple functional genomic approaches (Boehm et al., 2007). The first approach analysed kinases that (A) replaced either activated MEK or AKT and (B) drove cellular transformation of human epithelial cells as indicated by tumour formation in nude mice and *in vitro* by an anchorage independent growth assay. IKKε was one of four such kinases with transforming potential upon overexpression. Secondly, Boehm and colleagues used RNAi screens to knockdown expression of select kinases and found that IKKε was necessary for the growth and survival of several breast cancer cell lines such as ZR-75-1 cells. However, both IKKε and TBK-1 were required for MCF-7 viability, perhaps suggesting a level of redundancy between the two kinases. Lastly, they looked at expression of IKKε in 49 breast cancer cell lines and 30 primary breast

tumours and showed *IKBKE* was amplified in 16% and 30% respectively but found no correlation with ER or HER2 status. Immunohistochemistry of primary tumours also revealed nuclear localisation of c-Rel in 100% of tumours with *IKBKE* amplification. These results were the first to show the oncogenic potential of IKKε, whose overexpression lead to increase expression of NFκB target genes such as *MMP9* and *BCL3*. Importantly, these studies also demonstrated that knockdown of IRF3 and IRF7 did not suppress IKKε transforming capabilities thus further implicating the NFκB signalling pathway in breast cancer oncogenesis.

More recently, additional; mechanisms for IKKε oncogenic abilities have been elucidated (Figure 8). It was found that IKKε phosphorylates the cylindramatosis tumour suppressor (CYLD) (Hutti et al., 2009). CYLD possesses a deubiquitinating function that removes lysine-63 linked ubiquitin chains important for the activation of various adaptor proteins in the NFκB signalling pathway. Phosphorylation of CYLD precludes its ability to deubiquinate and inactivate its targets, leading to continued NFκB activation and increased basal activation (Hutti et al., 2009). Moreover, it was demonstrated that IKKε directly phosphorylates various other proteins involved in the activation of NFκB activation including Akt (independent of PI3K) and TRAF2 (Guo et al., 2011, Shen et al., 2012). TRAF2 is an E3-ubiquitin ligase that adds lysine-63 linked ubiquitin chains to other proteins thereby leading to NFκB activation (Shen et al., 2012). Zhou et al showed that IKKε is itself ubiquitinated by the TRAF2 containing complex, cIAP1/cIAP2/TRAF2. This complex adds lysine-68 linked ubiquitin chains to IKKε, which was shown to be vital for its NFκB dependent transforming capabilities (Zhou et al., 2013). Furthermore, stimulation of breast cancer cells with TNFα or IL-1β increased IKKε expression above basal levels, therefore further implying a role for inflammation and proinflammatory cytokines produced by cells of the stroma in cancer progression (Zhou et al., 2013). Guo and colleagues identified an

additional mechanism through which IKKε executes its oncogenic effect that involves the inhibition of transcription factor forkhead box O3 (FOXO3). FOXO3 functions to up-regulate genes involved in apoptosis and down-regulation of anti-apoptotic genes. Phosphorylation of FOXO3 by IKKε on serine-644 leads to abrogation of FOXO3 gene transcription thus reducing apoptosis of transformed cells (Guo et al., 2013). Most recently, Mukawere and colleagues investigated the role of oxidative stress on IKKε. It was shown that treatment of breast cancer cell lines with redox modulating dyes or silencing of NOX2, a superoxide-generating enzyme, inhibited IKKε expression and reduced the viability of breast cancer cells (Figure 8).

Constitutive STAT-1 activation has also been documented in both primary breast cancer samples and cell lines (Watson, 2001). On the one hand, STAT-1 has previously been deemed to act as a tumour suppressor within cancer cells due to increased death receptor and caspase transcription. However, recent studies have indicated that TNF-α can stimulate macrophages to release low levels of IFN-β, which activates STAT-1 to enhance pro-inflammatory cytokine production, thus amplifying tumour associated inflammation (Yarilina et al., 2008). Furthermore, as IKKε directly phosphorylates STAT-1 (Figure 8), IKKε overexpression may increase and prolong STAT-1 activity enhancing tumour-associated inflammation and early cancer progression (Clément et al., 2008).

Finally, IKKε has been implicated in increased resistance to chemotherapies and genotoxic stress in both breast and ovarian cancer. IKKε was shown to be up-regulated in metastatic ovarian cancer and facilitated resistance to cis-platin, the mainstay drug treatment for ovarian cancer (Hsu et al., 2012, Guo et al., 2009). Comparatively in breast cancer, IKKε expression was shown to contribute to resistance to the estrogen antagonist, tamoxifen (Figure 8). In breast cancer cells overexpression of IKKε resulted in increased resistance to tamoxifen whereas IKKε knockdown cells displayed sensitisation. Furthermore, IKKε was shown to phosphorylate estrogen receptor-α (ERα) on

serine-167 resulting in its transactivation and up-regulation of cyclin-D1, one such major target gene of ERα that drives cell cycle progression (Guo et al., 2010, Arnold and Papanikolaou, 2005). It has also become clear that IKKε serves to protect against DNA damage-induced cell death by a mechanism dependant on IKKε nuclear translocation and association with promyelotic leukaemia tumour suppressor (PML)(Renner et al., 2010). IKKε-dependent phosphorylation of PML is essential for IKKε nuclear retention. Once in the nucleus, IKKε undergoes SUMOylation, by topoisomerase I-binding arginine serine-rich protein (TOPORS). This post-translational modification necessitates IKKε ability to phosphorylate nuclear p65 at serine-468 and induce anti-apoptotic gene expression thus potentiating cell survival. Collectively, these findings signify additional NFκB-dependent and NFκB-independent mechanisms through which IKKε maintains its oncogenic effects in transformed cells and identify IKKε as a potential target in prevention of chemoresistant tumours (Figure 8).

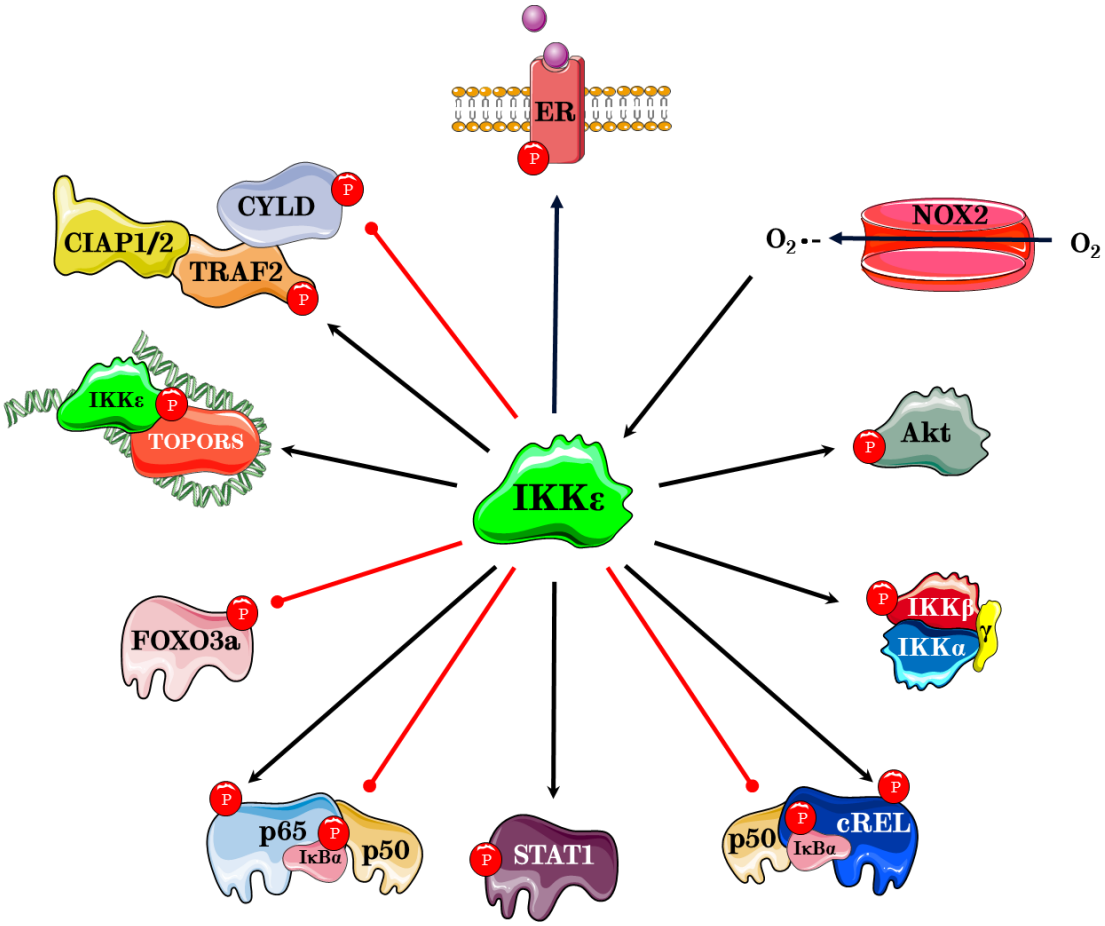

Figure 8. Existing mechanisms of IKKε oncogenic activity.

Overexpression of IKKε, linked to gene amplification and superoxide production leads to a variety of oncogenic activity. See text in section 1.4 for detailed description.

1.5 The role of IKKε in Bone Metastasis

Breast cancers preferentially colonise the skeleton (Coleman and Rubens, 1987) Previous work in our lab has demonstrated that IKKβ expression in breast cancer cells increases bone metastasis and osteolysis, however IKKε is the only member of the NFκB family to have been shown to be a breast cancer oncogene Several studies have demonstrated the role of NFκB activation in tumour growth and metastases. In breast cancer, NFκB (p65—50) activation leads to production of CXCR4, which enhances motility and subsequent homing to bone. (Helbig et al., 2003). Moreover, NFκB has been implicated in bone metastasis and the formation of osteolytic lesions (Park et al., 2006, Idris et al., 2009, Marino et al., 2018a, Peramuhendige et al., 2018). Recent work by our laboratory has evidenced that knockdown and pharmacological inhibition of IKKβ reduces breast cancer bone metastasis and osteolysis (Marino et al., 2018a, Marino et al., 2018b) . In addition, our recent work indicated that pharmacological inhibition of p65 with the inhibitor Parthenolide reduced breast cancer skeletal tumour growth and resulting osteolysis *in vivo* (Marino et al., 2017). As IKKε and its partner TBK-1 have been shown to directly and indirectly activate NFκB, it is plausible that IKKε may contribute to NFκB-mediated breast cancer motility and associated osteoclast formation. Similarly, IKKε activity has been shown to lead to the production of MMPs – critical mediators of ECM degradation and cancer invasion (Sweeney et al., 2005). Furthermore, pharmacological inhibition of IKKε/TBK-1 has been shown to reduce osteoclast formation *in vitro* and prevent ovariectomy induced bone loss *in vivo,* thus inhibition of IKKε within the bone microenvironment may prevent osteoclast formation and cancer-induced bone loss in models of breast cancer bone metastases. Thereby breaking the vicious cycle and the release of growth factors from the bone matrix may contribute to an inhibition of skeletal tumour growth of metastatic breast cancer.

1.6 The Aim of this Study

The NFκB pathway has been implicated in inflammation, bone remodelling and tumourigenesis. The aim of this study is to elucidate how modulation of IKKε through loss/gain of function and pharmacological inhibition affects breast cancer progression, skeletal tumour growth and osteolysis through the interaction of bone and cancer cells *in vivo* and *in vitro***.**

We hypothesise that inhibition of IKKε, both in breast cancer cells and the microenvironment reduces breast cancer growth, metastasis, skeletal tumour burden and osteolysis**.**

The specific aims of the work reported in this thesis are:

- To examine the expression of IKKε in breast cancer patient data sets and a panel of breast cancer cell lines
- To examine whether cancer-specific knockdown or overexpression of IKKε affects human breast cancer cell:
    - growth, migration and invasion *in vitro*
    - skeletal tumour growth *in vivo*
    - ability to induced-osteoclast formation and osteolysis *in vitro* and *in vivo*
    - ability to affect-osteoblast, growth, differentiation and activity *in vitro*
- To establish whether pharmacological inhibition of IKKε using the verified IKKε/TBK-1 inhibitor, Amlexanox:
    - Reduces breast cancer cell growth, migration and invasion *in vitro* and *in vivo*
    - Enhances the efficacy of clinically relevant chemotherapeutic agents *in vitro* and *in vivo*
    - Inhibits osteoclast signalling, formation and proliferation *in vitro*
    - Influences osteoblast growth, differentiation and activity *in vitro*
    - Reduces breast cancer bone metastasis, skeletal tumour growth and osteolysis *in vivo.*

Chapter 2

Materials & Methods

2 Materials and Methods

Reagents and suppliers used in this thesis can be found in Appendix 1.

2.1 Preparation of test compounds

The IKKε and TBK-1 inhibitor, Amlexanox was purchased from Tocris Bioscience (Bristol, UK), the IKKε inhibitors CAY10575 and CAY10576 were purchased from Cambridge Bioscience (Cambridge, UK; Table 2). For *in vitro* experiments, all compounds were prepared according to manufacturer's instructions. Amlexanox was prepared at 100mM in dimethyl sulfoxide (DMSO). Serial dilutions of the tested compounds were prepared and kept at -20°C. Concentrations used were determined by viability experiments, such that the concentration that had no effect on viability at a given time point were used.

Table 2. Inhibitors used and their targets

Compound	Targets (Concentration)
Amlexanox	IKKε/TBK-1 (1-2μM)
CAY10575	IKKε (15.μM)
CAY10576	IKKε (40nM), PDK1 (80nM)

2.2 Tissue Culture

2.2.1 Tissue culture media

Human CD14+ monocytes/macrophages, bone marrow cells, murine calvarial osteoblasts, MC3T3-E1 clone 4 were cultured in α-MEM supplemented with 10% foetal calf serum (FCS), 5% L-Glutamine, 100 U/ml penicillin and 100 g/ml streptomycin (standard αMEM). Human triple negative and claudin low parental MDA-MB-231 cancer cells were cultured in DMEM + Glutamax with 10% FCS, 100 U/ml penicillin and 100 μg/ml streptomycin (standard DMEM). All other human breast cancer cell lines, ZR-75-1 (ER positive – Luminal B), SK-BR-3

(HER2 enriched) and triple negative MDA-MB-468 (basal-like) were cultured in RPMI 1640 + Glutamax supplemented with 10% FCS, 5% L-Glutamine, 100 U/ml penicillin and 100 µg/ml streptomycin (standard RPMI). Tissue culture medium (DMEM, αMEM and RPMI) FCS, penicillin and streptomycin were obtained from Gibco, Thermofisher (Leicestershire, UK).

2.2.2 **Cell culture conditions**

Cell culture was performed in laminar flow hood sprayed with 70% (v/v) industrial methylated spirit prior to use. All solutions were warmed to 37°C before use. Plasticware supplied by various manufactures (Corning and Thermofisher) was bought pre-sterilised or autoclaved prior to use. All cultures were maintained under standard conditions of 5% CO_2: 95% air at 37°C in a humidified atmosphere. Phase-contrast microscopy was used routinely during the culture period in order to assess confluence or contamination of cultures.

2.2.3 **Cancer cell lines**

Human MDA-MB-231, MCF-7, ZR-75-1, SK-BR-3 and MDA-MB-468 breast cancer cell lines, Saos-2 osteoblast-like cells were purchased from ATCC (Manassas, VA, USA). The luciferase-expressing 4T1-Luc2 murine breast cancer cells and macrophage-like RAW264.7 cells were kindly donated by Dr. Munitta Muthana and Professor Dominique Heymann (University of Sheffield) respectively. Cancer cells were cultured in 25cm^2 or 75cm^2 flasks and passaged every 48-72 hours at a ratio of 1:5 MDA-MB- 231, 1:3 ZR-75-1, 1:3 SK-BR-3 1:5 MDA-MB-468, 1:10 4T1-Luc2, 1:5 Saos-2, 1:10 RAW264.7. The bone-seeking MDA-MB-231 sub-clone, MDA-BT1 (Marino et al., 2018a) were previously generated through *in vivo* passaging and donated by Dr. Nadia Rucci (University of L'Aquila) and sub-cultured at a ratio of 1:10. To subculture cells, the monolayer was washed in pre-warmed PBS and detached by treatment with trypsin. Standard medium was added at 2:1 ratio to trypsin in order to inactivate its proteolytic activity. The cell suspension was transferred to a fresh sterile 15 ml

tube that was then centrifuged at 300G for 5 minutes. The supernatant was removed and cells resuspended in 1 ml standard medium. A percentage of the suspension was placed into a new 25 or 75 cm^2 flask containing up to 15 ml standard medium. The remaining cells were counted and used for experiments.

2.2.4 **Preparation of Conditioned Medium**

Cancer cell conditioned mediuam was generated by the culturing of cancer cells in standard DMEM in 6 well plates. Once the cancer cells reached approximately 70% confluence, the cells were washed in PBS and 2ml of serum-free medium was added. Cells were then cultured for a further 16 hours under standard conditions and the conditioned medium obtained was then removed and filtered through a 0.2µm filter. Control conditioned medium was created from serum free medium cultured in the same way as cancer conditioned medium, but in a 6 well plate with no cancer cells present.

2.2.5 **Cell Viability**

The Alamar blue assay can be used to assess the viability of cells (O'Brien et al., 2000). Alamar Blue reagent (ThermoFisher) contains resazurin, a blue and weakly fluorescent dye. Alamar Blue is non-toxic to cells and is able to pass the cell membrane. The environment of respiring cells reduces resazurin to highly fluorescent resofurin. The degree of altered fluorescence is proportional to the number of living cells. MDA-BT1 cells were plated at a density of 3000 cells/well of a 96 well plate in 100µl of standard DMEM. Cells were allowed to adhere overnight and the following day medium was removed and replaced with compounds in DMEM containing 1% FCS. Cell Viability is measured by adding 10% (v/v) Alamar Blue reagent to each well. The plates are incubated for up to 3 hours. Fluorescence (excitation - 530 nm, emission - 590 nm) was detected using a SpectraMax® M5 microplate reader. AlamarBlue was also added to wells containing only standard media in order to correct for background fluorescence.

2.2.6 **Cancer cell motility**

2.2.6.1 2D directional migration

The wound healing assay was used to measure 2D directional migration of human MDA-BT1 (400 x 10^3 cells/well) breast cancer cells plated in 24-well plate in standard DMEM (Logan et al., 2013, Idris et al., 2009). After 24 hours, the confluent monolayer was treated with 5µg/ml of mitomycin-C for 2 hours to inhibit proliferation. The monolayer was scratched vertically using a 10µl pipette tip and the cells were washed eight times with serum free medium to remove any loose cells and debris. The drugs, solubilised in DMEM containing 1% FCS were added to the cells and the plate was placed in humidified microscope maintained at 37°C and 5% CO_2. Migration was monitored for 16 hours with an Olympus scanR time-lapse imaging system. Sequential images were captured at 30-minute intervals. Cell viability was measured using Alamar Blue assay at the end of the migration assays. Percentage of wound closure was calculated using T scratch software (Geback et al., 2009).

2.2.6.2 Cancer cell invasion

Cancer cell invasion was investigated using the Boyden chamber transwell invasion assay (Marino et al., 2018a). Pippette tips were left in -20°C freezer overnight. Growth factor reduced matrigel (Corning) was thawed on ice for 2 hours prior to usage. After defrosting, matrigel was diluted to a final concentration of 1.5mg/ml in ice-cold serum free medium. Corning™ 0.8 µm transwell inserts were inserted to a 24 well tissue culture plate. Diluted matrigel (20µl) was carefully pipetted into the insert using ice-cold tips and allowed to solidify for 3 hours at 37°C. Breast cancer cells were trypsinised and suspensions were prepared in serum free medium (3.2 x 10^4cells/ml). Once the matrigel was hardened, 200µl of cell suspension was added on to the transwell insert. Foetal calf serum (10% v/v) was used as a chemoattractant, thus 500µl of standard medium was placed in bottom of the 24-well plate and the transwell insert was added. The insert

containing plates were incubated at 37°C with 5% CO_2 for 72 hours. Following this, matrigel and non-invasive cells were removed from the interior part of the insert using a damp cotton bud. Cells were on the insert were fixed for 5 minutes in 100% ethanol followed by staining in haematoxylin and eosin (H&E). Inserts were placed in eosin (1% w/v) for 1 minute, rinsed in tap water, stained with haematoxylin for 5 minutes and rinsed again. Inserts were excised and mounted on superfrost plus glass slides using faramount mounting solution (Dako). Inserts were imaged using a bright field microscope 5x magnification. The area covered by invasive cells was analysed using ImageJ.

2.2.7 **Bone cell cultures**

2.2.7.1 Isolation of murine bone marrow cells

Bone marrow cells were isolated from the long bones (tibia and femur) of C57BL/6 female mice aged 8 weeks sacrificed by cervical dislocation as previously described (Takahashi et al., 2003, Sophocleous et al., 2015, Marino et al., 2014a). Sterilised equipment was used to perform the isolation. Briefly, the hind limbs were isolated and were placed in a Petri dish, the soft tissue and connective tissue that surrounds the bone was removed using a scalpel and the ends of each bone were cut off to reveal the bone marrow (Figure 9). To extract bone marrow cells (BM), the tibia were transferred to Eppendorf tubes with 500µl of standard αMEM and centrifuged at 400G for 5 minutes. This process was repeated twice. Bone marrow cells were passed through needles of decreasing gauge to generate a single cell suspension. The cell suspension was placed into a 15 ml tube and centrifuged at 400G for 3 minutes. The pellet was resuspended in an appropriate volume of standard αMEM and were plated in 96 well plates used for the generation of RANKL and M-CSF generated murine osteoclast cultures.

2.2.7.2 RANKL and M-CSF generated murine osteoclast cultures

Mouse BM cells isolated as described above were plated in 96-well at 150 x 10^3 cells/well in 100µl of standard αMEM with 25ng/ml murine M-CSF to facilitate

adherence (Marino et al., 2014, Sophocleous et al., 2015, Takahashi et al., 2003). After 48 hours, medium was replaced with standard αMEM supplemented with 100ng/ml RANKL and 25ng/ml M-CSF, Amlexanox and/or conditioned medium

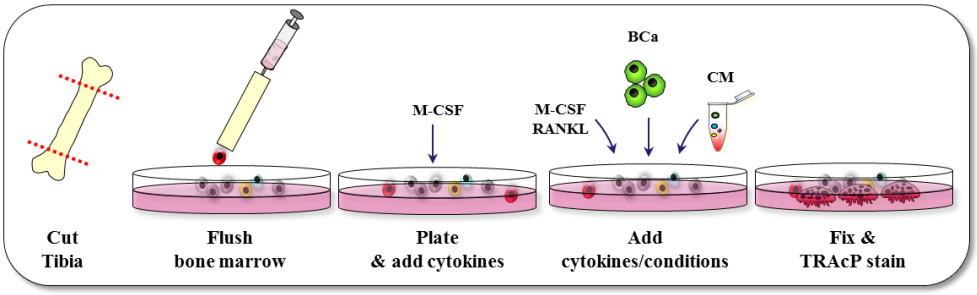

to a final volume of 150µl every 48 hours, while changing 50% of the medium supplemented with M-CSF and RANKL (Figure 9). Osteoclasts were identified using Tartrate-resistant Acid Phosphatase (TRAcP) staining as described below in section 2.2.8.

Figure 9. Generation of murine osteoclasts from tibia.
Schematic diagram of the isolation of murine total bone marrow from the long bones subsequent osteoclast formation in the presence of breast cancer cells/conditioned medium. See text in section 2.2.7.1 and 2.2.7.2 for details.

2.2.7.3 RANKL and M-CSF generated human osteoclast cultures

2.2.7.3.1 Isolation of peripheral blood mononuclear cells (PBMCs)

A source of osteoclast precursor cells can also be isolated from peripheral human blood. A volume equal to 100g of blood was drawn from healthy human volunteers in accordance with ethics given by the Ethics Committee of the University of Sheffield).

CD14+ cells were isolated as previously described (Marino et al., 2014a). Blood was diluted with twice the volume of EDTA buffer (2mM EDTA in PBS, 2-8°C). A volume of 25ml of diluted blood was transferred in to 50ml falcon tubes, where 14ml of Ficoll-Pacque (Sigma) was layered over the blood. Falcon tubes were centrifuged for 30 minutes at 20°C at 400G without brakes in order to separate out the blood. The white interphase containing peripheral blood mononuclear cells

(PBMCs) was aspirated and collected in a new 50ml falcon tube. PBMCs were resuspended and washed in 50ml of EDTA buffer. The cell suspension was centrifuged for 10 minutes at 20°C at 300G. The pellet was resuspended in 50ml EDTA buffer and centrifuged again for 10 minutes at 20°C at 200G. The pellet was resuspended in an appropriate amount of buffer and cell number was determined.

2.2.7.3.2 Isolation of CD14+ monocytes from PBMCs

The osteoclast precursor cells, CD14+ monocytes, can be isolated from PBMCs using antibodies specific for CD14 (Sorensen et al., 2007). PBMCs were isolated as described in section 2.2.7.3.1. Once the number of PBMCs was determined, cells were pelleted and then resuspended in 80µl of 2mM EDTA buffer with 0.5% (w/v) BSA per 10^7 total cells. To this suspension, 20µl of CD14 microbeads (Miltenyi Biotec) were added per 10^7 total cells. The cell and bead suspension was incubated for 15 minutes at 2-8°C. Cells were washed in 2mls EDTA buffer per 10^7 cells and centrifuged at 300g for 10 minutes. Following this, the CD14+ cells can be isolated using magnetic separation. The cells were resuspended in 500µl of buffer per 10^8 cells and loaded in to a MS magnetic column attached to a magnetic field. Three lots of washing using 500µl of buffer were performed to remove unbound cells. To elute bound $CD14^+$ cells, 1ml of buffer was added and a plunger was used remove cells. Cells were centrifuged as previously described and cell number was determined.

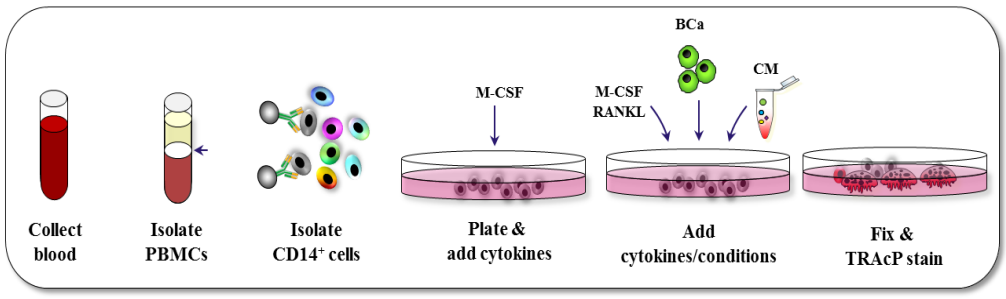

Figure 10. Isolation and generation of human osteoclasts from peripheral blood.

Schematic diagram of the isolation of human peripheral blood, isolation of CD14+ monocytes and subsequent osteoclast formation in the presence of breast cancer cells/conditioned medium. See text in section 2.2.7.3 for details.

2.2.7.4 Generation of osteoclast-like cells from RAW264.7 cells

RAW264.7 macrophage-like cells are plated in a 96-well plate at a density of 2000 cells/100µl of standard DMEM (Collin-Osdoby and Osdoby, 2012). The following day, RAW264.7 cells are given 100ng/ml of RANKL plus 10% v/v conditioned medium. Medium is refreshed after 48 hours with RANKL and conditioned medium. Cultures were stopped on day 5. Osteoclast-like cells are fixed and stained as seen in section 2.2.8.

2.2.8 **Characterization and identification of osteoclasts**

2.2.8.1.1 Culture fixation

To terminate the osteoclast cultures, the medium was removed and the adherent cells were rinsed twice with sterile PBS. Cells were then incubated in an appropriate volume (150µl for 96-well) of 4% (*v/v*) paraformaldehyde in PBS for 10 minutes at room temperature. Following fixation, the cells were rinsed twice with PBS and stored at 4°C in 70% ethanol (v/v).

2.2.8.1.2 Tartrate-resistant Acid Phosphatase (TRAcP) staining

Multinucleated osteoclasts were identified using TRAcP staining as previously described in (Marino et al., 2014a). Briefly, 100 µl of TRAcP staining solution (Appendix 2) was added to each well and plates were incubated at 37˚C for 30-60 minutes. The TRAcP staining solution was then removed and cells rinsed twice with sterile PBS and stored at 4°C in 70% (v/v) ethanol. TRAcP positive cells (TRAcP+) with 3 or more nuclei were considered to be osteoclasts and manually counted on a Zeiss Axiovert light microscope using a 10x and 20x objective lens.

2.2.9 **Osteoblast cultures**

2.2.9.1 Isolation of calvarial primary osteoblasts

Primary calvarial osteoblasts were isolated as previously described (Bakker and Klein-Nulend, 2012). Osteoblasts were obtained by sequential collagenase digestion from the calvarial bones of 2 days-old mice sacrificed by decapitation. The calvariae were removed, washed thoroughly in PBS and transferred to 15ml falcon tubes containing collagenase type 1 (1mg/ml) in PBS and incubated for 10 minutes at 37°C in a shaking water bath (Figure 11). Following the first digestion, the supernatant was discarded and the calvaria were incubated in fresh 5ml of collagenase type 1 for 30 minutes. The cell suspension obtained was mixed with 6 ml of standard αMEM (fraction 1). The remaining tissues were washed in PBS and treated for 10 minutes with 4 ml of 4 mM ethylenediaminetetraacetic acid (EDTA) in PBS at 37°C in a water bath with regular agitation. This cell suspension was then removed and mixed with 6 ml of standard αMEM (fraction 2). The remaining tissues were incubated in 4 ml of collagenase type 1 (1mg/ml) in PBS for 20 minutes in order to obtain the fraction 3. The three fractions were collected and centrifuged at 400G for 3 minutes. The cell pellet was resuspended in standard αMEM and cultured under standard conditions in 75cm^2 tissue culture flasks at a density of 3 calvariae per flask. The medium was changed 24 hours after seeding to remove non-adherent cells, and then every 48 hours until cells reached confluence.

2.2.9.2 Osteoblast viability

For studies of viability, osteoblasts were plated in 96-well plates (7 x 10^3 cells/well in 100µl of standard αMEM). After 24 hours, the desired treatments were added and left for 24 or 48 hours. Cell viability was analysed by the Alamar Blue assay (section 2.2.5).

2.2.9.3 Alkaline phosphatase assay

Alkaline phosphatase (ALP) is highly expressed by osteoblasts and thus is a marker of osteoblast differentiation (Taylor et al., 2014). This assay is a colorimetric assay based on the conversion of the colourless substrate p-nitrophenol phosphate (Sigma Aldrich) into a bright yellow p-nitrophenol by the enzyme, alkaline phosphatase. Osteoblasts were plated in 96-well plates at a density of 8 x 10^3 cells/well in 100µl of standard αMEM. After 24 hours, the cells were treated with the Amlexanox for 24 or 48 hours plus/minus conditioned medium from MDA-BT1 (20% v/v). Following treatment, the cell monolayer was rinsed with PBS and then incubated with 150µl of ALP lysis buffer (Appendix 3) for 20 minutes.

A serial dilution of p-nitrophenol (0 – 30 nM) was used to generate a standard curve. In a new 96-well plate, 50µl of the standard solutions and tested samples were plated in triplicates and 50µl of substrate solution was added on top. Absorbance was measured using a Molecular Devices SpectraMax M5 plate reader. The readings were taken at 414 nm at 37°C, at 5 minute intervals for 20 minutes. The activity of ALP was calculated from the linear part of the kinetic curve and was expressed as percentage of vehicle control. Alkaline Phosphatase activity was further normalised to cell number as determined by the Alamar Blue assay.

2.2.9.4 Bone nodule assay

For studies addressing osteoblast activity and bone nodule formation, Saos-2 osteoblasts were plated in 12-well plates (150 x 10^3 cells/well in 1 ml of standard DMEM). The following days, cultures were treated with the Amlexanox at the indicated concentration resuspended in αMEM supplemented with 50 µg/ml L-ascorbic acid and 10 mM beta-glycerophosphate (βGP) (osteogenic medium). The cells were cultured for up to 11 days and the medium was refreshed three times per week. At the end of the cultured period the cells were fixed in 70% (v/v) ethanol before staining.

2.2.9.4.1 Alizarin Red staining.

To quantify the formation of bone nodules by Saos-2 osteoblast-like cells, Alizarin Red S staining was used. Alizarin Red S bind binds to calcium deposited in mineralised tissues and cultures. This forms a complex that causes calcium uons to precipitate and form dark red deposits (Chang et al., 2000; Coelho et al., 2000).

Alizarin Red S powder (Sigma Aldrich) was first dissolved in deionised water to a final concentration of 40mM, the pH was adjusted with ~100µL of 37.5% HCl to a pH of 4.2. Ethanol was removed from fixed Saos-2 which were then rinsed thrice with PBS and then incubated with 1 ml per well of a 12-well plate with Alizarin Red S staining solution for 20 minutes on gentle rocking at room temperature. The staining solution was then removed and the culture was rinse thrice with de-ionized water and left to air-dry for 48 hours. Images of wells were taken on a standard scanner prior to destaining.

2.2.9.5 Destaining of osteoblast cultures.

In order to quantify mineralisation in stained osteoblast culture, a destaining solution consisting of 10% (w/v) cetylpyridinium chloride in 10mM sodium phosphate (pH 7.0) was used for 15 minutes at room temperature on a rocker. Alizarin Red S concentration was determined by absorbance measured at 562 nm on a Bio-Tek Synergy HT plate reader. Level of mineralisation was expressed as percentage of control.

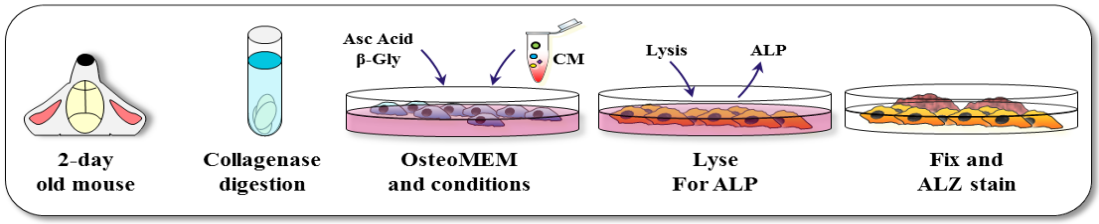

Figure 11. Isolation and characterisation of primary calvarial osteoblasts.
Calvaria from 2-day old mouse pups are digested with collagenase I. Osteoblasts are expanaded in standard αMEM and differentiated with OsteoMEM. Osteoblast maturation and activity are assessed by alkaline phosphatase activity and alizarin staining. See text in section 2.2.9 for more details.

2.2.9.6 Bone cells - conditioned medium co-cultures

For osteoclast – conditioned medium co-culture, mouse or human M-CSF dependent osteoclast precursors were plated in 96-well plates at 12 x 10^3 cells/well and 45 x10^3 cells/well in αMEM supplemented with 25ng/ml of M-CSF to allow attachment. After 48 hours, conditioned medium from different cancer cells (10% v/v), drug treatments, 100ng/ml RANKL and 25ng/ml of M-CSF were added to the bone marrow osteoclast precursors. The plates were cultured under standard conditions and treated with the desired compounds for 72-96 hours, while changing half of the medium supplemented with fresh conditioned medium, drug treatment, M-CSF and RANKL.

For osteoblast - conditioned medium co-culture, osteoblasts were plated in 96-well or 12-well plates at 8 x 10^3 cells/well in 100µl of standard αMEM, or 150 x 10^3 cells/well in 1 ml standard αMEM, respectively. In order to study the effect of breast cancer derived factors on osteoblast differentiation, osteoblast precursors were plated in 96-well plates and then treated with the desired compounds in presence and absence of conditioned medium (20% v/v) for 24 or 48 hours. In order to study the effect of breast cancer derived factors on osteoblasts activity, Osteoblasts were plated in 12-well plates and allowed to grow to confluency. Once confluent, osteoblasts were treated with the conditioned medium (20% v/v) or desired compounds resuspended in osteogenic medium in presence or absence of conditioned medium. The cells were cultured for up to 21 days and the medium was refreshed three times per week. At the end of the culture period, the cells were fixed in 70% (v/v) ethanol.

2.3 Molecular Biology techniques

2.3.1 Preparation of Luria-Bertani broth

Luria-Bertani (LB) broth (2% w/v) was dissolved in distilled water, autoclaved and the antibiotic for selection of transduced *E.coli* was added to LB broth once cooled at a final concentration of 100µg/ml. The antibiotic used was carbenicillin.

2.3.2 Preparation of LB/carbenicillin agar plates

Agar powder (4% w/v) was dissolved in distilled water. The solution was autoclaved and cooled at room temperature to around 50°C. Carbenicillin was added ad a concentration of (100µg/ml). LB agar media (20ml) was poured into 150mm petri dishes and left to set, then stored at 4°C.

2.3.3 Preparation of broth culture

A stab from the bacterial glycerol stock was added to 100 ml of LB broth in a 500ml conical flask to inoculate. The flasks were covered and left overnight at 37°C in a shaking incubator at 20G to allow for bacterial expansion. The next day, a High Speed QIAGEN Midi prep kit was used to isolate bacterial DNA from according to the manufacturer's instructions. Extracted DNA was quantified and assessed for purity using NanoDrop™ and stored at -20°C until further use. Glycerol stocks of LB culture were reserved by adding 15% glycerol to 85% bacterial suspension in a 2ml cryogenic vial and stored at -80°C.

2.3.4 Lentiviral gene delivery - Short Hairpin RNA (shRNA)

To generate knockdowns of IKKε expression in human osteotropic MDA-BT1 breast cancer cells a vector-based short hairpin RNA (shRNA) method was used according to manufacturer's instructions. Use of lentiviral vectors was approved by the University of Sheffield Biosafety Committee under project license GMO2014_11. Two TRC human individual clones ($IKK\varepsilon^{KD1}$ - TRCN0000010035 $IKK\varepsilon^{KD2}$ -TRCN0000010036; Table 3) and one empty vector control plKO.1 were

supplied in glycerol stocks (Thermo Scientific, Germany) ready for expansion in LB broth culture before use in transfection of MDA-BT1 breast cancer cells.

Table 3. Human IKKε ***targeting shRNA constructs and their target sequences***

Name	Construct	Targeting Sequence
$IKK\varepsilon^{KD1}$	TRCN0000010035	-TGCCCACAACACGATAGCCAT-
$IKK\varepsilon^{KD2}$	TRCN0000010036	-TGGGCAGGAGCTAATGTTTCG-

Nucleotide Basic Local Alignment Tool (BLASTn; NIH) confirmed that these constructs were specific for *IKBKE* mRNA and did not target the other IKK and IKK-related proteins including IKKα, IKKβ, IKKγ or TBK-1.

2.3.5 **Lentiviral transfection**

HEK29ET cells (1 x 10^5 cells/cm^2) were seeded in T25 flasks in 5 ml of standard DMEM. A transfection solution was generated by adding 5µg of indicated vector DNA (MOCK, $IKK\varepsilon^{KD1}$, $IKK\varepsilon^{KD2}$) to 5µg of PPAX vector DNA, 5µg of pMD2.G vector DNA (previously isolated by Dr. Silvia Marino) 40µl of Polyethylenimine (PEI) transfection reagent and 450 µl of serum free DMEM medium in 4.5ml of standard DMEM. Standard DMEM was removed from HEK-293ET cells and the monolayer was washed with PBS. The transfection medium (5ml) was added to HEK-293ET cells which were left under standard conditions for 24 hours. The transfection medium was then removed and fresh standard DMEM was added. The recipient MDA-BT1 (1x 10^4 cells/cm^2) were seeded into T25 flasks. On the fourth day, the virus containing medium was collected and briefly centrifuged. The viral supernatant (1ml) was added to 9ml of standard DMEM with polybrene (Sigma-Aldrich)at a final concentration of 5 µg/ ml. Back-up aliquots of viral medium were stored at -80°C. The viral solution was filtered through a 0.45 µm (low protein binding) filter. Filtered medium was added to the recipient MDA-BT1 cells. On the fifth day of the protocol, the medium from the recipient MDA-BT1 cells was removed and replaced with selection medium containing standard

DMEM and a concentration of puromycin, which would kill all non-transfected cells after 48 hours (1µg/ml)**.** The chosen selection concentration was determined by dose-response curves on non-transfected MDA-BT1 (data not shown). The transfected MDA-MB-231 cells were maintained in selection for at least two passages until knockdown was confirmed**.** The efficacy of the IKKε knockdown was determined by Western blot analysis (see section 0)**.**

2.3.6 **Lentiviral delivery of CRISPR activation particles**

To generate IKKε overexpressing MDA-BT1 cells, a lentiviral delivered CRISPR activation (CRISPRa) system was used. Control (only antibiotic resistance genes) and IKKε overexpressing lentiviral particles were purchased from Santa Cruz Biotechnology and transfections were carried out as per the manufacturer's instructions. The CRISPRa system is a repurposed version of the *Streptococcus pyogenes* bacterial CRISPR-Cas9 system. In *S. pyogenes* CRISPR-Cas9 functions to cleaves foreign DNA, however the CRISPRa system is used to enhances expression from an endogenous promoter (Perez-Pinera et al., 2013). The Cas9 nuclease has been mutated such that it loses its ability to cleave and is instead fused to three transcriptional activators (VP64, P65 and Rta) to form the dCas9-VPR protein. In addition to the mutated Cas9 protein a single guide RNA is also introduced. Guide RNAs are able to target upstream of the transcriptional start site (TSS) of a desired gene, bind the dCas9-VPR, guide the complex to the DNA target site, then the transcriptional activators are proximal to the TSS for up-regulation of the target gene (Chavez et al., 2015).

Recipient MDA-BT1 cells were seeded at a density of 1x 10^4 cells/cm^2 into 6 well plates. The following day (Day 1) 20µl of control viral particles containing only the antibiotic selection gene or CRISPR IKKε activating lentiviral particles were added to either well containing 2ml of standard DMEM plus 5µg/ ml polybrene (Sigma). On day 2, the viral containing medium was removed and replaced with standard DMEM. On day 3, the medium for the recipient MDA-BT1 cells was replaced with selection medium containing standard DMEM and concentrations of puromycin, hygromycin and blasticidin (Gibco), which would kill all non-transfected cells after 48 hours (1µg/ml, 500 µg/ml and 5 µg/ml respectively).

Concentrations were calculated by dose response curves on non-transfected MDA-BT1 (data not shown). The transfected MDA-BT1 cells were maintained in selection for at least two passages until overexpression was confirmed. The efficacy of the IKKε overexpression was determined by Western blot analysis (section 0)

2.3.7 **Small interfering RNA (siRNA) knockdown**

Generation of transient protein knockdown in breast cancer cells was carried out using siRNAs according to manufacturer's instructions. A pool of four annealed double – stranded RNA oligonucleotides (Table 4) against TBK-1 (M-003788-02-0005), IKKβ (M-003503-03-0005), p65 (M-003533-02-0005), IRF3 (M-006875-02-0005) or non-targeting pool no. 1 (D-001206-13-05) siRNAs were purchased from Dharmacon and reconstituted to a 20μM stock using 1x siRNA buffer (Dharmacon). Recipient cancer cells ($10x10^3$ cells/cm^2) were plated in standard DMEM and allowed to adhere overnight. The following day the indicated siRNA were added at a final concentration of 25nM with Dharmafect 1 transfection reagent (2.5 μg/ml; Dharmacon) in 80% antibiotic free standard DMEM and 20% serum free DMEM and left in standard conditions until indicated time points. Validation of knockdown was carried out using western blotting (section 0). Cancer cell viability, migration and ability to induce osteoclast formation were assayed by Alamar blue (section 2.2.5) wound healing (section 2.2.6.1) and osteoclast formation assays (see section 2.2.7.4).

Table 4. *A list of siRNA target sequences for human NFκB and IRF pathway members*

Human SMARTpool siRNA	Target Sequence
Non-Targeting	-UAGCGACUAAACACAAUCAA-
	-UAAGGCUAUGAAGAGAUAC-
	-AUGUAUUGGCCUGUAUUAG-
	-AUGAACGUGAAUUGCUCAA-
TBK-1	-GAACGUAGAUUAGCUUAUA-
	-UGACAGAGAUUUACUAUCA-
	-UAAAGUACAUCCACGUUA-
	-GGAUAUCGACAGCAGAUUA-
IKKβ	-GAAGUACCUGAACCUAGUU-
	-CCAAUAAUCUUAACAGUGU-
	-GGAUUCAGCUUCUCCUAA-
	-GUGGUGAGCUUAAUAAUG-
p65	-GGAUUGAGGAGAAACGUAA-
	-CUCAAGAAUCUGCCGAGUGA-
	-GAUUGAGGAGAAACGUAAA-
	-GGCUAUAACUCGCCUAGU-
IRF3	-GCAAAGAAGGGUUGCGUUU
	-AUGCACAGCAGGAGGAUU-
	-GGGAAGAGUGGGAGUUCGA-
	-CCAAGAGGCUCGUGAAUGGU-

Western Blot

Western blot was used to study protein expression and activity in bone and cancer cells as previously described in (Idris, 2012). Antibodies and their suppliers can be found in Appendix 7.

2.3.8 **Preparation of cell lysates**

Cells were plated in 12-well plates or 6-well plates at 150 x 10^3 cells/well and 500x10^3 cells/well respectively in standard medium until 70% confluence was reached. Medium was suctioned off and the cell monolayer was washed with ice-cold PBS. Cells were scraped in 60 µl (12-well) or 120µl (6-well) of RIPA lysis buffer (Appendix 4) supplemented with 2% (v/v) protease inhibitor cocktail (Sigma Aldrich, UK) and 0.4% (v/v) phosphatase inhibitor cocktail (Thermofisher, UK) and remained on ice 10 minutes or until cells were lysed. The cell lysate was transferred to a 500µl centrifuge tube and centrifuged at 14000G for 10 minutes at 4^{o}C. The supernatant fraction of proteins was collected, being careful not to disturb the pellet and stored at -20 ^{o}C until further use or used immediately.

2.3.9 **Measuring protein concentration**

Protein concentration of cell lysates was determined by the bicinchoninic acid (BCA) Pierce protein assay according to manufacturer's instructions (Pierce, USA) as previously described in (Idris, 2012). Serial dilutions of bovine serum albumin (BSA) (0-2000 µg/µl) were used to generate a standard curve. BCA standard dilutions (10 µl and protein samples (1:5 diluted in distilled H_2O) were plated in duplicates in a 96-well plate and 200µl of copper (II)-sulphate (diluted 1:50 with BCA) were added in each well and the plate incubated for 20-30 minutes at 37 ^{o}C. Absorbance was then measured at 562 nm on a Biotek Synergy HT plate reader and the protein concentration in each sample was calculated from the BSA standard curve.

2.3.10 **Gel electrophoresis**

In order to separate proteins by molecular weight, gel electrophoresis was performed using Criterion^{TM} XT BioRad (12% Bis-Tris) pre-cast gels,. Gels were placed into a vertical electrophoresis tank filled with electrophoresis running buffer (BioRad) diluted 1:10 in distilled water **.** Cell lysates (30-100µg, maximum 40µl) were mixed with 5x sample loading buffer (Appendix 4. **Buffers for Western blotting**) and heated to 95°C for 5 minutes and loaded into the well following a period of cooling at room temperature**.** Kaleidoscope pre-stained standard and Magic Marker XP (BioRad) western standards were used to identify molecular weights**.** Gels were run at constant voltage of 180V for 45-60 minutes dependant on the level of separation required**.**

2.3.11 **Electrophoretic transfer**

Separated proteins were transferred from polyacrylamide the gel to polyvinylidene difluoride (PVDF) pre-cut membranes (BioRad). PVDF membranes were activated in 100% methanol and then allowed to equilibrate in transfer buffer (BioRad) for 15 minutes**.** The blotting stack consisting of pre-soaked blot papers in transfer buffer, membrane, polyacrylamide gel, pre-soaked blot paper, was prepared and placed in the transfer apparatus (BioRad) at a constant voltage of 25V and a current of up to 1A for 7 minutes**.**

2.3.12 **Immunostaining and antibody detection**

Following transfer, the PVDF membrane was incubated at room temperature on a rocker for 60 minutes in 5% (w/v) non-fat dried milk in Tris buffer saline solution (TBS) supplemented with 0**.**1% (v/v) Tween 20 (TBST). This stage is to ensure that sufficient blocking of non-specific binding sites**.** The membrane was then washed in TBST for 15 minutes and this was repeated thrice**.** The membrane was placed in the specified primary antibody (Cell Signalling Technologies - 1:1000 or Santa Cruz 1:50 in 5% BSA in TBST) overnight at 4 ^{o}C with continuous rocking**.** The following day the membrane was washed three times in TBST for 15

minutes and incubated with the HRP-conjugated secondary antibody (1:5000 in 5% w/v dried non-fat milk in TBST; Jackson Laboratories) for 1 hour at room temperature gentle rocking. Following this stage, the antibody was removed and retained and the membrane was washed three times with TBST for 15 minutes each. Proteins on the membrane were visualised using, for the detection of the immunoreactivity complex, the Pierce SuperSignal® West Dura Extended Duration chemiluminescent detection system on a BioRad Imaging System. Signal intensity was quantified using ImageLab software from BioRad (Exeter, UK). Amount of protein of interest was normalised by housekeeping proteins (β-Actin). In some experiments, the membrane was incubated in stripping buffer (Appendix 4) for 3-6 minutes at 55^{o}C in a water both to remove all bound antibodies, then blocked again in blocking solution for 1 hour and re-probed with a different primary antibody and processed as described above.

2.3.13 **Measurement of tumour derived cytokines**

The Proteome Profiler Human XL Cytokine Array Kit (R&D Systems) was used to detect the expression of cytokines produced by human MDA-BT1 cells and the effect Amlexanox (30µM) has on these cytokines. The cytokine array kit was carried out according to manufacturer's instructions. Briefly, conditioned medium was generated as previously described (Preparation of Conditioned Medium) in the presence of 30µM Amlexanox (0.1% v/v) or DMSO however only a total of 500µl was prepared in in order to concentrate cytokines produced. Conditioned medium was collected and used immediately. The cytokine array membranes were incubated in blocking solution for one hour prior. Meanwhile, the samples were diluted with blocking solution to 1.5ml. The membranes were washed and then placed in the prepared samples at 4°C on a rocking platform overnight. The next day membranes were washed in the given wash buffer three times for 10 minutes each. The membranes were placed in the given secondary antibody cocktail for one hour on a rocker at room temperature before washing as previously mentioned. The membranes were covered with 1x streptavidin conjugated horseradish peroxidase (HRP) for 30 minutes. The washing steps were repeated. The membranes were then exposed to the chemiluminescent detection system and visualised using the BioRad system as section

2.4 Animal Studies

A variety of *in vivo* models were used to investigate how knockdown and pharmacological inhibition (alone and in combination with clinically relevant Docetaxel) affect primary tumour growth, development of metastasis, colonisation of the bone, skeletal tumour growth and osteolysis (Figure 12). All mice were placed on a 12-hour light-dark cycle with access to food and water *ad libitum*.

2.4.1 **Ethics**

All experimental protocols were approved by and performed in accordance with UK Home Office regulations under project licence 70/8964 and Italian Legislative Decree 116/9 and, Gazzetta Ufficiale della Repubblica Italiana no. 40, February 18, 1992.

2.4.2 **Intratibial Injection of breast cancer cells**

The effects of cancer-specific inhibition on skeletal tumour growth and osteolysis were investigated through intra-tibial injection of human MDA-MB-231-BT1 cells and was performed at the University of L'Aquila, Italy. Briefly, seven 4 week-old female BALB/c-nu/nu athymic mice **(**Charles River, Milan, Italy) per group were anesthetized with i.p injections of pentobarbital (60 mg/kg). Mice received intra-tibial injection of 5×10^3 human MDA-MB-231-BT IKKε-^{KD2} or IKKε-mock cells (Rucci et al., 2013). A 10µl suspension of the cells in PBS was injected using a 27½ gauge needle into the intramedullary space of the proximal tibiae. Animals were monitored weekly for the development of osteolytic lesions (Figure 13). Mice were anesthetized as before and subjected to X-ray analysis (36 KPV for 10 seconds) using a Cabinet X-ray system (Faxitron model n.43855A Buffalo Grove, IL, USA). Of note, two mock injected mice were killed by the anesthetic injection and thus bringing the mock group down to five. The experiment was terminated when significant osteolysis was observed. Animals were sacrificed after 21 days by carbon dioxide inhalation and cervical dislocation. Dissection was performed in L'Aquila by myself, lungs were observed for signs of macrometasases, although none were observed. Visceral organs and hind limbs were fixed in 10% buffered formalin and kept at 4°C.

2.4.3 **Intracardiac Injection of breast cancer cells**

The effects of pharmacological inhibition of IKKε, on the ability of breast cancer cells to colonise bone, tumour growth and osteolysis were assessed through intracardiac injection of murine 4T1-Luc2 cells (Wright et al., 2016). Intracardiac injection was performed at the University of Sheffield by Dr Ning Wang (Wang et al., 2015)(Figure 12). Sixteen 6-weeks old female BALB/c mice (Harlan, UK) were placed in the induction chamber of an anaesthetic machine filled with 2% isoflurane until sedated. Mice were placed supine on a sterile surgical platform with the forelimbs and hind limbs taped away from the torso. The chest was cleaned thoroughly with iodine (Sigma Aldrich). A 100µl suspension with $100x10^3$ 4T1-Luc2 cells in PBS was drawn up in to a 29G insulin needle. The needle was injected the left of the sternum, to reach the left ventricle. The cells were injected slowly and the needle removed, with pressure being held to the injection site for a moment. Mice were placed in an incubator heated to 22°C for 30-60 minutes to recover.

After 24 hours, mice were divided in to two groups of 8 mice and treated with the indicated compounds (Table 5). Intraperitoneal injections were performed by Mr. Richard J Allen using 25G needles. Animals were monitored thrice weekly for the development of metastasis using the IVIS system following injection of 100µl of D-luciferin (1.5mg/kg; Perkin Elmer). IVIS imaging was performed by Mr Richard Allen and myself. Ten days post treatment, animals developed hind-limb paralysis and the experiment was terminated. Animals were sacrificed by Mr Allen via cervical dislocation. Following sacrifice, the lungs, liver, spleen, kidneys, brain and hind limbs were harvested by myself. IVIS imaging was performed on organs *ex vivo* with organs and limbs being fixed in 4% paraformaldehyde for later processing by myself.

Table 5. Treatment regimens of mice following intracardiac injection.

Group	Treatment
Vehicle	200µl vehicle control i.p daily

Amlexanox	200µl Amlexanox (35mg/kg) i.p daily

2.4.4 **Orthotopic injection of breast cancer cells**

We studied the effects of treatment with Amlexanox, Docetaxel or a combination treatment on primary tumour growth and development of distant metastasis using the 4T1-Luc2 orthotopic injection model (Figure 12) performed by Dr. Penelope Ottewell. Prior to injection, a cell suspension containing 4T1-Luc2 ($10x10^7$/ml) of ice-cold 60% PBS, 39% growth factor reduced matrigel (Corning) and 1% trypan blue (Sigma Aldrich) and left on ice. Forty 6 week-old female BALB/c mice (Harlan, UK) were anesthetized as above and placed flat in a supine position on a surgical platform. Hair was removed from the mice inguinal surface and thoroughly cleaned with iodine as previously mentioned. A sterile scalpel was used to make a 1cm incision in the midline of the mouse abdomen. A 25G needle with a volume of 40µl of the cell suspension was injected into the fat pad of both the left and right inguinal breast. Incisions were closed with 2-3 5mm wound clips and placed in a heated incubator as before.

The following day mice were checked for tumour engraftment using IVIS Spectrum *In vivo* Imaging System (PerkinElmer, Buckinghamshire, UK). Following successful engraftment mice were divided in to four groups 10 mice per group and treated with i.p injections of vehicle, Amlexanox, Docetaxel or a combination (Table 6) carried out by Mrs. Diane Lefley**.** Animals monitored daily for cachexia (evaluated by body weight waste) and behavior**.** Drug treatments began the day following the injection and thus does not represent the treatment of a palpable tumour but rather a cell suspension of the cells in the fat pad. The size of each tumour was measured externally three times a week by measuring their two axes using a caliper and applying the formula of the volume of a sphere [$4/3\pi r^3$ where r is half the mean of the two axes]**.**

Once the tumour volume had reached the maximum volume of $1cm^3$, the tumours were resected by Dr. Penelope Ottewell**.** Briefly, mice were anaesthetised and an incision was made as before. Forceps were used to grip the skin and reveal the tumour. Blood vessels feeding the tumour and associated lymph nodes were

cortorised and the tumour resected using sterile scissors/scalpel.. In some cases, the tumour had invaded through the periosteum and in to the gut, deemed peritoneal metastasis, thus these mice were sacrificed. Incisions were closed with wound clips as before. Tumours were weighed and fixed in 10% buffered formalin by myself.

The development of metastases was monitored biweekly using the IVIS system. At the end of the experiment (when overt metastases were observed), mice were euthanized by cervical dislocation/cardiac exsanguination. The primary tumours and the lungs, brain, spleen and hind limbs of the animals were dissected formalin fixed (Appendix 5) for later processing. Data from this experiment is shown in both Figure 31 and Figure 57.

Table 6. ***Treatment regimens of mice following orthotopic injections of 4T1-Luc2 cells***

Group	Treatment
Vehicle	200µl vehicle control i.p daily
Amlexanox	100µl Amlexanox (35mg/kg) i.p daily 100µl of vehicle control i.p weekly
Docetaxel	100µl Docetaxel (15mg/kg) i.p weekly 100µl of vehicle control i.p daily
Combination	100µl Docetaxel (15mg/kg) i.p weekly 100µl Amlexanox (35mg/kg) i.p daily.

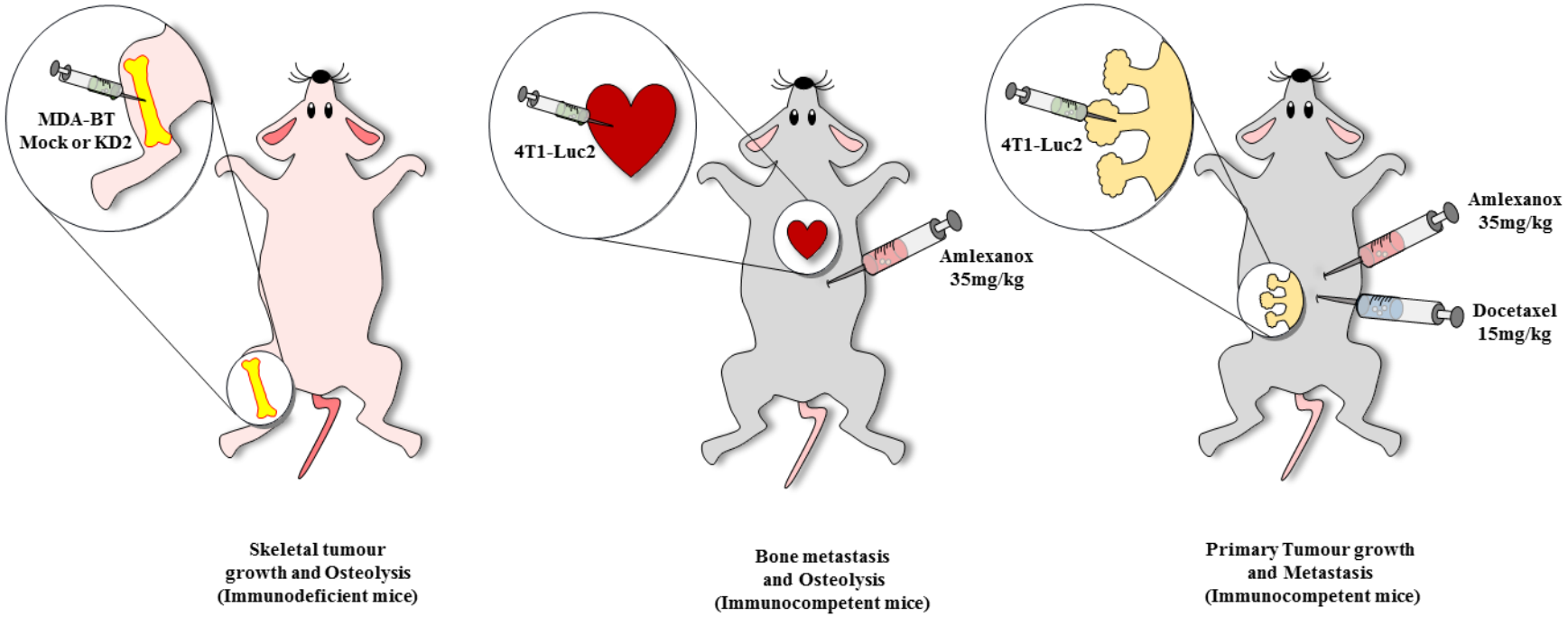

Figure 12. In vivo models used to study the role of IKKε in breast cancer primary tumour growth, bone metastasis, skeletal tumour growth and osteolysis

A) Athymic BALB/c nu/nu mice were injected intratibially with either mock transfected human breast cancer MDA-231 cells or MDA-231 IKKε knockdown cells ($IKK\varepsilon^{KD2.}$ B) BALB/c mice were injected intracardiacally with luciferase expressing 4T1 cells (4T1-Luc2) and given daily i.p injections of Amlexanox (35mg/kg) or weekly i.p injections of docetaxel (15mg/kg) or a combination of the two. C) BALB/c mice were injected in to the mammary fat pad with 4T1-Luc2 cells and given daily i.p injections of Amlexanox (35mg/kg) or weekly i.p injections of docetaxel (15mg/kg) or a combination of the two. Primary tumours were resected when they reached $1cm^3$, mice were monitored for development of metastases. Mice were sacrificed following detection of metastases using IVIS.

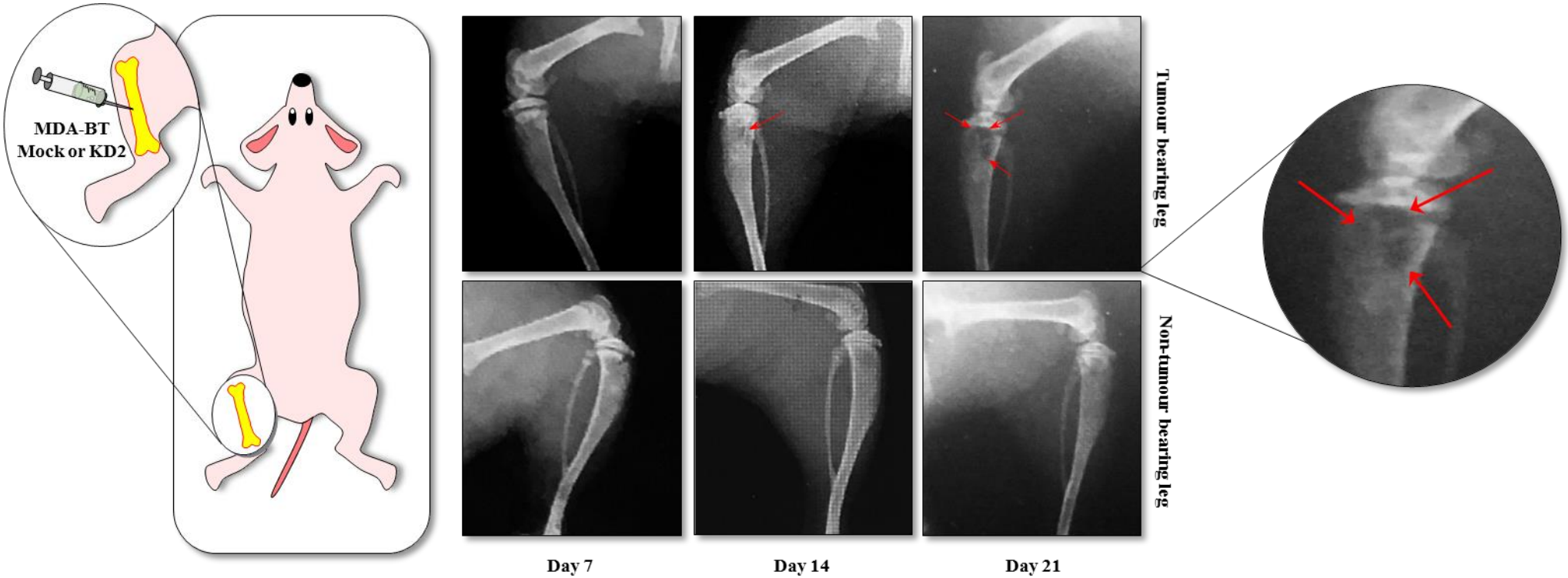

Figure 13. Development of osteolytic lesions following intratibial injection of MDA-BT1 cells.

A Schematic diagram of the intratibial injection of MDA-BT1 cells. B X-ray images of one mouse over three weeks following intratibial injection into the left tibia legs (top) and non-tumour bearing legs (bottom). Red arrow indicates the presence of osteolysis.

2.5 Histological processing of samples

2.5.1 Fixing of tissues

Hind limbs were trimmed of excess muscle and soft tissue to reveal bone. Limbs and internal organs were placed in 10% buffered formalin (Appendix 5) for 48 hours. Following this, samples were washed in PBS and then placed in 70% (v/v) ethanol and stored at 4°C for later processing.

2.5.2 Microcomputed tomography (µCT)

Microcomputed tomography (µCT) was employed to assess the bone structure and architecture following colonization and subsequent destruction of the bone by breast cancer cells (Campbell and Sophocleous, 2014). Hind limbs were scanned using an *ex vivo* scanning system (SkyScan). Hind limbs were wrapped in cellophane to prevent desiccation and placed upright in the scanner. Legs were scanned using an x-ray radiation source to 60kV and 150µA . The pixel size was set to 6µM for the intratibial injections 4.3µm for the intracardiac injections. NRecon software (Skyscan) was used to generate 3D image stacks by reconstructing the data from the rotation image projections. The beginning of the tibia on each leg was chosen as a reference point and 1000 frames below that were chosen for reconstruction (Table 5).

Table 7. Processes used for µCT analysis

Parameter	Description	Setting
Smoothing	Noise removed and image smoothed	Pixel width
Beam Hardening Factor Correction	Corrects for the absorbance of low energy x-ray on the outside of the specimen	9%
Ring correction level	Corrects for the non-linear behaviour of pixels causing ring artefacts	3

2.5.3 **Decalcification of hind limbs**

Hind limbs of mice were decalcified to remove mineral from the bone in order to provide quality sections such that the internal cellular structure remains intact. A chelating neutral EDTA buffer was chosen as it acts slowly, leaving the tissue intact and has little effect on conventional stains such as TRAcP. Hind limbs were placed in labelled histological cassettes (Fisher Scientific) submerged in neutral EDTA buffer. Cassettes were placed on a rocker at 20 RPM at 4°C. Neutral EDTA buffer was decanted and refreshed every 48 hours for 21 days.

2.5.4 **Embedding and sectioning of tissues**

Embedding of tissues in to paraffin blocks was performed as a service by the Skelet.AL lab (Sheffield, UK). Briefly, sections were dehydrated through various percentages of alcohols before placing in paraffin wax. Sectioning of tissues was performed on a Leica microtome (Leica microsystems, Germany) and sections of 4µm were placed on microscope slides before staining (Thermo Fisher, UK) by Danielle de Ridder.

2.5.5 **TRAcP staining of histological sections**

The TRAcP staining of osteoclasts in sections is carried out with similar methodology as the staining of osteoclasts in culture. Briefly, sections were rehydrated through xylene and alcohols (Table 8). Solutions are incubated in

Solution A (Appendix 2) for 30 minutes at 37°C. Solution A is removed and replaced with Solution B (Appendix 2) for 18 minutes. Sections are rinsed twice in running tap water to remove remaining solutions. Sections are then counterstained in Gill's Haemotoxylin for 20 sections. Washing in water will blue the sections. Sections are dehydrated by quickly reversing the steps in Table 8 so that the sections are in each solution for no more than 20 seconds. Sections can be mounted with DPX mounting medium and a coverslip.

Table 8. Process of dewaxing and rehydrating histological sections

Solution	Time (Minutes)	Process
100% Xylene	5	Dewax sections
100% Xylene	5	Dewax sections
100% Ethanol	5	Clear Xylene
100% Ethanol	5	Clear Xylene
95% Ethanol	5	Dehydrate sections
70% Ethanol	5	Dehydrate sections
dH_2O	1	Rinse sections

2.6 Gene expression analyses

Copy number variation (CNVs) and gene expression data were analysed using cBioPortal (Gao et al., 2013, Cerami et al., 2012). The Molecular Taxonomy of Breast Cancer International Consortium ((METABRIC (Curtis et al., 2012) and The Cancer Genome Atlas (TCGA (The Cancer Genome Atlas, 2012) studies were combined to analyze CNVs in a total of 2951 breast cancer patients. Only the METABRIC study had clinical data of the PAM50+Claudin Low molecular stratification thus was used to assess mRNA levels in each classification. For survival analysis, claudin-Low and Basal classifications were combined to form triple negative group. For analysis of association *IKBKE* copy number variations and metastasis, data from the Metastatic Breast Cancer Project was used (ongoing –published to cBioPortal (Cerami et al., 2012). Patients were separated in to those who were diploid for *IKBKE* or those who had increased expression (*IKBKE* duplication and amplification).

2.7 Statistical Analyses

Where appropriate comparison between groups was done by analysis of variance (ANOVA) followed by Bonferroni post-hoc test using GraphPad Prism 7. A student's T-test was used to determine the significance between two groups using GraphPad Prism 7. Kaplan-Meier curves were calculated in GraphPad Prism 7.0. To analyse significant differences between presence of metastasis i.e. yes metastasis or no metastasis contingency tables and Fisher's exact value were calculated. A p-value value of 0.05 or below was considered statistically significant, and a p-value of 0.01 or below highly statistically significant.

Chapter 3

IKKε INHIBITION REDUCES TRIPLE NEGATIVE BREAST CANCER CELL METASTATIC BEHAVIOUR

IN VITRO AND *IN VIVO*

3 Chapter 3

3.1 Summary

Metastasis to the skeleton occurs in up to 70% of breast cancer patients and is often deemed incurable (Coleman, 2001). IKKε is a breast cancer oncogene and has been shown to promote the formation of mammary tumours through activation of the NFκB pathway (Boehm et al., 2007). However, the role of IKKε in bone metastasis and skeletal tumour growth has yet to be assessed. In this study, we show that IKKε is amplified in around a fifth of breast cancer patients and is associated with triple negative breast cancers. In addition, this was associated with poorer overall survival in triple negative patients. Moreover, for the first time, we have shown an association between IKKε amplification and the development of bone metastasis.

Knockdown and pharmacological inhibition of IKKε reduced human triple negative and osteotropic MDA-MB-231 (MDA-BT1) growth, migration and invasion whilst overexpression was stimulatory. Mechanistic studies revealed that IKKε driven growth and migration are dependent on NFκB pathway expression. Furthermore, cancer specific inhibition of IKKε reduced skeletal tumour growth of MDA-BT1 cells following intratibial injection. In addition, for the first time, I have shown that pharmacological inhibition of IKKε reduced skeletal and primary tumour growth of syngeneic 4T1 mouse breast cancer cells. Overall, this chapter demonstrates that selective inhibition of IKKε in cancer cells and/or the environment can reduce both primary and skeletal tumour growth and thus may be of value in the treatment of breast cancer.

3.2 Introduction

Breast cancers are a highly heterogeneous group of diseases, thus efforts have been made to identify distinct intrinsic molecular subtypes such as the PAM50 stratification, which divides breast cancers in to luminal-A, luminal B, HER2, enriched, normal like and basal (Prat and Perou, 2010). Following these, the claudin-low group of highly metastatic triple negative breast cancers was added to these subtypes. Molecular stratification of cancer can be important in understanding clinical phenotypes, prognosis and response to therapies. It is important to identify genomic alterations and copy number variations (CNVs), namely chromosomal amplifications, deletions and rearrangements within these sub-types in order to develop novel targeted therapies that can be used as monotherapies or in combination with existing clinically relevant treatments to enhance patient survival and quality of life.

IKKε was first described as a breast cancer oncogene in 2007 by Boehm and colleagues (Boehm et al., 2007), who showed the overexpression of constitutively active and wild-type IKKε could cooperate with activated MAP kinase pathway signalling to induce the transformation of mammary epithelial cells leading to the formation of mammary tumours in mice. Furthermore, the authors showed that a third of breast cancer patient samples (n=30) express *IKBKE* CNVs, however they found no association of *IKBKE* gain/amplification with hormone receptor or HER2 status. They showed that *IKBKE* locus (1q32) amplification was present in 16.3% of breast cancer cell lines (n=49) and that its shRNA mediated inhibition in luminal A MCF7 and luminal B ZR-75-1 breast cancer cells caused a reduction in cell viability. Thereby, implicating IKKε as a breast cancer oncogene, which promotes the initiation of *de novo* tumours. In a follow-on study, Barbie and colleagues (2014) showed that *IKBKE* mRNA expression was upregulated in a subset of triple-negative breast cancers in patients (Barbie et al., 2014). Furthermore, they showed that IKKε expression lead to an IL-1β driven inflammatory phenotype and its pharmacological and shRNA-mediated inhibition reduced the growth of several

triple negative cell lines. They showed that inhibition of IKKε/TBK-1/JAK signalling slowed tumour growth however, when combined with a MEK inhibitor, this completely prevented tumour growth of primary triple negative patient-derived xenografts. These studies indicate that both inhibition of IKKε alone or in combination with other targets could be of value in the prevention and treatment of primary breast cancer; however, the validity of IKKε as a driver of metastatic breast cancer has yet to be examined.

3.3 Aim

The aims of this chapter were to assess the expression of IKKε in breast cancer and investigate the role of IKKε in breast cancer cell metastatic behaviour *in vitro* and *in vivo*.

These aims were achieved by examining:

- the presence of *IKBKE* CNVs in large clinical datasets
- the protein expression of IKKε in breast cancer cell lines
- the effects of stable shRNA mediated knockdown and pharmacological inhibition of IKKε on MDA-MB-231-BT breast cancer viability and migration *in vitro*
- the effects of stable CRISPRa mediated overexpression of IKKε on MDA-MB-231-BT breast cancer viability and migration *in vitro*
- The effect of shRNA mediated knockdown of IKKε on human MDA-BT1 breast skeletal growth *in vivo*
- The effect of Amlexanox on mouse 4T1-Luc2 breast cancer bone metastasis following intracardiac injection into syngeneic immunocompetent mice
- The effect of Amlexanox on mouse 4T1-Luc2 breast cancer general metastasis following intracardiac injection into syngeneic immunocompetent mice
- The effect of Amlexanox on mouse 4T1-Luc2 breast cancer primary tumour growth following orthotopic injection into syngeneic immunocompetent mice

3.4 Results

3.4.1 *IKBKE* copy number variation is associated with a shorter overall survival in triple negative breast cancers

Studies have indicated that breast cancer is primarily driven by genomic copy number variations (Ciriello et al., 2013). In addition, Boehm and colleagues showed that *IKBKE*, the gene encoding IKKε was amplified in around 30% of breast cancer patient samples. With this in mind, I first carried out a retrospective analysis of amplifications of the IKK genes in a large combined cohort of breast cancer patients. To do this I combined the Molecular Taxonomy of Breast Cancer International Consortium ((METABRIC (Curtis et al., 2012) and The Cancer Genome Atlas (TCGA (The Cancer Genome Atlas, 2012) cohorts which looked at putative CNVs in primary breast cancer patient samples, using cBioPortal (Cerami et al., 2012, Gao et al., 2013). This analysis revealed for the first time that *IKBKE* was the most amplified IKK gene, where it was amplified in 20.4% of breast cancer patients (Figure 14). Comparatively, *CHUK* (IKKα), *IKBKB* (IKKβ) and *TBK1* had copy number amplifications in 0.3%, 10% and 1.4% of breast cancer patients (n=2951) respectively. Further analysis of these cohorts revealed that only 35.5% of breast cancer patients being diploid for *IKBKE*, a very small percentage having deletions in the *IKBKE* locus (0.3%) and the remaining patients exhibiting duplications (43.5%).

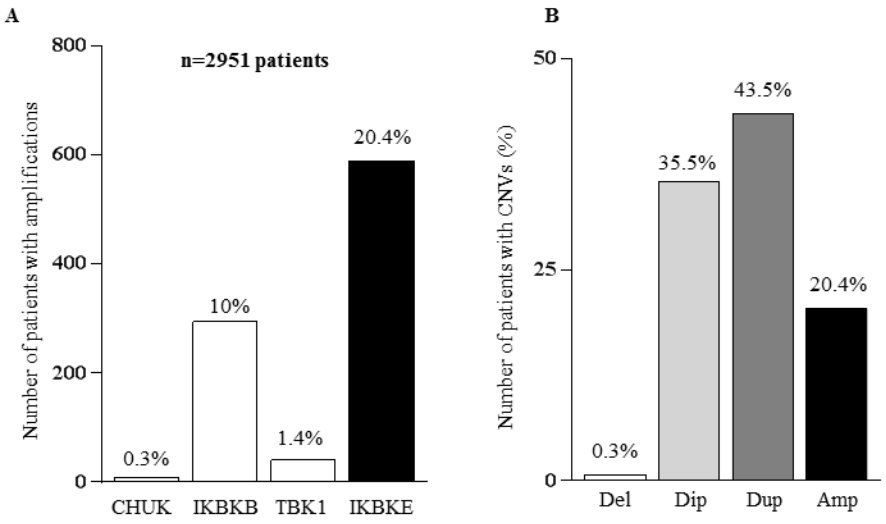

Figure 14. IKBKE copy number is amplified in a fifth of breast cancer patients.

A) Combined retrospective analysis of the METABRIC (Curtis et al., 2012) and TCGA 2012 (The Cancer Genome Atlas, 2012) studies revealed that 20% of breast cancer patients in a cohort of 2951 have copy number alterations in IKBKE. Comparatively, the other IKK genes, CHUK, IKBKB and TBK-1 only had copy number variation in 0.3%, 10% and 1.4% of breast cancer patients within the same cohort. **B)** Further analysis of these cohorts revealed that only 35.5% of patients were diploid for IKBKE, whereas 43.5% showed gain of IKBKE, 20.4% had amplifications and 0.7% had deletions of IKBKE. Del, deletion; dip, diploid; dup, duplication; amp, amplification

Next, I examined within which breast cancer molecular subgroup *IKBKE* expression is upregulated. Using the METABRIC cohort on the cBioPortal. *IKBKE* mRNA expression was found to be highest in the triple negative basal-like and claudin-low subgroups, significantly higher than luminal-A, luminal-B, HER2 enriched and normal-like (Figure 15). In addition, I also examined a panel of breast epithelial cells and different breast cancer cell lines for IKKε protein expression using Western Blot. In broad agreement with the METABRIC analysis, the two human triple negative cell lines MDA-MB-468 (basal-like) and MDA-MB-231 (claudin-low) breast cancer cell lines had the highest levels of IKKε when compared to non-transformed MCF10a breast epithelial cell line, with 7.5 ±1.33 ($p<0.001$) and 7.2 ±0.3 ($p<0.01$) fold higher levels of IKKε protein, respectively. The luminal B (ZR-75-1) and the HER-enriched (SK-BR-3) cell lines had also significantly higher IKKε expression than non-transformed breast epithelial cell line, MCF10a with 6.5 ±0.6 ($p<0.01$) and 4.7±0.5 ($p<0.05$) fold higher protein levels, respectively. There was no significant difference in IKKε expression between the luminal A MCF7 and MCF10A cells.

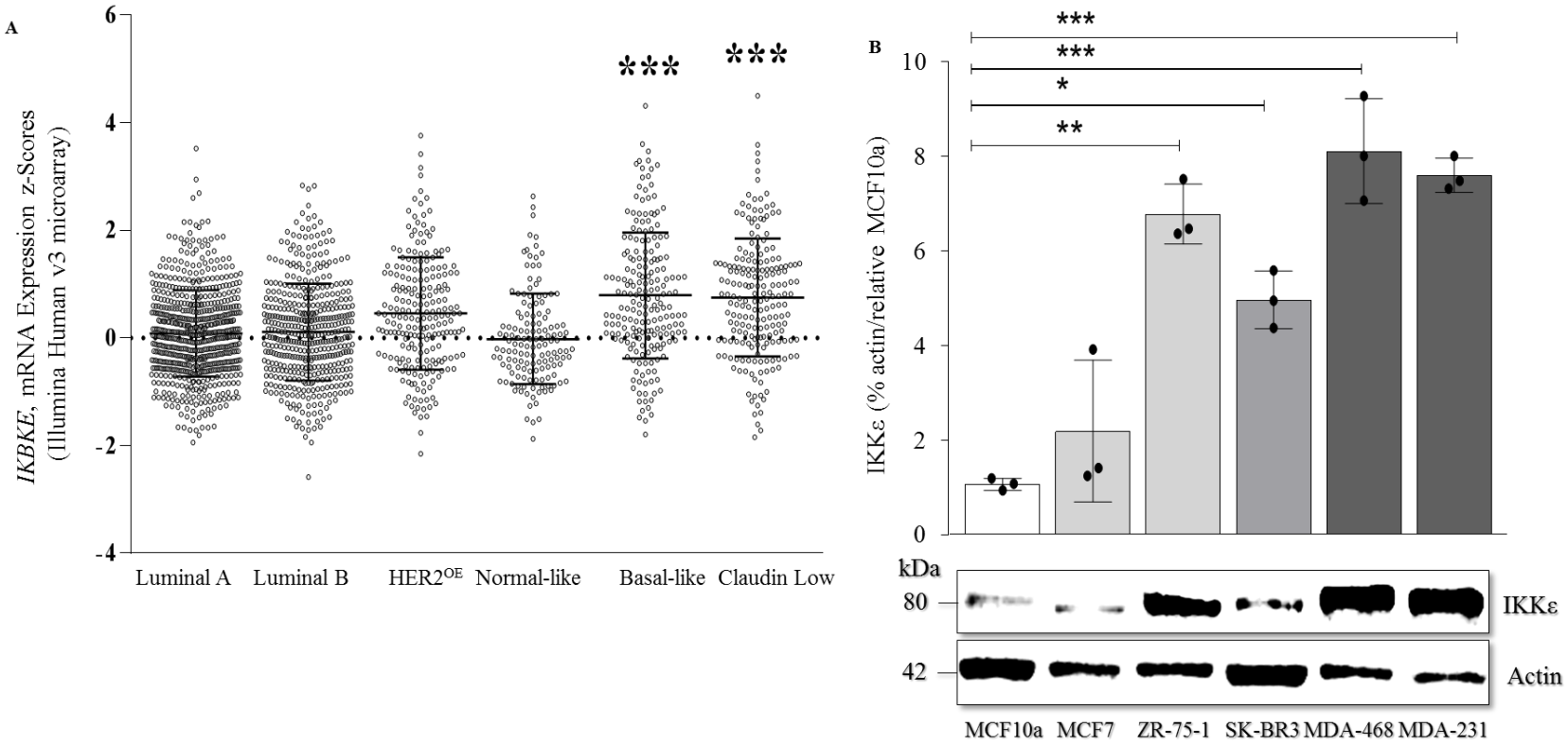

Figure 15. IKBKE expression is upregulated in basal-like and claudin low molecular breast cancer subtypes.

A) Analysis of the METABRIC study showed that *IKBKE* mRNA is most highly expressed in basal-like and claudin-low triple negative breast cancers compared to Luminal A, Luminal B, HER2-enriched, Normal-like molecular subtypes. *** $p < 0.001$ from total median. **B)** Western blot analysis of cell lysates from non-transformed breast epithelial cells (MCF10a), luminal A (MCF7), luminal B (ZR-75-1), HER2-enriched (SK-BR3), basal-like (MDA-468) and claudin-low (MDA-231) breast cancer cells showed IKKε is most highly expressed in basal-like and claudin-low triple negative breast cancer cells. Values are mean ± SD from 3 independent experiments. * $p < 0.05$; ** $p < 0.01$; *** $p < 0.001$ compared to non-transformed MCF10a

3.4.2 *IKBKE* CNVs are associated with reduced overall survival in TNBC

IKKε has previously been shown to be a breast cancer oncogene (Boehm et al., 2007). However, its role in tumour progression has never been evaluated. Therefore, I wanted to examine if there was an association between IKKε expression and overall survival in patients. Having shown there is an association with triple negative breast cancers, I analysed the METABRIC study survival data. These data (Figure 16) revealed that triple negative patients with gain or amplification of IKKε had a median overall survival of 78.6 months compared to those who were diploid who had a median overall survival of 99.7 months (21.1 month shorter overall survival, $p<0.05$). In a cohort of all breast cancer patients, *IKBKE* CNVs had no effect on overall survival in this study (Figure 16).

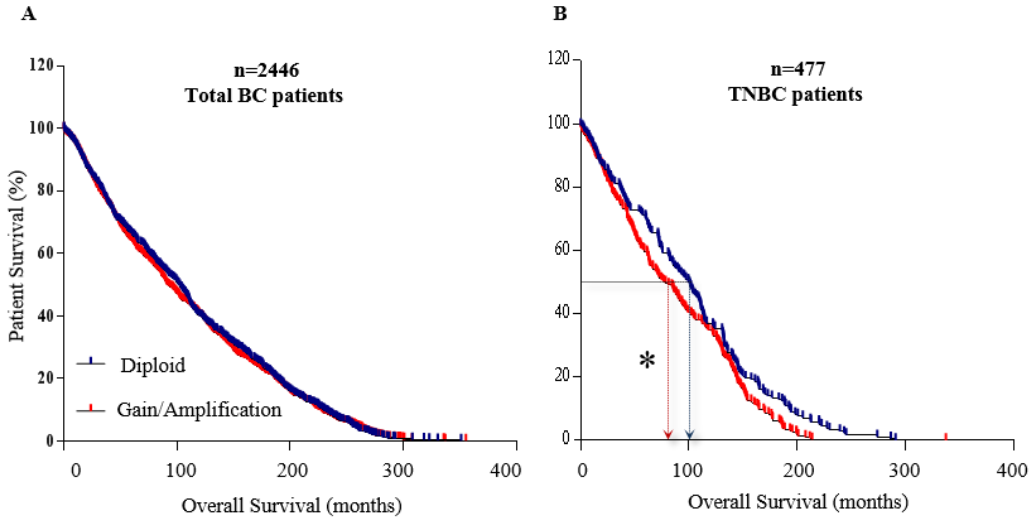

Figure 16. TNBC patients with IKBKE CNVs have significantly shorter overall survival
A) Combined retrospective analysis of the METABRIC and TCGA 2012 studies indicated that breast cancer patients with gain or amplification of IKBKE (n=1544) have no difference in overall survival to those diploid for IKBKE (n=871). B) Combined retrospective analysis of the METABRIC and TCGA 2012 studies indicated that breast cancer patients with triple negative and gain or amplification of IKBKE (n=285) have significantly reduced overall survival compared to triple negative breast cancer patients that are diploid for IKBKE (n=192) * $p<0.05$.

3.4.3 *IKBKE* CNVs are associated with bone metastasis

Breast cancer predominately metastasises to bone followed by lung, liver and brain. Thus I wanted to examine whether increased copy number of the *IKBKE* gene locus is associated with increased metastasis to common sites in patients. To do this I analysed data from the Metastatic Breast Cancer Project (provisional; n=155). In this study 13.79% of patient samples were diploid for *IKBKE*, 63.45% had duplications and 22.76% had amplifications of the *IKBKE* locus. Analysis of the metastatic locations, in Figure 17, shows that breast cancer patients with copy number variations of *IKBKE* had significantly more bone metastases compared with those who were diploid ($p<0.05$). Furthermore, when further stratified it was shown that an even higher percentage of patients who have amplifications of *IKBKE* developed bone metastases when compared to patients who were diploid for *IKBKE* ($P<0.05$). Interestingly, there was no difference between the percentage of patients in the two groups with lung, liver or CNS/brain metastases.

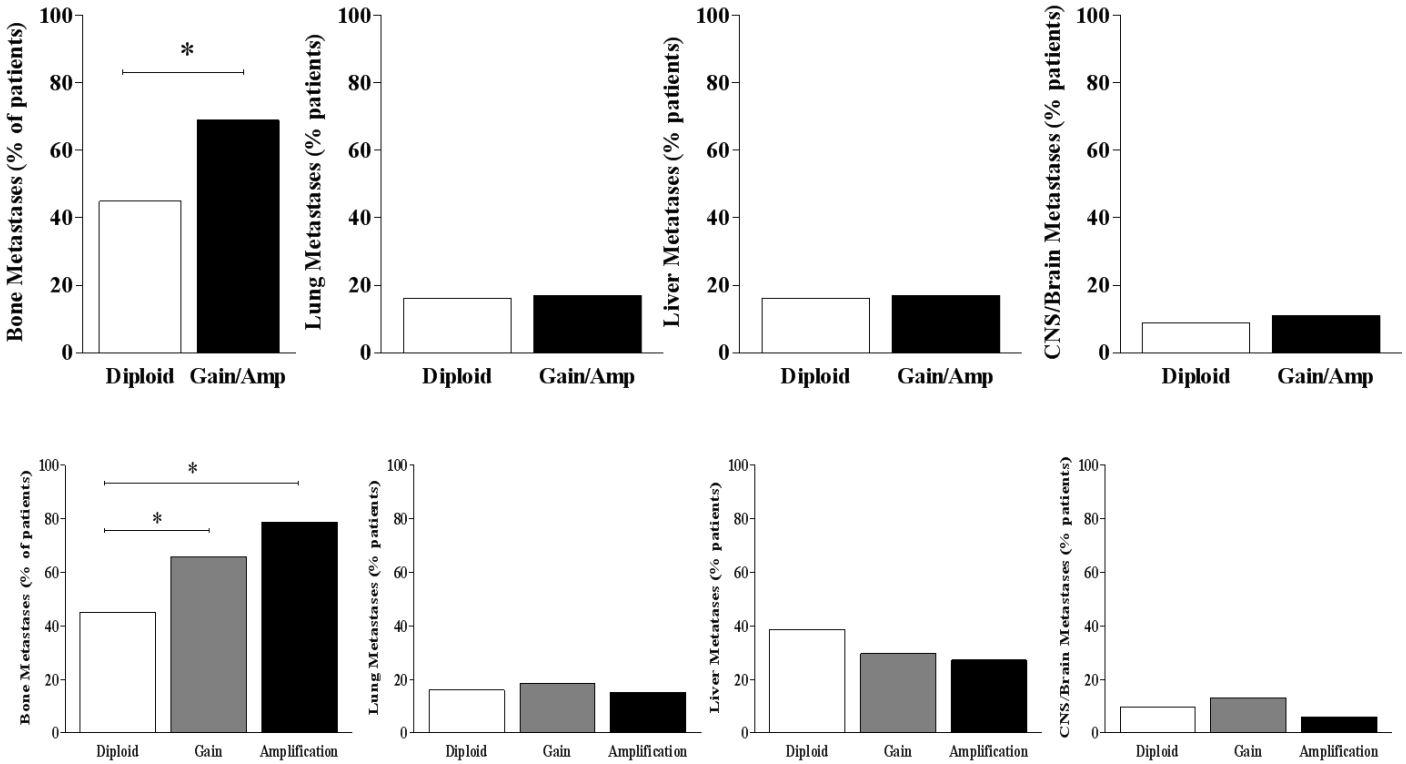

Figure 17. IKBKE CNVs are associated with bone metastasis.

Retrospective analysis of the association between *IKBKE* CNVs and site of breast cancer metastasis in the Metastatic Breast Cancer Project. The percentage of patients with metastasis at bone, lung, liver or CNS/brain. Diploid of *IKBKE* (n=31) ; Gain of *IKBKE* (N=91); Amplifications of *IKBKE* (n=33). * $p<0.05$ from diploid group.

3.4.4 **IKKε is expressed in both parental and osteotropic** MDA-MB-231 **breast cancer cells**

I had previously demonstrated that IKKε CNVs are associated with bone metastasis in breast cancer patients. Therefore, I assessed if IKKε was upregulated in the osteotropic human MDA-BT1 compared to parental MDA-MB-231 cells. As seen in Figure 18, IKKε was detected in both parental MDA-MB-231 and osteotropic MDA-BT1 cells, however, there was no significant difference in expression.

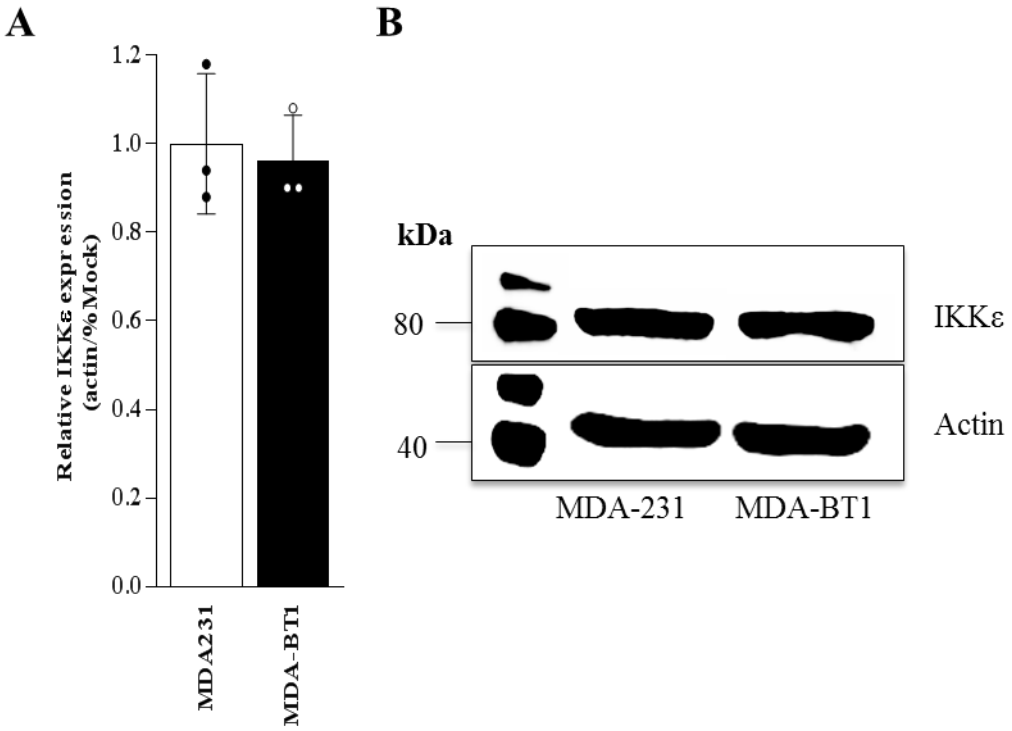

Figure 18. IKKε is expressed in triple negative parental and osteotropic MDA-MB-231**.**
A) Western blot quantification of cell lysates from human triple negative parental MDA-MB-231 and osteotropic MDA-BT1. Cell lysates were subject to western blot and probed with anti-IKKε and anti-Actin antibodies. Results are indicative of the mean from at least three independent results. B) Representative western blot photomicrograph from the experiment in A.

3.4.5 **IKKε expression was successfully knocked down in MDA-BT1 by shRNA**

To investigate the effects of IKKε inhibition on the metastatic behaviour of breast cancer cells I first stably knocked down IKKε in the human triple negative and osteotropic MDA-MB-231-BT cells using short-hairpin RNA (shRNA). MDA-MB-231-BT cells were transfected with a mock pLKO vector only containing a puromycin resistance gene or one of two independent shRNA constructs targeting IKKε were used to silence its expression. Following, one passage in standard DMEM after selection, cells were cultured in serum free medium and lysed. Lysates were collected at one, two and four weeks for the remaining experiments. Cell lysates underwent western blotting. Figure 19 shows that the two shRNA constructs successfully knocked down IKKε by 72.9% ±10.5 ($p<0.01$) and 86.7%±9.5 ($p <0.001$) for $IKK\varepsilon^{KD1}$ and $IKK\varepsilon^{KD2}$ respectively. Interestingly, the two IKKε mRNA targeting constructs also knocked down TBK-1 protein expression by 88.6 ±1.6 % ($p<0.001$) and 75.0 ±3.6% ($p <0.01$) for $IKK\varepsilon^{KD1}$ and $IKK\varepsilon^{KD2}$ respectively. Neither construct had any effect on the expression of the other IKK family of kinases namely IKKα and IKKβ.

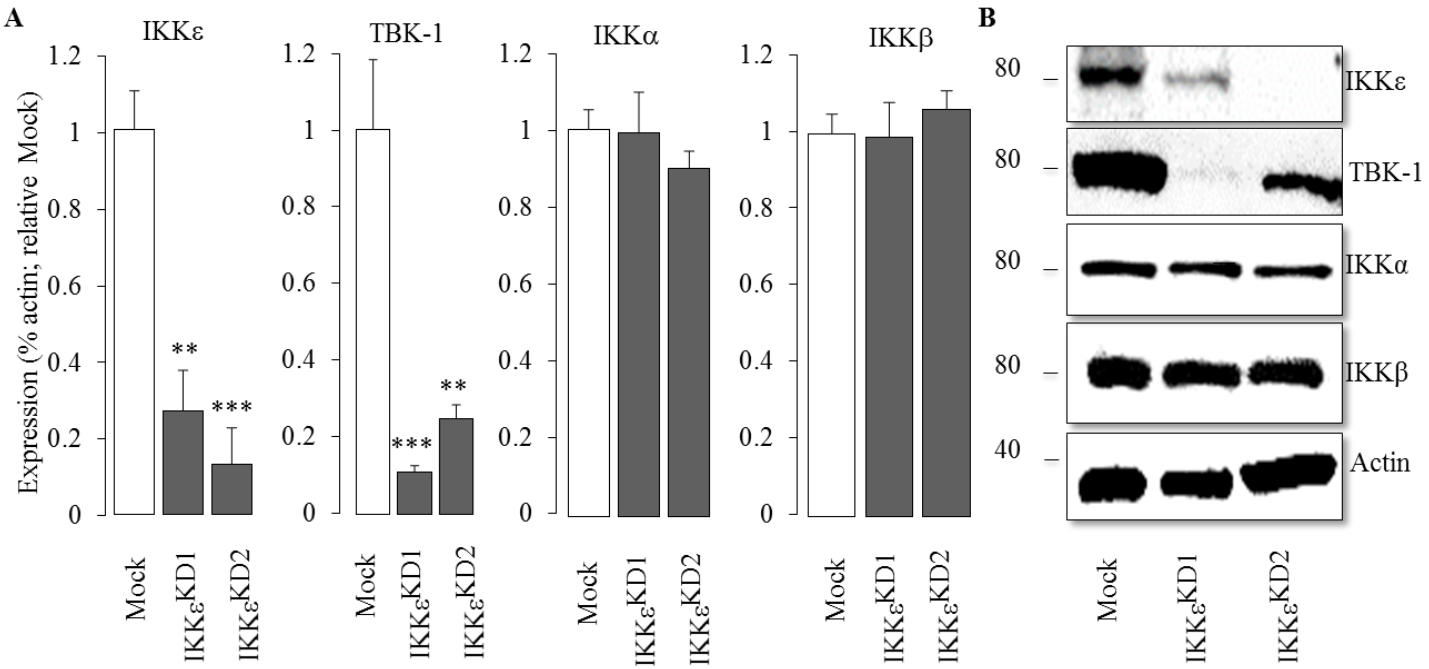

Figure 19. IKKε was successfully knocked down in MDA-231-BT using shRNA

A Western Blot quantification of the differential expression of IKKε, TBK-1, IKKα, IKKβ actin in total cell lysates obtained from mock control or MDA- BT1-IKKε^{KD1} and ^{KD2} breast cancer cells. **B** Representative images of the western blots described in **A.** Values are mean ± SD from at least three independent experiments; ** $p < 0.01$, *** $p<0.001$.

3.4.6 **IKKε was successfully overexpressed in MDA-BT1 using CRISPRa**

To further validate the role of IKKε in breast cancer bone metastases, I chose to also overexpress IKKε in the human triple negative and osteotropic MDA-BT1 cells using the Clustered Regularly Interspaced Short Palindromic Repeats Cas9 activation (CRISPRa) system. Lentiviral particles for CRISPR-Cas9 induced activation of IKKε or those containing a non-specific guide RNA as a control (mock) were incubated with MDA-BT1 cells as previously described. After selection, MDA-BT1 were cultured in selection-free medium for 72 hours and lysed. Lysates were subject to western blotting. As is evident in Figure 20, IKKε was successfully overexpressed in MDA-BT1 cells. CRISPRa led to a 5.2-fold increase ($p<0.05$) in IKKε expression in MDA-BT1IKKε^{OE} compared to MDA-BT1Mock cells. Overexpression of IKKε had no effect on protein expression of the homologous kinases TBK-1, IKKα, IKKβ (Figure 20).

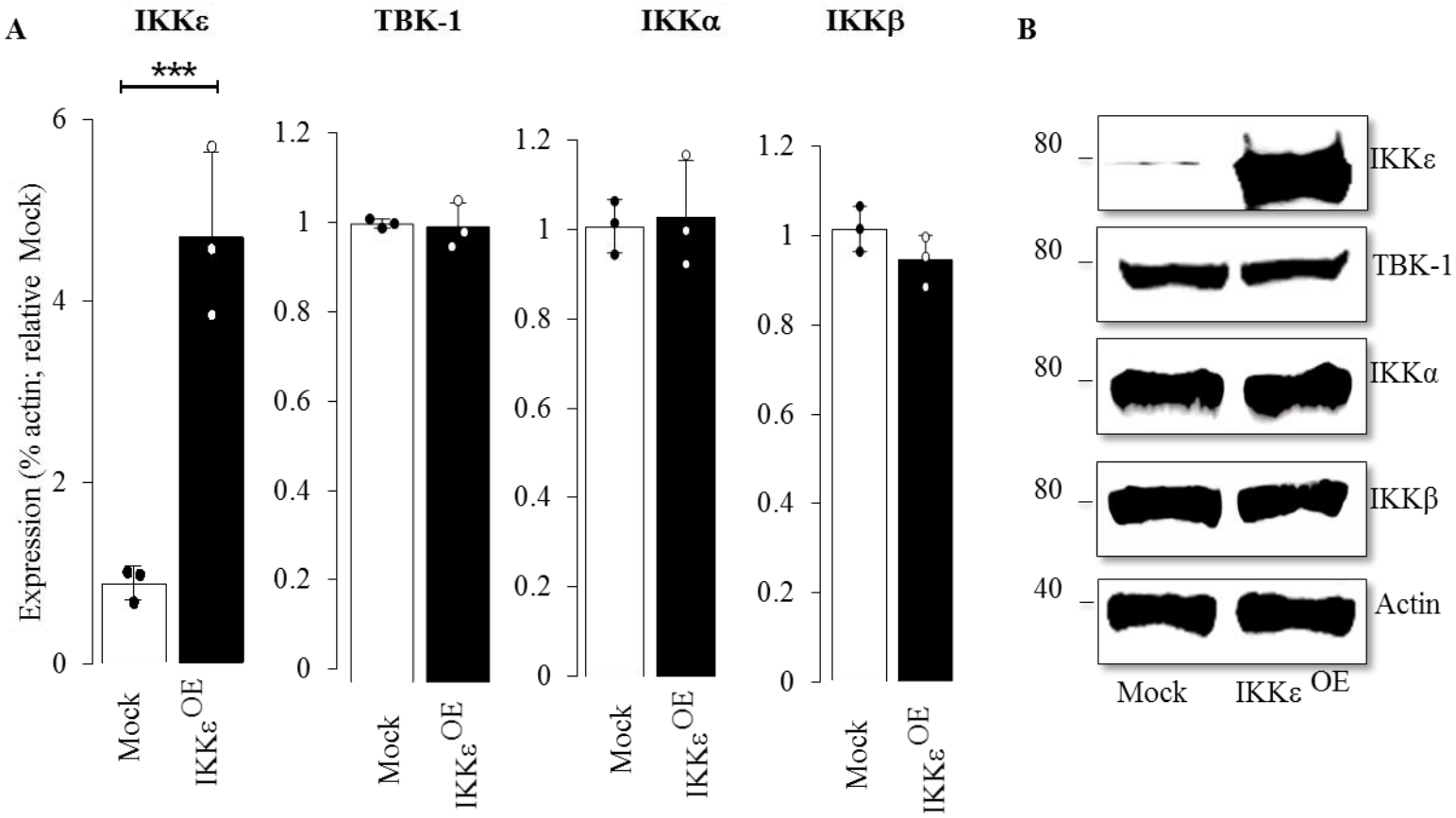

Figure 20. IKKε was successfully overexpressed in MDA-231-BT using CRISPRa.

A Western Blot quantification of the differential expression of IKKε, TBK-1, IKKα, IKKβ over actin in total cell lysates obtained from mock control or MDA- BT1-IKKε^{OE} breast cancer cells. B Representative images of the western blots described in A. Values are mean ± SD from at least three independent experiments; ** $p < 0.01$.

3.4.7 **Knockdown and pharmacological inhibition of IKKε reduces osteotropic breast cancer cell viability**

Several studies have indicated that inhibition of IKKε primary breast cancer cells reduces the viability and growth of primary breast cancer cells (Boehm et al., 2007, Barbie et al., 2014, Qin and Cheng, 2010). Therefore, I wanted to assess if IKKε regulates the growth and viability of MDA-BT1 cells. Firstly I wanted to examine how both knockdown and overexpression of IKKε in MDA-BT1 breast cancer cells affects cell viability (MDA-BT1 mock, IKKε^{KD1}, IKKε^{KD2} or MDA-BT1 mock and IKKε^{OE} cells were plated in a 96-well plate and allowed to grow in 1% FCS containing DMEM. Viability was assessed after 24, 48 (data not shown) and 72 hours (Figure 21). Knockdown of IKKε reduced MDA-BT1 cell viability by 20.3% ±1.7 (IKKε^{KD1}, p=0.003) and 37.3% ±6.4 (IKKε^{KD2}, p=0.001). Contrastingly, IKKε overexpression significantly increased MDA-BT1 cell viability by 31% ±1.2 (p<0.001) after 72 hours compared to MDA-BT1Mock (Figure 21).

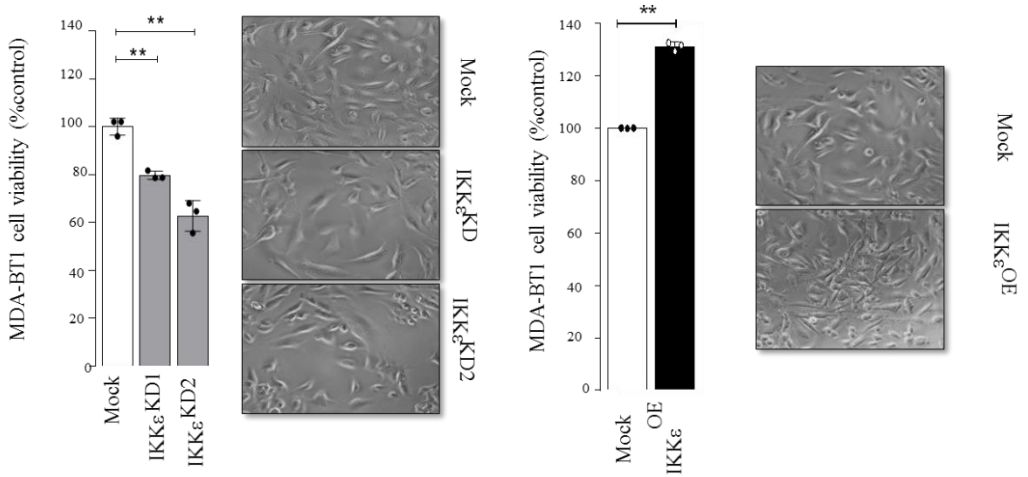

Figure 21. Knockdown of* IKKε *reduces MDA-BT1 cell viability whereas overexpression of* IKKε *enhances cell viability.

Panel (left) shows the viability of human MDA-BT1 mock (pLKO.1) and IKKε deficient MDA-BT1 ($IKK\varepsilon^{KD1}$ and $IKK\varepsilon^{KD2}$). Cell viability was determined using the Alamar Blue assay and expressed as a percentage of the values of the mock cells. Representative photomicrographs from cultures previously described are also shown. Right panel shows the viability of human MDA-BT1 mock (CRISPR) and IKKε overexpressing MDA-BT1 ($IKK\varepsilon^{OE}$) Representative photomicrographs from cultures previously described are also shown. The results shown are representative of three independent experiments. Values are mean ± SD from at least three independent experiments; ** $p < 0.01$ from mock control.

I also tested the effects of three verified IKKε inhibitors Amlexanox, CAY10575 and CAY10576 (Reilly et al., 2013) on the viability of MDA-BT1 cells using the Alamar Blue assay. As seen in Figure 22, at 30μM and 100μM all compounds significantly reduced MDA-BT1 viability after 48 and 72 hours of treatment. Although, no compound was able to give an accurate $IC_{50,}$ at 100μM Amlexanox (0.1% v/v) reduced MDA-BT1 viability by 37.5% ±3.6 after 72h in 1% FCS containing DMEM compared to DMSO (0.1% v/v) control.

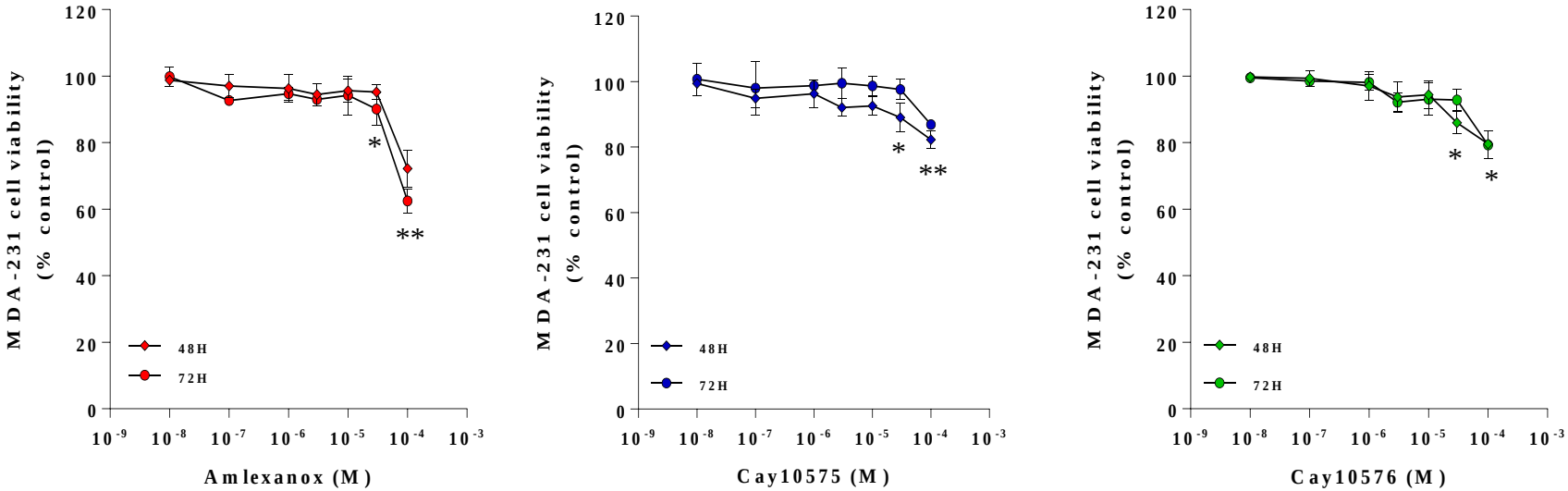

Figure 22. Pharmacological inhibition of IKKε reduces MDA-BT1 viability.

MDA-BT1 cells were plated in 96 well plates and treated with the indicated doses of Amlexanox, CAY10575 or CAY10576. Cell viability was determined using the Alamar Blue assay and expressed as a percentage of the values of the vehicle treated cells. Cell viability of the vehicle treated control was taken as 100%. Results shown are mean ± SD from at least 3 independent experiments from 48 and 72 hours of treatment. *p<0.05 **p<0.01, from vehicle treated MDA-BT1 human breast cancer cells. 72 hours of treatment. *p<0.05 **p<0.01, from vehicle treated MDA-BT1 human breast cancer cells.

3.4.8 **Amlexanox inhibited** IKKε**-driven growth in osteotropic breast cancer cells**

Once I established the effects of these compounds on the endogenous levels of IKKε, I tested the effects of Amlexanox on cell overexpressing IKKε. Amlexanox (10μM) had no effect on MDA-BT1 Mock cell viability (Figure 23). However, in stark contrast, Amlexanox (10μM) completely abolished IKKε driven cell viability (Figure 23) in MDA-BT1 IKKε^{OE}($p<0.01$).

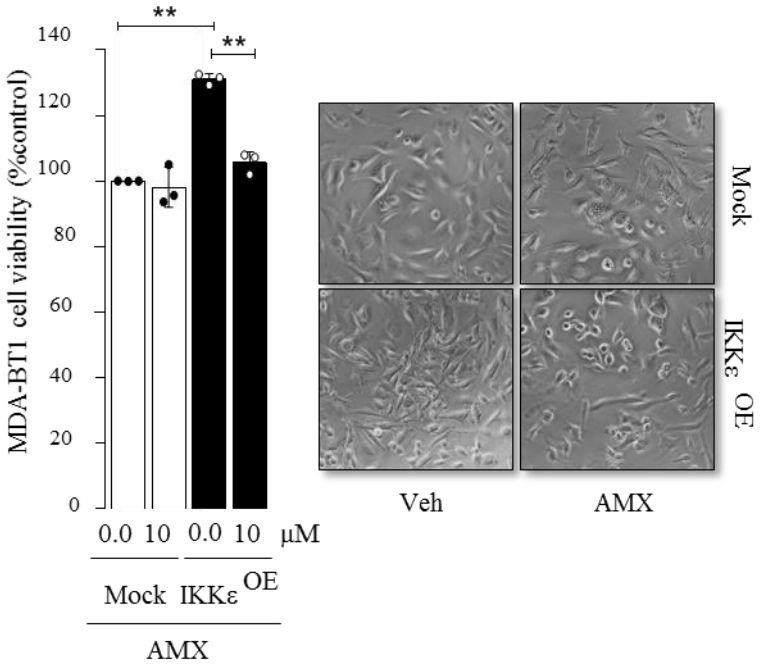

Figure 23. Amlexanox inhibits* IKKε*-driven MDA-BT1 viability.

The viability of human MDA-BT1 Mock and IKKε overexpressing MDA-BT1 (IKKε^{OE}) treated with either vehicle DMSO (0μM) or Amlexanox (10μM) after 72 hours. Representative photomicrographs from cultures previously described are also shown. The results shown are representative of three independent experiments. Values are mean ± SD from at least three independent experiments; ** $p < 0.01$ from vehicle-treated mock control. $^{++}$ $p < 0.01$ from vehicle-treated MDA-BT1 IKKε^{OE}.

3.4.9 **Knockdown and pharmacological inhibition of IKKε reduces osteotropic breast cancer motility**

Several studies have shown that IKKε contributes to breast cancer cell motility (Qing and Cheng, 2010). Here, I assessed the effects of pharmacological and shRNA mediated inhibition of IKKε on MDA-BT1 directional 2D migration using the wound healing assay (section 2.2.6.1). As shown below in Figure 24 and Figure 25, knockdown of IKKε reduced MDA-BT1 2D directed migration by 18.3% ±8.1 and 20.4±5.6% respectively after 12 hours compared to mock MDA-MB-231 ($p<0.01$). Similarly treatment of Mock MDA-BT1 with 10μM Amlexanox reduced 2D directed migration by 15.6 ±8.6% ($p<0.05$) after 12 hours when compared to vehicle treated mock cells. No difference in cell number was observed at the end of the experiment (16 hours) as assessed by the Alamar blue assay (Figure 24).

I also assessed the effects of overexpression of IKKε bone tropic MDA-MB-231 directional 2D migration using the wound healing assay. As shown in Figure 24 and Figure 25, overexpression of IKKε enhanced MDA-MB-231-BT1 2D directed migration by 21.1 ± 2.9% after 8 hours compared to mock MDA-MB-231-BT1 ($p<0.05$). I also treated IKKε overexpressing MDA-BT1 with Amlexanox (3μM), which completely abolished the effects of IKKε overexpression on cell migration.

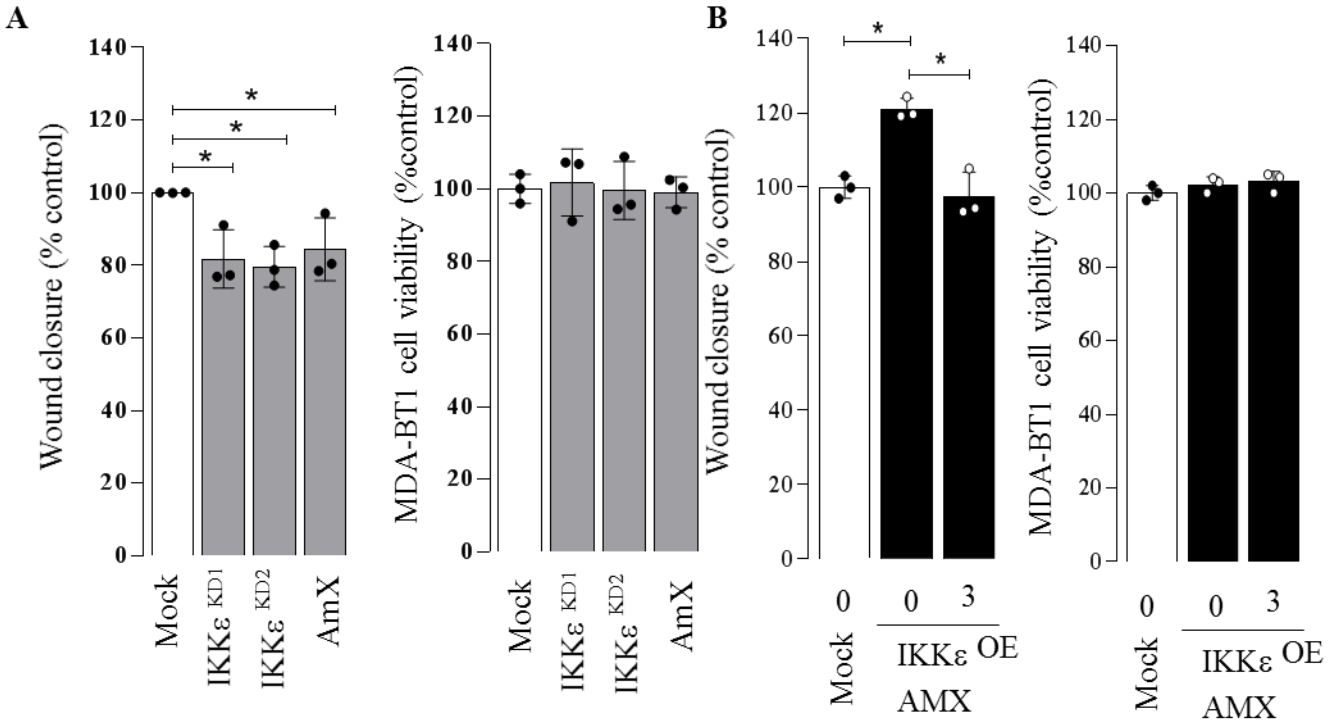

Figure 24. Inhibition of IKKε reduces MDA-BT1 2D cell migration whereas overexpression of IKKε enhances 2D cell migration

A (Left) shows the 2D directed migration of human MDA-BT1 mock (pLKO.1) and IKKε deficient MDA-BT1 ($IKK\varepsilon^{KD1}$ and $IKK\varepsilon^{KD2}$) after 12 hours. Migration was analysed using T-scratch software following a scratch assay. (Right) shows the cell viability at the end of the experiments (16 hours) and was determined using the Alamar Blue assay and expressed as a percentage of the values of the mock cells. B (Left) shows the 2D directed migration of human MDA-BT1 mock (CRISPR) and IKKε overexpressing MDA-BT1 ($IKK\varepsilon^{OE}$) treated with DMSO or Amlexanox 10μM at 8 hours. Migration was analysed using T-scratch software following a scratch assay. (Right) shows the cell viability at the end of the experiments (16 hours) and was determined using the Alamar Blue assay and expressed as a percentage of the values of the mock cells The results shown are representative of three independent experiments. Values are mean ± SD from at least three independent experiments; * $p < 0.01$ ** $p < 0.01$ from mock control; + $p < 0.05$ from DMSO treated MDA-BT1 $IKK\varepsilon^{OE}$.

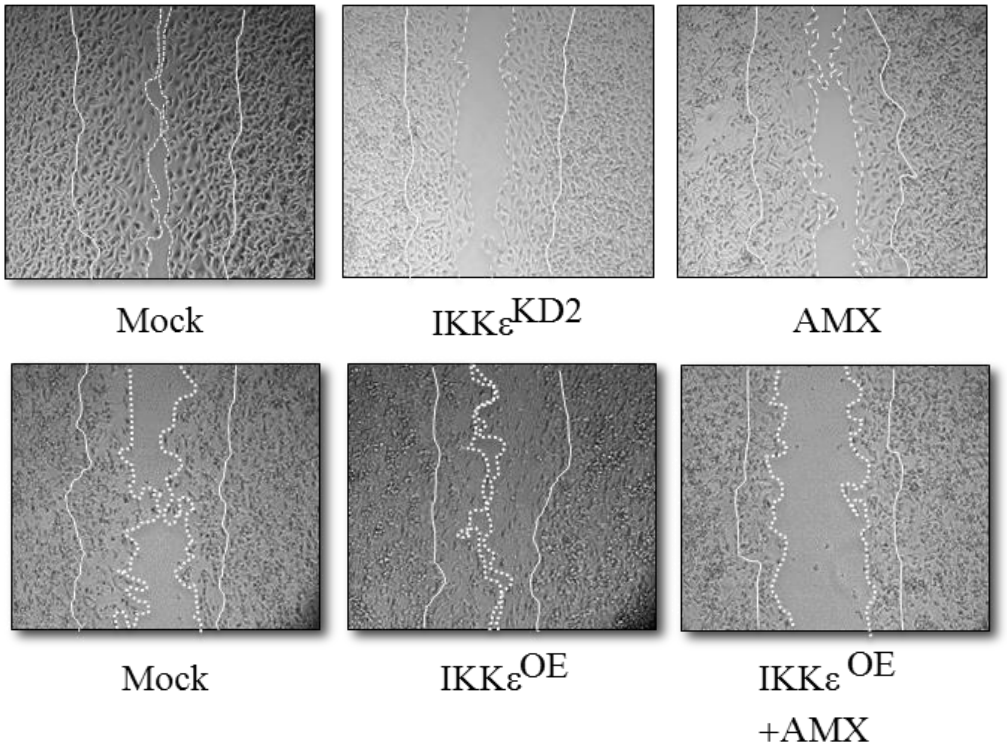

Figure 25. Pharmacological and shRNA mediated inhibition of IKKε reduces MDA-BT1 2D cell migration whereas overexpression of IKKε enhances 2D cell migration

Representative images from the experiments described in Figure 24.

3.4.10 **Knockdown and pharmacological inhibition of IKKε reduces osteotropic breast cancer invasion *in vitro*.**

A crucial stage in the metastatic process is the invasion of local tissues by tumour cells followed by extravasation into the circulatory system (Nguyen et al., 2009). Thus I assessed the effect of pharmacological inhibition, knockdown and overexpression of IKKε on the invasive capacity of MDA-BT1 cells using the transwell invasion assay (section 2.2.6.2). In brief, matrigel, an ECM-like substance, was coated over transwell inserts. MDA-BT1 deficient in or overexpressing IKKε or their relative controls were seeded on to the matrix in serum free medium containing either DMSO or Amlexanox. Standard DMEM was used as the chemoattractant in the bottom chamber (see section 2.2.6.2). Following 72 hours, cells were fixed, stained with H&E and quantified. As seen in Figure 26, both shRNA ($IKK\varepsilon^{KD1}$, 32.1± 5.7%, $p<0.01$ and $IKK\varepsilon^{KD2}$ 38.5± 3.5%, $p<0.01$) and pharmacological inhibition (42.2± 6.6%, $p<0.01$) of IKKε using Amlexanox reduced the invasive capacity of MDA-BT1 cells whereas overexpression was stimulatory (19.3± 7.5%, $p<0.01$). Again, addition of Amlexanox (3μM) to IKKε overexpressing MDA-BT1 cells completely prevented the IKKε driven invasiveness of these cells *in vitro*.

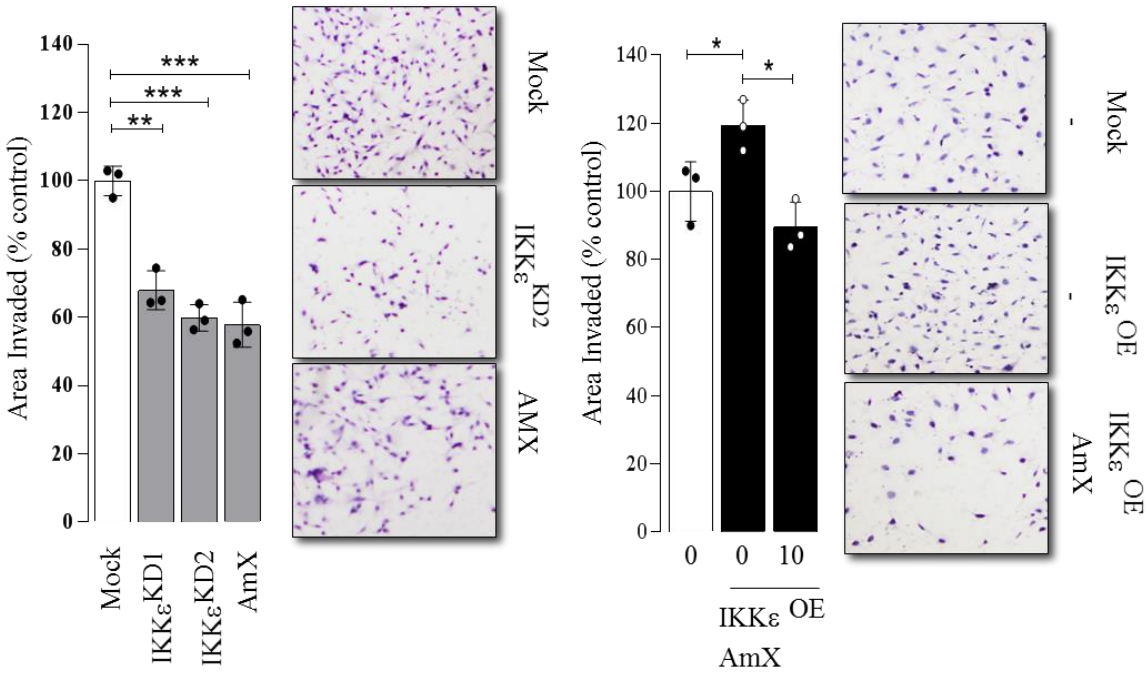

Figure 26. Pharmacological and shRNA mediated inhibition of IKKε reduces MDA-BT1 invasion whereas overexpression of IKKε enhances invasion

A (Left) shows the invasion of human MDA-BT1 mock (pLKO.1) and IKKε deficient MDA-BT1 ($IKK\varepsilon^{KD1}$ and $IKK\varepsilon^{KD2}$) or MDA-BT1 treated with Amlexanox (10μM) after 72 hours. (Right) Representative images from the experiment described. B (Left) shows the invasion of human MDA-BT1 mock (CRISPR) and IKKε overexpressing MDA-BT1 ($IKK\varepsilon^{OE}$) treated with DMSO or Amlexanox 10μM at 8 hours. (Right) Representative images from the experiment described. Invasive capacity was assessed by H&E staining; the area of invasive cells covered was quantified in Image J and assessed as a percentage of the relative MDA-BT1 mock. The results shown are representative of three independent experiments. Values are mean ± SD from at least three independent experiments; ** $p < 0.01$ from mock control; + $p < 0.05$ from DMSO treated MDA-BT1 $IKK\varepsilon^{OE}$.

3.4.11 **Knockdown and pharmacological inhibition of IKKε reduce NFκB activation in osteotropic breast cancer cells *in vitro***

The activation of the NFκB pathway through the phosphorylation and subsequent degradation of IκB proteins has been shown to be constitutively active in breast cancer cells (Adli and Baldwin, 2006). Additionally, NFκB activation has been shown to contribute to metastasis in breast cancer and other cancers (Huber et al., 2004, Park et al., 2006, Idris et al., 2009, Marino et al., 2018a). Both shRNA-mediated and pharmacological inhibition of IKKε have been shown to reduce MDA-BT1 cell viability, migration and invasion thus indicating a reduced metastatic potential. Therefore, I assessed the effects of shRNA-mediated and pharmacological inhibition of IKKε on the activation of IκBα (Figure 27). As shown in Figure 27, both shRNA ($IKK\varepsilon^{KD1}$ – 45.1± 11.6%, $p<0.05$; $IKK\varepsilon^{KD2}$ – 46.3 ± 5.0%, $p<0.05$) and pharmacological inhibition of IKKε (AmX100 – 48.4±18.2%, $p<0.05$) lead to a significant reduction in basal levels of phosphorylated IκBα when compared to vehicle treated MDA-BT1 cells. Consequently, $IKK\varepsilon^{KD1}$ (+34.8 ± 13.8%, $p<0.05$) and $IKK\varepsilon^{KD2}$ (+42.5 ± 12.6%, $p<0.05$) MDA-BT1 cells had significantly more IκBα protein overall compared to vehicle treated MDA-BT1 Mock cells suggestive of inhibition of IκBα degradation.

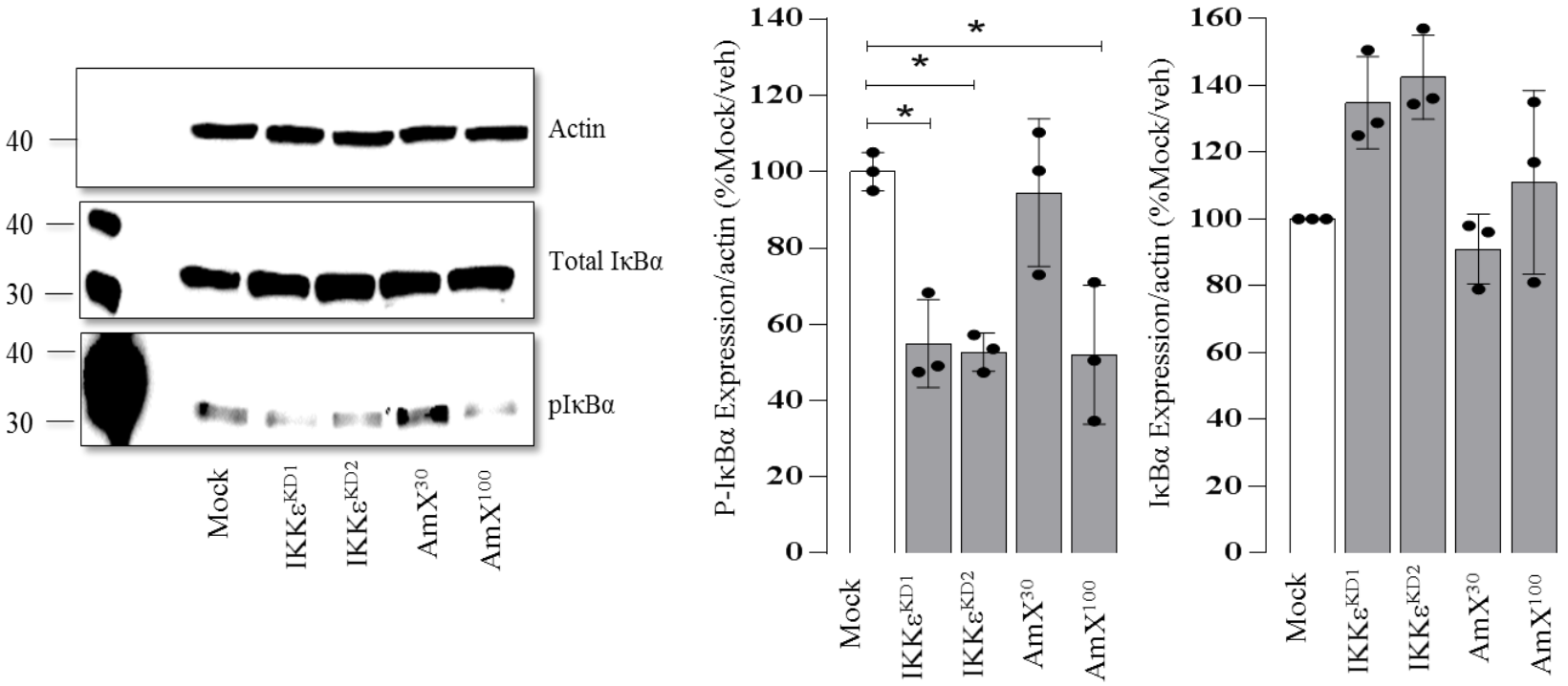

Figure 27. ShRNA- and pharmacological inhibition of IKKε reduces basal phosphorylation of IκBα and increases total IκBα in MDA-BT1 breast cancer cells

A Representative images of the western blots of the differential expression of serine-36 phosphorylated-IκBα (p- IκBα), total IκBα, over actin in total cell lysates of MDA-BT1. Lysates were obtained from mock control (pLKO.1)or MDA- BT1-IKK$\varepsilon^{KD1/KD2}$treated with vehicle or mock MDA-BT1 treated with the indicated concentrations of Amlexanox for 72 hours B Western blot quantification described in A. Values are mean ± SD from at least three independent experiments; * $p < 0.01$ from Mock vehicle treated MDA-BT1.

3.4.12 **IKKε driven breast cancer growth and motility is mediated through the NFκB pathway.**

Since IKKε was first suggested to be an oncogene, there have been various mechanisms that help to elucidate its role in tumourigenesis. Many of these have been via activation of transcription factors involved in survival and the production of proinflammatory factors. Boehm and colleagues showed, IKKε mediated tumourigenesis was conveyed through the NFκB pathway, specifically p65 and c-Rel. IRF3 has also been shown to be involved in antiapoptosis under genotoxic stress and in the production of pro-proliferative cytokines such as RANTES and IL-8 (Kim et al., 1999, Korherr et al., 2006). With this in mind, I assessed whether IKKε-driven breast cancer cell growth and motility was mediated through the NFκB and/or the IRF3 pathway. To do this, I knocked down key components of these pathways namely, TBK-1, IKKβ, p65 and IRF3 using pooled siRNA targeting in MDA-BT1-IKKε^{OE} and MDA-BT1 Mock cells. Each cell line was plated in 12-well plates and incubated with transfection medium and 5nM of the indicated siRNA or a scrambled siRNA (Scr). After 24, 48 and 72 hours, the cells were lysed and expression of indicated proteins was assessed using western blotting. After 24 hours no proteins were knocked down (data not shown) and after 48 hours IKKβ and p65 were not significantly knocked down (data not shown). However, after 72 hours all indicated proteins were successfully knocked down by their targeting siRNA in both MDA-BT1 mock and IKKε OE cells, whereas no significant difference was observed between protein expression between mock and IKKε^{OE} cells treated with scrambled siRNAs (Figure 28). TBK-1 expression was reduced by 89±6.2% ($p<0.001$) and 76.6 ±6.2% ($p<0.001$), IKKβ expression was reduced by 86.7 ±16.5% ($p<0.001$) and 67.4 ±25.8% ($p<0.01$), p65 expression was reduced by 43.2 ±22.5% ($p<0.05$) and 39.1 ±14.7% ($p<0.05$) and IRF3 expression was reduced by 87±4.0% ($p<0.001$) and 95.3±1.7% ($p<0.001$) in MDABT1 mock and IKKε^{OE} cells respectively.

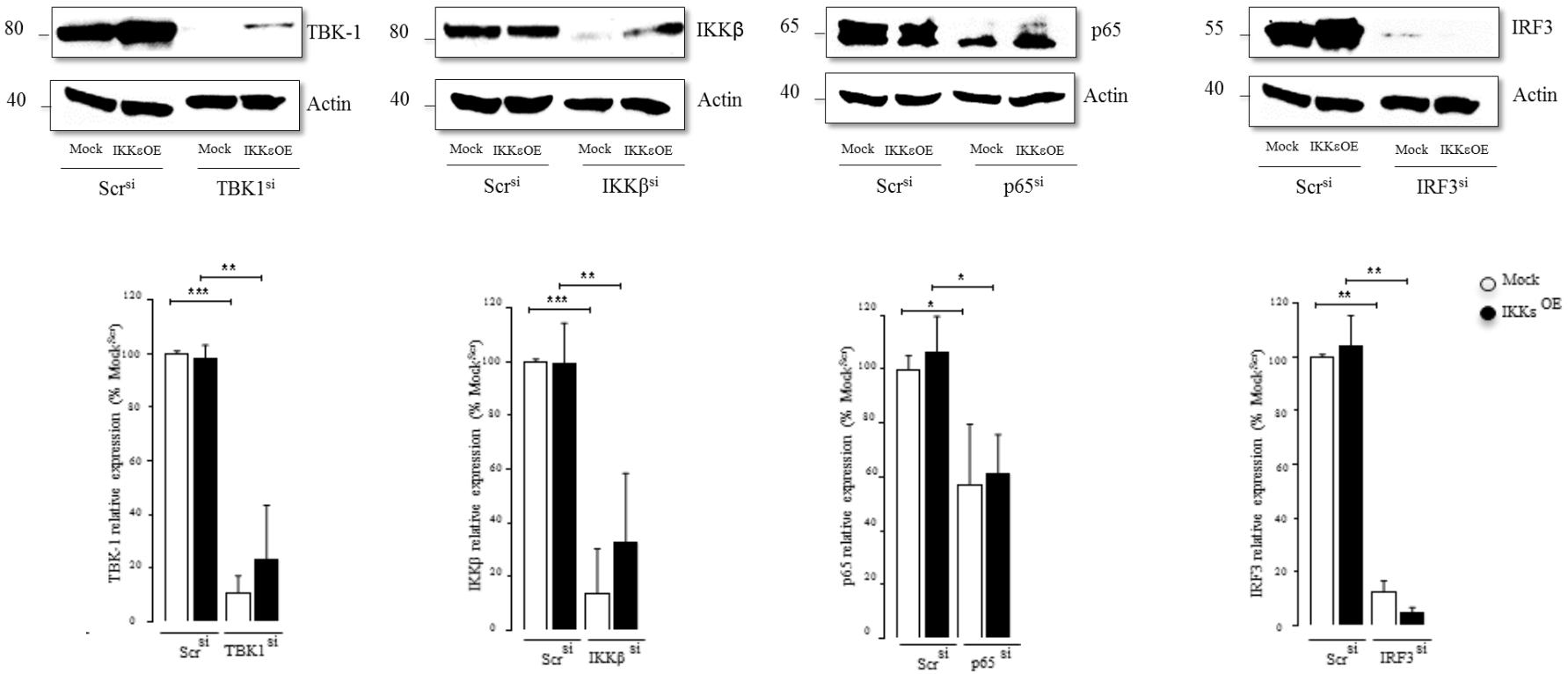

Figure 28.* TBK-1, *IKKβ, p65 and IRF3 were successfully knocked down by siRNA after 72 hours in MDA-BT1 Mock and IKKε^{OE}

(Top) Representative images of the western blots of the differential expression of TBK-1, IKKβ, p65 and IRF3 over actin in total cell lysates obtained from mock control or MDA- BT1-IKKεOE breast cancer cells treated with the indicated siRNA or a scrambled control (Scr). (Below) Western blot quantification of the respective siRNA knockdowns above. Values are mean ± SD from at least three independent experiments; Results are mean ± SD. * $p < 0.05$; ** $p < 0.01$; *** $p<0.001$.

After successful knockdown of each protein of interest I assessed the viability of these cells using Alamar blue assay. A non-transfected (NT) control was used as dsRNA in high concentrations induces cell death. After 72 hours, both NT and Scr treated IKKε^{OE} cells had significantly more cells compared to MDA-BT1 Mock controls. After 72 hours, only siRNA knockdown of IKKβ in MDA-BT1 Mock cells caused a significant reduction of viability (15.2± 1.5%; $p<0.05$) compared to Scramble siRNA treated control. SiRNA knockdown of IKKβ and p65 reduced MDA-BT1 IKKε^{OE} cell viability by 24.0 ± 5.3% ($p<0.05$) and 29.8 ± 5.5% ($p<0.05$) respectively compared to Scramble siRNA treated MDA-BT1 IKKε^{OE} cells.

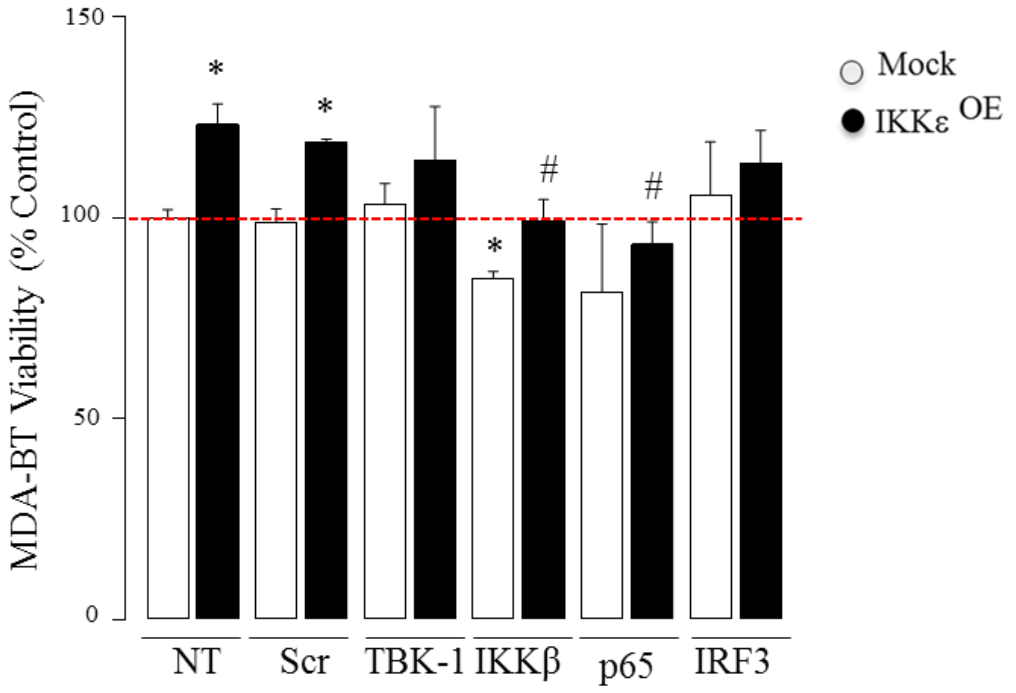

Figure 29. SiRNA knockdown of IKKβ and p65 inhibits IKKε-mediated increased cell viability.

MDA-BT1 Mock or IKKε^{OE} were plated in 12-well plates and treated with the indicated siRNAs, a scrambled siRNA or not transfected. Cell viability was measured after 72 hours using the Alamar Blue assay. Results are mean ± SD. * $p<0.05$ from Scr^{si} Mock; # $p<0.05$ from Scr^{si} IKKε^{OE} MDA-BT1 cells. Red dotted line indicates MDA-BT1 Mock baseline.

Overexpression of IKKε in MDA-BT1 lead to increased migration as assayed by the wound healing assay. Therefore, I aimed to explicate which pathway contributed to IKKε driven migration in these cells. Cells were plated and treated with indicated siRNA as before. After 72 hours, when confluence was reached migration was assessed using the wound healing assay (see section 2.2.6.1). As shown in Figure 30, overexpression of IKKε increased migration by 35.7 ± 8.1 % (NT; $p<0.05$) and 27.0 ± 9.3% (Scr; $p<0.05$) when compared to MDA-BT1 $Mock^{Scr}$. Knockdown of TBK-1, IKKβ and p65 significantly reduced migration of MDA-BT1 Mock when compared to Scramble siRNA treated Mock cells (Figure 30). Additionally, knockdown of TBK-1, IKKβ, p65 and IRF3 all inhibited the IKKε-driven migration of MDA-BT1 $IKK\varepsilon^{OE}$ cells after 16 hours.

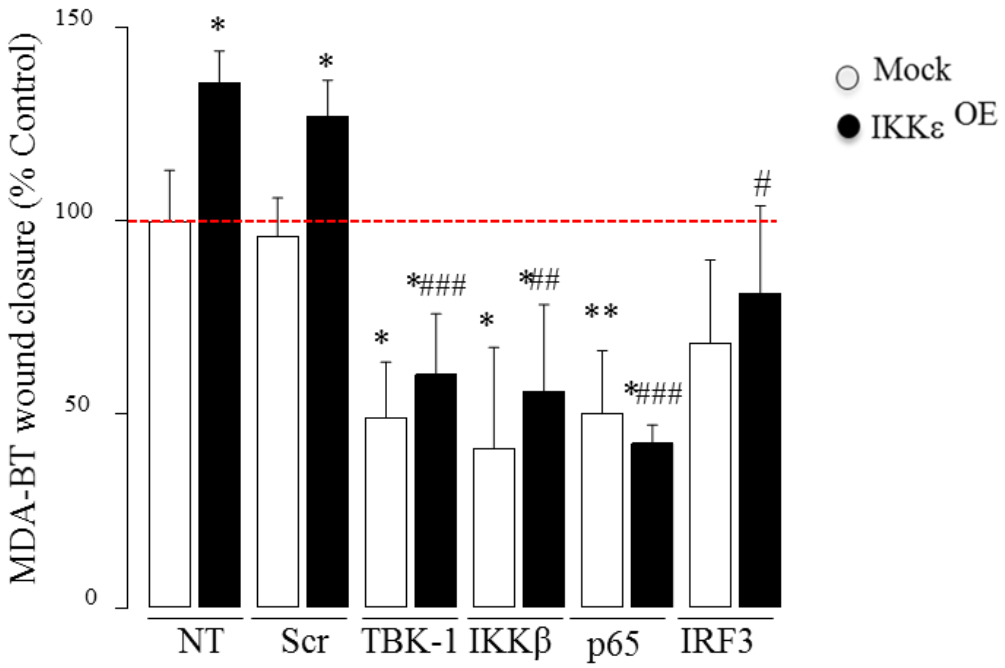

Figure 30. SiRNA knockdown of TBK-1***, IKKβ, p65 and IRF3 inhibit IKKε-mediated increased cell migration.***

MDA-BT1 Mock or $IKK\varepsilon^{OE}$ were plated in 24-well plates and treated with the indicated siRNAs, a scrambled siRNA or not transfected. After 72 hours, monolayer was scratched and cell migration was measure over time and analysed using T-scratch.. Results are mean ± SD. * $p<0.05$ from Scr^{si} Mock; ** $p<0.01$ from Scr^{si} Mock; # $p<0.05$ from Scr^{si} $IKK\varepsilon^{OE}$; ## $p<0.01$ from Scr^{si} $IKK\varepsilon^{OE}$; ### $p<0.01$ from Scr^{si} $IKK\varepsilon^{OE}$ MDA-BT1 cells. Red dotted line indicates MDA-BT1 Mock baseline.

3.4.13 **Amlexanox partially reduces primary tumour growth after 4T1-luc2 orthotopic injection**

IKKε has previously been described as a breast cancer oncogene, however, no compounds that directly inhibit IKKε have been examined on their ability to inhibit primary breast cancer growth (Boehm et al., 2007). Therefore, I tested the effects of IKKε on primary breast cancer tumour growth using the 4T1-Luc2 mouse breast cancer cells in syngeneic immunocompetent BALB/c. 4T1-Luc2 cells were injected orthotopically with $1x10^6$ cells being injected into each of the left and right mammary fat pads. The following day mice were injected with 1.5mg/kg D-Luciferin to check for tumour engraftment, where all mice developed tumours. The tumour was then measured with calipers. Mice were split in two groups (n=10/group) and administered vehicle (DMSO; 10% v/v in PBS), Amlexanox (35mg/kg/5-times-weekly (Figure 31A). The tumour volume was measured thrice weekly and was calculated using the volume of a sphere.

Treatments were initiated on day 0 (the day after orthotopic injection) and no significant effect was observed on primary tumour growth at days 3, 5 and 7 between vehicle- or Amlexanox -treated groups of mice. However, after day 9 the primary tumours of mice treated with Amlexanox showed a significant 31.73 ± 15.8% reduction ($p<0.05$).

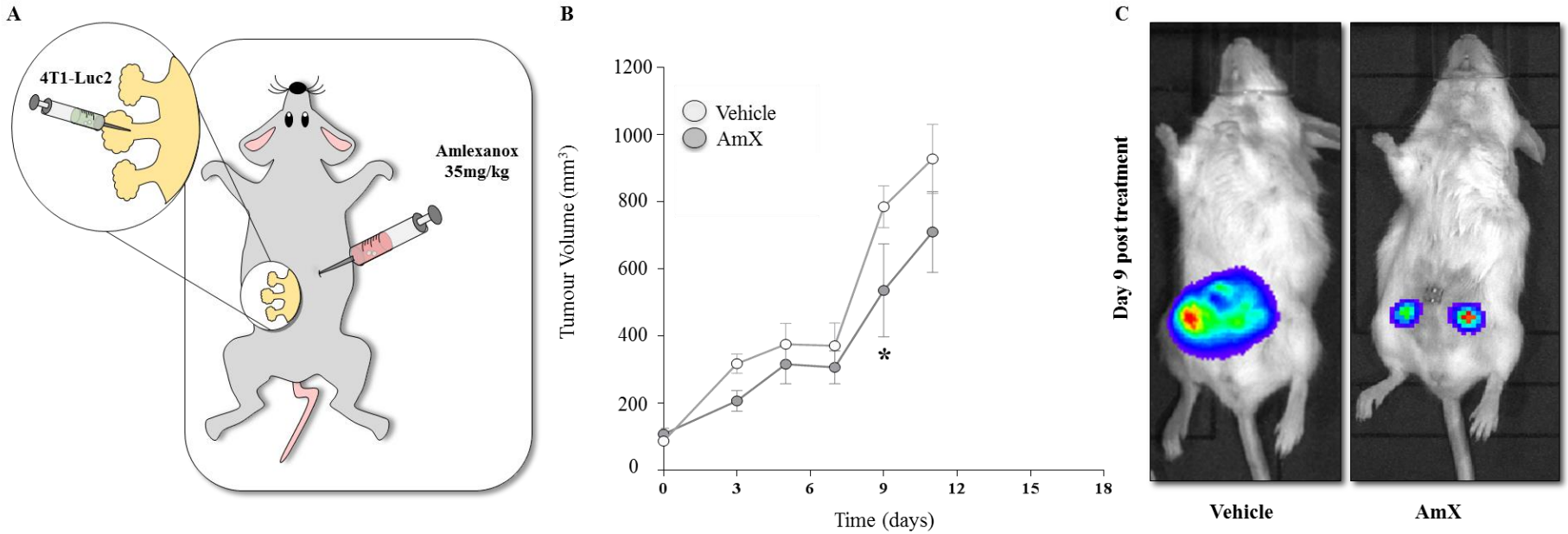

Figure 31. Treatment with Amlexanox partially reduces primary tumour growth of 4T1-Luc2 cells in vivo

A 4T1-Luc2 cells (1x10^6/100µl PBS/TB) were injected in to the left and right mammary fat pads of syngeneic BALB/c mice. Mice were split into four groups (n=10/group) and given daily i.p. injections of vehicle or Amlexanox (35mg/kg). B Primary orthotopic tumours were measured using callipers at the indicated time points. C. Mice were injected with D-luciferin and imaged using the IVIS system. Results shown are mean values ± SEM. * p<0.05 from vehicle treated group. Related to ***Figure 57***.

3.4.14 **Amlexanox reduces mouse 4T1 breast cancer metastatic growth *in vivo* following intracardiac injection**

In order to examine the effect of systemic IKKε inhibition on breast cancer cell skeletal growth we injected mouse 4T1-Luc2 breast cancer cells intracardiacally to mimic the dissemination of cancer cells throughout the circulatory system**.** *In vivo* bioluminescence of 4T1-Luc2 cells was detected every second day until the end of the experiment**.** Daily treatment with Amlexanox (35mg/kg) via i**.**p injection was initiated the following day**.** 4T1-Luc2 cells were detected in the hind limbs of mice 3 days after initial injection of cells in both vehicle and Amlexanox treated groups. Moreover, after 11 days of treatment Amlexanox reduced hind limbs tumour growth by 48.0 ±19.3% (Figure 32)

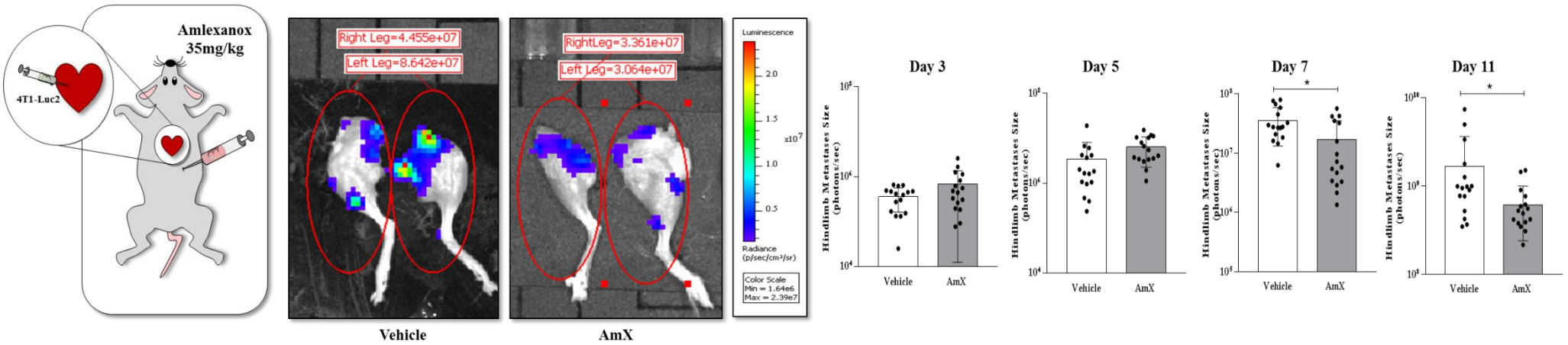

Figure 32 Amlexanox reduces skeletal tumour growth following intracardiac injection of 4T1-Luc2 mouse breast cancer cells

4T1-Luc2 cells ($1x10^5$/100µl PBS) were injected in to the left ventricle of syngeneic BALB/c mice. Mice were split into two groups (n=8/group) and given daily i.p. injections of vehicle or Amlexanox (35mg/kg) Development and relative size (photons/s) of hind limb metastases were monitored thrice weekly using the IVIS system. Results are mean values± SEM. *$p<0.05$ from vehicle treated mice.

As breast cancers, especially triple negative disease, spread to other sites in the body, namely lung, liver and brain in patients, I also looked at the general metastatic spread of the mouse 4T1-Luc2 cells. To do this I selected the body of the mouse quantified the metastatic growth over time using LivingImage software. Again, Figure 33 shows that Amlexanox reduced the general metastatic growth after 10 days of treatment ($p<0.05$).

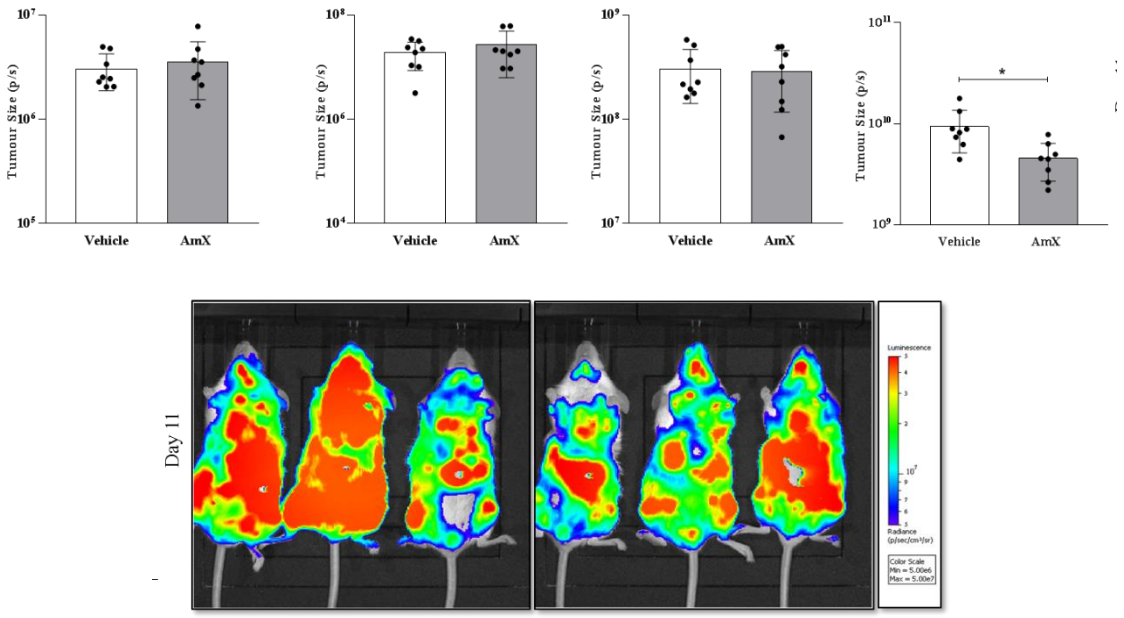

Figure 33. Amlexanox reduces general metastatic tumour growth following intracardiac injection of 4T1-Luc2 mouse breast cancer cells

4T1-Luc2 cells ($1x10^5$/100µl PBS) were injected in to the left ventricle of syngeneic BALB/c mice. Mice were split into two groups (n=8/group) and given daily i.p. injections of vehicle or Amlexanox (35mg/kg) Development and relative size (photons/s) of general metastases were monitored thrice weekly using the IVIS system. Results are mean values ± SEM *p<0.05 from vehicle treated mice.

In order to determine the organotropism of 4T1-Luc2 cells and in which organs Amlexanox reduced the growth of metastatic breast cancer, immediately following sacrifice and dissection, bioluminescence of the organs and hind limbs were assessed. Intracardiac injection of 4T1-Luc2 lead to the development of detectable metastases in the hind limbs (tibia and femur), lungs, liver, spleen and kidneys of mice (no brain metastases were detected). Bioluminescent signals were quantified using Living Image software. All eight mice per group developed metastases in the organs shown in Figure 34.

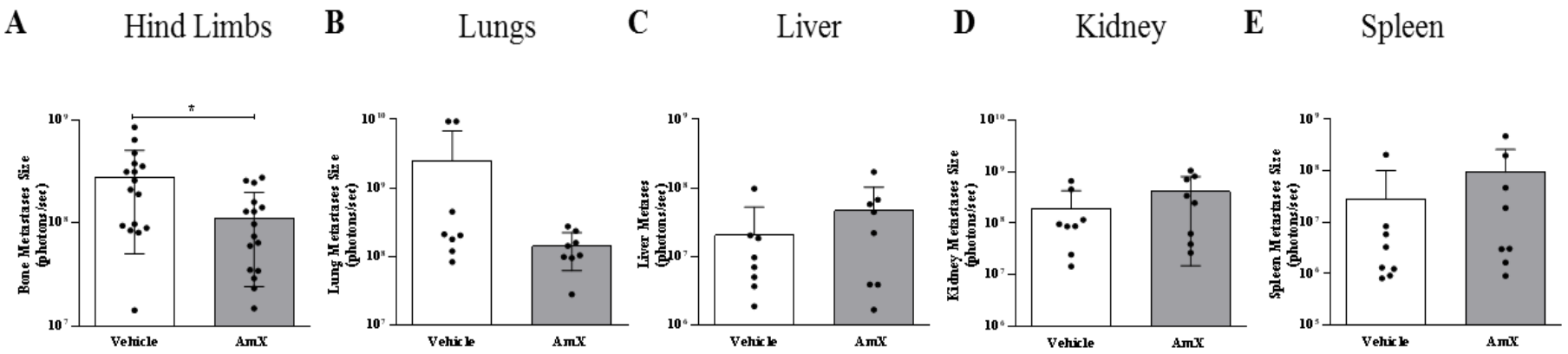

Figure 34. Amlexanox significantly reduced the size of skeletal hind limb but not metastatic lung, liver, kidney or spleen metastases of 4T1-Luc2 cells.

4T1-Luc2 cells (1x10^5/100µl PBS) were injected in to the left ventricle of syngeneic 6-week old immunocompetent BALB/c mice. Mice were split into two groups (n=8/group) and given daily i.p. injections of vehicle or Amlexanox (35mg/kg). After sacrifice, internal organs were collected and bioluminescence was detected. Relative size (photons/s) Hind Limbs (A), lungs (B), liver (C), kidney (D) and spleen (E) metastases are shown. All mice (8 per group) developed detectable metastases in these organs. . Results are mean values ± SEM ** $p<0.01$ from vehicle treated mice.

3.4.15 **Cancer-specific knockdown of IKKε in MDA-BT1 breast cancer cells reduces skeletal tumour growth *in vivo*.**

IKKε, a breast cancer oncogene, has been shown to contribute to the transformation of breast epithelial cells and the growth of cancer cells *in vitro* and *in vivo* (Boehm et al., 2007, Barbie et al., 2014, Qin and Cheng, 2010). However, the contribution of cancer-specific IKKε to breast cancer skeletal growth has not been investigated. In order to assess this, we injected MDA-BT1 Mock or MDA-BT1 IKKε^{KD2} cells intratibially in to female athymic BALB/c- nu/nu mice. The development of osteolytic lesions were monitored using weekly X-ray images (Figure 13). Mice were sacrificed after 21 days. Tumour bearing legs were processed and sectioned. Tumour size following TRAcP and eosin staining was determined on the Osteomeasure software. All mice in both groups (n=5 mock; n=7 IKKε^{KD2}) developed skeletal tumours, however, as seen in Figure 35, mice inoculated with MDA-BT1 IKKε^{KD2} cells had significantly smaller tumours (30.4±18.2%; $p<0.05$) than those inoculated with MDA-BT1-Mock cells after 21 days.

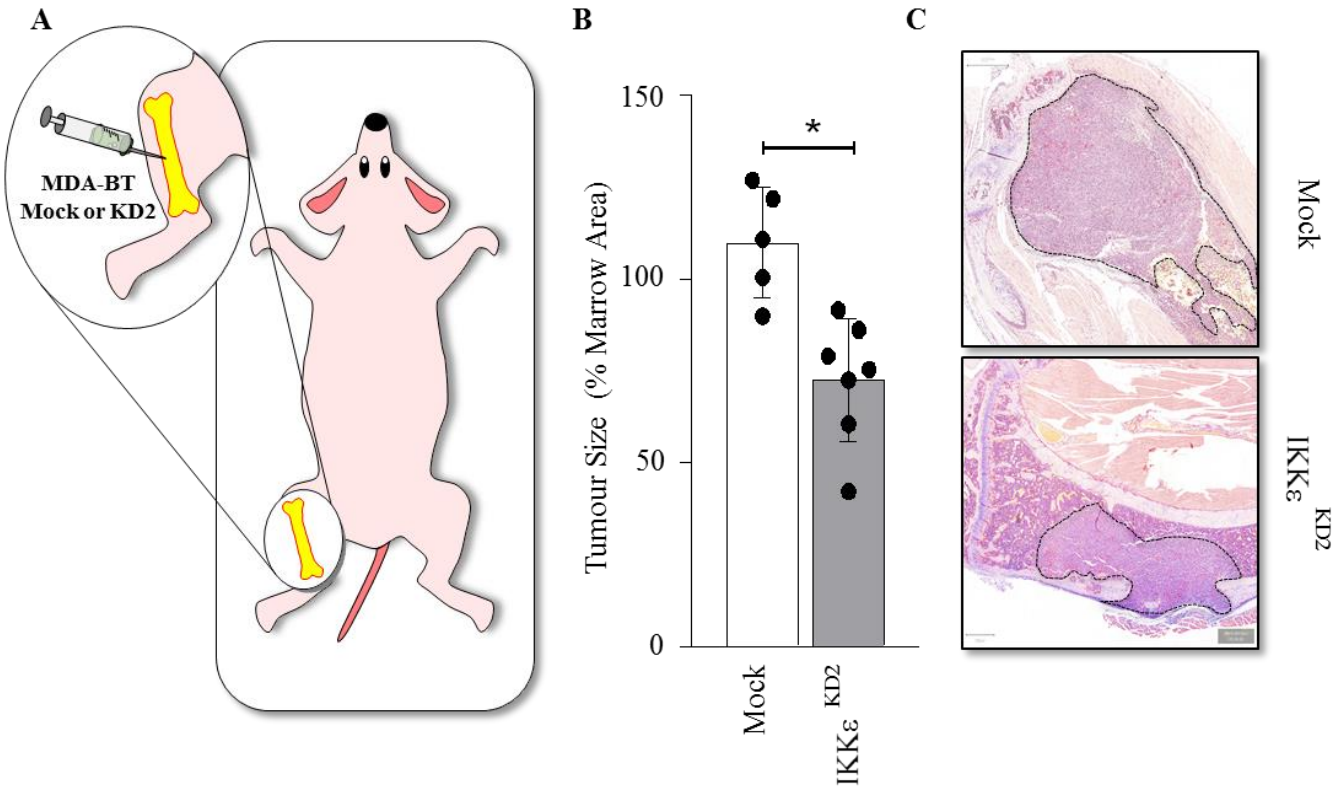

Figure 35. Breast cancer specific knockdown of IKKε reduces MDA-BT1 skeletal tumour growth in vivo

A) MDA-BT1 Mock (n=5) or IKKε^{KD2} cells (n=7) were injected intratibially in to athymic BALB/c nu/nu mice. The development of osteolytic lesions were monitored by x-ray. Mice were sacrificed 21-days post inoculation of tumour cells. B) Tumour Area was measured on histological sections stained for TRAcP and with H&E at 4x magnification on Osteomeasure software. Results are the mean ± SD from three non-consecutive depths. C) Representative Images from the experiment described in B. * $p<0.05$ from Mock MDA-BT1 tumours.

3.5 Discussion

IKKε has been implicated in breast cancer tumourigenesis and was found to be overexpressed in approximately 30% of breast cancer patient samples and 16% of breast cancer cell lines. Furthermore, several studies have shown the siRNA knockdown of IKKε reduces breast cancer cell growth, migration and invasion in various breast cancer cell lines (Boehm et al., 2007, Qin and Cheng, 2010).Upon overexpression, IKKε has been shown to phosphorylate and enhance IκB degradation leading to p65 activation and thus causing mammary oncogenesis. The aim of this chapter was to assess IKKε expression in breast cancer and to examine how IKKε contributes to breast cancer cell metastatic behaviour.

The development of sporadic breast tumours is thought to account for upwards of 90% of all breast cancers (Srihari et al., 2016). Whilst many breast cancers contain mutations in oncogenes and tumour suppressor genes, breast cancers are thought to be largely characterised by copy number variations (Ciriello et al., 2013). CNAs can affect cancer driver or suppressor genes and function to enhance development and ultimately the progression of cancers. Previous studies have shown that many IKKε overexpressing luminal breast cancer cell lines harbour an amplification of the *IKBKE* gene locus, whereas a subset of triple negative breast cancer cell lines were shown to overexpress IKKε without gene amplification. In this study, I combined the METABRIC and TCGA studies to look at CNVs of the IKKs and IKK-related proteins, IKKα and β and TBK-1 and IKKε respectively. This analysis confirmed that in primary breast cancers, IKKε is amplified in around a fifth of all breast cancer patients, whereas IKKβ was overexpressed in a tenth. Next, I looked to see if, IKKε mRNA expression was associated with any of the breast cancer molecular subtypes in the METABRIC study. Consistently, with Barbie and colleagues, I found that increased IKKε expression correlated with basal-like and claudin-low sub-types, which are generally considered triple negative (Barbie et al., 2014). In concordance with these results, western blot analysis of a panel of human breast cancer cell lines showed that IKKε was

overexpressed at the protein level in all breast cancer cells lines examined. Expression was significantly higher in the luminal B cell line ZR-75-1 and in the triple negative and highly metastatic basal-like MDA-468 and claudin-low MDA-MB-231 human breast cancer cell lines compared to the non-transformed breast epithelial cell line, MCF10a. Moreover, I assessed the effect of IKKε amplification and duplication on the survival of breast cancer patients in the aforementioned studies. When assessing all subtypes as a whole, IKKε overexpression/duplication had no effect on the overall survival of breast cancer patients. However, when looking at the survival of triple negative breast cancer patients, I found that those who were diploid for IKKε had a 21 months longer median survival than those with amplification or duplication. Unlike ER+ and HER2 amplified breast cancers, triple negative breast cancers have no known druggable targets, therefore these data indicate the a subset of triple negative breast cancers may benefit from inhibitors that target IKKε.

It is the spread of breast cancer to vital organs that leads to the death of patients and not the primary breast cancer; therefore, we may speculate from these data that IKKε does contribute to diseases recurrence and/or metastasis in these triple-negative patients. Neither the METABRIC nor TCGA cohorts had data on the sites of metastasis of the patients, thus I analysed data from the on-going Metastatic Breast Cancer Project. Although this cohort was smaller, this analysis revealed that patients with copy number variations for *IKBKE* had increased tendency to develop bone metastasis, thus IKKε may be ideal target to prevent bone metastasis in breast cancer patients. These results further validate the role of IKKε and related proteins in the regulation of triple negative and bone metastatic breast cancer cells.

With this in mind, I assessed how cancer-specific IKKε contributes to bone tropic MDA-MB-231 (MDA-BT1) breast cancer cell growth, migration and invasion. Here, IKKε regulates the growth of triple negative osteotropic breast cancer cells. I have demonstrated that knockdown or pharmacological inhibition of IKKε significantly reduced the growth of MDA-BT1 cells. Additionally, IKKε

overexpression enhanced the growth of these cells. All three compounds, not previously tested on their ability to reduce breast cancer cell growth, significantly reduced MDA-BT1 cell viability at high concentrations. However these concentrations are unlikely to be reached *in vivo*. Qing and Cheng (2014) showed inhibition of IKKε reduced the proliferation of luminal A MCF7 and HER2-enriched SK-BR-3 human breast cancer cells, not by inducing apoptosis as shown by annexin-V and propidium iodide staining, but by arresting cells in the G0/G1 phase of the cell cycle through downregulation of Cyclin-D (Qin and Cheng, 2010). Future studies should aim to assess whether inhibition of cell viability knockdown of IKKε in triple negative breast cancer cells is carried out through a similar mechanism.

The spreading of primary breast cancer to secondary sites such as bone and lung requires that cells become motile, detaching from the underlying basement membrane, invading through the ECM and entering the bloodstream. Here I showed that breast cancer specific IKKε regulates cell motility. Both pharmacological and shRNA-mediated inhibition of IKKε reduced MDA-BT1 migration and invasion. Contrastingly, IKKε overexpression in MDA-BT1 cells enhanced both migration and invasion. Besides, addition of Amlexanox to these cells completely prevented the IKKε driven invasion. Previous studies have demonstrated that activation of NFκB inhibition using a non-phosphorylatable IκBα reduces the ability of MDA-MB-231 cells to invade *in vitro.* In agreement with this, I have showed that, both knockdown and pharmacological inhibition of IKKε reduces basal levels of IκBα phosphorylation, leading to increased total levels of IκBα suggestive of reduced NFκB pathway activation.

Knockdown of IKKε was achieved through a lentivirally delivered plasmid that produces IKKε targeting shRNA. This targeting IKKε shRNA had no effect on the expression of canonical IKKs alpha and beta. Surprisingly, TBK-1 was also downregulated in these cells. To ensure that this was not due to direct targeting of TBK-1 mRNA, I carried out a BLAST search of the target sequence. The BLAST

search revealed that the sequences had 100% similarity with IKKε mRNA and no similarity with TBK-1, indicating that the knockdown is most likely not due to off target binding. The observed knockdown could be due to a feedback mechanism between IKKε and TBK-1. Additionally, Amlexanox the verified IKKε inhibitor has also been shown to inhibit TBK-1 at similar concentrations (Reilly et al., 2013). Therefore, regardless of what the mechanism may be, I cannot discount the fact that some of the observed effects in these cells may be due to the combined inhibition of both IKKε and TBK-1.

Breast cancer that has metastasised to the bone is considered incurable (Roodman, 2009). The median survival for patients with secondary breast cancer in the skeleton is between 19 and 25 months. Furthermore, breast cancers, once in the skeleton, influence the cells of the bone to produce predominantly osteolytic/mixed lesions and this is associated with significant morbidities such as hypercalcaemia, bone pain and pathological fractures (Coleman, 2001). Once breast cancer cells have homed to the bone, they must survive and ultimately begin to proliferate. Encouraged by the results that targeting of IKKε could inhibit MDA-BT1 metastatic behaviour I assessed the effect of both IKKε knockdown within the cancer cells on skeletal tumour growth and systemic IKKε/TBK-1 inhibition with Amlexanox on breast cancer metastasis and primary tumour growth using three models.

Here we showed that IKKε inhibition reduced the skeletal growth of MDA-BT1 cells *in vivo* following intratibial injection. Similar studies have shown that inhibition of NFκB pathway through knockdown of RANK or IKKβ and expression of inactive IκBα inhibit the ability of breast cancer cells to grow in the bone (Zheng et al., 2014, Marino et al., 2018a, Park et al., 2006). In the syngeneic model of breast cancer metastasis, in which murine breast cancer 4T1-luc2 are injected intracardiacally in to mice, I observed a significant reduction in the skeletal growth of 4T1-luc2 cells with Amlexanox treatment. This is the first study to show that pharmacological inhibition of IKKε/TBK-1 with Amlexanox can reduce the ability of breast cancer cells to grow within the bone. Considering the

fact that many patients present with stage II or stage III disease, we were also excited to assess the potential of Amlexanox as an inhibitor of primary tumour growth using the syngeneic 4T1-luc2 orthotopic model. However, Amlexanox only reduced primary tumour growth of the aggressive 4T1-luc2 cells at one time point. This perhaps suggests that IKKε/TBK-1 inhibition is more effective at reducing skeletal growth as those cells that thrive in the bone microenvironment upregulate members of the NFκB pathway. To that end, Sadanandam and colleagues demonstrated through characterising the gene expression profile of syngeneic breast cancer cells of differing metastatic potential, grown within the tumour bone microenvironment upregulated NFκB pathway members.

Having shown that IKKε inhibition could reduce tumour growth in three models of breast cancer I sought out to assess the mechanisms of which IKKε inhibition could reduce tumour growth. In one approach, I attempted to delineate the molecular pathways through which IKKε may drive the breast cancer metastatic phenotype. To do this, I utilised siRNA to knockdown proteins in MDA-BT1 Mock and IKKε^{OE} cells. TBK-1 was chosen as it forms a complex with IKKε to activate the NFκB and IRF3 transcription factors. IKKβ was also chosen as previous studies have postulated that neither IKKε nor TBK-1 are true IKK proteins as they are unable to directly target both serines on IκBα for degradation but function to stimulate the canonical pathway and enhance p65 transactivation through direct phosphorylation. These experiments revealed that knockdown of IKKβ and p65 reduced IKKε-driven and basal growth of MDA-BT1 cells, indicating that the NFκB pathway is responsible for IKKε-mediated enhanced viability. Whilst investigating motility, knockdown of TBK-1, IKKβ, p65 and IRF3 all reduced basal and IKKε-driven growth suggesting that both the NFκB and IRF3 pathways and their regulated factors contribute to IKKε driven motility *in vitro*.

In conclusion, these collective data demonstrate that IKKε is overexpressed in a subset of triple negative breast cancer patients and these patients have a reduced overall survival and an increased tendency to develop bone metastasis thus indicating IKKε as a viable target for the treatment of metastatic breast cancer**.** For the first time, I have shown that IKKε regulates the growth and motility of a human

bone tropic triple negative breast cancer cell line *in vitro* and that its inhibition via shRNA or with commercially available selective compounds can reduce *in vitro* metastatic phenotype. Similarly, these studies are the first to show that breast cancer specific knockdown of IKKε reduces the ability of an osteotropic triple negative breast cancer cell line to grow within the skeleton. Whilst previous studies have pharmacologically targeted the IKKε-driven cytokine network to reduce primary tumour growth, we are the first to show that direct pharmacological inhibition of IKKε and TBK-1 with Amlexanox reduces both primary and metastatic tumour growth *in vivo*. Overall, we have shown that targeting of the IKKε/TBK-1 axis may be a suitable therapy for all stages of breast cancer.

Chapter 4

IKKε INHIBITION PROTECTS AGAINST OSTEOLYSIS *IN VIVO*

4 Chapter 4

4.1 Summary

Skeletal metastases are accompanied by the formation of osteolytic and/or osteoblastic lesions. Osteolytic lesions result in enhanced osteoclast formation and activity which results in excessive weak resorption whilst osteoblastic lesions are characterised by deposition of weak disorganised bone. Bone metastases are associated with poor quality of life, hypercalcaemia and pathological fractures.

The IKK/NFκB pathway plays an important role in bone metastasis and osteolysis (Idris et al., 2009, Marino et al., 2018a, Peramuhendige et al., 2018). Here, I have shown that inhibition of IKKε reduces breast cancer- and RANKL-induced osteoclast formation *in vitro*, whilst overexpression of IKKε enhanced osteoclast formation. Mechanistic studies revealed that IKKε-driven breast cancer support for osteoclast formation required expression of either the NFκB or IRF3 signalling pathways. Moreover, inhibition of IKKε in breast cancer cells reduced the expression of inflammatory cytokines involved in osteoclast formation and activity such as M-CSF, TNFα and MMP9. Importantly, both breast cancer specific and pharmacological inhibition of IKKε reduced breast cancer associated osteoclast formation and osteolysis *in vivo*. Overall, this chapter demonstrates that IKKε is an attractive druggable target for the treatment of advanced breast cancer and the arising skeletal complications.

4.2 Introduction

Breast cancer commonly metastasises to the bone, with upwards of 70% of patients with secondary exhibiting disease skeletal involvement (Coleman, 2001, Lipton et al., 2009). Breast cancers tend to spread to highly vascularised bones, those with red marrow, such as the pelvic bones, sternum, and ribs (Chen et al., 2017). Once there, breast cancer cells disrupt not only bone cell activity and bone remodelling but also the immune system and haematopoiesis.

Following arrival in the skeleton, breast cancer cells produce factors that ultimately lead to increased osteoclast numbers (Guise, 2000). Osteolytic lesions arise because of enhanced osteoclastic bone resorption. Metastases with a net loss of bone are deemed osteolytic whilst those with enhanced deposition of bone are termed osteosclerotic/osteoblastic. Although osteoclastic bone resorption and osteoblastic mineral deposition are linked and both thought to occur in early metastases, breast cancers, are majority osteolytic (Macedo et al., 2017). The symptoms and clinical manifestations of osteolytic lesions include bone loss, bone pain, nerve compression syndrome, hypercalcaemia, pathological fractures and a reduced quality of life (Waning and Guise, 2014).

Early researchers suggested that osteolytic lesions were a result of the compression of the bone by an expanding tumour, coupled with resorption by the tumour cells. Although there is evidence to propose that tumour derived MMPs from breast cancers can resorb bone *in vitro* and *in vivo* (Lee et al., 2001), it is largely well accepted that the increase in osteoclast formation and activity influenced by the tumour cells that drives the formation of osteolytic lesions (Clohisy et al., 1995, Clohisy et al., 2000).

The observation that breast cancers metastasise to the skeleton has led to the conception of the vicious cycle paradigm (Mundy, 1997). In this concept, bone-homing breast cancer cells produce numerous growth factors and cytokines that stimulate osteoclast formation and enhance their activity. This increased osteoclastic bone resorption leads to the release of bone matrix-stored growth factors such as TGF-β, Insulin-like growth factors (IGFs) BMPs, FGF and VEGFs that can enhance tumour cell growth and cytokine release thus sustaining

osteoclast hyperactivity and the vicious cycle of bone metastasis (refer back to section 1.2.2 and Figure 5)

Whilst osteolytic lesions may be driven by enhanced OC formation, there is evidence to indicate that bone loss in these scenarios is, in part, a consequence of osteoblasts inability to deposit new matrix. Evidence from the literature suggests that bone metastatic cancer cells produce factors that inhibit osteoblast number and differentiation such as DKK-1, whilst enhancing osteoblast-derived osteoclastogenic cytokines such as IL-1, IL-6 and IL-8. In addition, within extensive bone metastatic lesions osteoblasts are almost absent (Phadke et al., 2006).

It is well established that activation of NFκB within osteoclasts and their precursors is essential for their formation and activity. RANKL produced by cells of the osteoblast lineage is essential for osteoclast formation, whilst other cytokines such as TNFα, CD40L and IL-1 aid in osteoclast formation and survival (Boyce et al., 2015). Additionally, NFκB activity within osteoblasts inhibits their differentiation and ability to mineralise. Furthermore, recent studies have indicated that the cancer-specific activation of NFκB through various members of the pathway, including IκBα, TRAF2 and IKKβ, contribute to osteoclast formation and osteolytic lesions. This was shown to be due to the production of numerous osteoclastogenic cytokines, (Park et al., 2006, Peramuhendige et al., 2018, Marino et al., 2018a). However, no studies to date have assessed the role of IKKε on the ability of breast cancer cells to influence osteoclastogenesis, osteoblast differentiation, skeletal tumour growth or osteolysis.

4.3 Aims

The aim of this chapter was to investigate the role of IKKε in human breast cancer and bone cell interactions *in vitro* and breast cancer skeletal tumour growth and osteolysis *in vivo*. The aims of this chapter will be realised by examining:

- The effect of knockdown and pharmacological inhibition of IKKε on skeletal tumour growth and osteolysis *in vivo*.
- The effect of on RANKL-induced and breast cancer support for osteoclastogenesis.
- The effect of knockdown and pharmacological inhibition of IKKε on breast cancer ability to influence osteoblast viability, differentiation and activity.

4.4 Results

4.4.1 **Cancer specific IKKε regulates breast cancer support for osteoclast formation.**

Osteolytic lesions are characterised by an increase in osteoclast number, size and bone resorption that fuels the growth of the cancer cells. With this is mind, I assessed how IKKε in cancers cells and osteoclast precursors regulates breast cancer support for osteoclastogenesis. I isolated human and mouse osteoclast precursor cells (see section 2.2.7) and co-cultured together with MDA-BT1 (IKKε $^{KD1/KD2}$, IKKε^{OE} and control) cells and RANKL (100ng/ml) and M-CSF (25ng/ml) for a total of 5 days. As shown in Figure 36, overexpression of IKKε in osteotropic MDA-BT1 enhances their ability to support human osteoclast formation by 45.2 ±15.9% ($p<0.05$) compared to mock transfected MDA-BT1. Addition of Amlexanox (1μM) to these cultures, prevented the IKKε-driven increase in MDA-BT1 IKKεOE cultures ($p<0.05$). Conversely, knockdown of IKKε in MDA-BT1 reduced their ability to support osteoclast formation as evidenced by a reduction of 36.5 ±9.8% and 39.4 ±7.5% for IKKε^{KD1} and IKKε^{KD2} co-cultures respectively. Again, addition of Amlexanox (1μM) to MDA-BT1 mock cultures also reduced their ability to support osteoclast formation by 54.7 ±10.4% . In mouse bone marrow co-cultures, those cultured with IKKε^{KD1} and IKKε^{KD2} had a reduction of 36.8±8.9% ($p<0.05$) and 32.9±5.9% ($p<0.05$) when compared to MDA-BT1 mock co-cultures.

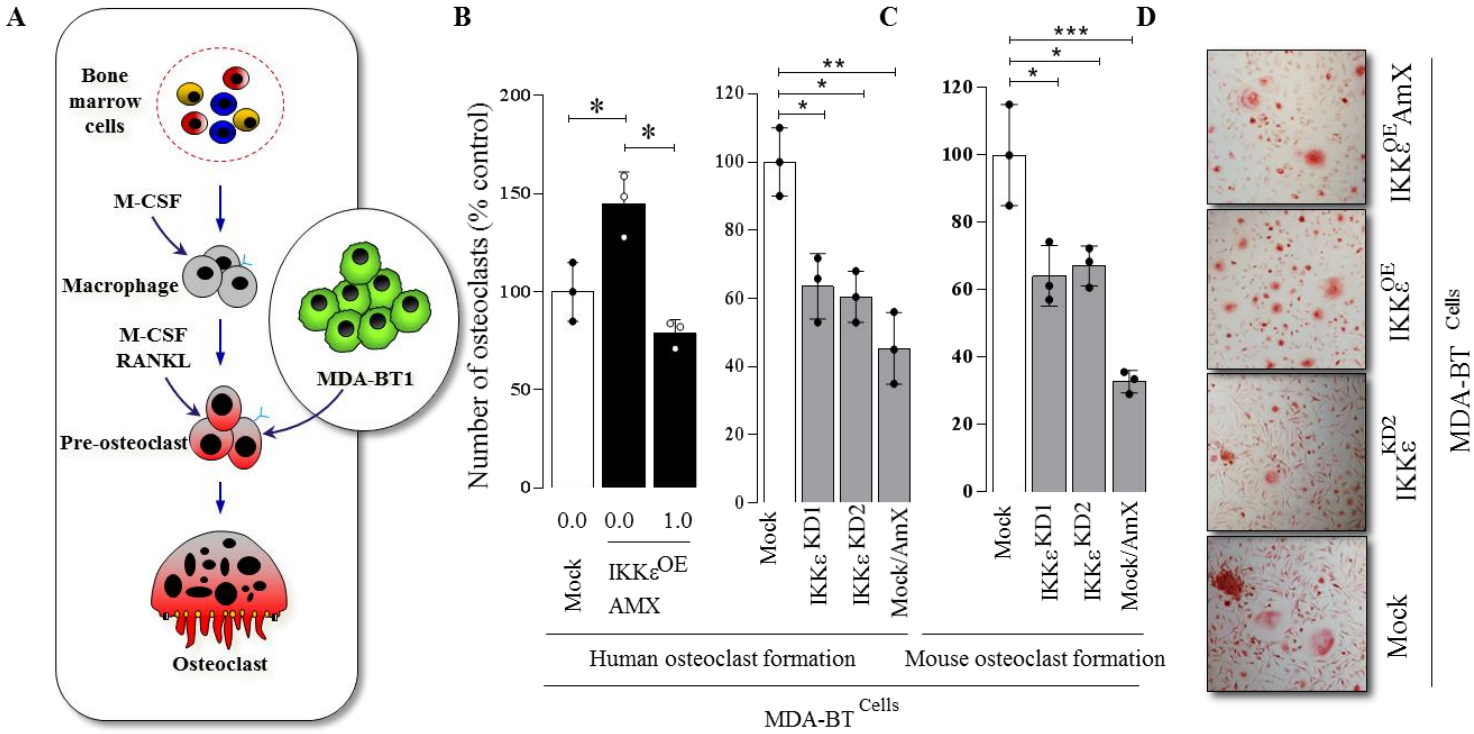

Figure 36. IKKε regulates breast cancer cell support for osteoclastogenesis

A) Schematic diagram of the experiment in B and C to generate osteoclasts. B) Number of human TRAcP+ multinucleated osteoclasts per well as a percentage of the Mock MDA-BT1 Cell treated well. AmX (1μM) or DMSO were added to the osteoclast precursors one hour before addition of Cells or cytokines (left) Number of human TRAcP+ multinucleated osteoclasts per well as a percentage of the Mock MDA-BT1 CM treated well. AmX (1μM) or DMSO were added to the osteoclast precursors one hour before addition of CM or cytokines (right). C) Number of mouse TRAcP+ multinucleated osteoclasts per well as a percentage of the Mock MDA-BT1 CM treated well. AmX (1μM) or DMSO were added to the osteoclast precursors one hour before addition of CM or cytokines. D) Representative images from the experiment in B

Breast cancers produce a number of factors that support osteoclast formation, therefore I wanted to see if IKKε supports osteoclast formation through the production of tumour derived factors. To do this I generated condition medium from MDA-BT1 IKKε deficient, IKKε overexpressing and their respective mock cells as previously described (section 2.2.4) and cultured it with mouse and human osteoclast precursor cells in the presence or absence of Amlexanox (Figure 37). Addition of MDA-BT1 IKKε^{OE} cell CM (10% v/v) to human macrophages increased osteoclast formation by 69.3± 6.3% ($p<0.01$) compared to MDA-BT1 Mock CM. Additionally, Amlexanox (0.3μM) completely prevented the increase in human osteoclast formation in cultures exposed to MDA-BT1 IKKε^{OE} condition medium. In accordance with these results, a reduction of 28.2± 5.1% and 34.7± 14.1% was observed in cultures exposed to MDA-BT1 IKKε^{KD1} and IKKε^{KD2} CM respectively, when compared to MDA-BT1 Mock CM. Moreover, Amlexanox (1μM) also significantly reduced MDA-BT1 Mock CM support for human osteoclast formation by 67.1± 9.9%. In mouse bone marrow cultures exposed to MDA-BT1 IKKε^{KD1} and ^{KD2} CM, a reduction of 54.6± 4.5% and 60.9± 2.1% respectively. Similarly, to human cultures, addition of Amlexanox to MDA-BT1 Mock CM treated murine osteoclast precursors reduced osteoclast formation by 81.7± 1.5% ($p<0.01$).

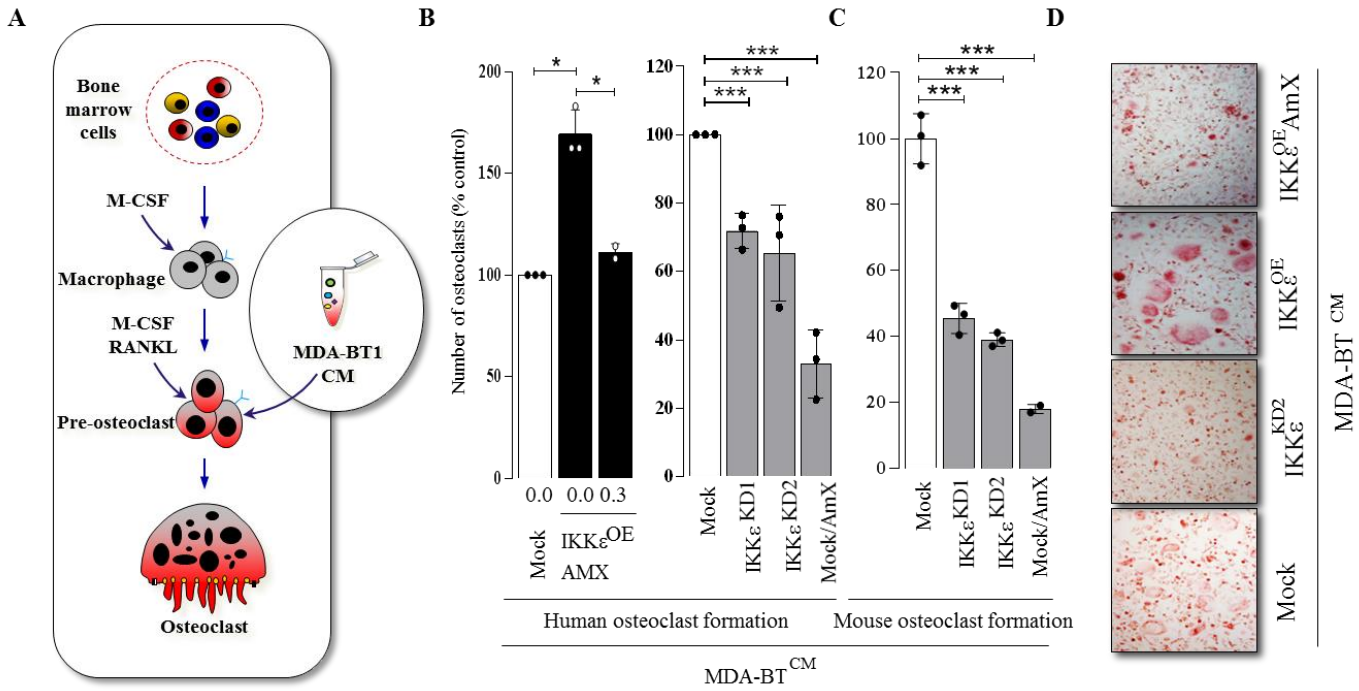

Figure 37. IKKε regulates breast cancer cell support for osteoclastogenesis through production of tumour derived factors.

A) Schematic diagram of the experiment in B and C to generate osteoclasts. B) Number of human TRAcP+ multinucleated osteoclasts per well as a percentage of the Mock MDA-BT1 CM treated well. AmX (0.3μM) or DMSO were added to the osteoclast precursors one hour before addition of CM or cytokines (left) Number of human TRAcP+ multinucleated osteoclasts per well as a percentage of the Mock MDA-BT1 CM treated well. AmX (1μM) or DMSO were added to the osteoclast precursors one hour before addition of CM or cytokines (right). C) Number of mouse TRAcP+ multinucleated osteoclasts per well as a percentage of the Mock MDA-BT1 CM treated well. AmX (1μM) or DMSO were added to the osteoclast precursors one hour before addition of CM or cytokines. D) Representative images from the experiment in B. *** $p<0.001$

4.4.2 **Knockdown of NFκB and IRF3 pathway inhibits** IKKε**-driven MDA-BT1 support for osteoclast formation**

In chapter 3, I showed that successful knockdown of the NFκB and IRF pathway members, namely TBK-1, IKKβ, p65 and IRF3 reduces IKKε-driven growth and migration in MDA-BT1 cells *in vitro*. I also wanted to assess which pathways were involved in IKKε-driven MDA-BT1 support for osteoclast formation, as both the NFκB and IRF3 pathways are known for regulating the production of proinflammatory factors and those involved in osteoclast formation. To do this, I used siRNA to knockdown TBK-1, IKKβ, p65 or IRF3 in both MDA-BT1 mock and IKKεOE and generated conditioned medium as described previously. The various conditioned medium (10% v/v) were added to RAW264.7 cells with 100ng/ml RANKL. Cultures were terminated after 120 hours. TRAcP staining was used to identify multinucleated (>3 nuclei) osteoclasts (see section 2.2.7). As seen in Figure 38, IKKε-over expression increases MDA-BT1 ability to support osteoclast formation *in vitro*. However, knockdown of TBK-1, IKKβ, p65 and IRF3 reduced osteoclast formation by 72.79±17.6% ($p<0.01$), 75.5±27.8% ($p<0.01$), 89.1±32.3% ($p<0.01$) and 103±24.5% ($p<0.01$) respectively compared to scramble treated MDA-BT1 $IKK\varepsilon^{OE}$ conditioned medium. Similarly, knockdown of TBK-1, IKKβ, p65 and IRF3 reduced support for osteoclast formation in Mock MDA-BT1 cells by 79.1 ± 21.5%, 55±9.8%, 32.5±8.1, 46.5±8.1% respectively compared to MDA-BT1 mock scramble conditioned medium.

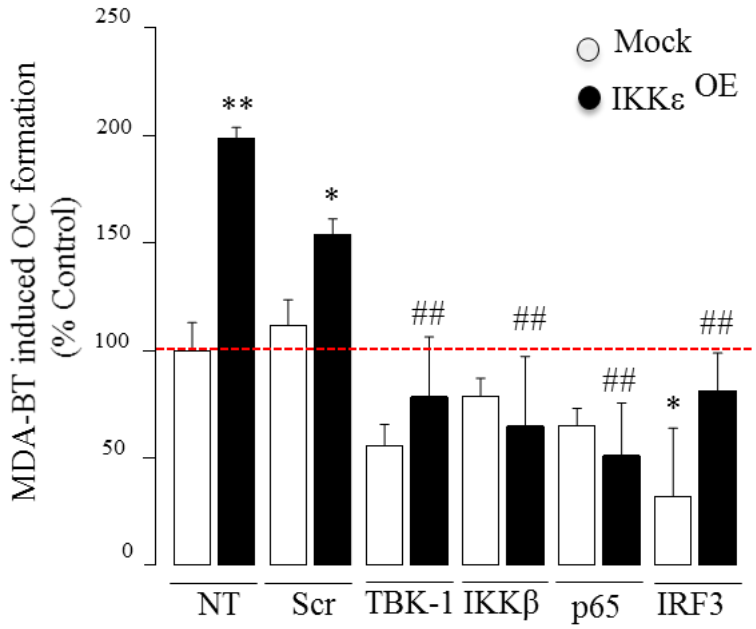

Figure 38. SiRNA knockdown of TBK-1, IKKβ p65 and IRF3 inhibits IKKε-mediated increased osteoclast formation.

MDA-BT1 Mock or IKKε^{OE} were plated in 12-well plates and treated with the indicated siRNAs, a scrambled siRNA or not transfected. Conditioned medium was collected and added (10% v/v) to RAW264.7 cells cultures with RANKL 100ng/ml every 48 hours for 120 hours. Cultures were fixed and TRAcP stained. Osteoclast were counted and expressed as a percentage of NT-Mock-BT1. Results are mean ± SD from at least three independent experiments. *$p < 0.05$ from MockScr^{si}; **$p<0.01$ from Mock Scr^{si} ## $p<0.01$ from IKKεOE Scr^{si} MDA-BT1 cells. Red dotted line indicates NT MDA-BT1 Mock baseline.

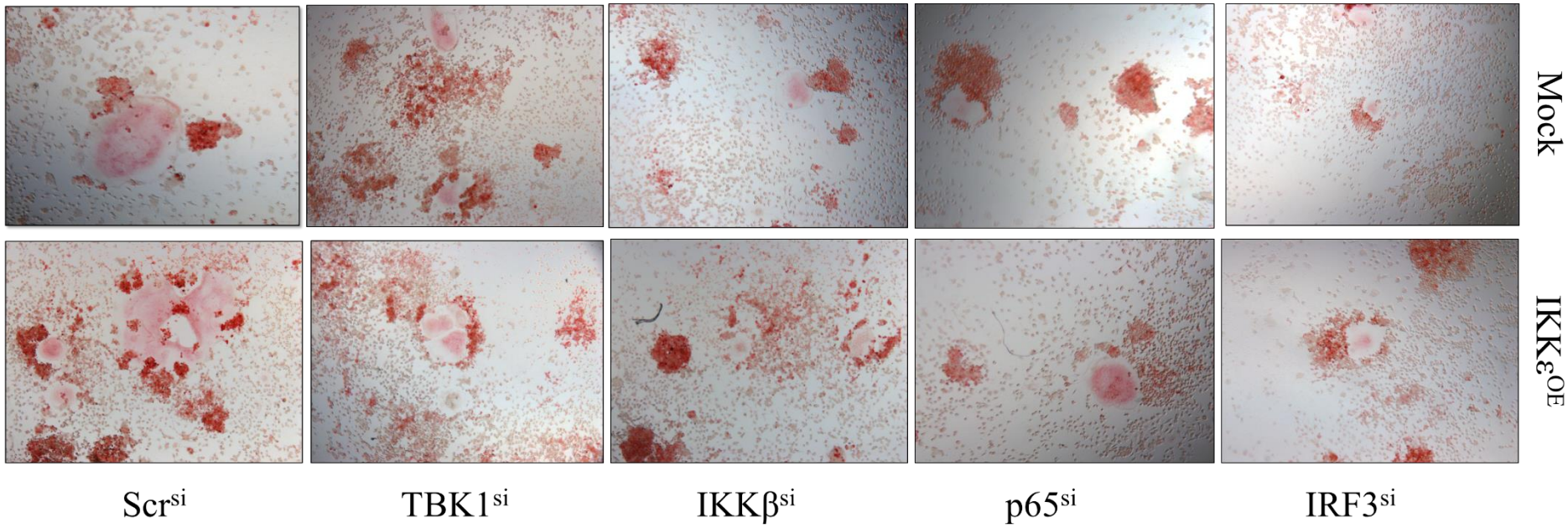

Figure 39 Knockdown of the NFκB and IRF3 pathways in MDA-BT1 Mock and IKKε ***OE cells reduced breast cancer support for osteoclast formation.***
RAW264.7 cells were plated in a 96-well plate and exposed to conditioned medium (10%v/v) from MDA-BT1 mock and IKKεOE cells treated with scramble siRNA or TBK-1, IKKβ, p65 or IRF3 targeting siRNA. Osteoclast-like cells were fixed, TRAcP stained and the number of TRAcP+ multinucleated OCs were counted. Above shows representative images**.**

4.4.3 IKKε **regulates tumour-derived proinflammatory cytokine production by osteotropic breast cancer cells**

The production of secreted factors by breast cancer cells has been shown to enhance cancer cell proliferation, migration, EMT-induction and priming of the metastatic niche for colonisation. Moreover, the NFκB pathway and IKKε are known to regulate a variety of cytokines and proinflammatory factors such as TNFα, MMP-9, IL-6, and IL-8 (Boehm et al., 2007, Adli and Baldwin, 2006, Peant et al., 2009, Barbie et al., 2014). Therefore, I examined the changes in cytokine production in MDA-BT1 cells in response to pharmacological inhibition of IKKε using Amlexanox. MDA-BT1 cells were treated with vehicle (0.01% v/v DMSO) or Amlexanox (30μM) for 24 hours. Conditioned medium was generated as previously described (See section 2.2.4). MDA-BT1-derived cytokines were measured using the Proteome Profiler Human XL Cytokine Array Kit (see section 2.3.13).

Of the 102 cytokines assayed. Six cytokines were upregulated by more than two-fold and fourteen were down regulated by more than two fold in MDA-BT1 cells treated with Amlexanox compared to vehicle treated cells (Figure 40). Amongst the cytokines that were upregulated in Amlexanox treated MDA-BT1 Mock cells compared to vehicle treated MDA-BT1 Mock cells were relaxin-2 (296.2%), angiogenin (281.4%), osteopontin (246.2%), Intercellular Adhesion Molecule 1 (ICAM; 243.0%), granulocyte-colony stimulating factor (G-CSF; 225.0%), extracellular matrix metalloproteinase inducer (EMMPRIN; 219.6%). Cytokines produced at 50% or less in MDA-BT1 cells exposed to Amlexanox include macrophage-colony stimulating factor (M-CSF; 47.5%), interleukin-24 (IL-24; 46.4%); tumour necrosis factor-alpha (TNFα; 44.8%), fms related tyrosine kinase 3 ligand (Flt-3 ligand; 43.3%) trefoil factor 3 (TFF3; 42.0%); chemokine C-X-C motif ligand 1 (CXCL1; 41.2%); Dickkopf-related protein 1 (DKK-1; 37.4%); matrix metalloproteinase-9 (MMP9; 37.3%); stromal –cell derived factor 1a (SDF1a; 33.7%); interleukin 23 (IL-23; 29.7%); adiponectin (22.1%); brain-derived neurotrophic factor (BDNF;7.9%); Cystatin C (7.9%); cluster of differentiation 30 (CD30; 3.8%)

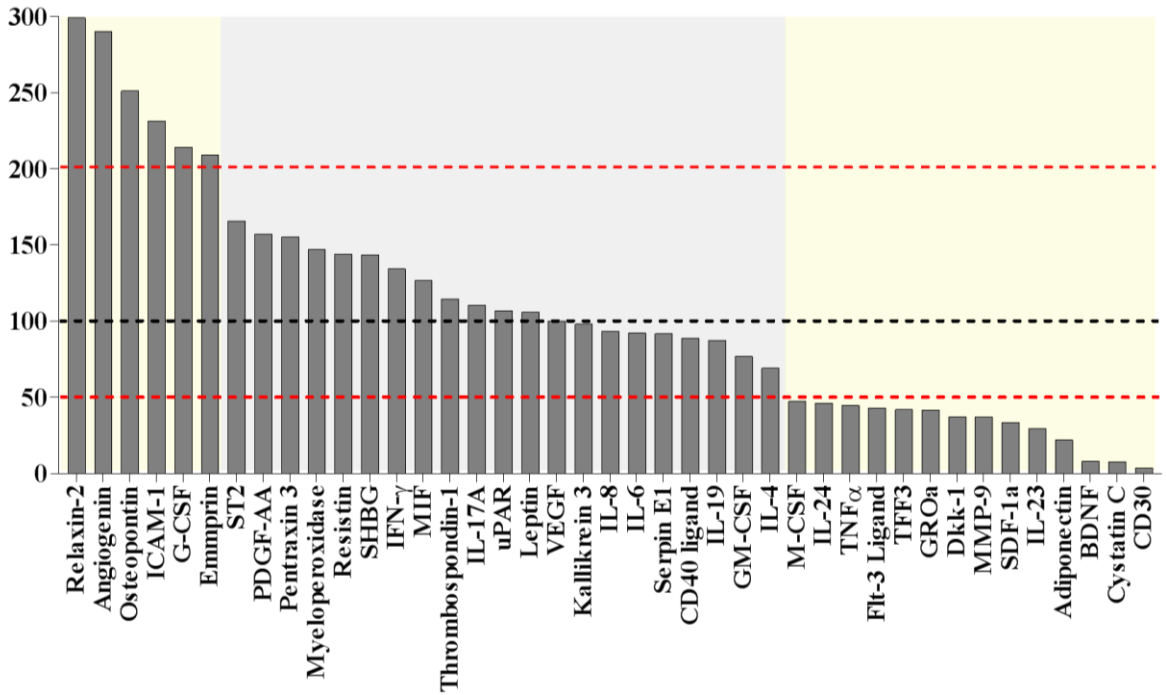

Figure 40. Differential expression of cytokines in the conditioned medium of MDA-BT1 cells treated with Amlexanox .

(Left) Quantification of cytokines in the conditioned medium of MDA-BT1 exposed to AmX for 24 hours compared to vehicle treated MDA-BT1. Yellow highlight shows upregulated and downregulated cytokines in conditioned medium of MDA-BT1 cells following treatment with AmX compared to vehicle treated MDA-BT1. Red dotted upper line indicates a 2.0 fold production of cytokines. Lower red dotted line indicates a 0.5-fold production in cytokine. These results are representative of an individual biological repeat. (Right) Venn diagram of differentially regulated breast cancer, bone metastatic, osteoclastic and osteoblastic mediators in MDA-BT1 CM in response to Amlexanox (30μM). See Table 9 for more details.

4.4.4 **Knockdown and pharmacological inhibition of** IKKε **have no effect on osteoblast viability, differentiation and activity**

Breast cancers once in the skeleton influence osteoblasts to produce disorganised woven bone resulting in osteoblastic metastases. With this is mind, I assessed the effects of cancer specific knockdown of IKKε in MDA-BT1 cells and pharmacological inhibition of IKKε/TBK-1 cells on viability, differentiation and activity. To do this calvarial osteoblasts were isolated as described (2.2.9.1). Osteoblasts were cultured in the presence of the indicated MDA-BT1 conditioned medium (20% v/v) with or without Amlexanox. After 3 days the osteoblast viability was measured (2.2.5) and the cells were lysed and assayed for alkaline phosphatase levels (2.2.9.3) as seen in, cancer-specific knockdown of IKKε had no effect on osteoblast viability or alkaline phosphatase activity. Similarly, pharmacological inhibition of IKKε with Amlexanox had no effect on osteoblast viability or alkaline phosphatase activity (Figure 41). Osteoblast-like Saos-2 cells were used to study the effect of inhibition of IKKε using Amlexanox on osteoblast activity. As shown in Figure 41D-E, pharmacological inhibition of IKKε in osteoblast-like cells had no effect on osteoblast activity in the presence of MDA-BT1 cell conditioned medium (20% v/v).

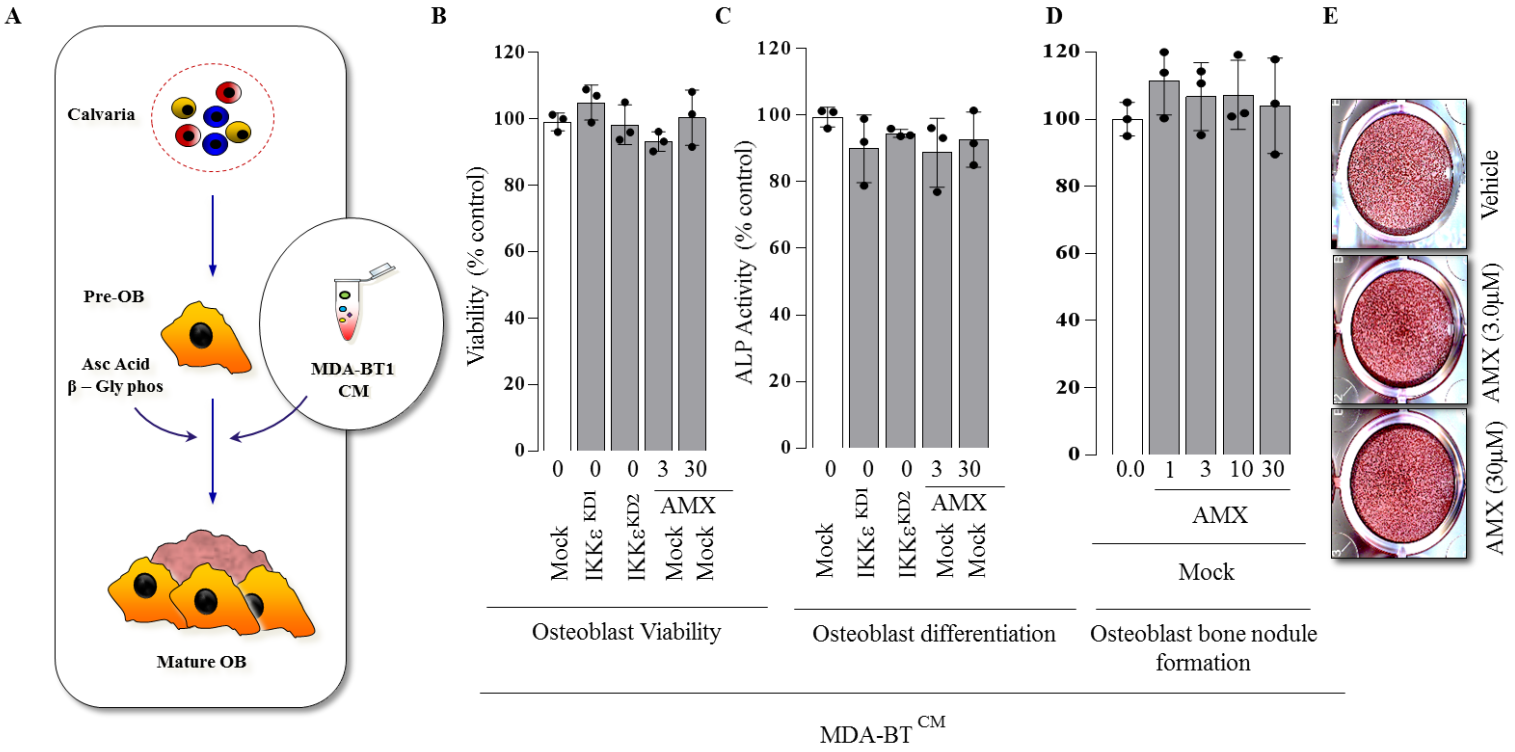

Figure 41. IKKε ***inhibition has no effect on osteotropic breast cancer cell support for osteoblast differentiation or activity.***

A) Schematic diagram of the experiment in B and C to isolate calvarial osteoblasts. B) Calvarial osteoblasts were co-cultured with 20% v/v MDA-BT1 Mock or IKKε$^{KD1/2}$ CM with DMSO or MDA-BT1 Mock CM plus AMX at the indicated concentrations for 72 hours. C) Cells were lysed and Alkaline phosphatase activity was measured. D Saos-2 osteoblast-like cells were co-cultured with 20% v/v MDA-BT1 Mock or IKKε$^{KD1/2}$ CM with DMSO or MDA-BT1 Mock CM plus AMX at the indicated concentrations for ten days, then fixed and stained with Alizarin red to show bone nodules. E. Representative images of the experiment in D. Results are mean ± SD from at least three independent experiments.

4.4.5 **Amlexanox inhibits RANKL-induced osteoclast formation without affecting osteoclast precursor viability**

A recent study by Zhang and colleagues showed that the verified IKKε/TBK-1 inhibitor reduced ovariectomy-induced bone loss in mice by osteoclast inhibition (Zhang et al., 2015). Thus, I aimed to examine whether IKKε/TBK-1 inhibition affects RANKL-induced human and mouse osteoclast formation in the absence of osteotropic breast cancer cells and their derived factors. Addition of RANKL (100ng/ml) to human CD14+ macrophages induced the formation of TRAcP positive multinucleated osteoclasts, and exposure to Amlexanox (1-3μM) significantly reduced the formation of osteoclasts by 29.6± 9.4% ($p<0.05$) and 48.4± 2.2% ($p<0.01$) (Figure 42) . Similarly, Amlexanox (1-3μM) reduced the formation of osteoclasts in RANKL stimulated mouse bone marrow cultures by 57.5± 3.3% ($p<0.01$) and 77.2 ± 3.4% ($p<0.01$) respectively (Figure 42).

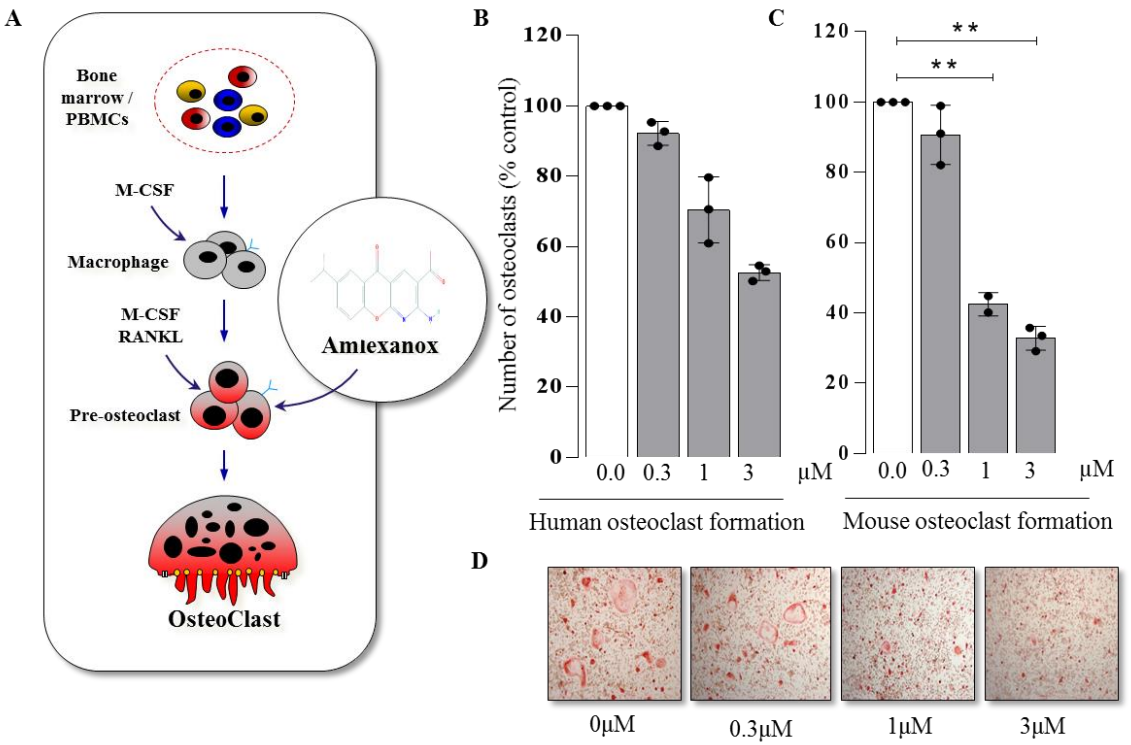

Figure 42. Amlexanox inhibits RANKL-induced human and mouse osteoclast formation.

A Schematic diagram of the experiment in B and C to generate osteoclasts. Bone marrow was isolated by flushing of mouse tibia. PBMCs were isolated from whole blood and CD14+ cells were selected for using antibody bound beads. MCSF was added for 48 hours to induce the differentiation to macrophages. RANKL and MCSF were added to induce osteoclast formation. Amlexanox was added at indicated concentrations and 50% of medium was refreshed every 48 hours until fixation and TRAcP staining. B Number of human TRAcP+ multinucleated osteoclasts per well as a percentage of the vehicle treated wells. C Number of human TRAcP+ multinucleated osteoclasts per well as a percentage of the vehicle treated wells. D Representative Images from the experiment described in B. Values are mean ± SD from at least three independent experiments; * $p < 0.05$, ** $p < 0.01$ from vehicle treated control.

As Amlexanox reduced the formation of osteoclasts following exposure to RANKL, I examined if this reduced osteoclast formation was due to a reduction in the viability of precursor cells**.** Human $CD14^{+}$ monocytes were cultured in MCSF for 48 hours to generate M-CSF dependant macrophages, which were exposed to various concentrations of Amlexanox**.** Amlexanox had no effect on the viability of human M-CSF dependant macrophage cells at concentrations that inhibited osteoclast formation for up to 5 days (Figure 43).

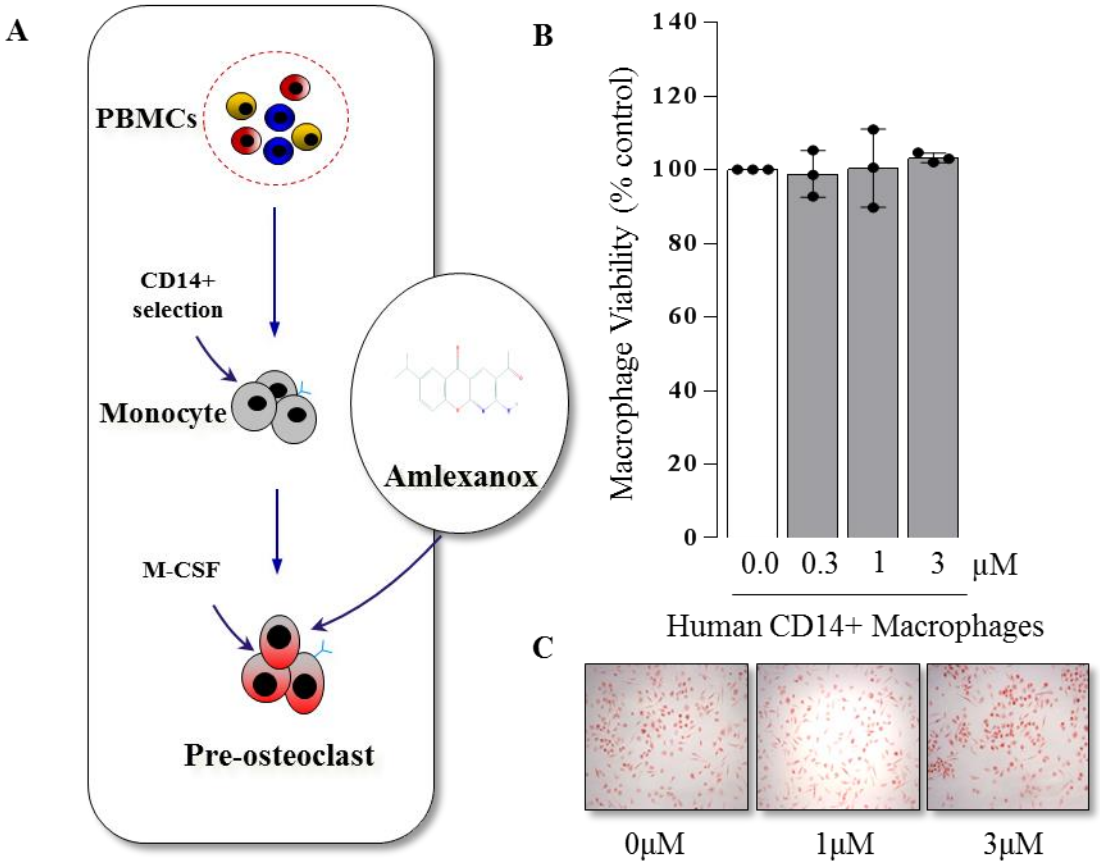

Figure 43. Amlexanox has no effect on human CD14+ MCSF generated macrophages

A. Schematic diagram of the experiment. PBMCs were isolated from whole blood and CD14+ cells were selected for using antibody bound beads. MCSF was added for 48 hours to induce the differentiation to macrophages. Amlexanox was added at indicated concentrations and 50% of medium was refreshed every 48 hours until fixation. B Relative cell viability at the end of the experiment as determined by Alamar Blue C Representative images of macrophage/osteoclast precursors following fixation and TRAcP staining. Values are mean ± SD from at least three independent experiments.

4.4.6 **Amlexanox inhibits RANKL- but not MDA-BT1 CM-induced phosphorylation of IκBα in osteoclast precursors**

RANKL and MCSF are essential cytokines for the formation, survival and activity of osteoclasts (Nakagawa et al., 1998, Fuller et al., 1993). However, only RANKL regulates the formation of osteoclasts through the phosphorylation of IκB and subsequent activation of NFκB (Boyce, 2013). In view of this, I went on to test the effects of Amlexanox on RANKL-induced phosphorylation of IκB by RANKL and osteotropic tumour cell derived factors (Figure 44). To do this, I exposed macrophage-like RAW264.7cells to RANKL following pre-treatment with vehicle or Amlexanox. Macrophage-like cells were lysed and subject to western blotting. RANKL (100ng/ml) increased the phosphorylation of IκBα by 3.26 fold ($p<0.05$), however, prior treatment with Amlexanox (10μM) prevented this increase (Figure 44). Moreover, 30μM of Amlexanox reduced phosphorylation of IκBα by 0.58 fold ($p<0.05$) of the basal levels of phosphorylation.

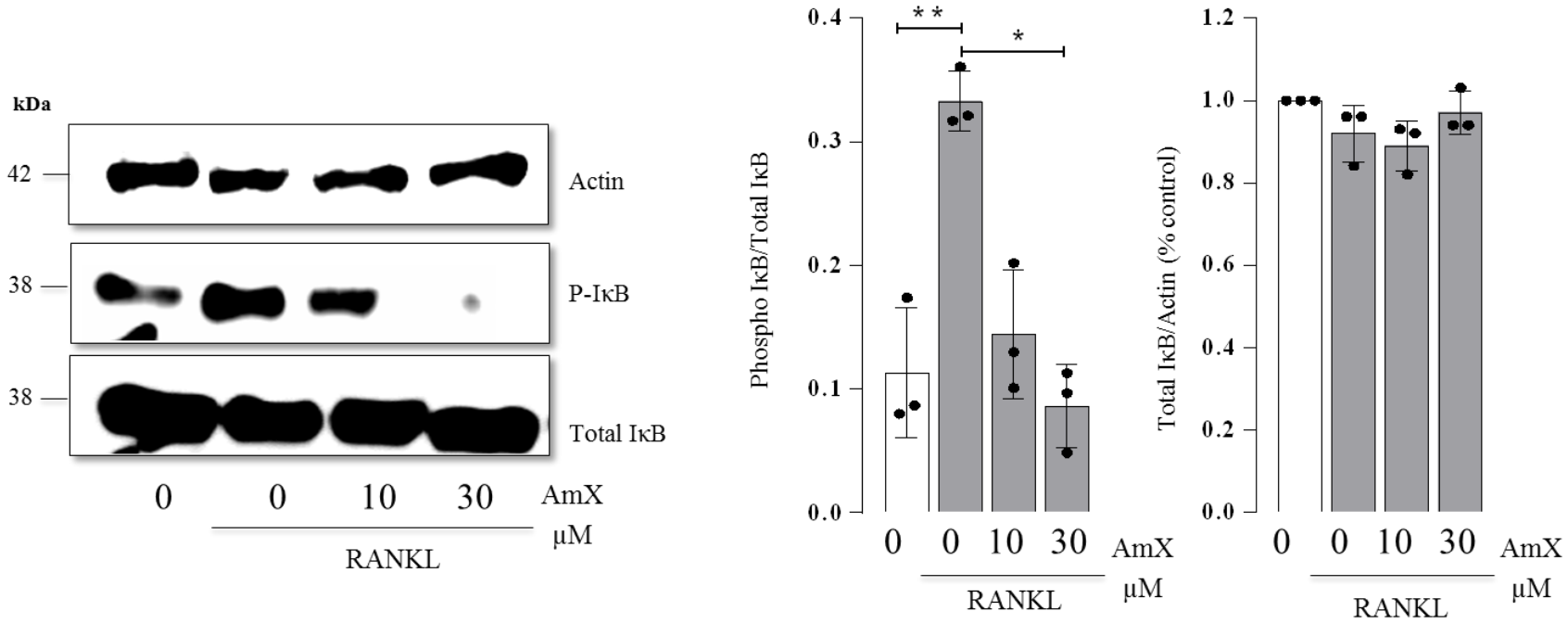

Figure 44. Amlexanox inhibits RANKL-induced phosphorylation of IκBα.

A) Western blot of mouse macrophage-like RAW264.*7*treated with vehicle (0.1% DMSO), Amlexanox (10 and 30 μM), for 1 hour prior to stimulation with vehicle (0.3% bovine serum albumin), RANKL (100 ng/ml) for 10 minutes. Total cellular protein was subjected to western blot analysis (70 μg/lane) using primary rabbit anti-phospho IκBα, rabbit anti-IκBα and rabbit anti-β-actin. The results shown are representative of three independent experiments. B) Quantification of the amount of phosphorylated IκBα over total IκBα (left) and total IκBα over actin as a percentage of vehicle control. Values are mean ± SD from at least three independent experiments; * $p<0.05$; ** $p < 0.01$.

Osteotropic breast cancer cells are able to support osteoclast formation through production of a variety of other factors including TNFα, IL-1, IL-6, IL-8, IL-23 IL-17, TGFβ, VEGF-A. In view of the above, I assessed whether Amlexanox was able to inhibit the phosphorylation of IκBα in macrophage-like osteoclast precursors. RAW264.7 were treated with DMSO (0.1%), Amlexanox (10 or 30μM) prior to stimulation with MDA-BT1 CM (20%) for ten minutes. RAW264.7were lysed and subject to western blotting. Western blot revealed that MDA-BT1 CM increased the phosphorylation of IκBα (5.72 fold increase, $p<0.001$) in RAW264.7 cells, leading to the degradation of IκBα (0.26 fold difference, $p<0.001$). Treatment with Amlexanox was not sufficient to significantly reduce the phosphorylation nor the degradation of IκBα (Figure 45). Interestingly, a trend towards more total IκBα was observed.

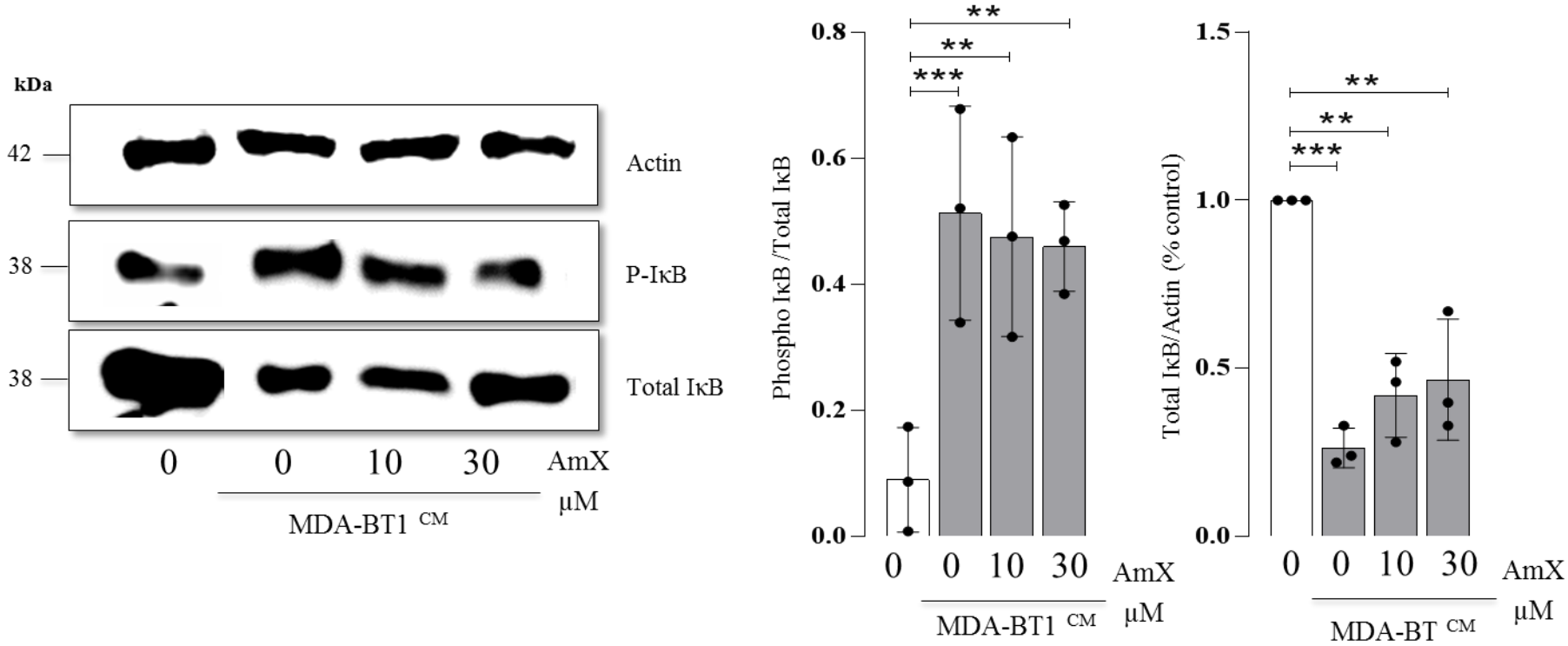

Figure 45. Amlexanox has no effect on MDA-BT1 CM induced phosphorylation and degradation of IκBα.

A) Western blot of mouse macrophage-like RAW.267 treated with vehicle (0.1% DMSO), Amlexanox (10 and 30 μM), for 1 hour prior to stimulation with control CM (20 % v/v) or MDA-BT1 CM (20 % v/v) for 10 minutes. Total cellular protein was subjected to western blot analysis (70 μg/lane) using primary rabbit anti-phospho-IκBα, rabbit anti-IκBα and rabbit anti-β-actin. The results shown are representative of three independent experiments. B) Quantification of the amount of phosphorylated IκBα over total IκBα (left) and total IκBα over actin as a percentage of vehicle control. Values are mean ± SD from at least three independent experiments; **p<0.01 , *** p < 0.001 from vehicle/Control CM treated control;

4.4.7 **Cancer-specific knockdown of IKKε in osteotropic breast cancer cells reduces osteolysis in mice**

The growth of breast cancer cells within the bone microenvironment often leads to the formation of osteolytic lesions**.** To examine the role of cancer specific IKKε on the ability to MDA-BT1 cells to induce osteolysis, IKKε knockdown ($IKK\varepsilon^{KD2}$) mock transfected MDA-BT1 cells were injected in to the left tibia of nude mice (see section 2.4.2) and monitored for the development of osteolytic lesions. Osteolysis was assessed using detailed μCT analysis of several features of the bone in the proximal tibial metaphysis. As shown in Figure 46, there was no significant difference in the total bone volume between mice intratibially injected with mock MDA-BT1 and MDA-BT1 $IKK\varepsilon^{KD2}$ cells.

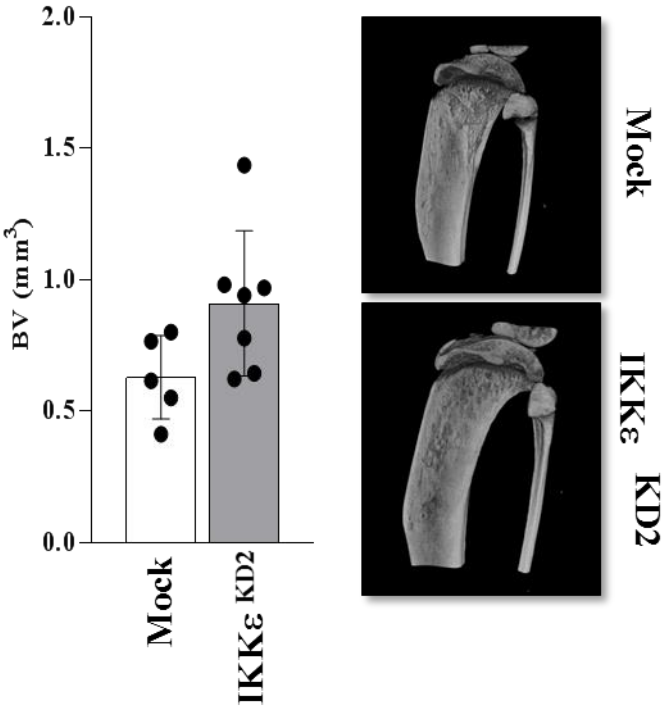

Figure 46. Knockdown of IKKε in MDA-BT1 had no effect on total bone volume.
4-week old athymic BALB/c nu/nu mice received injections of $4x10^3$ MDA-BT1 Mock or $IKK\varepsilon^{KD2}$ human breast cancer cells into the left tibiae and a sham injection of PBS into the right tibia. Animals were sacrificed 21 days after intratibial injection. Microcomputed tomography (μCT) was used to analyse changes in bone.

Detailed analysis of the trabecular and cortical compartments individually showed that mice injected with MDA-BT1 IKKε^{KD2} had significantly more trabecular bone (72.8± 36.2 %) at the end of the experiment as indicated by BV/TV ($p<0.05$ Figure 47A and F). Interestingly, breast cancer specific knockdown of IKKε had no significant effect in trabecular number (Figure 47B), trabecular thickness (Figure 47C) nor separation (Figure 47D), however, trabecular were significantly less porous (Figure 47E, 3.1 ± 1.4% reduction in porosity, $p<0.05$).

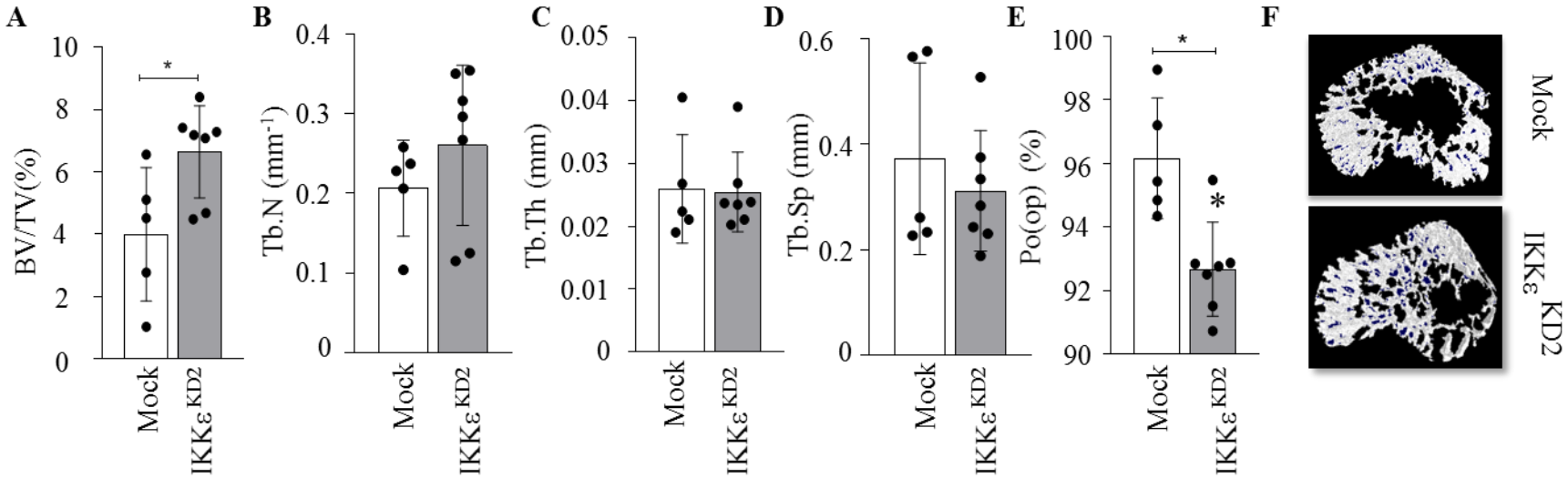

Figure 47. Breast cancer specific knockdown of IKKε reduces MDA-BT1 induced osteolysis in vivo

4-week old athymic BALB/c nu/nu mice received injections of $4x10^3$ MDA-BT1 Mock or IKKε^{KD2} human breast cancer cells into the left tibiae and a sham injection of PBS into the right tibia. Animals were sacrificed 21 days after intratibial injection. Microcomputed tomography (µCT) was used to analyse changes in bone. Trabecular parameters analysed were bone volume/tissue volume (BV/TV%; A), trabecular number (Tb.N; B) trabecular thickness (Tb.Th; C), separation (Tb.Sp; D) and porosity(Po(op)%; E) Representative 3D reconstructions are shown in panel F. Values are means ± standard deviation. Five mice in the mock injected group and seven mice in the IKKε^{KD2} group. *$p<0.05$ from mock MDA-BT1 injected legs.

Additionally I sought to evaluate the effect of knockdown of IKKε in MDA-BT1 on the osteolysis of cortical bone in mice. However, as shown in Figure 48, breast cancer specific knockdown of IKKε had no significant effect on cortical BV nor porosity.

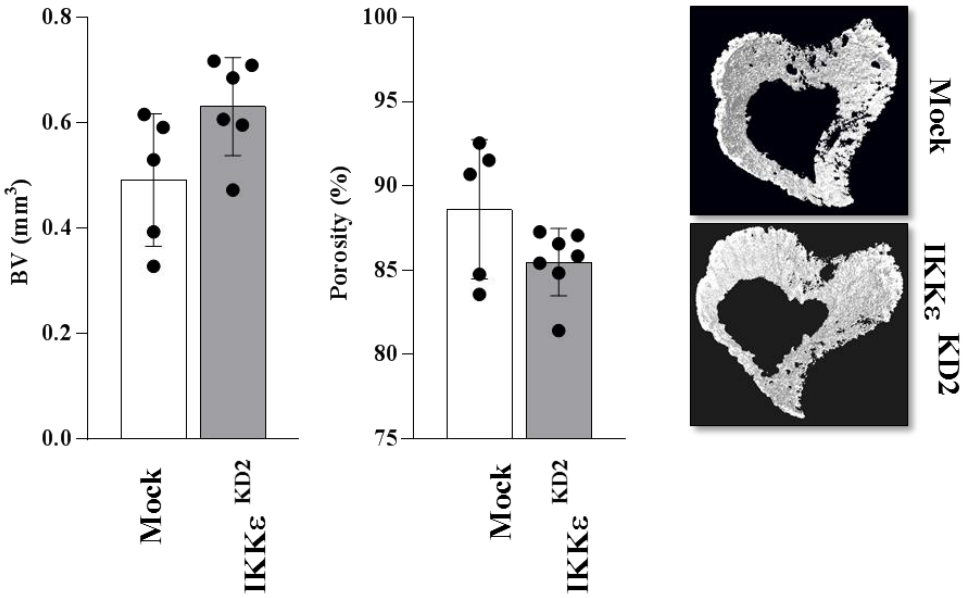

Figure 48. Breast cancer specific knockdown of IKKε has no effect on MDA-BT1 induced cortical osteolysis in vivo

4-week old athymic BALB/c nu/nu mice received injections of $4x10^3$ MDA-BT1 Mock or $IKK\varepsilon^{KD2}$ human breast cancer cells into the left tibiae and a sham injection of PBS into the right tibia. Animals were sacrificed 21 days after intratibial injection. Microcomputed tomography (μCT) was used to analyse changes in bone.

4.4.8 **Cancer-specific knockdown of IKKε in MDA-BT1 breast cancer cells reduces osteoclast formation but has no effect on osteoblasts**

To uncover the cellular changes associated with a reduction in bone loss in mice inoculated with MDA-BT1 IKKε^{KD2} cells, I carried out histomorphometric analysis of the mouse tibiae from the aforementioned experiment (Figure 49 and Figure 50). This analysis revealed there was a significant reduction in osteoclast number (40.7± 19.2% reduction; Figure 49A) but no difference in the size of osteoclasts formed (Figure 49B). Complementary to *in vitro* results, cancer cell-specific knockdown of IKKε had no effect on osteoblast number or activity as indicated by osteoblast number per bone surface (Ob.N/BS;Figure 49C) and osteoblast size (Ob.S/BS;Figure 49D)

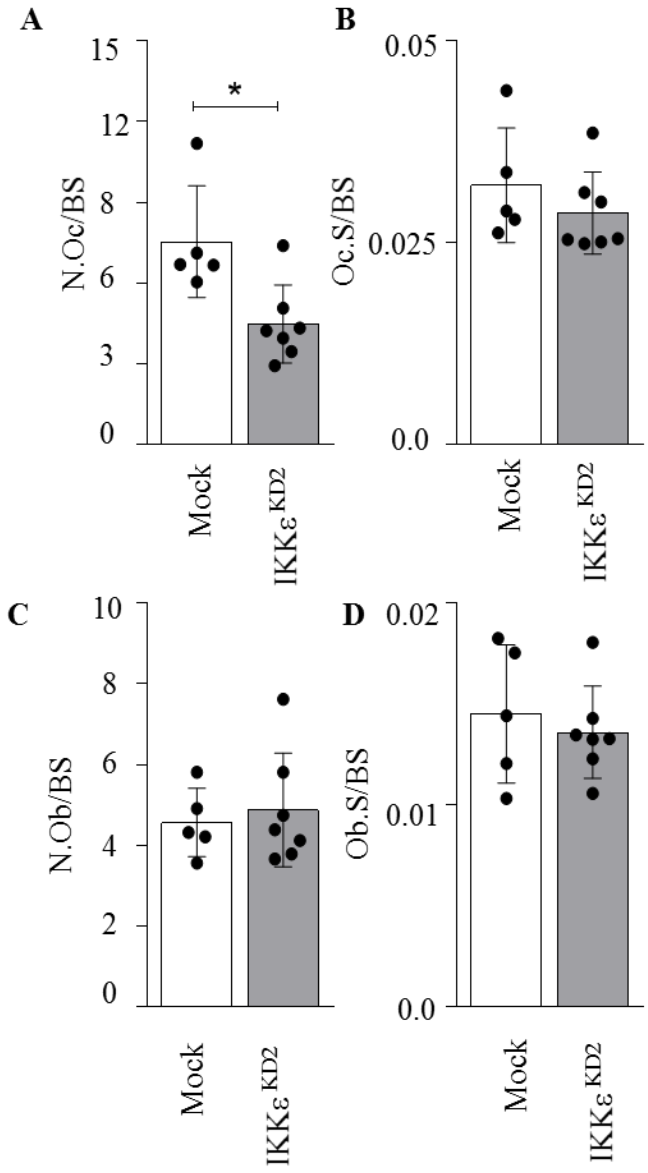

Figure 49. Breast cancer specific knockdown of IKKε reduces osteoclast formation associated with MDA-BT1, whilst having no effect on osteoclast size, osteoblast number or size.
4-week old athymic BALB/c nu/nu mice received injections of $4x10^3$ MDA-BT1 Mock or IKKε^{KD2} human breast cancer cells into the left tibiae and a sham injection of PBS into the right tibia. Animals were sacrificed 21 days after intratibial injection. A The number of osteoclasts per bone surface area and B the size of osteoclast per bone surface area. C The number of osteoblasts per bone surface area and D the size of osteoblast per bone surface area. Values are means ± standard deviation *$p<0.05$ from mock MDA-BT1 injected legs.

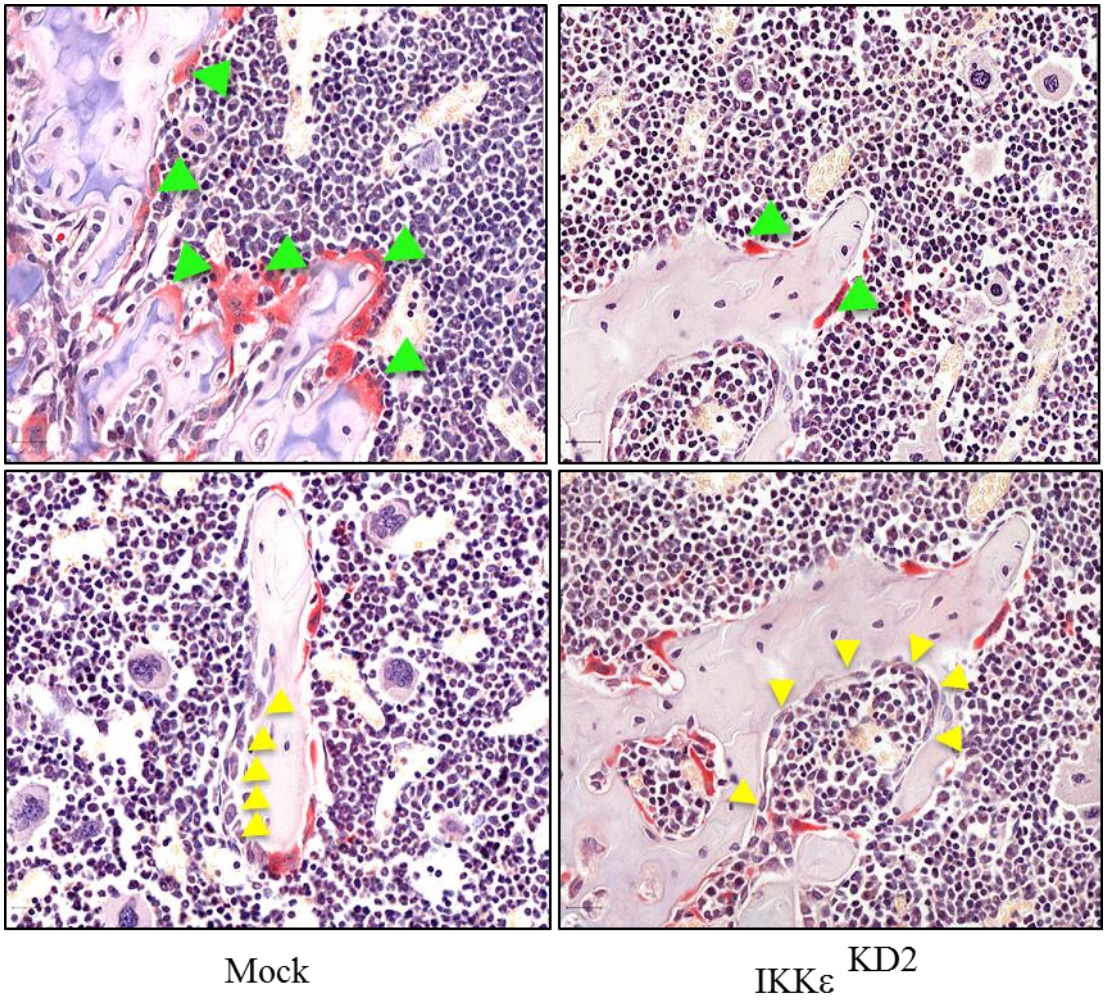

Figure 50. Breast cancer specific knockdown of IKKε reduces osteoclast number in vivo.
4-week old athymic BALB/c nu/nu mice received injections of $4x10^3$ MDA-BT1 Mock or $IKK\varepsilon^{KD2}$ human breast cancer cells into the left tibiae and a sham injection of PBS into the right tibia. Animals were sacrificed 21 days after intratibial injection. Representative images of the experiment described in Figure 49. Green arrows indicate TRAcP positive osteoclasts on the bone surface (top row). Yellow areas indicate cuboidal osteoblasts along bone surface (bottom row).

4.4.9 **Amlexanox reduced breast cancer induced osteolysis**

As cancer-specific IKKε inhibition reduced trabecular bone loss but not cortical, we hypothesised that host cells of the tumour microenvironment might be more involved. To examine this, we tested Amlexanox in immunocompetent mice using the 4T1-Luc2 model. I performed detailed μCT analysis of trabecular bone in the proximal right tibial metaphysis of mice injected intracardiacally with 4T1-Luc2 cells. This experiment revealed that mice treated with Amlexanox (35mg/kg/day) had significantly more bone (20.2±9.1% more; $p<0.05$) than vehicle treated mice.

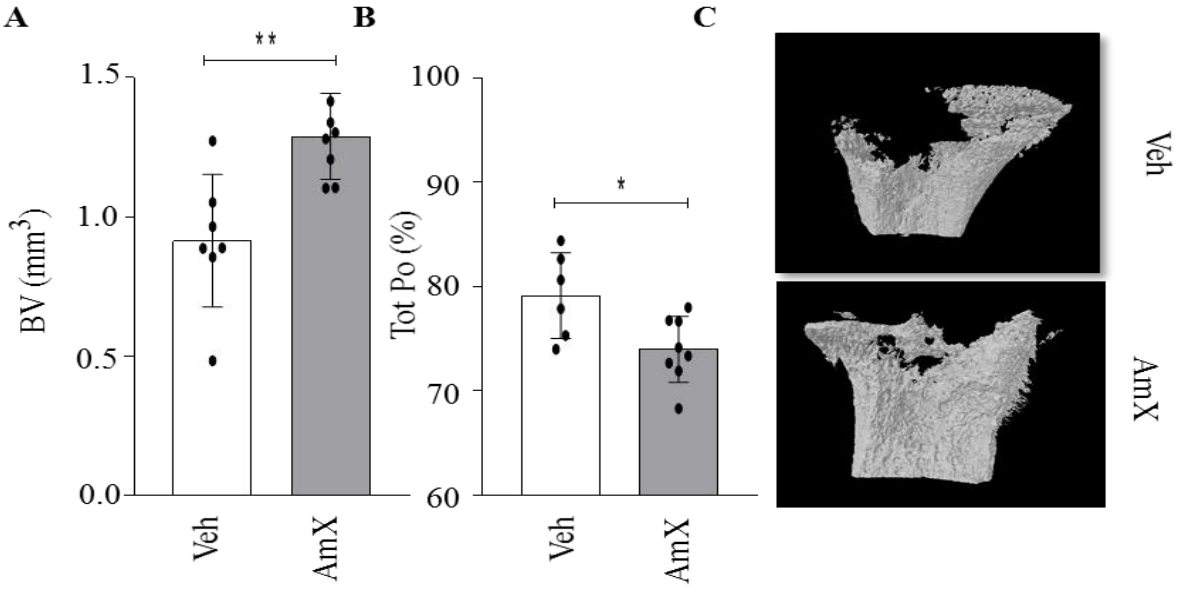

Figure 51. Amlexanox reduced 4T1-Luc2 induced osteolysis.
4T1-Luc2 cells ($1x10^5$/100μl PBS) were injected in to the left ventricle of syngeneic 6-week old immunocompetent BALB/c mice. Mice were split into two groups (n=8/group) and given daily i.p. injections of vehicle or Amlexanox (35mg/kg). After sacrifice, microcomputed tomography (μCT) was used to analyse changes in bone volume of the right tibia of mice.

Again I aimed to assess in which compartment there was a protection against bone loss by analysing the cortical and trabecular compartments individually. As seen in Figure 52A and F shows that mice treated with Amlexanox (35mg/kg) following intracardiac injection of 4T1-Luc2 cells had more trabecular bone at the end of the experiment as indicated by BV, however this did not reach significance. Further µCT analysis showed that there was no significant difference in trabecular number, spacing, or porosity (Figure 52B-C) between mice treated daily with Amlexanox or vehicle control.

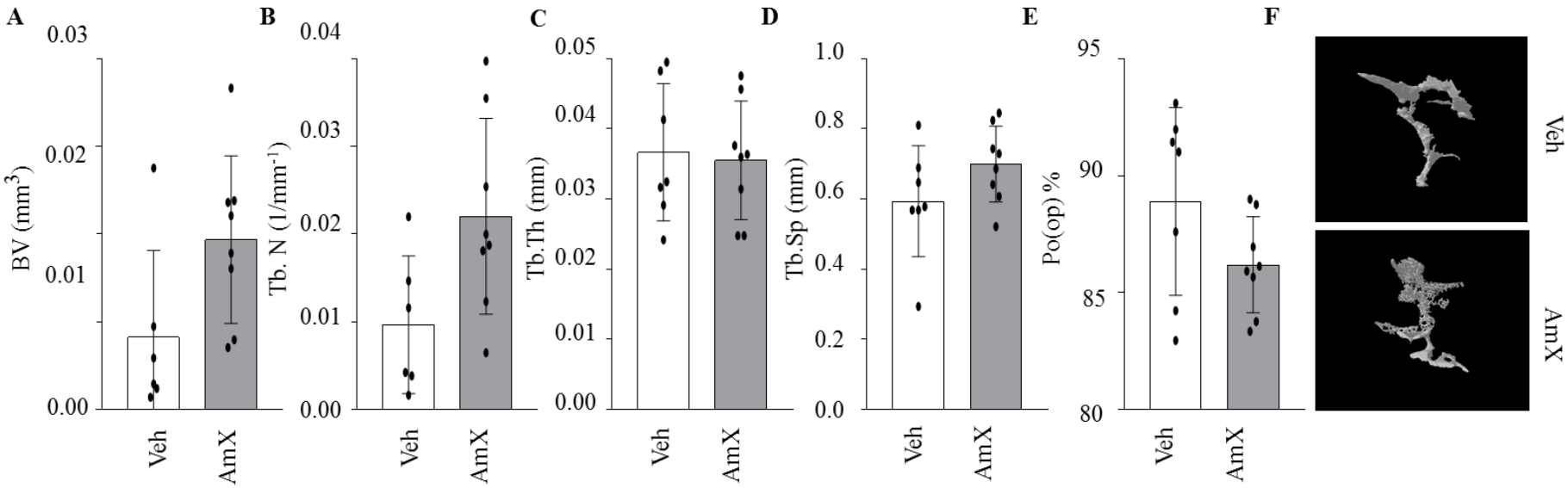

Figure 52. Amlexanox has no effect on trabecular bone parameters in mice following intracardiac injection of 4T1-Luc2 cells

4T1-Luc2 cells ($1x10^5$/100µl PBS) were injected in to the left ventricle of syngeneic 6-week old immunocompetent BALB/c mice. Mice were split into two groups (n=8/group) and given daily i.p. injections of vehicle or Amlexanox (35mg/kg). After sacrifice, microcomputed tomography (µCT) was used to analyse changes in bone of the right tibia of mice. Trabecular parameters analysed were bone volume (BV; A), trabecular number (Tb.N; B) trabecular thickness (Tb.Th; C), separation (Tb.Sp; D) and porosity (Po(op)%; E) Representative 3D reconstructions are shown in panel F. Values are means ± standard deviation. (8 mice per group)

The intracardiac injection of 4T1-Luc2 cells lead to a dramatic loss of trabecular bone after 11 days. During µCT scanning and analysis, it was evident that 4T1-Luc2 cells had caused significant osteolysis even in the cortex of the tibia; therefore, I also examined the cortical bone parameters (Figure 53A-C). These data indicate that daily treatment with Amlexanox lead to a significant protection of cortical bone loss (40.8 ± 16.4% more bone; $p<0.01$) and the cortical bone was significantly less porous (5.1 ± 1.2% less; $p<0.05$).

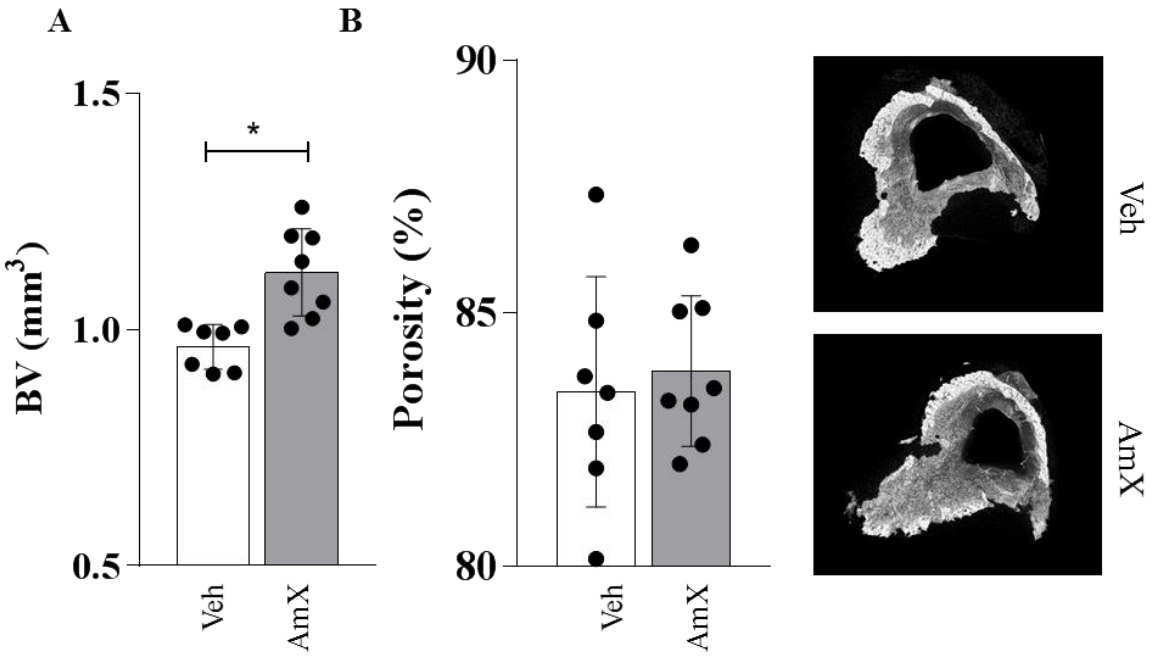

Figure 53. Amlexanox treated mice had more cortical bone than vehicle treated mice following intracardiac injection of 4T1-Luc2 cells

4T1-Luc2 cells ($1x10^5$/100µl PBS) were injected in to the left ventricle of syngeneic 6-week old immunocompetent BALB/c mice. Mice were split into two groups (n=8/group) and given daily i.p. injections of vehicle or Amlexanox (35mg/kg). After sacrifice, microcomputed tomography (µCT) was used to analyse changes in bone of the right tibia of mice. Cortical parameters analysed were bone volume (BV; A) and porosity (%; B). Representative 3D images of the cortical bone are shown in C. Values are means ± standard deviation. (8 mice per group) *$p<0.05$;**$p<0.01$ from vehicle treated control group.

4.5 Discussion

The IKK/NFκB pathway plays a key role in the formation and activation of osteoclast formation. (Chang et al., 2009a). Previous studies in our laboratories and in the literature have indicated that NFκB pathway in breast cancer cells contributes to their ability to grow, migrate, stimulate osteoclast formation and induce osteolysis (Idris et al., 2009, Marino et al., 2014, Peramuhendige et al., 2014, Park et al., 2006). However, the role of IKKε in breast cancer – bone cell interaction has yet to be investigated. The aim of this chapter was to assess both the cancer specific and bone cell contribution of IKKε to breast cancer support for osteoclast formation and osteoblast activity *in vitro* and *in vivo*.

In Chapter 3, I have shown that cancer-specific knockdown of IKKε reduced the skeletal tumour growth of MDA-BT1 cells *in vivo* following intratibial injection. Furthermore, pharmacological inhibition of IKKε also reduced the skeletal tumour growth of 4T1-luc2 cells *in vivo* following intracardiac injection. Following detailed microcomputed tomographic analysis, in this chapter I have shown that these observed reductions in tumour growth were accompanied by a reduction in osteolytic bone damage. In the intratibial model, I observed a reduction in bone loss in the trabecular of mice following injection of IKKε deficient breast cancer cells. Histomorphometry of these tibia revealed that these bones had no difference in osteoblast numbers but less osteoclasts. In the intracardiac model, there was no difference in the trabecular bone compartment. As there was very little trabeculae left at all, this may explain why we did not see a significant protection of bone in this aggressive model. However, we did observed a reduction in osteolysis of the cortical compartment. Mice treated with Amlexanox had more cortical bone compared to vehicle treated. As both knockdown and pharmacological inhibition of IKKε in cancer cells reduced cell viability *in vitro* (Chapter 3), we cannot yet conclude that the observed effect is not due to a cancer-specific effect on growth leading to less osteoclasts or rather the breast cancer cells are unable to stimulate osteoclast formation and subsequent osteolysis *in vivo* due to inhibition of the NFκB pathway in the environment. Although the overall reduction in tumour burden is likely due to both reduction of cancer-cell viability and osteoclast formation, future studies should address the effect of inhibiting IKKε in both the

cancer and the microenvironment on osteolysis in a model that removes growth inhibition as a factor such as the supracalvarial model of osteolysis. Here, conditioned medium from breast cancer cells is injected over the calvaria of young mice to induce osteolysis, thus one can examine how cancer-cell specific inhibition of IKKε may reduce osteolysis.

Here I have shown that in mouse bone marrow cultures, co-culture of MDA-BT1 cells deficient in IKKε or their conditioned medium greatly decreases their ability to support osteoclast formation Similarly, in human pre-osteoclast cultures, knockdown of IKKε in MDA-BT1 cells reduced their ability to support osteoclast formation; conversely, overexpression of IKKε in MDA-BT1 enhanced their support for osteoclast formation *in vitro*. In order to attempt to demarcate the pathways by which IKKε supports osteoclast formation, in a similar manner to chapter 3, I knocked down TBK-1, IKKβ, p65 and IRF3 using siRNA in both MDA-BT1 mock and IKKε^{OE} then added these conditioned media to osteoclast precursor cultures. Knockdown of all proteins examined significantly reduced breast cancer support for osteoclast formation and all reduced IKKε driven support for osteoclast formation suggesting that IKKε enhances osteoclast formation through activation of both the NFκB and IRF3 pathways. These data suggest that the activation of the IKKε/NFκB/IRF3 axis within breast cancer cells leads to the production of inflammatory factors that contribute to their ability to enhance osteoclast formation *in vitro*. Firstly, I assessed the proinflammatory factors that were regulated by Amlexanox. Amlexanox reduced the expression of several proinflammatory factors involved in breast cancer growth, metastasis and osteolysis such as TNFα, M-CSF, DKK-1, MMP-9, BDNF, IL-23 (Table 9). However, interestingly, Amlexanox also upregulated the production of several factors such as osteopontin, ICAM-1 and Emmprin, three factors which have been identified as molecules that promote breast cancer metastasis. In an elegant study carried out by the Massagué group, in which MDA-MB-231 cells were sequentially passaged through mice via intracardiac injection in order to isolate bone or lung metastatic variants, it was shown that osteopontin expression by breast cancer cells was significantly associated with increased bone metastasis and this correlated with reduced overall survival in patients (Kang et al., 2003). This could perhaps explain the reason why there was not an observed reduction in bone

metastasis in our 4T1-Luc2 model when treated with Amlexanox. Thus, significant work to understand the molecular mechanisms of how IKKε inhibition promotes the upregulation of these factors should be carried out. Nevertheless, treatment of mice with Amlexanox did partially reduce metastatic breast cancer growth in this model. Moreover, conditioned medium from cells deficient in IKKε failed to support osteoclastogenesis to the same level as IKKε replete cells suggesting that the factors downregulated or upregulated in response to IKKε inhibition play a role in breast cancer support for osteoclast formation.

Understanding the mechanisms that drive the bone metastatic vicious cycle are pertinent to designing new and effective therapeutics. Current therapies are designed to break the perpetual cycle of bone loss and tumour growth by targeting of osteoclasts. Bisphosphonates, a family of hydroxyapatite binding compounds, are endocytosed by osteoclasts leading to inhibition of the mevalonate pathway and the induction of apoptosis (Kavanagh et al., 2006). Bisphosphonates, the most potent being Zoledronic acid, and have been the gold standard of care for decades now. However, Denosumab, a monoclonal antibody against RANKL, has been shown to be superior in preventing skeletal-related events compared to Zoledronic acid in breast, prostate and myeloma patients (Stopeck, 2010). In this chapter, I tested the ability of Amlexanox to inhibit both breast cancer support for osteoclast formation and RANKL-induced osteoclast formation. Zhang and colleagues have previously shown that Amlexanox is able to reduce osteoclast formation *in vitro* and *in vivo,* though for the first time I have shown through addition of Amlexanox to cultures exposed to both RANKL and breast cancer conditioned medium that Amlexanox is also effective at inhibiting breast cancer support for osteoclastogenesis. Mechanistically, I showed that Amlexanox reduced the phosphorylation of IκBα in response to RANKL suggestive of NFκB inhibition, the essential transcription factor for osteoclast formation. Interestingly, Amlexanox was unable to reduce the phosphorylation of IκBα in response to MDA-BT1 CM. This could be due to the fact that the conditioned medium contains numerous cytokines that activate NFκB (TNFα, IL17A, CD40L) through the canonical pathway and thus inhibition of IKKε/TBK-1 is not sufficient to inhibit NFκB. In the other bone cell compartment, breast cancer cells also influence osteoblasts by inhibiting their differentiation and ability to mineralise, however,

no effect on osteoclast differentiation or mineralisation was observed in primary osteoblasts or Saos2 osteoblast-like cultures, exposed to MDA-BT1 conditioned medium. Of note, Amlexanox had no significant effects on osteoblasts either at concentration inhibitory to osteoclast-formation or higher. This study showed that Amlexanox reduced breast cancer skeletal tumour growth and the resultant osteolysis, however, pre-clinical data suggests that Zoledronic acid and OPG-Fc (Denosumab) inhibit osteolysis *in vivo* without affecting skeletal tumour growth (Buijs et al., 2009) , therefore it would be beneficial to test Amlexanox, Zoledronic acid and Denosumab comparatively on their ability to reduce breast cancer skeletal tumour burden of established bone metastases.

The NFκB pathway and its role in bone has long since been established. Expanding evidence is demonstrating that NFκB activation within cancer cells enables them to establish osteolytic tumours through the production of various inflammatory factors (Park et al., 2006, Idris et al., 2009, Peramuhendige et al., 2018, Marino et al., 2018a). This work has helped establish this role. Future studies, using cancer-specific CRISPR knockouts of the IKKs and the NFκB transcription factors should be carried out head-to-head to help establish which protein and at which level would be best to target to reduce skeletal tumour burden. Following this work, we may establish new treatments to compare or even combine with current bone targeted agents for the treatment of breast cancer associated osteolysis.

Table 9. Differentially regulated cytokines in MDA-BT1 following treatment with Amlexanox and their known effect on breast cancer, bone metastasis, osteoclasts and osteoblasts.

Protein	Breast cancer	Bone metastasis	Osteoclasts	Osteoblasts	Ref
Relaxin-2	↑↓	-	↑	↑	(Radestock et al., 2008, Binder et al., 2002, Duarte et al., 2014)
Angiogenin (ANG)	↑↓	-	↑↓	-	(Montero et al., 1998, Morita et al., 2008)
Osteopontin (OPN)	↑	↑	↑	↓	(Chellaiah et al., 2003, Holm et al., 2014, Chakraborty et al., 2008, Kruger et al., 2014)
ICAM-1	↑	↓	↑	↓	(Guo et al., 2014, Yang et al., 2015, Fernandes et al., 2008)
Emmprin	↑	-	↑	-	(Nishioku et al., 2016, Zhou et al., 2005)
M-CSF	↑	↑	↑	-	(Mancino et al., 2001, Ide et al., 2008, Richardsen et al., 2015)
TNFα	↑	↑	↑	↓	(Lam et al., 2000, Abbas et al., 2003)
FLT3 ligand	↓	-	↑	-	(Lean et al., 2001, Braun et al., 1999)
TFF3	↑	↑	-	-	(Pandey et al., 2014, Kannan et al., 2010)
CXCL1	↑	↑	↑	↑	(Hardaway et al., 2015, Acharyya et al., 2012)
DKK1	↑	↑	↑	↓	(Qiang et al., 2008, Mariz et al., 2015, Fujita and Janz, 2007)
MMP9	↑	↑	↑	↔	(Mehner et al., 2014)

SDF1a	↑↓	↑	↑	↓	(Sun et al., 2014, Roccaro et al., 2014, Yu et al., 2003, Shahnazari et al., 2013)
G-CSF	↑	↑	↑	↓	(Hirbe et al., 2007, Christopher and Link, 2008)
IL-23	↑	↑	↓	↔	(Teng et al., 2010, Kamiya et al., 2007)
Adiponectin	↑↓	↓	↓	↑	(Landskroner-Eiger et al., 2009, Liu et al., 2013, Oshima et al., 2005)
BDNF	↑	↑	↑	↑	(Yang et al., 2012, Choi et al., 2016, Sun et al., 2012, Ida-Yonemochi et al., 2017)
Cystatin C	↑	-	↓	↑	(Završnik et al., 2017, Lerner et al., 1997, Danjo et al., 2007)
CD30	-	-	-	-	

An upwards arrow (↑) represents an increase in breast cancer or bone (any cancer) metastasis, osteoclasts formation and osteoblast activity whereas a downwards arrow (↓) represents an inhibition. Both upwards and downwards arrows (↑↓) indicates both an increase and decrease reported. Horizontal arrows (↔) denotes no change in breast cancer or bone (any cancer) metastasis, osteoclasts formation and osteoblast activity. A hyphen (-) designates no reported effect. Cytokines above the red line are upregulated and those below are downregulated.

Chapter 5

Combined administration of Amlexanox and Docetaxel reduces breast cancer metastasis *in vivo*

5 Chapter 5

5.1 Summary

The treatment of triple negative breast cancers often relies on a surgery, radiotherapy or chemotherapy. NFκB activity has been demonstrated to a be a potential mechanism of resistance to mainstay chemotherapies in triple negative breast cancer (Chuang et al., 2002). In this chapter, I demonstrate that pharmacological inhibition of IKKε enhances the cytotoxic effects of a panel of chemotherapeutic agents at inhibiting triple negative breast cancer cell viability *in vitro* and has synergy with a number including FDA-approved standard of care Docetaxel. In addition, treatment of breast cancer cells with Docetaxel increased IKKε expression *in vitro*.

Next I demonstrated, for the first time, that combined administration of Amlexanox and Docetaxel significantly and consistently inhibits mammary tumour growth in mice. In addition, combined administration of Amlexanox and Docetaxel significantly reduced the development of metastasis and lead to a significantly longer overall survival when compared to vehicle or either treatment as a monotherapy. Overall, this chapter demonstrates that inhibition of IKKε in combination with clinically relevant chemotherapies may be of use for the treatment of local and advanced triple negative breast cancer.

5.2 Introduction

Triple negative breast cancer is a highly heterogeneous group of breast cancers that affects up to 20% of all breast cancer patients (Ferlay et al., 2015). Therapies that target hormones and their receptors such as aromatase inhibitors or tamoxifen and HER2-targeting drugs such as trastuzumab lack efficacy in triple negative diseases owing to their lack of receptor status. Thus chemotherapy remains the standard of care for triple negative disease. A tumour that remains localised can be treated with various surgical options. Moreover, systemic delivery of chemotherapy can be administered in an attempt to eliminate disseminated cancer cells. In the case of overt metastatic disease chemotherapy is used to improve quality of life and extend progression-free and overall-survival. Many chemotherapies such as Docetaxel, paclitaxel, doxorubicin, cyclophosphamide and 5-flurouracil function to cause DNA or cytoskeletal damage or target vital cellular pathways such as rapamycin and thus, whilst being efficacious, have systemic and often serious adverse side effects(Malhotra and Perry, 2003).

Single agent treatment has shown promising results in preclinical and clinical studies, however, often do not eradicate later stage aggressive disease owing to various mechanisms of resistance that arise in these heterogeneous tumours. Recent scientific efforts have been focusing on combination therapies in an attempt to improve overall survival in multiple cancers, including breast cancer. Combination therapy, is the administration of two or more drugs with usually differing modes of action to enhance the efficacy of both drugs. In fact, around 80% of all clinical trials in triple negative breast cancers are exploring the efficacy of combination treatments (Chalakur-Ramireddy and Pakala, 2018).

A body of increasing evidence has shown that activation of the NFκB pathway has been shown to be a key contributing factor to chemoresistance. Moreover, a variety of chemotherapies such as taxanes and anthracyclines have been shown to activate the NFκB pathway and its contribution to chemoresistance mediated through the activation of a variety of anti-apoptosis and survival genes such as Bcl-2, Bcl-xl, XIAP and Survivin (Chuang et al., 2002, Li and Sethi, 2010). Furthermore, a number of studies in the past decade have implicated IKKε in both NFκB-dependent and independent resistance to chemotherapies. Following genotoxic

stress via DNA damaging agents, IKKε has been found to translocate to the nucleus where it phosphorylates p65 at serine-468 to induce gene expression that prevent apoptosis (Renner et al., 2010). Furthermore, IKKε has been shown to promote resistance to tamoxifen in ER+ breast cancers and carboplatin resistance in ovarian cancers (Guo et al., 2010, Guo et al., 2009) . In previous chapters, I have shown that inhibition of IKKε using shRNA or pharmacologically with Amlexanox reduces both skeletal and primary tumour growth of breast cancer cells, therefore I hypothesised that combined administration of IKKε with a clinically relevant compound would reduce the growth and metastasis of triple negative breast cancer cells *in vitro* and *in vivo*.

5.3 Aims

The aim of this chapter was to assess whether pharmacological inhibition of IKKε using Amlexanox enhances the efficacy of clinically relevant chemotherapeutic agents on breast cancer cells *in vitro***.** In addition, I aimed to test the if combined administration of Amlexanox with a chemotherapeutic agent in the neoadjuvant setting reduces primary tumour growth, the occurrence of metastasis and improves survival in a 4T1-Luc2 model *in vivo***.** The aims of this chapter will be realised by examining:

- The effect of chemotherapies alone and in combination with Amlexanox on breast cancer cell viability *in vitro***.**
- The effect of chemotherapeutic agents on IKKε expression *in vitro***.**
- The effect of Amlexanox, Docetaxel and their combined administration on mouse 4T1-Luc2 breast cancer primary tumour growth *in vivo***.**
- The effect of Amlexanox, Docetaxel and their combined administration on mouse 4T1-Luc2 breast cancer and the development of metastases following primary orthotopic tumour removal *in vivo***.**

5.4 Results

5.4.1 **Amlexanox enhances the efficacy of a panel of several chemotherapeutic agents**

Triple-negative breast cancers currently have no targeted therapies like ER/PR and HER2 expressing breast cancers. Thus in their absence, patients are often administered chemotherapeutics, as single or combination therapies. Activation of the NFκB pathway has been shown to be a mechanism of chemoresistance in several cancers including breast and pharmacological inhibition of the pathway enhances efficacy (Baldwin, 2001, Sweeney et al., 2005, Zhang et al., 2009). For these reasons, I decided to test the effects of combined administration of Amlexanox with various clinically relevant compounds with different modes of action on the viability of parental MDA-MB-231 cells. All compounds alone achieved IC_{50} values in the micromolar range except Docetaxel, paclitaxel and doxorubicin, which had IC_{50} values in the nanomolar after 72 hours (Figure 54 and Table 10). Interestingly, cyclophosphamide was only effective in the milimolar range. Amlexanox (30μM) significantly reduced the IC_{50} values of all compounds tested apart from doxorubicin (Table 10).

Table 10. Half maximal inhibitory concentration (IC_{50}) values of chemotherapeutic agents alone or combined with Amlexanox (30μM) on MDA-231 cell viability after 72 hours

Compound	IC_{50} (μM)		
	Single Agent	+AmX (30μM)	p-value
Docetaxel	0.01414	0.00016	<0.0001
Doxorubicin	0.57	0.08	0.633
Rapamycin	14.04	0.3012	0.0004
Tamoxifen	4.38	0.65	0.0156
Cyclophoshamide	8741	801.5	0.0012
Paclitaxel	0.0112	0.00183	0.0006
5-Fluorouracil	330.7	70.54	<0.0001

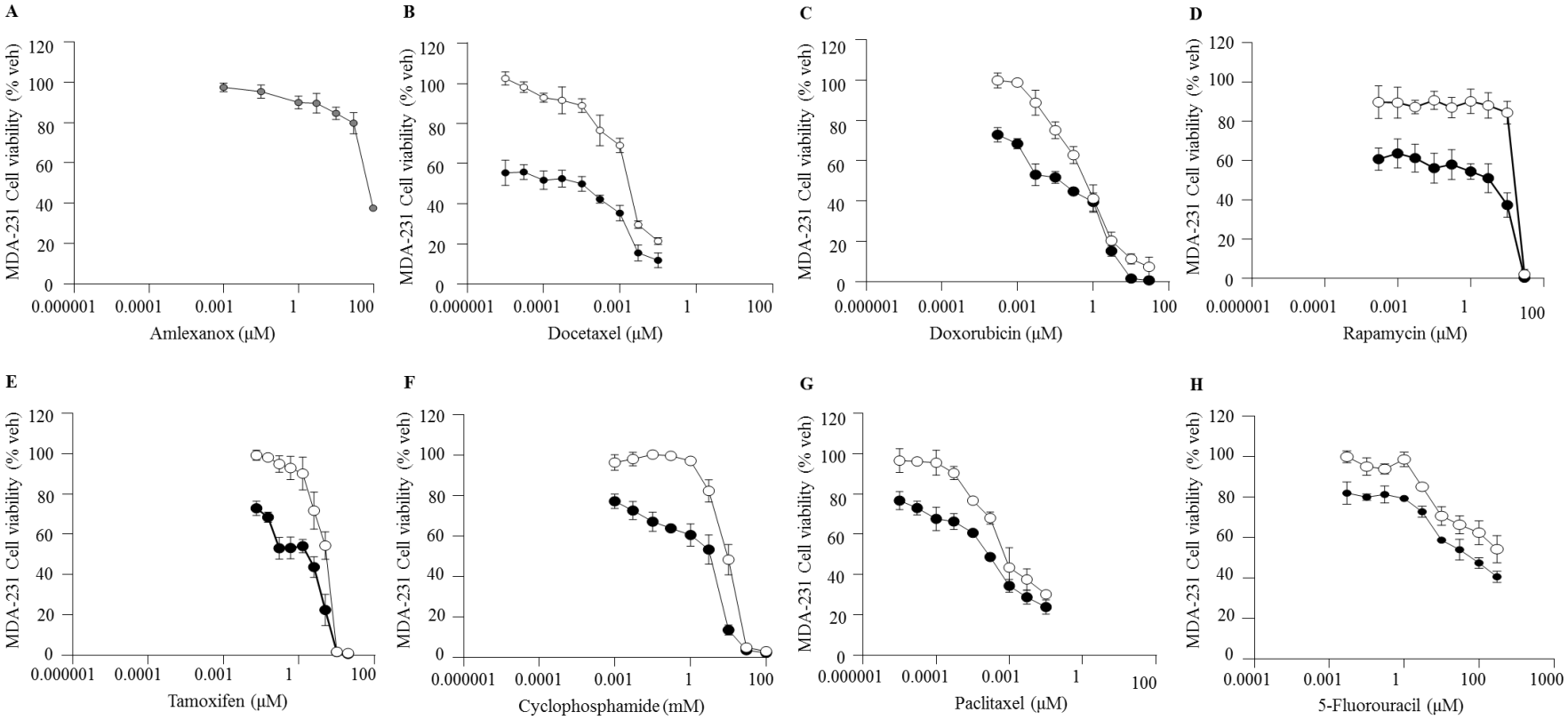

Figure 54. Amlexanox enhances the efficacy of a panel of chemotherapeutic agents

MDA-BT1 cells were plated in 96 well plates and treated with the indicated of Amlexanox (A) or the indicated doses of Docetaxel (B), Doxorubicin (C), Rapamycin (D), Tamoxifen (E), Cyclophosphamide (F), Paclitaxel (G), 5-Fluorouracil (H), alone (white circles) or with Amlexanox (30µM; black circles). Cell viability was determined using the Alamar Blue assay and expressed as a percentage of the values of the vehicle treated cells. Values are means ± standard deviation from at least three independent experiments.

5.4.2 **Docetaxel increases the expression of IKKε in** MDA-MB-231 **cells**

Many cancers develop resistance mechanisms to aid in survival leading to the development of resistant tumours. Therefore, it is important to find drug combinations that are synergistic such that results that are more effective are achieved, at lower doses and thus avoiding side effects. For this reason, I used the Chou-Talalay Method using CompuSyn Software to calculate the Combination Index values of the indicated drug combinations. Briefly, a drug combination that has a CI value of <1 would be deemed synergistic, equal to 1 is additive and 1 to ∞ is antagonistic. CI values of each concentration of the combinations were then plotted against the fraction-affected value (Fa). CompuSyn analysis revealed that Docetaxel, Rapamycin, Doxorubicin acted synergistically with Amlexanox at all doses tested (Figure 55). Tamoxifen, Paclitaxel, and Cyclophosphamide were mostly synergistic at more effective concentrations of chemotherapy, however were partially antagonistic at lower Fa values. Interestingly, the combination of 5-Fluorouracil and Amlexanox (30μM) were shown to be antagonistic with the majority of CI values greater than 1 (Figure 55).

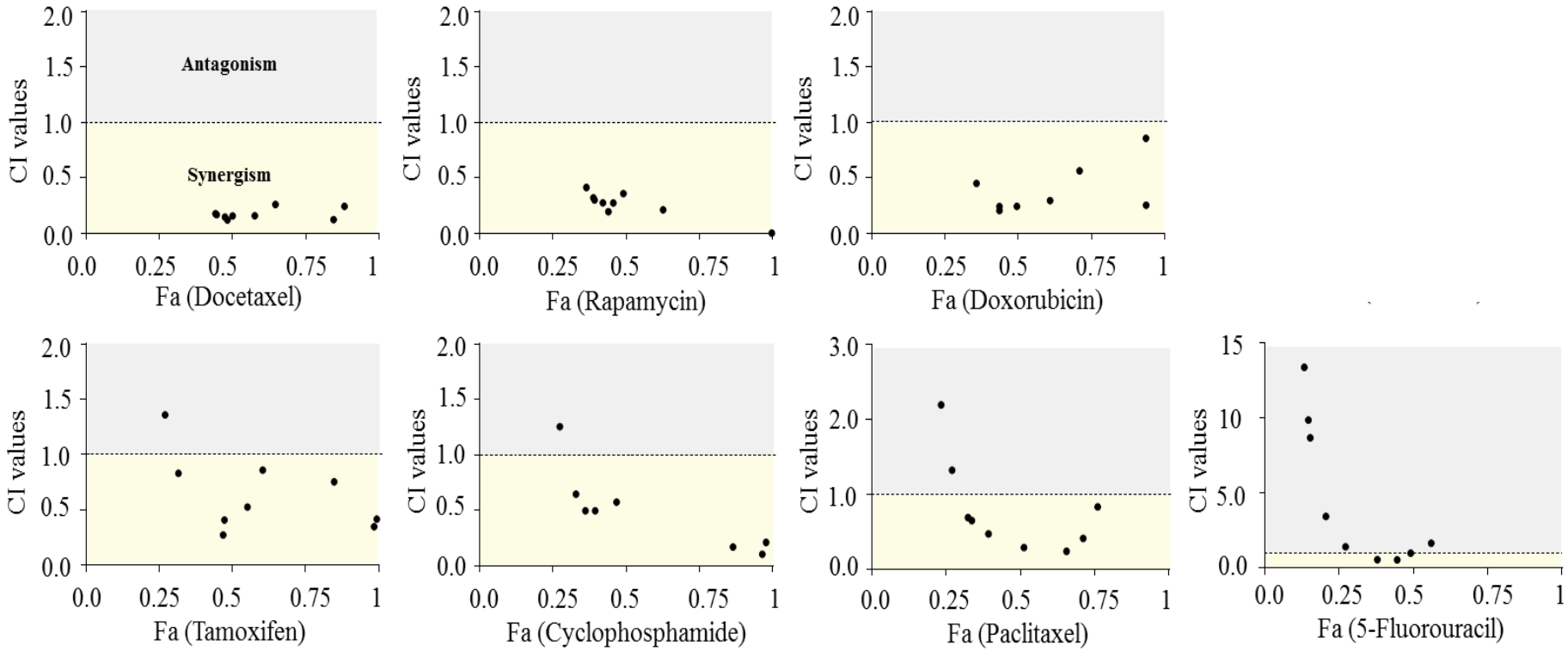

Figure 55. Amlexanox and Docetaxel, Rapamycin and Doxorubicin act synergistically at all doses whereas Tamoxifen, Cyclophosphamide, Paclitaxel and 5-Fluorouracil are antagonistic at lower doses

MDA-231 cells were plated in 96-well plates and treated with Docetaxel (A), Rapamycin (B), Doxorubicin (C), Tamoxifen (D), Cyclophosphamide (E), Paclitaxel (F), 5-Fluorouracil (G), alone) or with Amlexanox (30µM). Cell viability was determined using the Alamar Blue assay. The Chou-Talalay Method was used to calculate CI values plotted against Fa values to assess potential drug combination synergy. Synergistic CI <1 (yellow), Additive = 1 (dotted line), Antagonistic CI>1 (grey) Values are calculated using the means from at least three independent experiments

Owing to the fact that one of the potential benefits of finding new synergistic combinations of therapeutic agents is the potential to use them at lower concentrations to reduce side effects in the patient whilst maintaining efficacy, I decided to eliminate the chemotherapeutics (Tamoxifen, Cyclophosphamide, Paclitaxel, and 5-Fluorouracil) which I have shown to be antagonistic at lower doses. Following this, I examined the effect of chemotherapy treatment on the expression of IKKε in parental MDA-MB-231 breast cancer cells.

Treatment with Docetaxel (1nM) significantly increased the expression of IKKε by 48.3 ± 11.3% ($p<0.05$) compared to DMSO-treated control after 72 hours (Figure 56). Exposure to Rapamycin (10μM) had no effect on IKKε expression after 72 hours compared to DMSO-treated control (Figure 56). Interestingly, treatment with Doxorubicin (10nM) significantly reduced IKKε expression by 37.4± 16.8% ($p<0.05$; Figure 56).

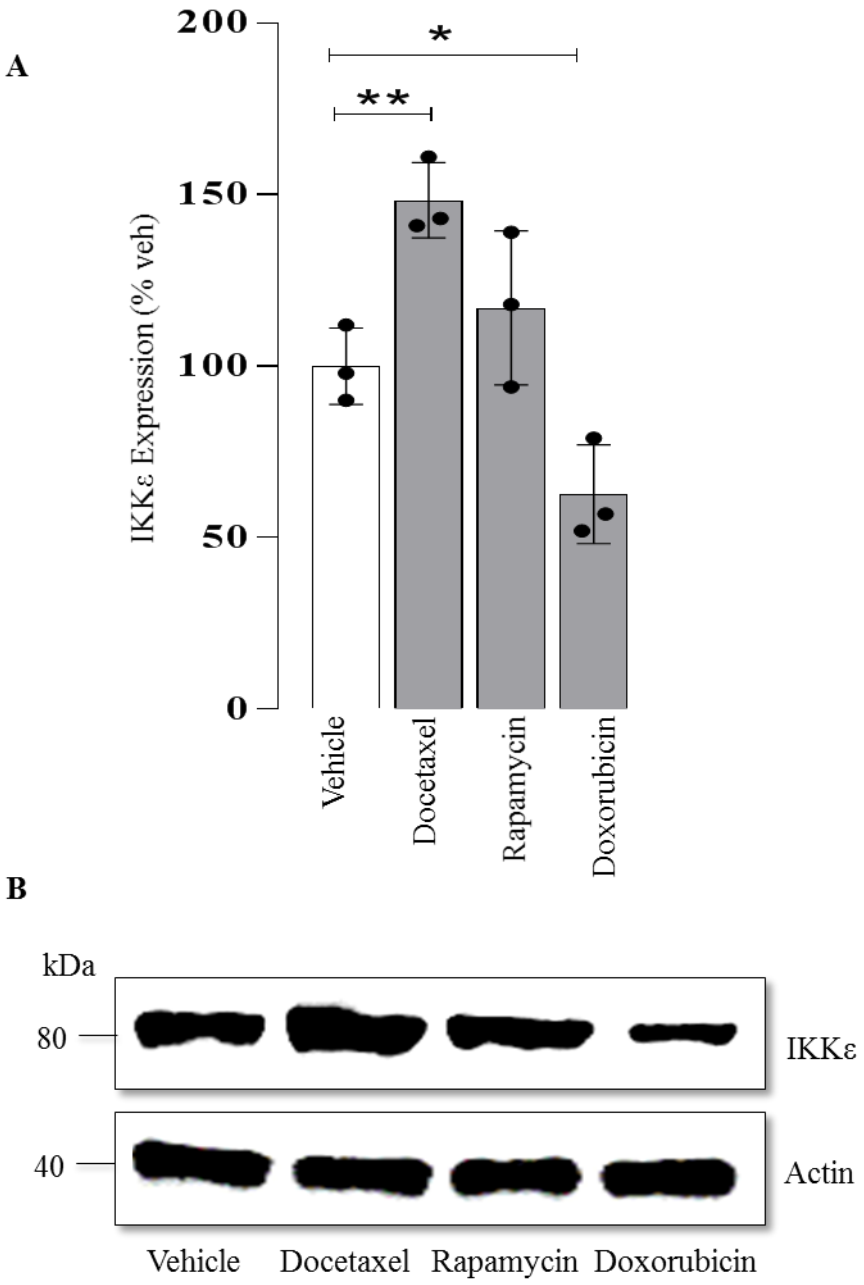

Figure 56. Docetaxel increases expression of IKKε in MDA-231 cells

Parental MDA-231 cells were exposed to Docetaxel (1nM), Rapamycin (10μM), Doxorubicin (10nM) or vehicle (DMSO) for 72 hours. Cells were lysed and total cellular protein was subjected to western blot analysis (70 μg/lane) using primary rabbit anti-IKKε and rabbit anti-β-actin. A) Quantification of the amount IKKε as a percentage of vehicle treated control. B) Representative Western blot image from the experiment described. Values are mean ± SD from at least three independent experiments; *$p<0.05$ from vehicle treated control

5.4.3 **Combined administration of Amlexanox significantly inhibits mammary tumour growth in mice.**

In Chapter 3, I have shown that Amlexanox (35mg/kg/5-day) reduced the growth of skeletal breast cancer metastases following intracardiac injection of 4T1-Luc2 cells in immunocompetent BALB/c mice**.** However, the majority of breast cancer patients do not present with advance disease, rather where the tumour remains localized**.** With this in mind, we wanted to test the effects of Amlexanox, Docetaxel and the combined administration of either agent in the neoadjuvant setting**.** To do this, we again utilised 4T1-Luc2 mouse breast cancer cells in syngeneic immunocompetent BALB/c, however, this time 4T1-Luc2 cells were injected orthotopically with $1x10^6$ cells being injected into each of the left and right mammary fat pads. The following day mice were injected with 1.5mg/kg D-Luciferin to check for tumour engraftment, where all mice developed tumours. The tumour was then measured with callipers. Mice were randomized to four groups (n=10/group) and administered vehicle (DMSO; 10% v/v in PBS), Amlexanox (35mg/kg/5-times-weekly), Docetaxel (15mg/kg/week) or the combination of either treatment (Figure 57A). The tumour volume was measured thrice weekly and was calculated using the volume of a sphere. When at least one of the tumours per mouse reached the maximum volume of $1000mm^3$, they were then surgically resected

Treatments were initiated on day 0 (the day after orthotopic injection) and no significant effect was observed on primary tumour growth at days 3, 5 and 7 between vehicle-, Amlexanox-, Docetaxel- or Combination-treated groups of mice. However, after Day 9 the primary tumours of combination treated mice had the largest reduction in tumour growth, with a 56.5± 23.1% reduction compared to vehicle treated controls (Figure 57B), whereas mice treated with Amlexanox showed a significant 31.73 ± 15.8% reduction, Docetaxel treated mice had a 29.1± 17.2% reduction and. Furthermore, the observed reduction in combination treated mice was significant when compared to Docetaxel as a single agent. Additionally, this significant reduction in tumour growth was maintained to the following time point, Day 11. There was a reduction of 37.9 ± 27.3% and 59.5 ± 17.7 % in primary

tumour growth of Docetaxel and Combination treated mice, respectively compared to vehicle treated control mice. Detailed statistical analyses can be seen in Table 11. Correspondingly, the combination treatment of Amlexanox and Docetaxel delayed the last tumours reaching maximum volume until day 18, compared to all mice in the vehicle control and Amlexanox treated groups reaching the maximum tumour volume of $1000mm^3$ by day 11 of treatment, the Docetaxel group reached maximum volume at day 16 and the combination group reached maximum volume at Day 17.

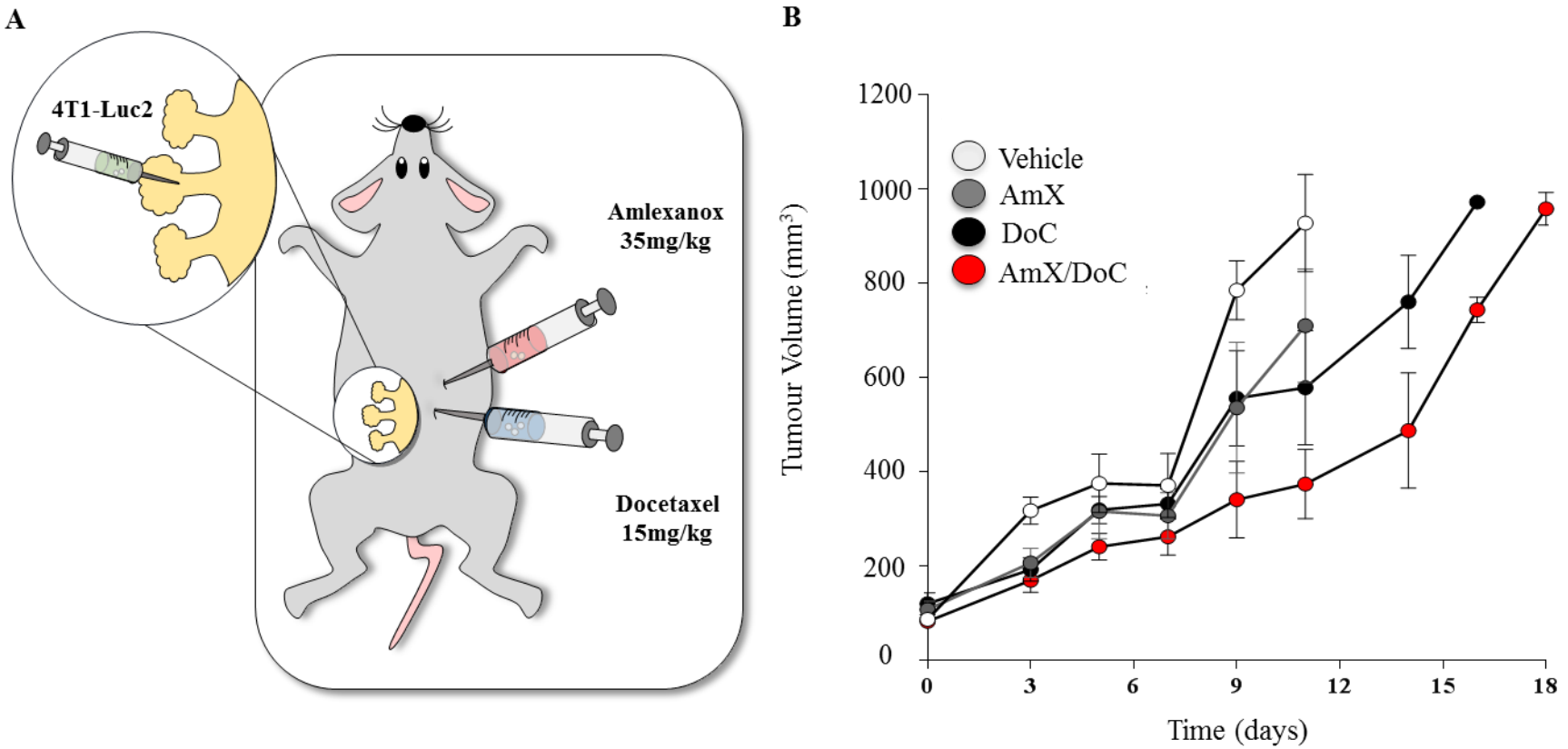

Figure 57. Combined administration of Amlexanox and Docetaxel significantly reduces primary tumour growth of 4T1-Luc2 cells after orthotopic injection.
A 4T1-Luc2 cells ($1x10^6$/100µl PBS/TB) were injected in to the left and right mammary fat pads of syngeneic BALB/c mice. Mice were split into four groups (n=10/group) and given daily i.p. injections of vehicle or Amlexanox (35mg/kg) or weekly Docetaxel (15mg/kg) or a combination of Amlexanox and Docetaxel. Primary orthotopic tumours were measured using callipers at the indicated time points. Results shown are mean values ± SEM. Related to figure ***Figure 31***.

Table 11. Detailed Statistical Comparisons of the 4T1-Luc2 primary tumour volume from mice treated with vehicle, Amlexanox, Docetaxel or Combination (Amlexanox and Docetaxel)

Comparison	Day 0		Day 3		Day 5		Day 7		Day 9		Day 11		Day 14		Day 16		Day 18	
	Summary	p-value	Summary	p-value	Summary	p-value	Summary	p-value	Summary	p-value	Summary	p-value	Summary	p-value	Summary	p-value	Summary	p-value
Veh vs. AmX	ns	0.9888	ns	0.2953	ns	0.7824	ns	0.799	*	0.036	ns	0.2292	NA	-	NA	-	NA	-
Veh vs. Doc	ns	0.9527	ns	0.1941	ns	0.7941	ns	0.9377	*	0.0318	***	0.0005	NA	-	NA	-	NA	-
Veh vs. Com	ns	0.9998	ns	0.0898	ns	0.145	ns	0.3925	****	<0.0001	****	<0.0001	NA	-	NA	-	NA	-
AmX vs. Doc	ns	0.9977	ns	0.9959	ns	>0.9999	ns	0.9797	ns	0.9956	ns	0.6597	NA	-	NA	-	NA	-
AmX vs. Comb	ns	0.9797	ns	0.9382	ns	0.6479	ns	0.9086	ns	0.1489	*	0.0197	NA	-	NA	-	NA	-
Doc vs. Comb	ns	0.9317	ns	0.9849	ns	0.5995	ns	0.6835	*	0.049	ns	0.0879	ns	0.1322	ns	0.1322	NA	-

Multiple comparisons were calculated using Two-way ANOVA followed by Tukeys Test on GraphPad Prism 7.0. Comparison of two groups at Day 16 and Day 18 were calculated using student's T-test. NS denotes 'not significant'; NA denotes 'not applicable' where statistical comparisons were not possible. Related to Figure 57

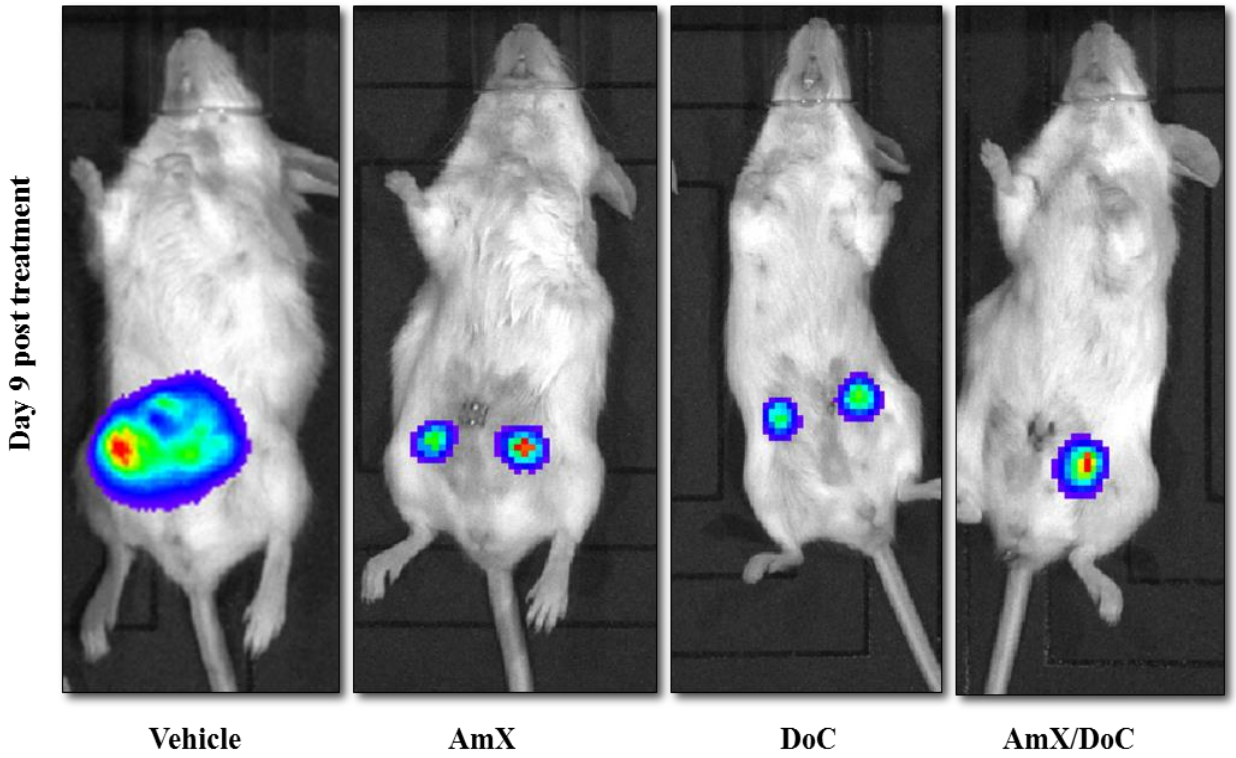

Figure 58. Representative images of tumour growth with Amlexanox, Docetaxel and combination treatment in mice.

4T1-Luc2 cells ($1x10^6$/100µl PBS/TB) were injected in to the left and right mammary fat pads of syngeneic BALB/c mice. Mice were split into four groups (n=10/group) and given daily i.p. injections of vehicle or Amlexanox (35mg/kg) or weekly Docetaxel (15mg/kg) or a combination of Amlexanox and Docetaxel. IVIS system was used to detect in vivo primary tumours at day 9 following 1.5mg/kg injection of D-luciferin.

5.4.4 **Combined administration of Amlexanox and Docetaxel had no significant effect on primary tumour weight following removal.**

In order to assess for the development of distant overt metastases using the IVIS system, it was important to allow the primary tumours to reach the same end point of 1000mm^3. Upon removal, the tumours were weighed and no significant difference in primary tumour weight was observed between vehicle, Amlexanox, Docetaxel or Combination treated mice.

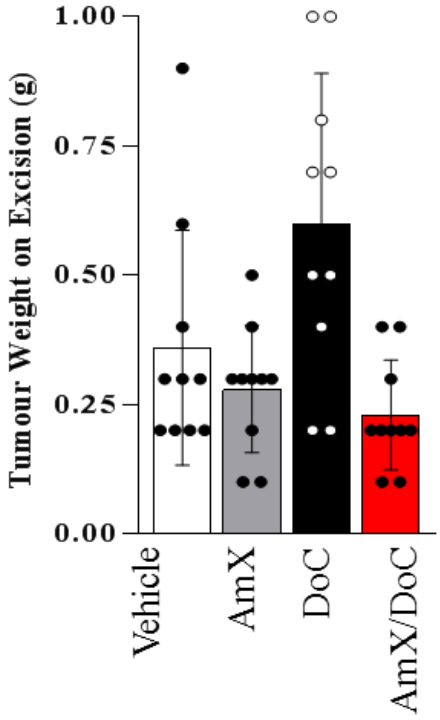

Figure 59. No significant difference in tumour weight between groups following tumour removal
4T1-Luc2 cells (1x10^6/100µl PBS/TB) were injected in to the left and right mammary fat pads of syngeneic BALB/c mice. Mice were split into four groups (n=10/group) and given daily i.p. injections of vehicle or Amlexanox (35mg/kg) or weekly Docetaxel (15mg/kg) or a combination of Amlexanox and Docetaxel. Upon surgical resection, primary tumours were weighed. Results shown are mean ± SD.

5.4.5 **Combined administration of Amlexanox and Docetaxel reduced body weights of mice**

Amlexanox has been shown to reduce body weight of obese mice (Reilly et al., 2013). Furthermore, Docetaxel can cause significant unwanted side effects as a single agent in patients such as anaemia, loss of appetite, nausea, diarrhoea and weight loss thus it was important to regularly monitor the behaviour and body weight of the mice. As seen in Figure 60, neither Amlexanox nor Docetaxel had any significant effect on the body weight of mice compared to the vehicle treated group. However, from 7 to 21 days of combination treatment, this group had significantly lower body weight than compared to vehicle treated mice (day 7 $p<0.05$; day 14 $p<0.001$; day 21 $p<0.05$). Of note, mice given combined administration of Amlexanox and Docetaxel did appear distressed in the hours after treatments. Although, it is important to note that the none of the mice lost more than 20% of their body weight, the allowed threshold.

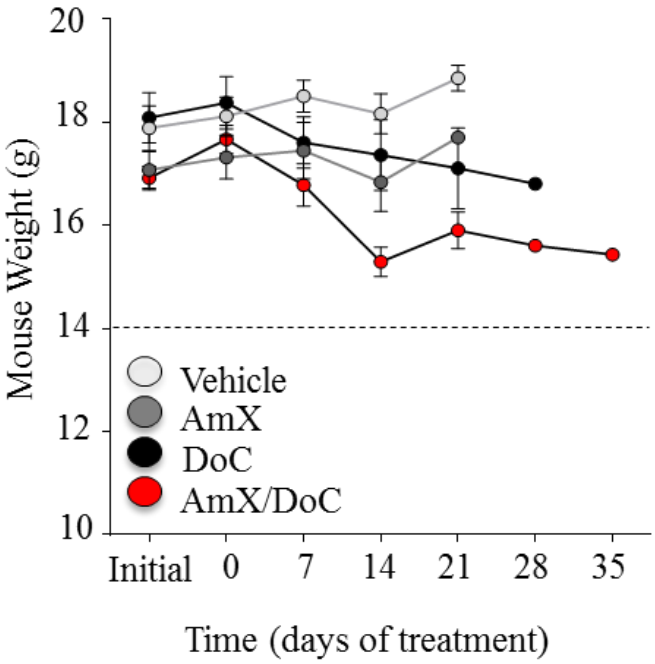

Figure 60. Combined administration of Amlexanox and Docetaxel reduced body weights of mice.

4T1-Luc2 cells ($1x10^6$/100µl PBS/TB) were injected in to the left and right mammary fat pads of syngeneic BALB/c mice. Mice were split into four groups (n=10/group) and given daily i.p. injections of vehicle or Amlexanox (35mg/kg) or weekly Docetaxel (15mg/kg) or a combination of Amlexanox and Docetaxel. Mice were weighed at the indicated time points. Results shown are mean ± SD. Dotted line indicates 80% of starting mean body weight. Detailed statistical analysis shown in Table 12.

Table 12. Detailed Statistical Comparisons of the mouse body weights from groups treated with vehicle, Amlexanox, Docetaxel or Combination (Amlexanox and Docetaxel)

Comparison	Initial		Day 0		Day 7		Day 14		Day 21	
	Summary	P-value	Summary	P-value	Summary	P-value	Summary	P-value	Summary	P-value
Veh vs. AmX	ns	0.480	ns	0.491	ns	0.317	ns	0.43	ns	0.88
Veh vs. Doc	ns	0.985	ns	0.968	ns	0.460	ns	0.67	ns	0.35
Veh vs. AmX/Doc	ns	0.318	ns	0.856	*	0.029	***	0.001	*	0.02
AmX vs. Doc	ns	0.283	ns	0.283	ns	0.243	ns	0.94	ns	0.97
AmX vs. AmX/Doc	ns	0.992	ns	0.992	ns	0.926	ns	0.27	ns	0.54
Doc vs. AmX/Doc	ns	0.167	ns	0.167	ns	0.591	*	0.02	ns	0.35

Multiple comparisons were calculated using Two-way ANOVA followed by Tukeys Test on GraphPad Prism 7**.**0**.** NS denotes ‘not significant’; Related to Figure 60

5.4.6 **Combined administration of Amlexanox and Docetaxel prolonged metastasis-free survival in mice**

Following the removal of the primary tumour, I observed the development of secondary metastases. The development of metastases was monitored bi-weekly after the removal of the primary tumours using the IVIS system. Upon detection of a secondary metastasis, the primary end goal was reached and mice were sacrificed. As shown in Figure 61, vehicle treated mice had a median metastasis free survival of 17 days however, combined administration of daily Amlexanox to weekly Docetaxel significantly increased the median metastasis free survival by 1.82-fold to 31 days ($p<0.001$). Moreover, Amlexanox treated mice also had a median metastasis free survival of 17 days. Docetaxel treated mice had a median survival of 21 days; however this was not significantly longer than vehicle treated mice (Figure 61).

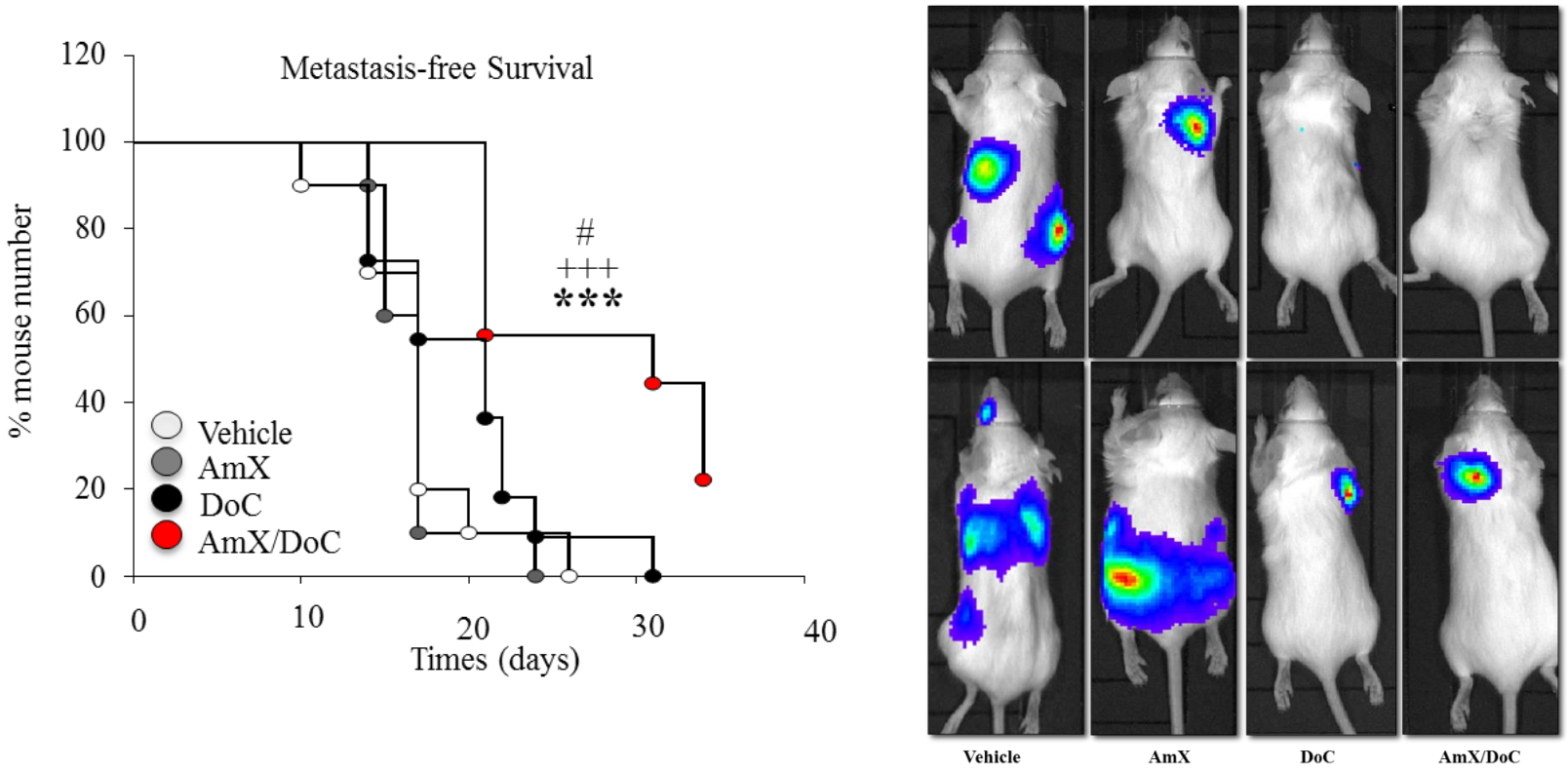

Figure 61. Combined administration of Amlexanox and Docetaxel prolonged metastasis-free survival in mice.

4T1-Luc2 cells ($1x10^6$/100µl PBS/TB) were injected in to the left and right mammary fat pads of syngeneic BALB/c mice. Mice were split into four groups (n=10/group) and given daily i.p. injections of vehicle or Amlexanox (35mg/kg) or weekly Docetaxel (15mg/kg) or a combination of Amlexanox and Docetaxel. Following primary tumour removal, mice were monitored for the development of metastasis using IVIS system. Mice were sacrificed following detection of tumour. **A** Metastasis free survival curves for the 4 treatment groups. **B** Representative IVIS images at two time points. *** $p<0.001$ from vehicle treatment; $p<0.001$ from Amlexanox treatment; # $p<0.05$ from Docetaxel treatment.

5.4.7 **Combined administration of Amlexanox and Docetaxel reduces breast cancer metastases in mice.**

Breast cancers preferentially spread to bone, lung, liver and brain (Wu et al., 2016). Following sacrifice, the internal organs were collected and imaged in the IVIS system. *Ex vivo* bioluminescence analysis revealed that vehicle-treated mice developed an average of 3 metastases however, combined administration of Amlexanox and Docetaxel markedly reduce the number of metastases observed to an average of 1.1 per mouse ($p<0.01$). There was no significant change in the average number of metastases observed in mice treated with Amlexanox or Docetaxel as single agents, with each group developing an average of 3.6 and 2.9 respectively

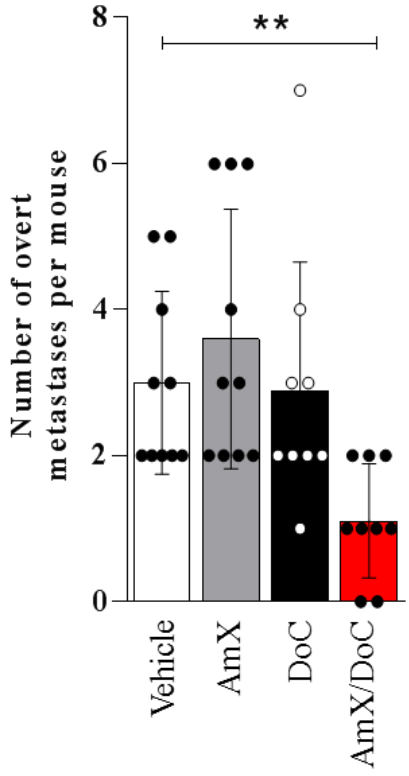

Figure 62. Combined administration of Amlexanox and Docetaxel reduced metastases in mice. 4T1-Luc2 cells ($1x10^6$/100µl PBS/TB) were injected in to the left and right mammary fat pads of syngeneic BALB/c mice. Mice were split into four groups (n=10/group) and given daily i.p. injections of vehicle or Amlexanox (35mg/kg) or weekly Docetaxel (15mg/kg) or a combination of Amlexanox and Docetaxel. Following primary tumour removal, mice were monitored for the development of metastasis using IVIS system. Mice were sacrificed following detection of metastases. Organs were collected and ex vivo bioluminescence was performed using the IVIS system. Results shown are mean ± SD. ** $p< 0.01$ from vehicle treated controls.

Further *ex vivo* examination of the individual organs and the femur and tibiae bones of the mice using bioluminescence revealed that control mice developed lung, bone, brain and spleen metastases (no liver or kidney metastases were observed in this model). Mice also developed peritoneal metastases, in which the metastases had invaded from the primary tumour and through the peritoneum in to the gut. Combined administration of Amlexanox and Docetaxel significantly reduced lung and spleen metastases (compared to vehicle-, Amlexanox-, and Docetaxel-treated mice). Additionally combined administration of Amlexanox and Docetaxel reduced the number of invasive peritoneal metastases compared to vehicle and single agent Amlexanox (Table 13). In concordance with the previous results, mice given either Amlexanox or Docetaxel developed metastases in these organs also and no significant difference in the incidence of organ specific metastases was observed.

Table 13. The incidence of secondary metastases in BALB/c mice treated with vehicle, Amlexanox, docetaxel or a combination treatment in the neoadjuvant setting.

	Frequency of Metastasis			
Organ	- -	AmX -	- Doc	AmX Doc
Lung	10/10	9/10	10/10	6/9*+#
Bone	3/40	7/40	5/40	0/36
Brain	1/10	3/10	2/10	0/9
Spleen	7/10	6/10	5/10	0/9*+#
Peritoneal	9/10	9/10	6/10	4/9*+

Fisher's exact test was used to calculate statistical differences between metastatic incidences. *$p<0.05$ from vehicle; + $p<0.05$ from Amlexanox treated; # $p<0.05$ from Docetaxel treatment.

5.4.8 **Amlexanox, Docetaxel and their combination had no significant effect on the individual size of metastases in mice.**

Having shown that the combination of both Amlexanox and Docetaxel significantly reduce metastatic development following orthotopic injection of 4T1-Luc2 cells yet neither Amlexanox (35-mg/kg/5-times weekly) nor Docetaxel (15mg/kg/weekly) alone reduced the incidence of overt metastases thus I decided to see if either treatment alone and in combination was sufficient to reduce the size of metastatic tumours in the organs collected. As seen in Figure 63, a trend to smaller lung metastases was observed in the single and combination treated groups, however, this trend was not significant. Similarly, no significant difference was observed in the size of brain or spleen metastases in mice treated with Amlexanox, Docetaxel or Combination treatments compared to vehicle treated control mice. No differences in volume of bone metastases were observed between mice treated with control or single drug, alone, however, no bone metastases were detected following combination treatment.

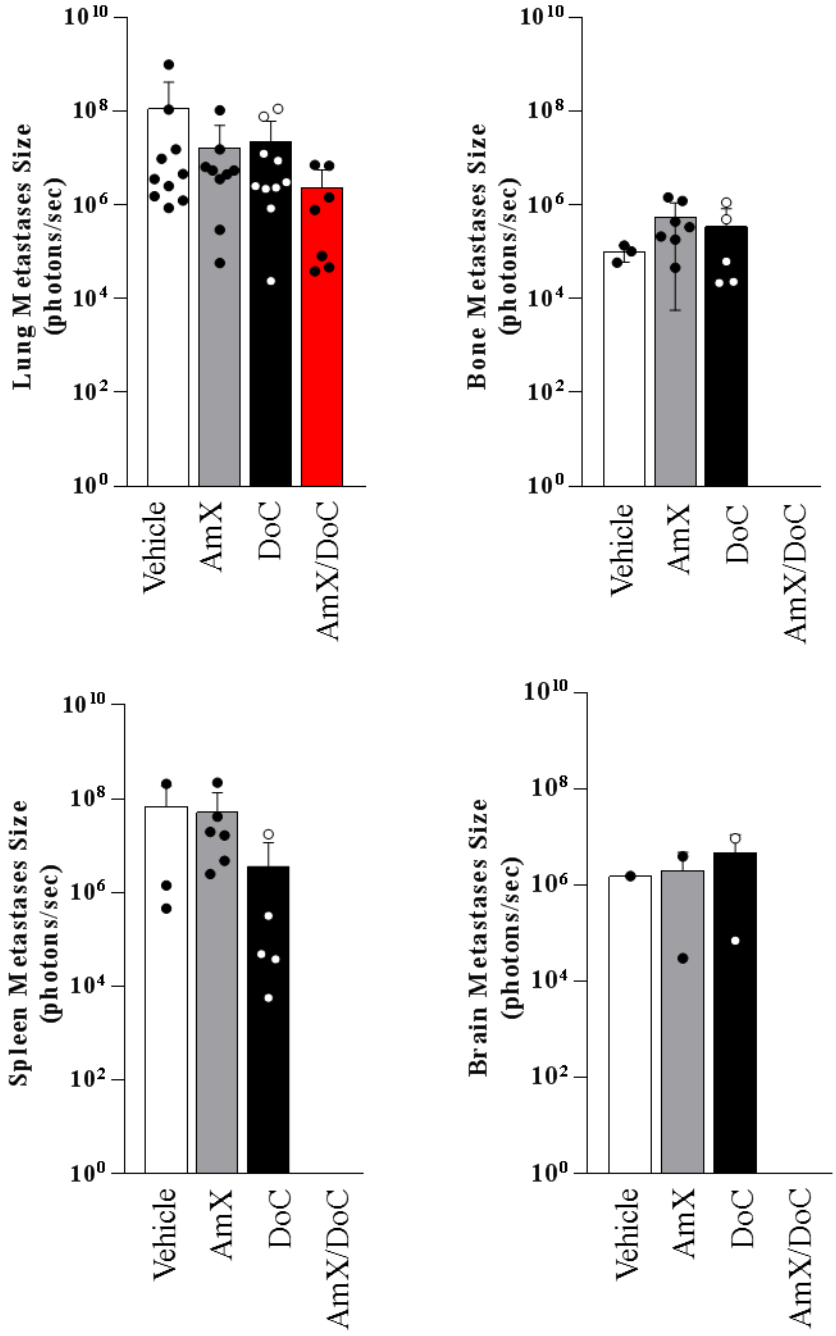

Figure 63. Amlexanox, Docetaxel and their combination had no significant effect on the size of metastases in mice ex vivo.

4T1-Luc2 cells ($1x10^6$/100µl PBS/TB) were injected in to the left and right mammary fat pads of syngeneic BALB/c mice. Mice were split into four groups (n=10/group) and given daily i.p. injections of vehicle or Amlexanox (35mg/kg) or weekly Docetaxel (15mg/kg) or a combination of Amlexanox and Docetaxel. Mice were sacrificed following detection of metastases. Organs were collected and ex vivo bioluminescence was used to calculate the size of tumours in organs. Results shown are mean ± SD.

5.5 Discussion

Aberrant expression and regulation of the NFκB signalling cascade is implicated in the oncogenesis and progression of various haematological and solid malignancies including breast cancer through mediation of cell death, cell cycle progression and inflammatory processes (Baldwin, 2001). Recent studies have showed that a multitude of chemotherapeutics activate the NFκB signalling pathway, which in this context functions to prevent apoptosis via induction of anti-apoptotic genes. In the preceding chapters, I have shown that Amlexanox alone reduces *in vitro* breast cancer cell growth and skeletal tumour growth of triple negative breast cancer cells *in vivo*. Here, I wanted to assess whether pharmacological inhibition of IKKε could enhance the effects of chemotherapies.

Firstly, I tested a panel of clinically available FDA-approved chemotherapies alone or in combination with Amlexanox on triple negative breast cancer cell viability *in vitro.* Amlexanox reduced the IC_{50} value of all of the chemotherapies tested and higher doses were synergistic in their action, however, at lower doses the combination of paclitaxel, tamoxifen, cyclophosphamide or 5-flurouracil with Amlexanox was found to be antagonistic. Chemotherapies, although efficacious in prolonging disease-free and overall survival following the removal of the primary tumour, often have unwanted side effects that halt their continued use in clinics such as cardiotoxicity, anaemia, diarrhoea, and hair loss**.** One of the potential benefits of combination therapies may be using chemotherapies at lower doses to avoid or reduce adverse side-effects. Thus those that had demonstrated antagonistic potential were eliminated from further studies. Further studies showed that Docetaxel treatment increased IKKε expression, whilst rapamycin and doxorubicin had no effect and reduced expression respectively. Encouraged by these results, I went on to test the effects of combined treatment of Amlexanox and Docetaxel in the neoadjuvant setting *in vivo*.

Localised breast cancer has a favourable outlook, with around a 95% 5-year survival rate**.** Management of breast cancer varies greatly depending on the size; grade and receptor status however usually includes surgery, radiation and/or systemic delivery of therapy. Breast cancers, in humans can have a long latency period and relapses in secondary organs develop many years after the removal of the primary tumour**.**

Therefore, I used a model that recapitulates the human condition but in a shorter time space. In this model, combined treatment of Amlexanox and Docetaxel reduced primary tumour growth and the number of overt metastases and enhanced metastasis-free survival following surgical removal of the primary tumour, significantly more so than vehicle or either agent alone. Interestingly, combination treated mice also lost significantly more weight than vehicle treated mice or either agent alone. Of note, a study by Reilly and colleagues showed that Amlexanox prevented diet-induced obesity in mice by inducing thermogenesis, potentially explaining the reduction in weight loss (Reilly et al., 2013).

A number of studies have previously shown that IKKε contributes to chemoresistance in various cancer models (Guo et al., 2009, Guo et al., 2010). However, no studies to date have combined Amlexanox with clinically relevant chemotherapies to reduce breast cancer cell growth *in vitro* or *in vivo*. Future studies, using platforms such as Nanostring, should aim to elucidate the mechanisms through which combined treatment of Amlexanox and Docetaxel reduce tumour growth and metastasis. In addition, further preclinical studies should also aim to assess different dosing and scheduling strategies in order to minimise potential side effects whilst maximising the observed anti-cancer effects of these two FDA-approved drugs, such that first in man trials could be carried out. Together, these data implicate IKKε in Docetaxel resistance and identify it as potential target for the treatment of breast cancer in combination with taxanes and other chemotherapies.

Chapter 6

General Discussion

6 Chapter 6

6.1 General Discussion

The IKK/NFκB signalling pathway plays a role in the development of breast cancer (Lee et al., 2007, Hu et al., 2004), and inflammation-induced bone loss (Ruocco et al., 2005, Idris et al., 2010, Otero et al., 2010, Park et al., 2007, Idris et al., 2009). Past studies have implicated both the canonical and non-canonical NFκB pathways in the regulation of breast cancer bone metastasis (Park et al., 2007), and recent work by our laboratories has found that pharmacological and cancer specific inhibition of these pathways reduces the progression of breast cancer osteolytic metastastasis (Idris et al., 2009). Furthermore, a recent study by Zhang and colleagues showed that pharmacological inhibition of the IKK-related kinases, IKKε and TBK-1 significantly reduced ovariectomy-induced bone loss *in vivo* (Zhang et al., 2015).

Interestingly, IKKε is the only IKK family member that has been deemed a breast cancer oncogene through its activation of the NFκB pathway (Boehm et al., 2007). However, its contribution to breast cancer bone metastasis has not been previously investigated. Here I provide evidence for a previously unknown role of IKKε in the regulation of skeletal tumour growth and breast cancer induced osteolysis. Previous studies have shown that overexpression of IKKε in normal mammary epithelial cells results in tumourigenesis and primary tumour growth (Boehm et al., 2007) . Originally, these studies found no association with hormone receptor positive, HER2 overexpressing or triple negative breast cancer using a small cohort of patients, however, after retrospectively assessing two independent large cohorts of breast cancer patients, this study has found that IKKε is amplified in around 20% of breast cancer patients and that its expression is associated with triple negative disease. This is in

agreement with previous studies that found IKKε to be linked to a subset of inflammation-driven triple negative breast cancers (Barbie et al., 2014). Furthermore, using larger patient cohorts, I have shown that high expression of IKKε is associated with a significantly shorter overall survival. With this in mind I expanded on these aforementioned studies where I have shown that IKKε regulates breast cancer cell metastatic and osteotropic potential in two independent triple negative breast cancer models.

I demonstrated that overexpression of IKKε in an aggressive osteotropic variant of MDA-MB-231 (MDA-BT1) enhances cell growth, migration and invasion *in vitro.* Additionally, IKKε overexpression in MDA-BT cells also enhanced their ability to support osteoclastogenesis, a characteristic of bone metastatic breast cancers. The increased osteotropic capacities of these cells could be abrogated through siRNA-mediated inhibition of the IRF3 or NFκB signalling pathways. Preceding studies have shown that IKKε-induced transformation is dependent on p65 and not IRF3 and similarly, I have shown that IKKε driven growth is dependent on NFκB rather than IRF3. However, IKKε-driven osteoclast formation was driven by both NFκB and IRF3 pathways, both pathways having been previously implicated in cancer cell secretion of inflammatory factors. Conversely, inhibition of IKKε in MDA-BT using either shRNA or pharmacologically using the IKKε/TBK-1 inhibitor, Amlexanox significantly reduced the growth, migration, invasion and ability to support osteoclast formation of osteotropic MDA-MB-231 breast cancer cells. Inhibition of IKKε was associated with a reduction in a variety of proinflammatory cytokines, osteoclastic cytokines and matrix remodeling proteins. Furthermore, knockdown of IKKε in the aggressive osteotropic sub-clone of MDA-MB-231 cells significantly reduced skeletal tumour

burden and their ability to cause osteolysis in immuno-deficient mice thus implicating a prior unidentified role of IKKε in breast cancer skeletal tumour growth.

Osteotropic breast cancer cells acquire the capability to promote osteolysis by influencing the differentiation of osteoclasts and osteoblasts (Yoneda and Hiraga, 2005, Siclari et al., 2006, Zhang et al., 2013). We, and others, have previously reported that pharmacological inhibition of NFκB activity reduced bone loss through inhibition of osteoclastic bone resorption and stimulation of osteoblast differentiation (Otero et al., 2010, Chang et al., 2009b, Alles et al., 2010, Ruocco et al., 2005, Idris et al., 2010). The findings of the present study expand on these observations and demonstrate that pharmacological inhibition of IKKε/TBK-1 in the tumour bone microenvironment using the inhibitor, Amlexanox significantly reduced skeletal tumour growth and the resultant osteolysis caused by murine 4T1 breast cancer cells in immunocompetent mice. Mechanistic studies revealed that Amlexanox prevented the RANKL-induced phosphorylation of IκB in macrophages cells and RANKL induced osteoclast formation *in vitro.* These data further suggest that suppression of IKKε/NFκB in the bone microenvironment suppresses osteoclast formation and skeletal tumour burden in mice.

IKKε and NFκB signalling have been implicated in the growth of primary breast cancer and its resultant metastasis to distant sites (Boehm et al., 2007, Barbie et al., 2014, Qin and Cheng, 2010, Park et al., 2007, Peramuhendige et al., 2018). With this in mind, we aimed to examine the efficacy of IKKε/TBK-1 inhibition using Amlexanox on primary tumour growth. As a single agent, Amlexanox reduced the tumour growth of syngeneic mouse breast cancer cells following orthotopic injection yet had no effect on the number of metastases or metastasis-free survival of mice following removal of the

primary tumour. Considering that targeting of a single pathway, is unlikely to provide long-term benefits in terms of metastatic spread, secondary tumour growth and overall patient survival in a disease as complex as breast cancer, we also evaluated the effects of Amlexanox in combination with FDA-approved Docetaxel (Zeichner et al., 2016). Amlexanox exerted a synergistic effect with Docetaxel resulting in a significant reduction of primary tumour growth, a reduction in the number of overt metastases and almost a 2-fold improvement in metastasis-free survival when compared to vehicle or either treatment as a single-agent. However, I did observe that mice given the combination treatment lost significantly more body weight than those treated with individual agents. From a clinical point-of-view weight loss and cachexia are serious complications of cancer and its treatments for breast cancer patients. In a similar vein, NFκB and cytokine production is a vital part of the innate immune system (Bonizzi and Karin, 2004). In addition breast cancer patients who take Docetaxel often suffer with neutropenia (Montero et al., 2005). Although not addressed in this study, subsequent studies should assess levels of white blood cells in mice treated with the combination of Amlexanox and Docetaxel. Impairment of the immune system is a serious adverse complication for advanced breast cancer patients (Montero et al., 2005).

Irrespective of the potential downsides, the observed synergism between Amlexanox and Docetaxel in inhibiting tumour growth and recurrent metastases *in vivo* suggests the combination of Docetaxel and therapeutic targeting of IKKε/TBK-1 may be of value of the treatment of metastatic breast cancers. In addition, these findings lend credence to the notion that blocking more than one aspect of metastatic breast cancer may have added benefits to chemotherapy in terms of clinical outcomes.

Collectively, the results of the present study demonstrate that IKKε plays a significant role in the regulation of bone metastasis, skeletal tumour growth, osteolysis and enhanced bone cell activity associated with advanced breast cancer. These results offer new insight into the crosstalk between breast cancer cells and bone cells of the tumour microenvironment, and provide evidence to show that disruption of IKKε/TBK-1, alone or in combination with clinically relevant chemotherapies such as taxanes, may have potential therapeutic efficacy in all stages of breast cancer.

6.2 On-going and Future studies

6.2.1 **IKKε, bone metastasis and osteolysis**

In this study, I have demonstrated that pharmacological inhibition and knockdown of IKKε reduces breast cancer skeletal tumour growth and subsequent osteolysis. However, as the tumour growth and osteolysis were both reduced, we cannot yet deem if IKKε is necessary for breast cancer induced osteolysis or only a reduction in skeletal tumour growth. In a similar manner, Amlexanox reduced breast cancer skeletal tumour growth and osteolysis. In order to address this issue, conditioned medium from MDA-BT1 Mock and MDA-BT1 IKKε^{KD} should be injected supracalvarially in to mice to induce osteolysis thus removing the effect of tumour growth inhibition (Marino et al., 2014a, Marino et al., 2018a, Peramuhendige et al., 2018). In addition, it would be beneficial to address the effect of Amlexanox alone and in combination with Docetaxel on bone metastasis and skeletal colonisation. To do this, mice should be pre-treated with Amlexanox and/or Docetaxel before injection of bone-seeking breast cancer cells such as MDA-MB-231-I.V/B02 (Nutter et al., 2014, Peyruchaud et al., 2001). Similar studies have sought to establish the effects of combined administration of anti-cancer and anti-resorptive agents (zoledronic acid) on skeletal tumour burden (Ottewell et al., 2008). However, owing to the fact that Amlexanox functions as both an anti-resorptive and an anti-cancer agent, the combination of Amlexanox and Docetaxel may be superior at inhibiting skeletal tumour growth in the osseous microenvironment.

6.2.2 **Combined administration of chemotherapies and IKKε inhibitors**

In this study I have shown that IKKε is a potential druggable target for the treatment of metastatic triple negative breast cancer in the 20% of breast cancer patients whose tumours harbour CNVs of IKKε. These patients have a significantly shorter overall survival and these data suggests that targeting IKKε may provide life prolonging benefit. With this in mind, future pre-clinical studies should aim to optimise the scheduling and dosing of IKKε inhibitors with Docetaxel in order to reduce adverse side-effects and enhance the efficacy of the combination at reducing metastatic spread of breast cancers and improving patient survival. Furthermore, future studies could also address if inhibition of IKKε can be combined with targeted treatments. ER+ and HER2-enriched breast cancers are often treated with therapies such as tamoxifen and Herceptin respectively. Activation of NFκB has been shown to play a role in response to both tamoxifen and Herceptin resistance (Guo et al., 2010, Zhou et al., 2007, Kanzaki et al., 2016) therefore it may be pertinent to explore whether IKKε inhibition in combination with these and other chemotherapies may be of value in overcoming resistance and enhancing patient survival.

In this study I have demonstrated that Amlexanox acts synergistically with rapamycin in triple negative breast cancer cells. Everolimus, a derivative of Sirolimus (Rapamycin) is approved for the treatment of metastatic ER+ breast cancers in combination with hormone-therapy (Baselga et al., 2012). The BOLERO-2 trial indicated that everolimus reduced the incidence of breast cancer progression in bone (i.e., development of new skeletal metastases) in the overall patient population (Gnant et al., 2013). Furthermore, the combination of everolimus and hormone therapy (exemestane) reduced progressive bone disease in patients with bone metastases at baseline (Gnant et al., 2013). The reduction in skeletal lesion progression is postulated to be due the effects of everolimus on bone remodelling. Everolimus and Rapamycin have both been shown to inhibit osteoclast formation and resorption in pre-clinical models (Kneissel et al., 2004). Therefore, it would be interesting to test the added effects of Amlexanox in this combination as Amlexanox similarly reduces osteoclast formation and activity whilst inhibiting breast cancer skeletal growth.

6.2.3 **Combined administration of immunotherapies and IKKε inhibitors**

The remarkable success of immunotherapies in cancers such as lung and melanoma, revealed the suppressive power of T-cell anti-tumour immunity (CiRen et al., 2016, Gandhi et al., 2018). Immunotherapies are treatments that aim to enhance the patient's own immune system to eliminate cancer cells. Often in tumours, cancer cells have developed mechanisms to evade the innate and adaptive immune system. Tumour cells upregulate molecules like programmed death receptor ligand-1 (PDL-1) and others which bind to inhibitory receptors on the surface of T-cells such as programmed death receptor-1 and cytotoxic T-lymphocyte-associated protein 4 (CTLA-4). These receptors function to induce T-cell anergy and apoptosis thus inhibiting an anti-tumour response. The most trialled and successful immunotherapies so far in breast cancer have been PD1 blockade with around 20% of patients exhibiting a significant improvement (Nanda et al., 2016), thus there is still a need to enhance the efficacy of immunotherapies for the treatment of breast cancer.

Recently, it was demonstrated that IKKε acts as a negative regulator of CD8+ (cytotoxic) T-cell activity (Zhang et al., 2016). IKKε phosphorylates the transcription factor NFATc1 upon T-cell activation to inhibit prolonged activation of T-cells. Zhang and colleagues went on to demonstrate that knockout of IKKε in CD8+ reduces metastatic tumour burden and significantly improves survival in a mouse model of melanoma. In this study we demonstrated that IKKε inhibition reduces skeletal and primary tumour growth of breast cancer cells. Our unpublished data indicates that Amlexanox inhibits macrophage- and TNFα-induced expression of PDL1 by cancer cells (Gkanatsiou, Bishop and Idris, *unpublished data*) and thus, it would be interesting to assess how pharmacological inhibition of IKKε in combination with immunotherapies such as PD-1/CTLA-4 inhibitors affects primary and metastatic tumour growth of breast cancer cells in mouse models. Current work in our own laboratory is investigating the link between IKK/NFκB activity and anti-tumour T-cell responses.

6.2.4 **The role of IKKε inhibitors in obesity-driven breast cancers**

Obesity has become pandemic and studies suggest that a high-fat diet and obesity enhance the incidence of cancers including breast cancer (Meldrum et al., 2017). Current studies suggest that obese breast cancer patients have a significantly poorer

prognosis than their healthy counterparts (Protani et al., 2010). In addition, it has been suggested that obesity enhances the development of metastasis via production of proinflammatory cytokines that alter the metastatic niche (Quail et al., 2017)

In recent years, a number of studies have demonstrated that IKKε and TBK-1 are both upregulated in adipose tissue in response to a high-fat diet (Chiang et al., 2009). In addition, they demonstrated that targeted deletion of adipose IKKε prevented diet-induced obesity and reduced adipose inflammation. Furthermore, in a follow-up study by Reilly and colleagues, it was shown that Amlexanox causes reversible weight loss and reduction of adipose inflammation in obese mice. In this study I have demonstrated that IKKε is overexpressed in ~20% of breast cancer patients. Therefore one could postulate that pharmacological inhibition of IKKε in obese patients may serve to reduce adipose inflammation and resultant metastatic spread. Future studies should assess the role of obesity in breast cancer growth and metastasis and whether pharmacological inhibition of IKKε can reduce or even prevent obesity driven breast cancers.

Appendices

Appendices

Appendix 1. List of reagents and manufacturers.

Materials and reagents	Supplier	Experiment
1.5ml Eppendorf tubes with cap	Starlab, Milton Keynes, UK	Western blot/TC
12% Criterion™ TGX™ Precast Midi Protein Gel, 12+2 well	Bio-Rad Laboratories, Hertfordshire, UK	WB
4-Nitrophenyl phosphate disodium salt hexahydrate powder	Scientific laboratory supplies (SLS), Nottingham UK	ALP
Acetic Acid Glacial	Sigma Aldrich, Dorset, UK	TRAcP
Agar powder	Sigma Aldrich, Dorset, UK	Transfection protocol
AlamarBlue™ reagent	Invitrogen, Paisley, UK	Viability
Alizarin Red S	Sigma Aldrich, Dorset, UK	Mineralization
Amlexanox	Tocris Bioscience, Bristol, UK	Drug treatments
Anti-CD14 microbeads human	Miltenyi Biotech, Gladbach, Germany	Human OC
BD microlance needles (19, 21 and 25G)	Fisher Scientific, Leicestershire, UK	Isolation
Bicinchoninic acid (BCA) solution	Sigma Aldrich, Dorset, UK	BCA assay
Blasticidin	Sigma Aldrich, Dorset, UK	Transfection protocol
Bovine serum albumin	Sigma Aldrich, Dorset, UK	Antibodies
Carbenicillin	Fisher Scientific, Leicestershire, UK	Transfection protocol
CAY10575	Cambridge Bioscience, Cambridge, UK	Drug treatments
CAY10576	Cambridge Bioscience, Cambridge, UK	Drug treatments
Centrifuge tubes 15ml	Scientific laboratory supplies (SLS), Nottingham UK	TC
Centrifuge tubes 50ml	Fisher Scientific, Leicestershire, UK	TC/WB
Cetyl pyridinium chloride monohydrate	Sigma Aldrich, Dorset, UK	Destain
Clarity Western ECL Substrate	Bio-Rad Laboratories, Hertfordshire, UK	WB
Collagenase (type 1A)	Sigma Aldrich, Dorset, UK	Primary OB
Copper (II)-sulfate	Sigma Aldrich, Dorset, UK	BCA assay
Corning™ Transwell™ Multiple Well Plate with Permeable Polycarbonate Membrane Inserts	Corning, Flintshire, UK	Invasion assay
Cover slips	Fisher Scientific, Leicestershire, UK	Any histology
DAKO	Sigma Aldrich, Dorset, UK	Invasion assay

Diethanolamin	Sigma Aldrich, Dorset, UK	TRAcP staining
DL-Dithiothreitol (DTT)	Sigma Aldrich, Dorset, UK	Strip WB/ Sample buffer
DMSO	Sigma Aldrich, Dorset, UK	Freezing
DPX mounting medium	Sigma Aldrich, Dorset, UK	Slide mounting (TRAcP)
Dulbecco's Minimum Essential Medium (DMEM)	Fisher Scientific, Leicestershire, UK	TC
ECL solution	Bio-Rad Laboratories, Hertfordshire, UK	WB
EDTA	Sigma Aldrich, Dorset, UK	Lysis
EDTA Buffer, sterile`	Sigma Aldrich, Dorset, UK	OC
Electrophoresis power supply	Bio-Rad Laboratories, Hertfordshire, UK	WB
Ethanol Absolute	Sigma Aldrich, Dorset, UK	Transfection protocol
Fetal calf serum (FCS)	Fisher Scientific, Leicestershire, UK	TC
Filter Tips any size	Starlab, Milton Keynes, UK	General
Glycine	Acros organics, Geel, Belgium	Sample buffer
Histopaque	Sigma Aldrich, Dorset, UK	Isolation of PBMCs
Human recombinant RANKL	Gift from Dr. Patrick Mollat (Proskelia SASU)	Osteoclast assays
Hygromycin	Sigma Aldrich, Dorset, UK	Transfection protocol
Jackson ImmunoResearch Anti-rabbit secondary ab	Stratech Scientific Unit, Newmarket Suffolk, UK	WB
Kaleidoscope Pre-stained standards	Bio-Rad Laboratories, Hertfordshire, UK	WB
L-Ascorbic acid	Sigma Aldrich, Dorset, UK	Mineralization
Luria-Bertani (LB) Broth	Sigma Aldrich, Dorset, UK	Transfection protocol
Magic Marker	Invitrogen, Paisley, UK	WB
Magnesium chloride	Sigma Aldrich, Dorset, UK	ALP
Matrigel, Growth Factor Reduced	Corning, Flintshire, UK	TC/Invivo
M-CSF mouse recombinant	R & D Systems, Abingdon, UK	OC
Methanol	VWR International LTD, Leicestershire, UK	WB
Minimum Essential Medium (αMEM)	Fisher Scientific, Leicestershire, UK	TC
MS Columns	Miltenyi Biotech, Gladbach, Germany	Human OC
N,N-Dimethylformamide	Sigma Aldrich, Dorset, UK	TRAcP
Napthol-AS-BI-phosphate	Sigma Aldrich, Dorset, UK	TRAcP
Neubauer Haemocytometer	Hawksley, Lancing, UK	General/TC
Paraformaldehyde	Taab Lab, Berkshire, UK	Fixation

Pararosanilin	Sigma Aldrich, Dorset, UK	TRAcP
Penicillin/Streptomycin	Fisher Scientific, Leicestershire, UK	TC
Phosphatase inhibitor cocktail	Fisher Scientific, Leicestershire, UK	WB
Phosphate buffered saline	Fisher Scientific, Leicestershire, UK	TC
Pierce™ Bovine Serum Albumin Standard Pre-Diluted Set	Fisher Scientific, Leicestershire, UK	BSA
Pipette tips (all sizes)	Starlab, Milton Keynes, UK	General
Polybrene	Sigma Aldrich, Dorset, UK	Transfection protocol
Polyethylenimine	Sigma Aldrich, Dorset, UK	Transfection protocol
Protease inhibitor cocktail	Sigma Aldrich, Dorset, UK	WB
Proteome Profiler XL Cytokine Array Kit	R & D Systems, Abingdon, UK	WB
Puromycin	Sigma Aldrich, Dorset, UK	Transfection protocol
Roswell Park Memorial Institute (RPMI)	Sigma Aldrich, Dorset, UK	TC
Scalpel, disposable	VWR International LTD, Leicestershire, UK	TC
Scissors (fine points and spring bow handles)	S Murray & Co Ltd, Surrey, UK	TC
Sodium acetate trihydrate	VWR International LTD, Leicestershire, UK	TRAcP
Sodium barbiturate	Sigma Aldrich, Dorset, UK	TRAcP
Sodium chloride	Sigma Aldrich, Dorset, UK	General
Sodium dodecyl sulphate (SDS)	Bio-Rad Laboratories, Hertfordshire, UK	WB
Sodium hydroxide	VWR International LTD, Leicestershire, UK	Decalcification
Sodium phosphate	Sigma Aldrich, Dorset, UK	Destain
Sodium tartrate dibasic dihydrate	Sigma Aldrich, Dorset, UK	TRAcP
Starguard® laboratory gloves	Starlab, Milton Keynes, UK	General
Sterile filter (0.2 and 0.45µm)	Pall lifesciences, Portsmouth, UK	TC
Stripettes (5, 10, 25 and 50ml)	Fisher Scientific, Leicestershire, UK	General
Superfrost Plus™ Adhesion Microscope Slides	Fisher Scientific, Leicestershire, UK	Histo
Syringes (all sizes)	Fisher Scientific, Leicestershire, UK	In vivo
Tissue culture 25, 75, 175cm^2 flasks	Fisher Scientific, Leicestershire, UK	TC
Tissue culture microplates (6, 12, 24, 48 and 96-well plates)	Corning, Flintshire, UK	TC
Transblot Turbo midi Size PVDF membrane	Bio-Rad Laboratories, Hertfordshire, UK	WB
Transblot Turbo midi Size Transfer stacks	Bio-Rad Laboratories, Hertfordshire, UK	WB

Tris	Sigma Aldrich, Dorset, UK	WB
Tris-Base	Sigma Aldrich, Dorset, UK	Transfection protocol
Tris-EDTA buffer	Sigma Aldrich, Dorset, UK	WB
Tris-Glycine buffer 10x	Bio-Rad Laboratories, Hertfordshire, UK	WB
Tris-HCl	Sigma Aldrich, Dorset, UK	Transfection protocol
Triton X-100™	Sigma Aldrich, Dorset, UK	RIPA
Trizma® base	Sigma Aldrich, Dorset, UK	WB
Trizma® hydrochloride	Sigma Aldrich, Dorset, UK	WB
Trypan Blue	Fisher Scientific, Leicestershire, UK	TC/In vivo
Trypsin/EDTA	Sigma Aldrich, Dorset, UK	TC
Tween-20	Acros organics, Geel, Belgium	WB
Western blot tips	Starlab, Milton Keynes, UK	WB
Xylene	Sigma Aldrich, Dorset, UK	Histology
β-glycerophosphate disodium	Sigma Aldrich, Dorset, UK	Mineralization

Appendix 2. Solutions for TRAcP staining of osteoclasts *in vitro*.

Solution	Method
Naphthol-AS-BI-phosphate	10 mg/ml Naphthol-AS-BI-phosphate in Dimethylformamide
Veronal buffer	1.17 g sodium acetate anhydrous and 2.94g sodium barbiturate both dissolved in 100 ml of dH_2O
Acetate buffer	0.82 g sodium acetate anhydrous dissolved in 100 ml of dH_2O and pH adjusted to 5.2 with 0.6 ml glacial acetic acid made up to 100 ml with dH_2O
Pararosanilin	1 g Pararosanilin dissolved in 20 ml of dH_2O and 5 ml of 5M HCl added to it The solution was heated carefully whilst stirring and filtered after cooling.
TRAcP Staining Solution	The TRAcP staining solution was freshly prepared by mixing solution A and B as outlined below. ***Solution A*** 150 ml of Napthol-AS-BI-phosphate 750 ml of Veronal buffer 900 ml Acetate buffer 900 ml Acetate buffer with 100 mM Sodium Tartate ***Solution B*** 120 ml of Pararosanilin 120 ml of Sodium Nitrate (4% w/v)

Appendix 3. Solutions for Alkaline phosphatase detection in osteoblasts

Solution	Method
Diethanolamine (DEA)/MgCl2 buffer	1 M DEA and 1 M MgCl2 made up in 100 ml dH2O and pH adjusted to 9.8. Left at room temperature for 24 hours
ALP Lysis buffer	0.05% Triton X-100 added to DEA/MgCl2 buffer
p-Nitrophenol standard solution	p-Nitrophenol standards (1.25 – 30 nM) prepared in lysis buffer
Substrate solution	20 mM p-nitrophenol-phopshate made up in DEA/MgCl2 buffer and pH adjusted to 9.8

Appendix 4**.** Buffers for Western blotting

Solution	Method
RIPA Lysis buffer	1% Triton 100X, 0.5% (w/v) Sodium Deoxycholate, 0.1% (w/v) Sodium Dodecyl Sulphate (SDS), 50 mM Tris-HCl (pH 7.4) and 150 mM Sodium Chloride were dissolved in dH_2O.
20X TBS	60.5g TrisBASE in 1L dH_2O adjust pH to 7.9 with 79g TrisHCl. Add 3M (175.32g) NaCl.
1x TBS-Tween (TBST) wash buffer	Dilute 20X TBS in dH_2O (1:19). Add 0.1% Tween-20. Shake well.
5X Sample loading buffer	0.63g of TrisHCl in 5.2ml of dH_2O (pH6.8; alter pH with TrisBase), 1g of DL-Dithiothreitol (DDT), Add 1.3g SDS and put at 37˚ degrees on the stirrer to dissolve

Appendix 5**.** Buffered Formalin for fixation

Solution	Method
10% buffered formalin	8g sodium dihydrogen orthophosphate dehydrate, disodium hydrogen orthophosphate dehydrate, 37% formaldehyde in 2L warmed dH_2O.

Appendix 6**.** Solutions for decalcification of mouse hind limbs

Solution	Method
EDTA-decal	500g EDTA-disodium salt in 3.5L of dH_2O added gradually with continual stirring, followed by addition of 50g sodium hydroxide pellets. Store at 4°C

Appendix 7 . List of Antibodies

Antibody	Host Species	Supplier
anti-IKKα	rabbit	Cell Signalling Technologies
anti-IKKβ	rabbit	Cell Signalling Technologies
anti-IKKε	rabbit	Cell Signalling Technologies
anti-TBK-1	rabbit	Cell Signalling Technologies
anti-IRF3	rabbit	Cell Signalling Technologies
anti-p65	rabbit	Cell Signalling Technologies
anti-Phospho-IκBα	rabbit	Cell Signalling Technologies
anti-IκBα	rabbit	Cell Signalling Technologies
Anti-actin	rabbit	Sigma Aldrich
Anti-rabbit secondary	goat	Jackson Laboratories

Bibliography

ABBAS, S., ZHANG, Y. H., CLOHISY, J. C. & ABU-AMER, Y. 2003. Tumor necrosis factor-alpha inhibits pre-osteoblast differentiation through its type-1 receptor. *Cytokine,* 22**,** 33-41.

ACHARYYA, S., OSKARSSON, T., VANHARANTA, S., MALLADI, S., KIM, J., MORRIS, P. G., MANOVA-TODOROVA, K., LEVERSHA, M., HOGG, N., SESHAN, V. E., NORTON, L., BROGI, E. & MASSAGUE, J. 2012. A CXCL1 paracrine network links cancer chemoresistance and metastasis. *Cell,* 150**,** 165-78.

ADLI, M. & BALDWIN, A. S. 2006. IKK-i/IKKepsilon controls constitutive, cancer cell-associated NF-kappaB activity via regulation of Ser-536 p65/RelA phosphorylation. *J Biol Chem,* 281**,** 26976-84.

ALAM, A. S., GALLAGHER, A., SHANKAR, V., GHATEI, M. A., DATTA, H. K., HUANG, C. L., MOONGA, B. S., CHAMBERS, T. J., BLOOM, S. R. & ZAIDI, M. 1992. Endothelin inhibits osteoclastic bone resorption by a direct effect on cell motility: implications for the vascular control of bone resorption. *Endocrinology,* 130**,** 3617-24.

ALLES, N., SOYSA, N. S., HAYASHI, J., KHAN, M., SHIMODA, A., SHIMOKAWA, H., RITZELER, O., AKIYOSHI, K., AOKI, K. & OHYA, K. 2010. Suppression of NF-kappaB increases bone formation and ameliorates osteopenia in ovariectomized mice. *Endocrinology,* 151**,** 4626-4634.

ALLISON, K. H. 2012. Molecular pathology of breast cancer: what a pathologist needs to know. *Am J Clin Pathol,* 138**,** 770-80.

ARNOLD, A. & PAPANIKOLAOU, A. 2005. Cyclin D1 in Breast Cancer Pathogenesis. *J Clin Oncol,* 23**,** 4215-4224.

BAKKER, A. D. & KLEIN-NULEND, J. 2012. Osteoblast isolation from murine calvaria and long bones. *Methods Mol Biol,* 816**,** 19-29.

BALDWIN, A. S. 2001. Control of oncogenesis and cancer therapy resistance by the transcription factor NF-kappaB. *J Clin Invest,* 107**,** 241-6.

BARBIE, T. U., ALEXE, G., AREF, A. R., LI, S., ZHU, Z., ZHANG, X., IMAMURA, Y., THAI, T. C., HUANG, Y., BOWDEN, M., HERNDON, J., COHOON, T. J., FLEMING, T., TAMAYO, P., MESIROV, J. P., OGINO, S., WONG, K.-K., ELLIS, M. J., HAHN, W. C., BARBIE, D. A. & GILLANDERS, W. E. 2014. Targeting an IKBKE cytokine network impairs triple-negative breast cancer growth. *J Clin Inv,* 124**,** 5411-5423.

BARTON, V. N., GORDON, M. A., RICHER, J. K. & ELIAS, A. 2016. Anti-androgen therapy in triple-negative breast cancer. *Ther Adv Med Oncol,* 8**,** 305-8.

BASELGA, J., CAMPONE, M., PICCART, M., BURRIS, H. A., 3RD, RUGO, H. S., SAHMOUD, T., NOGUCHI, S., GNANT, M., PRITCHARD, K. I., LEBRUN, F., BECK, J. T., ITO, Y., YARDLEY, D., DELEU, I., PEREZ, A., BACHELOT, T., VITTORI, L., XU, Z., MUKHOPADHYAY, P., LEBWOHL, D. & HORTOBAGYI, G. N. 2012. Everolimus in postmenopausal hormone-receptor-positive advanced breast cancer. *N Engl J Med,* 366**,** 520-9.

BINDER, C., HAGEMANN, T., HUSEN, B., SCHULZ, M. & EINSPANIER, A. 2002. Relaxin enhances in-vitro invasiveness of breast cancer cell lines by up-regulation of matrix metalloproteases. *Mol Hum Reprod,* 8**,** 789-96.

BOEHM, J. S., ZHAO, J. J., YAO, J., KIM, S. Y., FIRESTEIN, R., DUNN, I. F., SJOSTROM, S. K., GARRAWAY, L. A., WEREMOWICZ, S.,

RICHARDSON, A. L., GREULICH, H., STEWART, C. J., MULVEY, L. A., SHEN, R. R., AMBROGIO, L., HIROZANE-KISHIKAWA, T., HILL, D. E., VIDAL, M., MEYERSON, M., GRENIER, J. K., HINKLE, G., ROOT, D. E., ROBERTS, T. M., LANDER, E. S., POLYAK, K. & HAHN, W. C. 2007a. Integrative genomic approaches identify IKBKE as a breast cancer oncogene. *Cell,* 129**,** 1065-79.

BONIZZI, G. & KARIN, M. 2004. The two NF-kappaB activation pathways and their role in innate and adaptive immunity. *Trends Immunol,* 25**,** 280-8.

BONNARD, M., MIRTSOS, C., SUZUKI, S., GRAHAM, K., HUANG, J., NG, M., ITIE, A., WAKEHAM, A., SHAHINIAN, A., HENZEL, W. J., ELIA, A. J., SHILLINGLAW, W., MAK, T. W., CAO, Z. & YEH, W. C. 2000. Deficiency of T2K leads to apoptotic liver degeneration and impaired NF-kappaB-dependent gene transcription. *Embo J,* 19**,** 4976-85.

BOYCE, B. F. 2013. Advances in osteoclast biology reveal potential new drug targets and new roles for osteoclasts. *J Bone Miner Res,* 28**,** 711-22.

BOYCE, B. F., XIU, Y., LI, J., XING, L. & YAO, Z. 2015. NF-κB-Mediated Regulation of Osteoclastogenesis. *Endocrinol Metab,* 30**,** 35-44.

BRAUN, S., PANTEL, K., MULLER, P., JANNI, W., HEPP, F., KENTENICH, C. R., GASTROPH, S., WISCHNIK, A., DIMPFL, T., KINDERMANN, G., RIETHMULLER, G. & SCHLIMOK, G. 2000. Cytokeratin-positive cells in the bone marrow and survival of patients with stage I, II, or III breast cancer. *N Engl J Med,* 342**,** 525-33.

BRAUN, S. E., CHEN, K., BLAZAR, B. R., ORCHARD, P. J., SLEDGE, G., ROBERTSON, M. J., BROXMEYER, H. E. & CORNETTA, K. 1999. Flt3 ligand antitumor activity in a murine breast cancer model: a comparison with granulocyte-macrophage colony-stimulating factor and a potential mechanism of action. *Hum Gene Ther,* 10**,** 2141-51.

BUIJS, J. T., QUE, I., LOWIK, C. W., PAPAPOULOS, S. E. & VAN DER PLUIJM, G. 2009. Inhibition of bone resorption and growth of breast cancer in the bone microenvironment. *Bone,* 44**,** 380-6.

BULEK, K., LIU, C., SWAIDANI, S., WANG, L., PAGE, R. C., GULEN, M. F., HERJAN, T., ABBADI, A., QIAN, W., SUN, D., LAUER, M., HASCALL, V., MISRA, S., CHANCE, M., ARONICA, M., HAMILTON, T. & LI, X. 2011. IKKi is required for interleukin 17-dependent signaling associated with neutrophilia and pulmonary inflammation. *Nat Immunol,* 12**,** 844-52.

BUSS, H., DORRIE, A., SCHMITZ, M. L., HOFFMANN, E., RESCH, K. & KRACHT, M. 2004. Constitutive and interleukin-1-inducible phosphorylation of p65 NF-{kappa}B at serine 536 is mediated by multiple protein kinases including I{kappa}B kinase (IKK)-{alpha}, IKK{beta}, IKK{epsilon}, TRAF family member-associated (TANK)-binding kinase 1 (TBK1), and an unknown kinase and couples p65 to TATA-binding protein-associated factor II31-mediated interleukin-8 transcription. *J Biol Chem,* 279**,** 55633-43.

CAMPBELL, G. M. & SOPHOCLEOUS, A. 2014. Quantitative analysis of bone and soft tissue by micro-computed tomography: applications to ex vivo and in vivo studies. *Bonekey Rep,* 3.

CERAMI, E., GAO, J., DOGRUSOZ, U., GROSS, B. E., SUMER, S. O., AKSOY, B. A., JACOBSEN, A., BYRNE, C. J., HEUER, M. L., LARSSON, E., ANTIPIN, Y., REVA, B., GOLDBERG, A. P., SANDER, C. & SCHULTZ, N. 2012. The cBio cancer genomics portal: an open platform for exploring multidimensional cancer genomics data. *Cancer Discov,* 2**,** 401-4.

CHAKRABORTY, G., JAIN, S., PATIL, T. V. & KUNDU, G. C. 2008. Down-regulation of osteopontin attenuates breast tumour progression in vivo. *J Cell Mol Med,* 12**,** 2305-18.

CHALAKUR-RAMIREDDY, N. & PAKALA, S. 2018. Combined drug therapeutic strategies for the effective treatment of Triple Negative Breast Cancer. *Biosci Rep,* 38.

CHANG, J., WANG, Z., TANG, E., FAN, Z., MCCAULEY, L., FRANCESCHI, R., GUAN, K., KREBSBACH, P. H. & WANG, C. Y. 2009a. Inhibition of osteoblastic bone formation by nuclear factor-kappaB. *Nat Med,* 15**,** 682-9.

CHANG, J., WANG, Z., TANG, E., FAN, Z., MCCAULEY, L., FRANCESCHI, R., GUAN, K., KREBSBACH, P. H. & WANG, C. Y. 2009b. Inhibition of osteoblastic bone formation by nuclear factor-kappaB. *Nat.Med.,* 15**,** 682-689.

CHAU, T. L., GIOIA, R., GATOT, J. S., PATRASCU, F., CARPENTIER, I., CHAPELLE, J. P., O'NEILL, L., BEYAERT, R., PIETTE, J. & CHARIOT, A. 2008. Are the IKKs and IKK-related kinases TBK1 and IKK-epsilon similarly activated? *Trends Biochem Sci,* 33**,** 171-80.

CHAVEZ, A., SCHEIMAN, J., VORA, S., PRUITT, B. W., TUTTLE, M., E, P. R. I., LIN, S., KIANI, S., GUZMAN, C. D., WIEGAND, D. J., TER-OVANESYAN, D., BRAFF, J. L., DAVIDSOHN, N., HOUSDEN, B. E., PERRIMON, N., WEISS, R., AACH, J., COLLINS, J. J. & CHURCH, G. M. 2015. Highly efficient Cas9-mediated transcriptional programming. *Nat Methods,* 12**,** 326-8.

CHELLAIAH, M. A., KIZER, N., BISWAS, R., ALVAREZ, U., STRAUSS-SCHOENBERGER, J., RIFAS, L., RITTLING, S. R., DENHARDT, D. T. & HRUSKA, K. A. 2003. Osteopontin deficiency produces osteoclast dysfunction due to reduced CD44 surface expression. *Mol Biol Cell,* 14**,** 173-89.

CHEN, W. Z., SHEN, J. F., ZHOU, Y., CHEN, X. Y., LIU, J. M. & LIU, Z. L. 2017. Clinical characteristics and risk factors for developing bone metastases in patients with breast cancer. *Sci Rep,* 7**,** 11325.

CHIANG, S. H., BAZUINE, M., LUMENG, C. N., GELETKA, L. M., MOWERS, J., WHITE, N. M., MA, J. T., ZHOU, J., QI, N., WESTCOTT, D., DELPROPOSTO, J. B., BLACKWELL, T. S., YULL, F. E. & SALTIEL, A. R. 2009. The protein kinase IKKε regulates energy expenditure, insulin sensitivity and chronic inflammation in obese mice. *Cell,* 138**,** 961-75.

CHOI, B., LEE, E. J., SHIN, M. K., PARK, Y. S., RYU, M. H., KIM, S. M., KIM, E. Y., LEE, H. K. & CHANG, E. J. 2016. Upregulation of brain-derived neurotrophic factor in advanced gastric cancer contributes to bone metastatic osteolysis by inducing long pentraxin 3. *Oncotarget,* 7**,** 55506-17.

CHRISTOPHER, M. J. & LINK, D. C. 2008. Granulocyte colony-stimulating factor induces osteoblast apoptosis and inhibits osteoblast differentiation. *J Bone Miner Res,* 23**,** 1765-74.

CHUANG, S. E., YEH, P. Y., LU, Y. S., LAI, G. M., LIAO, C. M., GAO, M. & CHENG, A. L. 2002. Basal levels and patterns of anticancer drug-induced activation of nuclear factor-kappaB (NF-kappaB), and its attenuation by tamoxifen, dexamethasone, and curcumin in carcinoma cells. *Biochem Pharmacol,* 63**,** 1709-16.

CIREN, B., WANG, X. & LONG, Z. 2016. The evaluation of immunotherapy and chemotherapy treatment on melanoma: a network meta-analysis. *Oncotarget,* 7**,** 81493-511.

CIRIELLO, G., MILLER, M. L., AKSOY, B. A., SENBABAOGLU, Y., SCHULTZ, N. & SANDER, C. 2013. Emerging landscape of oncogenic signatures across human cancers. *Nat Genet,* 45**,** 1127-33.

CLOHISY, D. R., OGILVIE, C. M. & RAMNARAINE, M. L. 1995. Tumor osteolysis in osteopetrotic mice. *J Orthop Res,* 13**,** 892-7.

CLOHISY, D. R., PERKINS, S. L. & RAMNARAINE, M. L. 2000. Review of cellular mechanisms of tumor osteolysis. *Clin Orthop Relat Res***,** 104-14.

CLÉMENT, J.-F., MELOCHE, S. & SERVANT, M. J. 2008. The IKK-related kinases: from innate immunity to oncogenesis. *Cell Research,* 18**,** 889-899.

COLEMAN, R. 2001. Metastatic bone disease: clinical features, pathophysiology and treatment strategies. *Cancer Treatment Reviews,* 27**,** 165-176.

COLEMAN, R. E. & RUBENS, R. D. 1987. The clinical course of bone metastases from breast cancer. *Br J Cancer,* 55**,** 61-6.

COLLIN-OSDOBY, P. & OSDOBY, P. 2012. RANKL-mediated osteoclast formation from murine RAW 264.7 cells. *Methods Mol Biol,* 816**,** 187-202.

CURTIS, C., SHAH, S. P., CHIN, S. F., TURASHVILI, G., RUEDA, O. M., DUNNING, M. J., SPEED, D., LYNCH, A. G., SAMARAJIWA, S., YUAN, Y., GRAF, S., HA, G., HAFFARI, G., BASHASHATI, A., RUSSELL, R., MCKINNEY, S., LANGEROD, A., GREEN, A., PROVENZANO, E., WISHART, G., PINDER, S., WATSON, P., MARKOWETZ, F., MURPHY, L., ELLIS, I., PURUSHOTHAM, A., BORRESEN-DALE, A. L., BRENTON, J. D., TAVARE, S., CALDAS, C. & APARICIO, S. 2012. The genomic and transcriptomic architecture of 2,000 breast tumours reveals novel subgroups. *Nature,* 486**,** 346-52.

DAI, J., KITAGAWA, Y., ZHANG, J., YAO, Z., MIZOKAMI, A., CHENG, S., NOR, J., MCCAULEY, L. K., TAICHMAN, R. S. & KELLER, E. T. 2004. Vascular endothelial growth factor contributes to the prostate cancer-induced osteoblast differentiation mediated by bone morphogenetic protein. *Can Res,* 64**,** 994-9.

DANJO, A., YAMAZA, T., KIDO, M. A., SHIMOHIRA, D., TSUKUBA, T., KAGIYA, T., YAMASHITA, Y., NISHIJIMA, K., MASUKO, S., GOTO, M. & TANAKA, T. 2007. Cystatin C stimulates the differentiation of mouse osteoblastic cells and bone formation. *Biochem Biophys Res Commun,* 360**,** 199-204.

DUARTE, C., KOBAYASHI, Y., KAWAMOTO, T. & MORIYAMA, K. 2014. RELAXIN enhances differentiation and matrix mineralization through Relaxin/insulin-like family peptide receptor 2 (Rxfp2) in MC3T3-E1 cells in vitro. *Bone,* 65**,** 92-101.

EDDY, S. F., GUO, S., DEMICCO, E. G., ROMIEU-MOUREZ, R., LANDESMAN-BOLLAG, E., SELDIN, D. C. & SONENSHEIN, G. E. 2005. Inducible IkappaB kinase/IkappaB kinase epsilon expression is induced by CK2 and promotes aberrant nuclear factor-kappaB activation in breast cancer cells. *Cancer Res,* 65**,** 11375-83.

ERIKSEN, E. F. 2010. Cellular mechanisms of bone remodeling. *Rev Endocr Metab Disord,* 11**,** 219-27.

EVERTS, V., DELAISSE, J. M., KORPER, W., NIEHOF, A., VAES, G. & BEERTSEN, W. 1992. Degradation of collagen in the bone-resorbing compartment underlying the osteoclast involves both cysteine-proteinases and matrix metalloproteinases. *J Cell Physiol,* 150**,** 221-31.

FERLAY, J., SOERJOMATARAM, I., DIKSHIT, R., ESER, S., MATHERS, C., REBELO, M., PARKIN, D. M., FORMAN, D. & BRAY, F. 2015. Cancer

incidence and mortality worldwide: sources, methods and major patterns in GLOBOCAN 2012. *Int J Cancer,* 136**,** E359-86.

FERNANDES, J. C., SHI, Q., BENDERDOUR, M., LAJEUNESSE, D. & LAVIGNE, P. 2008. An active role for soluble and membrane intercellular adhesion molecule-1 in osteoclast activity in vitro. *J Bone Miner Metab,* 26**,** 543-50.

FUJITA, K. & JANZ, S. 2007. Attenuation of WNT signaling by DKK-1 and -2 regulates BMP2-induced osteoblast differentiation and expression of OPG, RANKL and M-CSF. *Mol Cancer,* 6**,** 71.

FULLER, K., OWENS, J. M., JAGGER, C. J., WILSON, A., MOSS, R. & CHAMBERS, T. J. 1993. Macrophage colony-stimulating factor stimulates survival and chemotactic behavior in isolated osteoclasts. *J Exp Med,* 178**,** 1733-44.

GANDHI, L., RODRIGUEZ-ABREU, D., GADGEEL, S., ESTEBAN, E., FELIP, E., DE ANGELIS, F., DOMINE, M., CLINGAN, P., HOCHMAIR, M. J., POWELL, S. F., CHENG, S. Y., BISCHOFF, H. G., PELED, N., GROSSI, F., JENNENS, R. R., RECK, M., HUI, R., GARON, E. B., BOYER, M., RUBIO-VIQUEIRA, B., NOVELLO, S., KURATA, T., GRAY, J. E., VIDA, J., WEI, Z., YANG, J., RAFTOPOULOS, H., PIETANZA, M. C. & GARASSINO, M. C. 2018. Pembrolizumab plus Chemotherapy in Metastatic Non-Small-Cell Lung Cancer. *N Engl J Med,* 378**,** 2078-2092.

GAO, J., AKSOY, B. A., DOGRUSOZ, U., DRESDNER, G., GROSS, B., SUMER, S. O., SUN, Y., JACOBSEN, A., SINHA, R., LARSSON, E., CERAMI, E., SANDER, C. & SCHULTZ, N. 2013. Integrative analysis of complex cancer genomics and clinical profiles using the cBioPortal. *Sci Signal,* 6**,** pl1.

GARNERO, P., BOREL, O., BYRJALSEN, I., FERRERAS, M., DRAKE, F. H., MCQUENEY, M. S., FOGED, N. T., DELMAS, P. D. & DELAISSE, J. M. 1998. The collagenolytic activity of cathepsin K is unique among mammalian proteinases. *J Biol Chem,* 273**,** 32347-52.

GEBACK, T., SCHULZ, M. M., KOUMOUTSAKOS, P. & DETMAR, M. 2009. TScratch: a novel and simple software tool for automated analysis of monolayer wound healing assays. *Biotechniques,* 46**,** 265-74.

GNANT, M., BASELGA, J., RUGO, H. S., NOGUCHI, S., BURRIS, H. A., PICCART, M., HORTOBAGYI, G. N., EAKLE, J., MUKAI, H., IWATA, H., GEBERTH, M., HART, L. L., HADJI, P., EL-HASHIMY, M., RAO, S., TARAN, T., SAHMOUD, T., LEBWOHL, D., CAMPONE, M. & PRITCHARD, K. I. 2013. Effect of everolimus on bone marker levels and progressive disease in bone in BOLERO-2. *J Natl Cancer Inst,* 105**,** 654-63.

GUISE, T. A. 2000. Molecular mechanisms of osteolytic bone metastases. *Cancer,* 88**,** 2892-8.

GUO, J. P., COPPOLA, D. & CHENG, J. Q. 2011. IKBKE protein activates Akt independent of phosphatidylinositol 3-kinase/PDK1/mTORC2 and the pleckstrin homology domain to sustain malignant transformation. *J Biol Chem,* 286**,** 37389-98.

GUO, J. P., SHU, S. K., HE, L., LEE, Y. C., KRUK, P. A., GRENMAN, S., NICOSIA, S. V., MOR, G., SCHELL, M. J., COPPOLA, D. & CHENG, J. Q. 2009. Deregulation of IKBKE is associated with tumor progression, poor prognosis, and cisplatin resistance in ovarian cancer. *Am J Pathol,* 175**,** 324-33.

GUO, J. P., SHU, S. K., ESPOSITO, N. N., COPPOLA, D., KOOMEN, J. M. & CHENG, J. Q. 2010. IKKϵ Phosphorylation of Estrogen Receptor α Ser-167

and Contribution to Tamoxifen Resistance in Breast Cancer*. *J Biol Chem,* 285**,** 3676-84.

GUO, J. P., TIAN, W., SHU, S., XIN, Y., SHOU, C. & CHENG, J. Q. 2013. IKBKE phosphorylation and inhibition of FOXO3a: a mechanism of IKBKE oncogenic function. *PLoS One,* 8**,** e63636.

GUO, P., HUANG, J., WANG, L., JIA, D., YANG, J., DILLON, D. A., ZURAKOWSKI, D., MAO, H., MOSES, M. A. & AUGUSTE, D. T. 2014. ICAM-1 as a molecular target for triple negative breast cancer. *Proc Natl Acad Sci U S A,* 111**,** 14710-5.

GUPTA, G. P., NGUYEN, D. X., CHIANG, A. C., BOS, P. D., Y., K. J., NADAL, C., GOMIS, R. R., KATIA, M.-T. & MASSAGUÉ, J. 2007. Mediators of vascular remodelling co-opted for sequential steps in lung metastasis. *Nature,* 446**,** 765-770.

HANAHAN, D. & WEINBERG, R. A. 2011. Hallmarks of Cancer: The Next Generation. *Cell,* 144**,** 646-674.

HARDAWAY, A. L., HERROON, M. K., RAJAGURUBANDARA, E. & PODGORSKI, I. 2015. Marrow adipocyte-derived CXCL1 and CXCL2 contribute to osteolysis in metastatic prostate cancer. *Clin Exp Metastasis,* 32**,** 353-68.

HARRIS, J., OLIÈRE, S., SHARMA, S., SUN, Q., LIN, R., HISCOTT, J. & GRANDVAUX, N. 2006. Nuclear Accumulation of cRel following C-Terminal phosphorylation by TBK1/IKKε. *The,* 177**,** 2527-2535.

HAYDEN, M. S. & GHOSH, S. 2004. Signaling to NF-kappaB. *Genes Dev,* 18**,** 2195-224.

HELBIG, G., CHRISTOPHERSON, K. W., 2ND, BHAT-NAKSHATRI, P., KUMAR, S., KISHIMOTO, H., MILLER, K. D., BROXMEYER, H. E. & NAKSHATRI, H. 2003. NF-kappaB promotes breast cancer cell migration and metastasis by inducing the expression of the chemokine receptor CXCR4. *J Biol Chem,* 278**,** 21631-8.

HEMMI, H., TAKEUCHI, O., SATO, S., YAMAMOTO, M., KAISHO, T., SANJO, H., KAWAI, T., HOSHINO, K., TAKEDA, K. & AKIRA, S. 2004. The roles of two IkappaB kinase-related kinases in lipopolysaccharide and double stranded RNA signaling and viral infection. *J Exp Med,* 199**,** 1641-50.

HILAKIVI-CLARKE, L., CABANES, A., KERR, L., BOUKER, K. B. & CLARKE, R. 2002. Do estrogens always increase breast cancer risk? *The Journal of Steroid Biochemistry and Molecular Biology,* 80**,** 163–174.

HIRBE, A. C., ULUCKAN, O., MORGAN, E. A., EAGLETON, M. C., PRIOR, J. L., PIWNICA-WORMS, D., TRINKAUS, K., APICELLI, A. & WEILBAECHER, K. 2007. Granulocyte colony-stimulating factor enhances bone tumor growth in mice in an osteoclast-dependent manner. *Blood,* 109**,** 3424-31.

HOLM, E., GLEBERZON, J. S., LIAO, Y., SORENSEN, E. S., BEIER, F., HUNTER, G. K. & GOLDBERG, H. A. 2014. Osteopontin mediates mineralization and not osteogenic cell development in vitro. *Biochem J,* 464**,** 355-64.

HOSHINO, A., COSTA-SILVA, B., SHEN, T. L., RODRIGUES, G., HASHIMOTO, A., MARK, M. T., MOLINA, H., KOHSAKA, S., DI GIANNATALE, A., CEDER, S., SINGH, S., WILLIAMS, C., SOPLOP, N., URYU, K., PHARMER, L., KING, T., BOJMAR, L., DAVIES, A. E., ARARSO, Y., ZHANG, T., ZHANG, H., HERNANDEZ, J., WEISS, J. M., DUMONT-COLE, V. D., KRAMER, K., WEXLER, L. H., NARENDRAN, A.,

SCHWARTZ, G. K., HEALEY, J. H., SANDSTROM, P., LABORI, K. J., KURE, E. H., GRANDGENETT, P. M., HOLLINGSWORTH, M. A., DE SOUSA, M., KAUR, S., JAIN, M., MALLYA, K., BATRA, S. K., JARNAGIN, W. R., BRADY, M. S., FODSTAD, O., MULLER, V., PANTEL, K., MINN, A. J., BISSELL, M. J., GARCIA, B. A., KANG, Y., RAJASEKHAR, V. K., GHAJAR, C. M., MATEI, I., PEINADO, H., BROMBERG, J. & LYDEN, D. 2015. Tumour exosome integrins determine organotropic metastasis. *Nature,* 527**,** 329-35.

HSU, S., KIM, M., HERNANDEZ, L., GRAJALES, V., NOONAN, A., ANVER, M., DAVIDSON, B. & ANNUNZIATA, C. M. 2012. IKKε coordinates invasion and metastasis of ovarian cancer. *Can Res,* 72**,** 5494-504.

HU, M. C., LEE, D. F., XIA, W., GOLFMAN, L. S., OU-YANG, F., YANG, J. Y., ZOU, Y., BAO, S., HANADA, N., SASO, H., KOBAYASHI, R. & HUNG, M. C. 2004. IkappaB kinase promotes tumorigenesis through inhibition of forkhead FOXO3a. *Cell,* 117**,** 225-37.

HUANG, J., LIU, T., XU, L. G., CHEN, D., ZHAI, Z. & SHU, H. B. 2005. SIKE is an IKK epsilon/TBK1-associated suppressor of TLR3- and virus-triggered IRF-3 activation pathways. *Embo J,* 24**,** 4018-28.

HUANG, W., GHISLETTI, S., PERISSI, V., ROSENFELD, M. G. & GLASS, C. K. 2009. Transcriptional integration of TLR2 and TLR4 signaling at the NCoR de-repression checkpoint. *Mol Cell,* 35**,** 48-57.

HUBER, M. A., AZOITEI, N., BAUMANN, B., GRUNERT, S., SOMMER, A., PEHAMBERGER, H., KRAUT, N., BEUG, H. & WIRTH, T. 2004. NF-kappaB is essential for epithelial-mesenchymal transition and metastasis in a model of breast cancer progression. *J Clin Invest,* 114**,** 569-81.

HUNTER, G. K. & GOLDBERG, H. A. 1993. Nucleation of hydroxyapatite by bone sialoprotein. *Proc Natl Acad Sci U S A,* 90**,** 8562-5.

HUTTI, J. E., SHEN, R. R., ABBOTT, D. W., ZHOU, A. Y., SPROTT, K. M., ASARA, J. M., HAHN, W. C. & CANTLEY, L. C. 2009. Phosphorylation of the tumor suppressor CYLD by the breast cancer oncogene IKKepsilon promotes cell transformation. *Mol Cell,* 34**,** 461-72.

IDA-YONEMOCHI, H., YAMADA, Y., YOSHIKAWA, H. & SEO, K. 2017. Locally Produced BDNF Promotes Sclerotic Change in Alveolar Bone after Nerve Injury. *PLoS One,* 12**,** e0169201.

IDE, H., HATAKE, K., TERADO, Y., TSUKINO, H., OKEGAWA, T., NUTAHARA, K., HIGASHIHARA, E. & HORIE, S. 2008. Serum level of macrophage colony-stimulating factor is increased in prostate cancer patients with bone metastasis. *Hum Cell,* 21**,** 1-6.

IDRIS, A. I., KRISHNAN, M., SIMIC, P., LANDAO-BASSONGA, E., MOLLAT, P., VUKICEVIC, S. & RALSTON, S. H. 2010. Small molecule inhibitors of I{kappa}B kinase signaling inhibit osteoclast formation in vitro and prevent ovariectomy-induced bone loss in vivo. *FASEB J.,* 24**,** 4545-4555.

IDRIS, A. I., LIBOUBAN, H., NYANGOGA, H., LANDAO-BASSONGA, E., CHAPPARD, D. & RALSTON, S. H. 2009. Pharmacologic inhibitors of IkappaB kinase suppress growth and migration of mammary carcinosarcoma cells in vitro and prevent osteolytic bone metastasis in vivo. *Mol Cancer Ther,* 8**,** 2339-47.

KAMIYA, S., NAKAMURA, C., FUKAWA, T., ONO, K., OHWAKI, T., YOSHIMOTO, T. & WADA, S. 2007. Effects of IL-23 and IL-27 on

osteoblasts and osteoclasts: inhibitory effects on osteoclast differentiation. *J Bone Miner Metab,* 25**,** 277-85.

KANG, Y., SIEGEL, P. M., SHU, W., DROBNJAK, M., KAKONEN, S. M., CORDON-CARDO, C., GUISE, T. A. & MASSAGUE, J. 2003. A multigenic program mediating breast cancer metastasis to bone. *Cancer Cell,* 3**,** 537-49.

KANNAN, N., KANG, J., KONG, X., TANG, J., PERRY, J. K., MOHANKUMAR, K. M., MILLER, L. D., LIU, E. T., MERTANI, H. C., ZHU, T., GRANDISON, P. M., LIU, D. X. & LOBIE, P. E. 2010. Trefoil factor 3 is oncogenic and mediates anti-estrogen resistance in human mammary carcinoma. *Neoplasia,* 12**,** 1041-53.

KANZAKI, H., MUKHOPADHYA, N. K., CUI, X., RAMANUJAN, V. K. & MURALI, R. 2016. Trastuzumab-Resistant Luminal B Breast Cancer Cells Show Basal-Like Cell Growth Features Through NF-κB-Activation. *Monoclon Antib Immunodiagn Immunother,* 35**,** 1-11.

KAVANAGH, K. L., GUO, K., DUNFORD, J. E., WU, X., KNAPP, S., EBETINO, F. H., ROGERS, M. J., RUSSELL, R. G. & OPPERMANN, U. 2006. The molecular mechanism of nitrogen-containing bisphosphonates as antiosteoporosis drugs. *Proc Natl Acad Sci U S A,* 103**,** 7829-34.

KERLIKOWSKE, K., GARD, C. C., TICE, J. A., ZIV, E., CUMMINGS, S. R. & MIGLIORETTI, D. L. 2017. Risk Factors That Increase Risk of Estrogen Receptor-Positive and -Negative Breast Cancer. *J Natl Cancer Inst,* 109.

KIM, T., KIM, T. Y., SONG, Y. H., MIN, I. M., YIM, J. & KIM, T. K. 1999. Activation of interferon regulatory factor 3 in response to DNA-damaging agents. *J Biol Chem,* 274**,** 30686-9.

KNEISSEL, M., LUONG-NGUYEN, N. H., BAPTIST, M., CORTESI, R., ZUMSTEIN-MECKER, S., KOSSIDA, S., O'REILLY, T., LANE, H. & SUSA, M. 2004. Everolimus suppresses cancellous bone loss, bone resorption, and cathepsin K expression by osteoclasts. *Bone,* 35**,** 1144-56.

KORHERR, C., GILLE, H., SCHÄFER, R., KOENIG-HOFFMANN, K., DIXELIUS, J., EGLAND, K. A., PASTAN, I. & BRINKMANN, U. 2006. Identification of proangiogenic genes and pathways by high-throughput functional genomics: TBK1 and the IRF3 pathway. *Proc Natl Acad Sci U S A,* 103**,** 4240-5.

KRAVCHENKO, V. V., MATHISON, J. C., SCHWAMBORN, K., MERCURIO, F. & ULEVITCH, R. J. 2003. IKKi/IKKepsilon plays a key role in integrating signals induced by pro-inflammatory stimuli. *J Biol Chem,* 278**,** 26612-9.

KRUGER, T. E., MILLER, A. H., GODWIN, A. K. & WANG, J. 2014. Bone Sialoprotein and Osteopontin in Bone Metastasis of Osteotropic Cancers. *Crit Rev Oncol Hematol,* 89**,** 330-41.

KRZESZINSKI, J. Y. & WAN, Y. 2015. New therapeutic targets for cancer bone metastasis. *Trends Pharmacol Sci,* 36**,** 360-73.

LAM, J., TAKESHITA, S., BARKER, J. E., KANAGAWA, O., ROSS, F. P. & TEITELBAUM, S. L. 2000. TNF-alpha induces osteoclastogenesis by direct stimulation of macrophages exposed to permissive levels of RANK ligand. *J Clin Invest,* 106**,** 1481-8.

LANDSKRONER-EIGER, S., QIAN, B., MUISE, E. S., NAWROCKI, A. R., BERGER, J. P., FINE, E. J., KOBA, W., DENG, Y., POLLARD, J. W. & SCHERER, P. E. 2009. Proangiogenic contribution of adiponectin toward mammary tumor growth in vivo. *Clin Cancer Res,* 15**,** 3265-76.

LEAN, J. M., FULLER, K. & CHAMBERS, T. J. 2001. FLT3 ligand can substitute for macrophage colony-stimulating factor in support of osteoclast differentiation and function. *Blood,* 98**,** 2707-13.

LEE, D. F., KUO, H. P., CHEN, C. T., HSU, J. M., CHOU, C. K., WEI, Y., SUN, H. L., LI, L. Y., PING, B., HUANG, W. C., HE, X., HUNG, J. Y., LAI, C. C., DING, Q., SU, J. L., YANG, J. Y., SAHIN, A. A., HORTOBAGYI, G. N., TSAI, F. J., TSAI, C. H. & HUNG, M. C. 2007. IKK beta suppression of TSC1 links inflammation and tumor angiogenesis via the mTOR pathway. *Cell,* 130**,** 440-55.

LEE, J., WEBER, M., MEJIA, S., BONE, E., WATSON, P. & ORR, W. 2001. A matrix metalloproteinase inhibitor, batimastat, retards the development of osteolytic bone metastases by MDA-MB-231 human breast cancer cells in Balb C nu/nu mice. *Eur J Cancer,* 37**,** 106-13.

LEHMANN, B. D., BAUER, J. A., CHEN, X., SANDERS, M. E., CHAKRAVARTHY, A. B., SHYR, Y. & PIETENPOL, J. A. 2011. Identification of human triple-negative breast cancer subtypes and preclinical models for selection of targeted therapies. *J Clin Invest,* 121**,** 2750-67.

LERNER, U. H., JOHANSSON, L., RANJSO, M., ROSENQUIST, J. B., REINHOLT, F. P. & GRUBB, A. 1997. Cystatin C, and inhibitor of bone resorption produced by osteoblasts. *Acta Physiol Scand,* 161**,** 81-92.

LI, F. & SETHI, G. 2010. Targeting transcription factor NF-kappaB to overcome chemoresistance and radioresistance in cancer therapy. *Biochim Biophys Acta,* 1805**,** 167-80.

LI, X., KONG, X., HUO, Q., GUO, H., YAN, S., YUAN, C., MORAN, M. S., SHAO, C. & YANG, Q. 2011. Metadherin enhances the invasiveness of breast cancer cells by inducing epithelial to mesenchymal transition. *Cancer Sci,* 102**,** 1151-7.

LIPTON, A., UZZO, R., AMATO, R. J., ELLIS, G. K., HAKIMIAN, B., ROODMAN, G. D. & SMITH, M. R. 2009. The Science and Practice of Bone Health in Oncology: Managing Bone Loss and Metastasis in Patients With Solid Tumors. *J Natl Compr Canc Netw,* 7**,** S1-S30.

LIU, L. Y., WANG, M., MA, Z. B., YU, L. X., ZHANG, Q., GAO, D. Z., WANG, F. & YU, Z. G. 2013. The Role of Adiponectin in Breast Cancer: A Meta-Analysis. *PLoS One.*

LOGAN, J. G., SOPHOCLEOUS, A., MARINO, S., MUIR, M., BRUNTON, V. G. & IDRIS, A. I. 2013. Selective tyrosine kinase inhibition of insulin-like growth factor-1 receptor inhibits human and mouse breast cancer-induced bone cell activity, bone remodeling, and osteolysis. *J Bone Miner Res,* 28**,** 1229-42.

MACEDO, F., LADEIRA, K., PINHO, F., SARAIVA, N., BONITO, N., PINTO, L. & GONCALVES, F. 2017. Bone Metastases: An Overview. *Oncol Rev,* 11.

MALHOTRA, G. K., ZHAO, X., BAND, H. & BAND, V. 2010. Histological, molecular and functional subtypes of breast cancers. *Cancer Biol Ther,* 10**,** 955-60.

MALHOTRA, V. & PERRY, M. C. 2003. Classical chemotherapy: mechanisms, toxicities and the therapeutic window. *Cancer Biol Ther,* 2**,** S2-4.

MANCINO, A. T., KLIMBERG, V. S., YAMAMOTO, M., MANOLAGAS, S. C. & ABE, E. 2001. Breast cancer increases osteoclastogenesis by secreting M-CSF and upregulating RANKL in stromal cells. *J Surg Res,* 100**,** 18-24.

MANDERS, K., VAN DE POLL-FRANSE, L. V., CREEMERS, G. J., VREUGDENHIL, G., VAN DER SANGEN, M. J., NIEUWENHUIJZEN, G.

A., ROUMEN, R. M. & VOOGD, A. C. 2006. Clinical management of women with metastatic breast cancer: a descriptive study according to age group. *BMC Cancer,* 6**,** 179.

MARINO, S., LOGAN, J., G., MELLIS, D. & CAPULLI, M. 2014. Generation and culture of osteoclasts. *BoneKEy Reports,* 3.

MARINO, S., BISHOP, R. T., LOGAN, J. G., MOLLAT, P. & IDRIS, A. I. 2017. Pharmacological evidence for the bone-autonomous contribution of the NFκB/Beta-catenin axis to breast cancer related osteolysis. *Can Lett,* 410**,** 180-190.

MARINO, S., BISHOP, R. T., CAPULLI, M., SOPHOCLEOUS, A., LOGAN, J. G., MOLLAT, P., MOGNETTI, B., VENTURA, L., SIMS, A. H., RUCCI, N., RALSTON, S. H. & IDRIS, A. I. 2018a. Regulation of breast cancer induced bone disease by cancer-specific IKKβ. *Oncotarget,* 9**,** 16134-48.

MARINO, S., BISHOP, R. T., MOLLAT, P. & IDRIS, A. I. 2018b. Pharmacological Inhibition of the Skeletal IKKbeta Reduces Breast Cancer-Induced Osteolysis. *Calcif Tissue Int*.

MARIZ, K., INGOLF, J. B., DANIEL, H., TERESA, N. J. & ERICH-FRANZ, S. 2015. The Wnt inhibitor dickkopf-1: a link between breast cancer and bone metastases. *Clin Exp Metastasis,* 32**,** 857-66.

MEHNER, C., HOCKLA, A., MILLER, E., RAN, S., RADISKY, D. C. & RADISKY, E. S. 2014. Tumor cell-produced matrix metalloproteinase 9 (MMP-9) drives malignant progression and metastasis of basal-like triple negative breast cancer. *Oncotarget,* 5**,** 2736-49.

MELDRUM, D. R., MORRIS, M. A. & GAMBONE, J. C. 2017. Obesity pandemic: causes, consequences, and solutions-but do we have the will? *Fertil Steril,* 107**,** 833-839.

MONTERO, A., FOSSELLA, F., HORTOBAGYI, G. & VALERO, V. 2005. Docetaxel for treatment of solid tumours: a systematic review of clinical data. *Lancet Oncol,* 6**,** 229-39.

MONTERO, S., GUZMAN, C., CORTES-FUNES, H. & COLOMER, R. 1998. Angiogenin expression and prognosis in primary breast carcinoma. *Clin Cancer Res,* 4**,** 2161-8.

MORITA, Y., MATSUYAMA, H., SERIZAWA, A., TAKEYA, T. & KAWAKAMI, H. 2008. Identification of angiogenin as the osteoclastic bone resorption-inhibitory factor in bovine milk. *Bone,* 42**,** 380-7.

MUNDY, G. R. 1997. Mechanisms of bone metastasis. *Cancer,* 80**,** 1546-56.

NAKAGAWA, N., KINOSAKI, M., YAMAGUCHI, K., SHIMA, N., YASUDA, H., YANO, K., MORINAGA, T. & HIGASHIO, K. 1998. RANK is the essential signaling receptor for osteoclast differentiation factor in osteoclastogenesis. *Biochem Biophys Res Commun,* 253**,** 395-400.

NANDA, R., CHOW, L. Q., DEES, E. C., BERGER, R., GUPTA, S., GEVA, R., PUSZTAI, L., PATHIRAJA, K., AKTAN, G., CHENG, J. D., KARANTZA, V. & BUISSERET, L. 2016. Pembrolizumab in Patients With Advanced Triple-Negative Breast Cancer: Phase Ib KEYNOTE-012 Study. *J Clin Oncol,* 34**,** 2460-7.

NEGI, P., KINGSLEY, P. A., JAIN, K., SACHDEVA, J., SRIVASTAVA, H., MARCUS, S. & PANNU, A. 2016. Survival of Triple Negative versus Triple Positive Breast Cancers: Comparison and Contrast. *Asian Pac J Cancer Prev,* 17**,** 3911-6.

NGUYEN, D. X., BOS, P. & MASSAGUÉ, J. 2009. Metastasis: from dissemination to organ-specific colonization. *Nature Reviews Cancer,* 9**,** 274-284.

NGUYEN, D. X. & MASSAGUÉ, J. 2007. Genetic determinants of cancer metastasis. *Nature Reviews Genetics,* 8**,** 341-352.

NISHIOKU, T., TERASAWA, M., BABA, M., YAMAUCHI, A. & KATAOKA, Y. 2016. CD147 promotes the formation of functional osteoclasts through NFATc1 signalling. *Biochem Biophys Res Commun,* 473**,** 620-4.

NUTTER, F., HOLEN, I., BROWN, H. K., CROSS, S. S., EVANS, C. A., WALKER, M., COLEMAN, R. E., WESTBROOK, J. A., SELBY, P. J., BROWN, J. E. & OTTEWELL, P. D. 2014. Different molecular profiles are associated with breast cancer cell homing compared with colonisation of bone: evidence using a novel bone-seeking cell line. *Endocr Relat Cancer,* 21**,** 327-41.

O'BRIEN, J., WILSON, I., ORTON, T. & POGNAN, F. 2000. Investigation of the Alamar Blue (resazurin) fluorescent dye for the assessment of mammalian cell cytotoxicity. *The FEBS Journal,* 267**,** 5421-5426.

OFFICE FOR NATIONAL STATISTICS 2014. Cancer Registration Statistics, England, 2012,. *Cancer Registration Statistics.*

OSHIMA, K., NAMPEI, A., MATSUDA, M., IWAKI, M., FUKUHARA, A., HASHIMOTO, J., YOSHIKAWA, H. & SHIMOMURA, I. 2005. Adiponectin increases bone mass by suppressing osteoclast and activating osteoblast. *Biochem Biophys Res Commun,* 331**,** 520-6.

OTERO, J. E., DAI, S., ALHAWAGRI, M. A., DARWECH, I. & ABU-AMER, Y. 2010. IKKbeta activation is sufficient for RANK-independent osteoclast differentiation and osteolysis. *J.Bone Miner.Res.,* 25**,** 1282-1294.

OTTEWELL, P. D., DEUX, B., MONKKONEN, H., CROSS, S., COLEMAN, R. E., CLEZARDIN, P. & HOLEN, I. 2008. Differential effect of doxorubicin and zoledronic acid on intraosseous versus extraosseous breast tumor growth in vivo. *Clin Cancer Res,* 14**,** 4658-66.

PAGET, S. 1989. The distribution of secondary growths in cancer of the breast. 1889. *Cancer Metastasis Rev,* 8**,** 98-101.

PANDEY, V., WU, Z. S., ZHANG, M., LI, R., ZHANG, J., ZHU, T. & LOBIE, P. E. 2014. Trefoil factor 3 promotes metastatic seeding and predicts poor survival outcome of patients with mammary carcinoma. *Breast Cancer Res,* 16**,** 429.

PARK, B. K., ZHANG, H., ZENG, Q., DAI, J., KELLER, E. T., GIORDANO, T., GU, K., SHAH, V., PEI, L., ZARBO, R. J., MCCAULEY, L., SHI, S., CHEN, S. & WANG, C.-Y. 2006. NF-|[kappa]|B in breast cancer cells promotes osteolytic bone metastasis by inducing osteoclastogenesis via GM-CSF. *Nat Med,* 13**,** 62-69.

PARK, B. K., ZHANG, H., ZENG, Q., DAI, J., KELLER, E. T., GIORDANO, T., GU, K., SHAH, V., PEI, L., ZARBO, R. J., MCCAULEY, L., SHI, S., CHEN, S. & WANG, C. Y. 2007. NF-kappaB in breast cancer cells promotes osteolytic bone metastasis by inducing osteoclastogenesis via GM-CSF. *Nat Med.,* 13**,** 62-69.

PEANT, B., DIALLO, J. S., DUFOUR, F., LE PAGE, C., DELVOYE, N., SAAD, F. & MES-MASSON, A. M. 2009. Over-expression of IkappaB-kinase-epsilon (IKKepsilon/IKKi) induces secretion of inflammatory cytokines in prostate cancer cell lines. *Prostate,* 69**,** 706-18.

PERAMUHENDIGE, P., MARINO, S., BISHOP, R. T., DANIËLLE, D. R., KHOGEER, A., BALDINI, I., CAPULL, M., RUCCI, N. & IDRIS, A. I. 2018. TRAF2 in osteotropic breast cancer cells enhances skeletal tumour growth and promotes osteolysis. *Sci Rep,* 8**,** 39.

PEREZ, E. A., ROMOND, E. H., SUMAN, V. J., JEONG, J. H., DAVIDSON, N. E., GEYER, C. E., JR., MARTINO, S., MAMOUNAS, E. P., KAUFMAN, P. A. & WOLMARK, N. 2011. Four-year follow-up of trastuzumab plus adjuvant chemotherapy for operable human epidermal growth factor receptor 2-positive breast cancer: joint analysis of data from NCCTG N9831 and NSABP B-31. *J Clin Oncol,* 29**,** 3366-73.

PEREZ-PINERA, P., KOCAK, D. D., VOCKLEY, C. M., ADLER, A. F., KABADI, A. M., POLSTEIN, L. R., THAKORE, P. I., GLASS, K. A., OUSTEROUT, D. G., LEONG, K. W., GUILAK, F., CRAWFORD, G. E., REDDY, T. E. & GERSBACH, C. A. 2013. RNA-guided gene activation by CRISPR-Cas9-based transcription factors. *Nat Methods,* 10**,** 973-6.

PEROU, C. M., SORLIE, T., EISEN, M. B., VAN DE RIJN, M., JEFFREY, S. S., REES, C. A., POLLACK, J. R., ROSS, D. T., JOHNSEN, H., AKSLEN, L. A., FLUGE, O., PERGAMENSCHIKOV, A., WILLIAMS, C., ZHU, S. X., LONNING, P. E., BORRESEN-DALE, A. L., BROWN, P. O. & BOTSTEIN, D. 2000. Molecular portraits of human breast tumours. *Nature,* 406**,** 747-52.

PETERS, R. T., LIAO, S. M. & MANIATIS, T. 2000. IKKepsilon is part of a novel PMA-inducible IkappaB kinase complex. *Mol Cell,* 5**,** 513-22.

PEYRUCHAUD, O., WINDING, B., PECHEUR, I., SERRE, C. M., DELMAS, P. & CLEZARDIN, P. 2001. Early detection of bone metastases in a murine model using fluorescent human breast cancer cells: application to the use of the bisphosphonate zoledronic acid in the treatment of osteolytic lesions. *J Bone Miner Res,* 16**,** 2027-34.

PHADKE, P. A., MERCER, R. R., HARMS, J. F., JIA, Y., FROST, A. R., JEWELL, J. L., BUSSARD, K. M., NELSON, S., MOORE, C., KAPPES, J. C., GAY, C. V., MASTRO, A. M. & WELCH, D. R. 2006. Kinetics of metastatic breast cancer cell trafficking in bone. *Clin Cancer Res,* 12**,** 1431-40.

POMERANTZ, J. L. & BALTIMORE, D. 1999. NF‐κB activation by a signaling complex containing TRAF2, TANK and TBK1, a novel IKK‐related kinase. *EMBO,* 18**,** 6694-6704.

POND, G. R., SONPAVDE, G., FIZAZI, K., DE BONO, J. S., BASCH, E. M., SCHER, H. I. & SMITH, M. R. 2018. Cabozantinib for metastatic castration-resistant prostate cancer (mCRPC) following docetaxel: Combined analysis of two phase III trials.

PRAT, A. & PEROU, C., M. 2010. Deconstructing the molecular portraits of breast cancer. *Molecular Oncology,* 5**,** 5-23.

PROTANI, M., COORY, M. & MARTIN, J. H. 2010. Effect of obesity on survival of women with breast cancer: systematic review and meta-analysis. *Breast Cancer Res Treat,* 123**,** 627-35.

QIANG, Y. W., BARLOGIE, B., RUDIKOFF, S. & SHAUGHNESSY, J. D., JR. 2008. Dkk1-induced inhibition of Wnt signaling in osteoblast differentiation is an underlying mechanism of bone loss in multiple myeloma. *Bone,* 42**,** 669-80.

QIN, B. & CHENG, K. 2010. Silencing of the IKKε gene by siRNA inhibits invasiveness and growth of breast cancer cells. *Breast Cancer Research,* 12**,** 1.

QUAIL, D. F., OLSON, O. C., BHARDWAJ, P., WALSH, L. A., AKKARI, L., QUICK, M. L., CHEN, I. C., WENDEL, N., BEN-CHETRIT, N., WALKER, J., HOLT, P. R., DANNENBERG, A. J. & JOYCE, J. A. 2017. Obesity alters the lung myeloid cell landscape to enhance breast cancer metastasis through IL5 and GM-CSF. *Nat Cell Biol,* 19**,** 974-987.

RADESTOCK, Y., HOANG-VU, C. & HOMBACH-KLONISCH, S. 2008. Relaxin reduces xenograft tumour growth of human MDA-MB-231 breast cancer cells. *Breast Cancer Res,* 10**,** R71.

RAKHA, E. A., SORIA, D., GREEN, A. R., LEMETRE, C., POWE, D., NOLAN, C., JM, G., BALL, G. & ELLIS, I. 2014. Nottingham Prognostic Index Plus (NPI+): a modern clinical decision making tool in breast cancer. *British Journal of Cancer,* 110**,** 1688-1697.

REILLY, S. M., CHIANG, S. H., DECKER, S. J., CHANG, L., UHM, M., LARSEN, M. J., RUBIN, J. R., MOWERS, J., WHITE, N. M., HOCHBERG, I., DOWNES, M., YU, R., LIDDLE, C., EVANS, R. M., OH, D., LI, P., OLEFSKY, J. M. & SALTIEL, A. R. 2013. An inhibitor of the protein kinases TBK1/IKKε improves obesity-related metabolic dysfunctions. *Nat Med,* 19**,** 313-21.

RENNER, F., MORENO, R. & SCHMITZ, M. L. 2010. SUMOylation-dependent localization of IKKepsilon in PML nuclear bodies is essential for protection against DNA-damage-triggered cell death. *Mol Cell,* 37**,** 503-15.

RICHARDSEN, E., UGLEHUS, R. D., JOHNSEN, S. H. & BUSUND, L. T. 2015. Macrophage-colony stimulating factor (CSF1) predicts breast cancer progression and mortality. *Anticancer Res,* 35**,** 865-74.

ROCCARO, A. M., SACCO, A., PURSCHKE, W. G., MOSCHETTA, M., BUCHNER, K., MAASCH, C., ZBORALSKI, D., ZÖLLNER, S., VONHOFF, S., MISHIMA, Y., MAISO, P., REAGAN, M. R., LONARDI, S., UNGARI, M., FACCHETTI, F., EULBERG, D., KRUSCHINSKI, A., VATER, A., ROSSI, G., KLUSSMANN, S. & GHOBRIAL, I. M. 2014. SDF-1 inhibition targets the bone marrow niche for cancer therapy. *Cell Rep,* 9**,** 118-28.

ROODMAN, G. 2009. Pathophysiology of Bone Metastases. *In:* D., K., V., V. & E, C. (eds.) *Bone Metastases.* Dordecht: Springer.

RUCCI, N., CAPULLI, M., VENTURA, L., ANGELUCCI, A., PERUZZI, B., TILLGREN, V., MURACA, M., HEINEGARD, D. & TETI, A. 2013. Proline/arginine-rich end leucine-rich repeat protein N-terminus is a novel osteoclast antagonist that counteracts bone loss. *J Bone Miner Res,* 28**,** 1912-24.

RUOCCO, M. G., MAEDA, S., PARK, J. M., LAWRENCE, T., HSU, L. C., CAO, Y., SCHETT, G., WAGNER, E. F. & KARIN, M. 2005. I{kappa}B kinase (IKK){beta}, but not IKK{alpha}, is a critical mediator of osteoclast survival and is required for inflammation-induced bone loss. *J Exp.Med.,* 201**,** 1677-1687.

SHAHNAZARI, M., CHU, V., WRONSKI, T. J., NISSENSON, R. A. & HALLORAN, B. P. 2013. CXCL12/CXCR4 signaling in the osteoblast regulates the mesenchymal stem cell and osteoclast lineage populations. *FASEB J,* 27**,** 3505-13.

SHEN, R. R., ZHOU, A. Y., KIM, E., LIM, E., HABELHAH, H. & HAHN, W. C. 2012. IκB Kinase ε Phosphorylates TRAF2 To Promote Mammary Epithelial Cell Transformation. *Mol Cell Biol,* 32**,** 4756-68.

SHIMADA, T., KAWAI, T., TAKEDA, K., MATSUMOTO, M., INOUE, J., TATSUMI, Y., KANAMARU, A. & AKIRA, S. 1999. IKK-i, a novel lipopolysaccharide-inducible kinase that is related to IkappaB kinases. *Int Immunol,* 11**,** 1357-62.

SHIOZAWA, Y., PEDERSEN, E. A., HAVENS, A. M., JUNG, Y., MISHRA, A., JOSEPH, J., KIM, J. K., PATEL, L. R., YING, C., ZIEGLER, A. M., PIENTA,

M. J., SONG, J., WANG, J., LOBERG, R. D., KREBSBACH, P. H., PIENTA, K. J. & TAICHMAN, R. S. 2011. Human prostate cancer metastases target the hematopoietic stem cell niche to establish footholds in mouse bone marrow. *J Clin Invest,* 121**,** 1298-312.

SHIOZAWA, Y., PEDERSEN, E. A., PATEL, L. R., ZIEGLER, A. M., HAVENS, A. M., JUNG, Y., WANG, J., ZALUCHA, S., LOBERG, R. D., PIENTA, K. J. & TAICHMAN, R. S. 2010. GAS6/AXL axis regulates prostate cancer invasion, proliferation, and survival in the bone marrow niche. *Neoplasia,* 12**,** 116-27.

SICLARI, V. A., GUISE, T. A. & CHIRGWIN, J. M. 2006. Molecular interactions between breast cancer cells and the bone microenvironment drive skeletal metastases. *Cancer Metastasis Rev.,* 25**,** 621-633.

SOPHOCLEOUS, A., MARINO, S., LOGAN, J. G., MOLLAT, P., RALSTON, S. H. & IDRIS, A. I. 2015. Bone Cell-autonomous Contribution of Type 2 Cannabinoid Receptor to Breast Cancer-induced Osteolysis. *Journal of Biological Chemistry,* 290.

SORENSEN, M. G., HENRIKSEN, K., SCHALLER, S., HENRIKSEN, D. B., NIELSEN, F. C., DZIEGIEL, M. H. & KARSDAL, M. A. 2007. Characterization of osteoclasts derived from CD14+ monocytes isolated from peripheral blood. *J Bone Miner Metab,* 25**,** 36-45.

SRIHARI, S., KALIMUTHO, M., LAL, S., SINGLA, J., PATEL, D., SIMPSON, P. T., KHANNA, K. K. & RAGAN, M. A. 2016. Understanding the functional impact of copy number alterations in breast cancer using a network modeling approach. *Mol Biosyst,* 12**,** 963-72.

STOPECK, A. 2010. Denosumab findings in metastatic breast cancer. *Clin Adv Hematol Oncol,* 8**,** 159-60.

SUN, C. Y., CHU, Z. B., SHE, X. M., ZHANG, L., CHEN, L., AI, L. S. & HU, Y. 2012. Brain-derived neurotrophic factor is a potential osteoclast stimulating factor in multiple myeloma. *Int J Cancer,* 130**,** 827-36.

SUN, Y., MAO, X., FAN, C., LIU, C., GUO, A., GUAN, S., JIN, Q., LI, B., YAO, F. & JIN, F. 2014. CXCL12-CXCR4 axis promotes the natural selection of breast cancer cell metastasis. *Tumour Biol,* 35**,** 7765-73.

SWEENEY, S. E., HAMMAKER, D., L., B. D. & S., F. G. 2005. Regulation of c-Jun Phosphorylation by the IκB Kinase-ε Complex in Fibroblast-Like Synoviocytes. *J Immunol,* 174**,** 6424-6430.

TAKAHASHI, N., UDAGAWA, U., S, T. & SUDA, T. 2003. Generating Murine Osteoclasts from Bone Marrow. *In:* MIEP HELFRICH, S. H. R. (ed.) *Bone Research Protocols.* Springer.

TAYLOR, S. E., SHAH, M. & ORRISS, I. R. 2014. Generation of rodent and human osteoblasts. *Bonekey Rep,* 3**,** 585.

TENG, M. W., ANDREWS, D. M., MCLAUGHLIN, N., VON SCHEIDT, B., NGIOW, S. F., MOLLER, A., HILL, G. R., IWAKURA, Y., OFT, M. & SMYTH, M. J. 2010. IL-23 suppresses innate immune response independently of IL-17A during carcinogenesis and metastasis. *Proc Natl Acad Sci U S A,* 107**,** 8328-33.

TENOEVER, B. R., NG, S. L., CHUA, M. A., MCWHIRTER, S. M., GARCIA-SASTRE, A. & MANIATIS, T. 2007. Multiple functions of the IKK-related kinase IKKepsilon in interferon-mediated antiviral immunity. *Science,* 315**,** 1274-8.

THE CANCER GENOME ATLAS, N. 2012. Comprehensive molecular portraits of human breast tumours. *Nature,* 490**,** 61.

TYE, C. E., RATTRAY, K. R., WARNER, K. J., GORDON, J. A., SODEK, J., HUNTER, G. K. & GOLDBERG, H. A. 2003. Delineation of the hydroxyapatite-nucleating domains of bone sialoprotein. *J Biol Chem,* 278**,** 7949-55.

VAN SANT, C., WANG, G., ANDERSON, M. G., TRASK, O. J., LESNIEWSKI, R. & SEMIZAROV, D. 2007. Endothelin signaling in osteoblasts: global genome view and implication of the calcineurin/NFAT pathway. *Mol Cancer Ther,* 6**,** 253-61.

WANG, N., REEVES, K. J., BROWN, H. K., FOWLES, A. C. M., DOCHERTY, F. E., OTTEWELL, P. D., CROUCHER, P. I., HOLEN, I. & EATON, C. L. 2015. The frequency of osteolytic bone metastasis is determined by conditions of the soil, not the number of seeds; evidence from in vivo models of breast and prostate cancer. *J Exp Clin Cancer Res,* 34.

WANING, D. L. & GUISE, T. A. 2014. Molecular mechanisms of bone metastasis and associated muscle weakness. *Clin Cancer Res,* 20**,** 3071-7.

WATSON, C. J. 2001. Stat transcription factors in mammary gland development and tumorigenesis. *J Mammary Gland Biol Neoplasia,* 6**,** 115-27.

WEIGELT, B., MACKAY, A., A'HERN, R., NATRAJAN, R., TAN, D. S., DOWSETT, M., ASHWORTH, A. & REIS-FILHO, J. S. 2010. Breast cancer molecular profiling with single sample predictors: a retrospective analysis. *Lancet Oncol,* 11**,** 339-49.

WEIGELT, B., PETERSE, J. L. & VAN 'T VEER, L. J. 2005. Breast cancer metastasis: markers and models. *Nat Rev Cancer,* 5**,** 591-602.

WELTE, T. & ZHANG, X. H. 2015. Interleukin-17 Could Promote Breast Cancer Progression at Several Stages of the Disease. *Med Inflamm,* 2015.

WRIGHT, L. E., OTTEWELL, P. D., RUCCI, N., PEYRUCHAUD, O., PAGNOTTI, G. M., CHIECHI, A., BUIJS, J. T. & STERLING, J. A. 2016. Murine models of breast cancer bone metastasis. *Bonekey Rep,* 5.

WU, Q., LI, J., ZHU, S., WU, J., CHEN, C., LIU, Q., WEI, W., ZHANG, Y. & SUN, S. 2017. Breast cancer subtypes predict the preferential site of distant metastases: a SEER based study. *Oncotarget,* 8**,** 27990-6.

YANG, M., LIU, J., PIAO, C., SHAO, J. & DU, J. 2015. ICAM-1 suppresses tumor metastasis by inhibiting macrophage M2 polarization through blockade of efferocytosis. *Cell Death Dis,* 6**,** e1780.

YANG, X., MARTIN, T. A. & JIANG, W. G. 2012. Biological influence of brain-derived neurotrophic factor on breast cancer cells. *Int J Oncol,* 41**,** 1541-6.

YARILINA, A., PARK-MIN, K. H., ANTONIV, T., HU, X. & IVASHKIV, L. B. 2008. TNF activates an IRF1-dependent autocrine loop leading to sustained expression of chemokines and STAT1-dependent type I interferon-response genes. *Nat Immunol,* 9**,** 378-87.

YERSAL, O. & BARUTCA, S. 2014. Biological subtypes of breast cancer: Prognostic and therapeutic implications. *World J Clin Oncol,* 5**,** 412-24.

YIN, J. J., POLLOCK, C. B. & KELLY, K. 2005. Mechanisms of cancer metastasis to the bone. *Cell Research,* 15**,** 57-62.

YONEDA, T. & HIRAGA, T. 2005. Crosstalk between cancer cells and bone microenvironment in bone metastasis. *Biochem.Biophys.Res.Commun.,* 328**,** 679-687.

YU, X., HUANG, Y., COLLIN-OSDOBY, P. & OSDOBY, P. 2003. Stromal cell-derived factor-1 (SDF-1) recruits osteoclast precursors by inducing chemotaxis,

matrix metalloproteinase-9 (MMP-9) activity, and collagen transmigration. *J Bone Miner Res,* 18**,** 1404-18.

ZAVRŠNIK, J., BUTINAR, M., PREBANDA, M. T., KRAJNC, A., VIDMAR, R., FONOVIĆ, M., GRUBB, A., TURK, V., TURK, B. & VASILJEVA, O. 2017. Cystatin C deficiency suppresses tumor growth in a breast cancer model through decreased proliferation of tumor cells. *Oncotarget,* 8**,** 73793-809.

ZEICHNER, S. B., TERAWAKI, H. & GOGINENI, K. 2016. A Review of Systemic Treatment in Metastatic Triple-Negative Breast Cancer. *Breast Cancer (Auckl),* 10**,** 25-36.

ZHANG, D., QIU, L., JIN, X., GUO, Z. & GUO, C. 2009. Nuclear factor-kappaB inhibition by parthenolide potentiates the efficacy of Taxol in non-small cell lung cancer in vitro and in vivo. *Mol Cancer Res,* 7**,** 1139-49.

ZHANG, J., FENG, H., ZHAO, J., FELDMAN, E. R., CHEN, S. Y., YUAN, W., HUANG, C., AKBARI, O., TIBBETTS, S. A. & FENG, P. 2016. IκB Kinase ε Is an NFATc1 Kinase that Inhibits T Cell Immune Response. *Cell Rep,* 16**,** 405-18.

ZHANG, X. H., JIN, X., MALLADI, S., ZOU, Y., WEN, Y. H., BROGI, E., SMID, M., FOEKENS, J. A. & MASSAGUE, J. 2013. Selection of bone metastasis seeds by mesenchymal signals in the primary tumor stroma. *Cell,* 154**,** 1060-73.

ZHANG, Y., GUAN, H., LI, J., FANG, Z., CHEN, W. & LI, F. 2015. Amlexanox Suppresses Osteoclastogenesis and Prevents Ovariectomy-Induced Bone Loss. *Sci Rep,* 5**,** 13575.

ZHENG, Y., CHOW, S. O., BOERNERT, K., BASEL, D., MIKUSCHEVA, A., KIM, S., FONG-YEE, C., TRIVEDI, T., BUTTGEREIT, F., SUTHERLAND, R. L., DUNSTAN, C. R., ZHOU, H. & SEIBEL, M. J. 2014. Direct crosstalk between cancer and osteoblast lineage cells fuels metastatic growth in bone via auto-amplification of IL-6 and RANKL signaling pathways. *J Bone Miner Res,* 29**,** 1938-49.

ZHOU, A. Y., SHEN, R. R., KIM, E., LOCK, Y. J., XU, M., CHEN, Z. J. & HAHN, W. C. 2013. IKKepsilon-mediated tumorigenesis requires K63-linked polyubiquitination by a cIAP1/cIAP2/TRAF2 E3 ubiquitin ligase complex. *Cell Reports,* 3**,** 724-33.

ZHOU, S., LIU, C., WU, S. M. & WU, R. L. 2005. [Expressions of CD147 and matrix metalloproteinase-2 in breast cancer and their correlations to prognosis]. *Ai Zheng,* 24**,** 874-9.

ZHOU, Y., YAU, C., GRAY, J. W., CHEW, K., DAIRKEE, S. H., MOORE, D. H., EPPENBERGER, U., EPPENBERGER-CASTORI, S. & BENZ, C. C. 2007. Enhanced NFκB and AP-1 transcriptional activity associated with antiestrogen resistant breast cancer. *BMC Cancer,* 7**,** 59.

Copyright

The following figures were created in part using Servier Medical Art (SMART Creative commons license) and may have been edited it some aspects:

- Figure 2. Schematic diagram of tumourigenesis and the metastatic process.
- Figure 3. Patterns of breast cancer metastatic dissemination.
- Figure 5. The bone metastatic process.
- Figure 6. Canonical and non-canonical NFκB activation.
- Figure 7. IKKε/TBK-1 signalling pathways in innate immunity.
- Figure 8. Existing mechanisms of IKKε oncogenic activity.